MOLECULAR MECHANISMS UNDERLYING THE ADAPTATION OF *LEISHMANIA* TO PURINE STRESS

By

Jessica Lindsay Martin

A DISSERTATION

Presented to The Department of Biochemistry and Molecular Biology

and the Oregon Health & Science University

School of Medicine

in partial fulfillment of the requirements for the degree of

Doctor of Philosophy

August 2015

School of Medicine

Oregon Health & Science University

CERTIFICATE OF APPROVAL

This is to certify that the PhD dissertation of

Jessica Lindsay Martin

has been approved

_____

Buddy Ullman, PhD (Mentor)

_____

Scott Landfear, PhD (Committee Chair)

_____

Nicola Carter, PhD (Member)

_____

Ujwal Shinde, PhD (Member)

_____

Show-Ling Shyng, PhD (Member)

Acknowledgments

I am forever indebted to Nicola and Buddy for introducing me to the world of parasitology and connecting me to such a wonderful research community, I look forward to always being a part of it. Thank you both for supporting me, challenging me, and allowing me to pursue my own path. I have learned so much from every member of the laboratory Phil, Jan, Marie-Pierre, Radika, Caslin, Tamara, Mike, I could fill pages upon pages of memories and experiences with each of you that have shaped not only my graduate career but who I am as a person, I am grateful for all the time we've spent together and all you've taught me.

Thank you to my advisory committee (Bill, Scott, Ujwal, and Show-Ling) for your mentorship and advice and for teaching me what it means to have a successful career in research.

Josh thank you for taking a chance on me all those years ago and inviting me to PNNL and Charles, perhaps against your better judgment, for allowing me to come back! To everyone who asked in 2009: I can finally say I'm a postdoc! Sorry about the flood. Kristin, you have always been such an inspiration to me, both in science and life, thank you.

I cannot thank everyone who has ever been on the 7th floor of RJH enough for putting up with my antics. I've had so much fun getting to know and work alongside you all. Thayer, Musil, Kabat, Skach lab, everyone!

Thank you to everyone in the OHSU cores for holding my hand through some tough moments. Thank you to the custodial staff for keeping me company late at night in the lab, it's been great getting to know you, all the laughs, and keeping me safe. You are all wonderful.

To all of my classmates and students that I've met along the way, not only did you all make me feel less alone in this isolating process, you made my experience really, really great. I will always cherish our friendships and hope to collaborate in the future! Alison, thank you for Brazil.

Amber, Danielle, Jenna, and Carly, there just aren't words to thank you enough for your friendship. You are incredible women and I'm so excited for what the future will bring each of you (hopefully all of us back together!).

Clark and Mark, thanks for supporting dissertation station, and removing me from it when necessary. And for the food. That was essential.

To the ARCS foundation, thank you. Jean, Jamie, and Shelley, you are incredible and I am so lucky to know each of you.

To Barbara, thank you for the opportunity, I can't wait to start working together!

To my family, thank you. Thank you. Thank you. Especially my mom and my sister; I love you.

I simply do not have the space or the words to express my appreciation for everyone who has contributed to my life and dissertation; please know that I am grateful.

"There are two ways to do research: the right way, and over again."

-Armando Jardim, PhD

Table of Contents

List of Tables

List of Figures

Abbreviations

3'NT/NU – 3'-nucleotidase/nuclease

AAH – adenine aminohydrolase

ACN – acetonitrile

ADE – adenine

ADO – adenosine

ADSS – adenylosuccinate synthetase

AK – adenosine kinase

AMPDA -- adenosine monophosphate deaminase

AMPK – AMP-activated protein kinase

AMT – accurate mass and time

APRT – adenine phosphoribosyltransferase

ASL – adenylosuccinate lyase

ATG8 – autophagy-related protein 8

CDS – coding sequence

CL – Cutaneous leishmaniasis

DME-L – Dulbecco's Modified Eagle medium with *Leishmania* additions

DTT – Dithiothreitol

ESI – electrospray ionization

GDA – guanine deaminase

GEO – NCBI Gene Expression Omnibus

GK – guanylate kinase

GMPR – guanosine monophosphate reductase

GMPS – guanosine monophosphate synthase

GO – gene ontology

GPCR – G-protein coupled receptor

GUA – guanine

GUO – guanosine

H_2DCFDA – 2'7'-dichlorodihydrofluorescein diacetate

HBSS-G – Hank's balanced salt solution with glucose

HGPRT – hypoxanthine-guanine phosphoribosyltransferase

HYP – hypoxanthine

IAA – iodoacetamide

IAGNH – purine-specific nucleoside hydrolase

IGNH – 6-hydroxypurine nucleoside hydrolase

IMPDH – inosine monophosphate dehydrogenase

INO – inosine

kDNA – kinetoplast DNA

LC-MS/MS – liquid chromatography tandem mass spectrometry

LdNT1, LdNT2, LdNT3, LdNT4

MAP2 – membrane-bound acid phosphatase

MCL – Mucocutaneous leishmaniasis

MTA - methylthioadenosine

MTAP – methylthioadenosine phosphorylase

NCBI – National Center for Biotechnology Information

NGS – next generation sequencing

NH – non-specific nucleoside hydrolase

PDE – phosphodiesterase

PE – phosphatidylethanolamine

qRT-PCR – quantitative reverse transcriptase polymerase chain reaction

RFU – relative fluorescence units

RLU – relative light units

Rluc – *Renilla* luciferase

RNA-seq – RNA sequencing (whole transcriptome shotgun sequencing)

ROS – reactive oxygen species

SAM – S-adenosylmethionine

SAMSYN – S-adenosylmethionine synthetase

SCX – strong cation exchange

SL – spliced leader

SPE – solid phase extraction

TCA – tricarboxylic acid cycle

TEAB – triethylammonium bicarbonate

TFA – trifluoroacetic acid

TMT – tandem mass tag

TOR – target of rapamycin

UMPS – uridine monophosphate synthase

UMSBP – universal minicircle sequence binding protein

UTR – untranslated region

XAN – xanthine

XAO – xanthosine

XPRT – xanthine phosphoribosyltransferase

VL – Visceral leishmaniasis

VSP4 – vacuolar protein sorting-associated protein 4

Thesis overview

Leishmania are the causative agent of *leishmaniasis*, a disease with many forms, the most severe of which is ultimately fatal if left untreated. Unfortunately, no vaccine is available, and resistance is emerging to currently employed therapeutics, many of which are costly and difficult to administer. Because the parasite must respond and adapt to a number of environmental insults throughout its lifecycle, including nutrient scarcity, inhibiting its mechanisms of adaptation is an attractive area for chemotherapeutic intervention. My thesis research focuses on the molecular mechanisms that allow *Leishmania* to persist in a non-dividing, but metabolically active, quiescent-like state for months in the absence of an extracellular purine—a nutrient essential for growth.

The introduction begins with a brief review of the unique biology of *Leishmania* as well as the current knowledge of nutrient sensing and adaptation in these parasites. Chapter 2 describes the global investigation into changes of both the proteome and transcriptome in response to the removal of purines from the parasite's extracellular environment. These data reveal an extensive remodeling at both the protein and transcript level, highlighting how a few subtle increases or decreases of enzymes in a common pathway can lead to substantial metabolite changes, for example, increased intracellular proline. The data reveal a frequent discordant relationship between mRNA expression and protein abundance, thereby emphasizing the role of translation and posttranslational regulatory mechanisms.

The studies in Chapter 2 lead to the question of *how* the parasite senses these nutrient fluctuations, especially in the absence of canonical sensing and signaling mechanisms. My work in Chapter 3 details the investigation of internal versus external nutrient sensing mechanisms, showing for the first time that extracellular purine sensing occurs through perturbations in intracellular pools. Furthermore, by employing a cell line defective in purine interconversion, my thesis research determined that perturbation of the adenine-containing nucleotides alone is both necessary and sufficient for the adaptation of the parasite to purine stress—the first mechanistic insight for nutrient sensing in these parasites.

Chapter 4 concludes this dissertation by showcasing the utility of the mutant cell line described in Chapter 3 as a model for investigating molecular regulatory mechanisms. Preliminary studies into purine-pool specific protein abundance and phosphorylation are described. The long-term implications of such a robust model system for nutrient adaptation are discussed. In closing, it is my belief that the data generated by the studies described in this thesis will be useful many times over, not only in the understanding of the basic biology of the parasite, but also in combating a debilitating disease.

Chapter 1

INTRODUCTION

1.1 PARASITES

A parasite, from the Greek *parasitos*, is one who lives at the expense of another. While initially used to describe people who take from others while offering nothing in return, the word parasite, as used in biology today, indicates an organism that takes all that it needs from its host, often resulting in harm to the host. By defining this group based on behavior, the word parasite encompasses viruses, prokaryotes, and single and multicellular eukaryotes.

1.2 TRYPANOSOMATIDS

Domain Eukaryota, kingdom Excavata, phylum Euglenozoa, class Kinetoplastida, order Trypanosomatida.

Classification

The class Kinetoplastida is divided into two subclasses: Prokinetoplastina and Metakinetoplastina, the former consists of order Protokinetoplastida with later of orders Eubodonida, Parabodonida, Neobodonida and Trypanosomatida. Members of Kinetoplastida can be free-living, commensalic, or parasitic, however, all members of Trypansomatida are parasitic (1). Trypanosomatida are

attractive research subjects due to their global health burden, responsible for over 37 million infections of *Trypanosoma brucei, Trypanosoma cruzi,* and *Leishmania* species, the causative agents of African sleeping sickness, Chagas disease, and leishmaniasis respectively (See section 1.3) (1). These organisms also warrant investigation at the molecular level as they are evolutionarily distant from animals, plants, and fungi (2), with particularly unique biological features to be described in the following sections.

Kinetoplast

Kinetoplast DNA (**kDNA**) has been described as "the most structurally complex mitochondrial DNA in nature" (3). kDNA is the mitochondrial DNA of trypanosomatids. It is a giant DNA network found in the cell's single large mitochondrion and is comprised of thousands of catenated circular DNAs of two types, minicircles and maxicircles (Fig 1.1) (4, 5). Minicircles range in size from 0.5 to 10 kb, depending on the species, and are found in thousands of copies, which are heterogeneous in sequence. Maxicircles are typically found in a few dozen identical copies, ranging in size from 20 to 40 kb, again depending on the species (3-5). With the exception of tRNAs, the genes encoded within the maxicircles are for typical mitochondrial gene products, such as ribosomal RNAs and complexes involved in cellular respiration. However, some of these protein-coding genes are encrypted, meaning the transcripts must undergo the extensive posttranscriptional RNA editing process of inserting and deleting hundreds of uridine residues at specific sites, using "guide" RNAs. While both mini and

maxicircles encode gRNAs, the only known function for minicircles is to encode these gRNAs (3-5).

Glycosome

Glycosomes are considered "divergent peroxisomes;" these protein-dense membrane-bound organelles compartmentalize a variety of metabolic enzymes, including those involved in glycolysis (for which the organelle is named) (6) as well as parts of the pentose-phosphate pathway, purine salvage, pyrimidine biosynthesis, energy homeostasis, beta-oxidation, ether-lipid biosynthesis, squalene synthesis, and oxidative stress pathways (7). However, the defining characteristic of peroxisomes—H_2O_2 metabolism, has been lost entirely from *Trypanosoma* and *Leishmania* (8, 9) but is retained in other kinetoplastids, showing that this activity was likely lost after the incorporation of glycolytic enzymes. Much speculation surrounds the evolutionary advantage and general role of this organelle, including glycolytic flux and minimization of toxic intermediates (10-12), facilitating the development of parasitism (13), and in keeping with the theme of this dissertation, that the fluctuations in nutrient availability drove the origin and further evolution of glycosomes (13).

Genome and Gene Regulation

Currently, it is estimated that the *Leishmania donovani* genome encodes 8195 genes, 8083 of which are expected to be protein coding (14, 15), the study described in Chapter 2 identified 4109 proteins (16) when using *L. infantum* as

the reference genome (as it was the most comprehensive available at the time).

A proteogenomic analysis of the *L. donovani* proteome in both the promastigote and amastigote stages identified 3999 proteins in total, 1090 and 603 identifications unique to each life cycle stage, respectively (17). Further studies of specific lifecycle stages will likely lead to more complete coverage of the *L. donovani* proteome as well as reanalysis of existing mass spectrometry data against the refined genome sequences. Trypanosomes exhibit polycistronic gene transcription (18) meaning that clusters of genes are co-transcribed by RNA polymerase II; these genes are typically functionally unrelated (19). These large polycistronic pre-mRNAs are processed into monocistronic units via *trans*-splicing, a mechanism in which a 39-nt spliced leader (**SL**) capped sequence is attached to the 5' end of mRNAs and the 3' end is polyadenylated (19, 20). In addition to being functionally unrelated, the individual genes transcribed in a polycistronic unit can demonstrate different steady-state levels, indicating that mRNA abundance regulation is occurring through post-transcriptional processes (21). No evidence exists for the differential regulation of RNA polymerase II transcription of genes or gene clusters, and very few transcription factors are predicted in the leishmanial genome, and more significantly, none of which have been verified (18, 21).

1.3 *LEISHMANIA*

Discovery of *Leishmania*

In 1903, William Leishman, a Scottish army doctor, published his observation of ovoid bodies in a spleen smear from an infected British solider, he attributed these to a degenerate form of *Trypanosomes* (22). Around this same time, Charles Donovan, a professor of physiology at Madras University also found "Leishman bodies" in a splenic biopsy. It was later confirmed that Leishman and Donovan had identified the same bodies—the amastigote form of the parasite, now known as *Leishmania donovani*, named by Ronald Ross in their honor (23). It should be noted that others including Cunningham, Borovsky, Wright, Lindenberg, and Vianna also independently identified this parasite at about the same time (24). The race was on to identify this parasite's vector. It wasn't until nearly forty years later, in 1942, that studies confirmed the vector for *Leishmania* is the phlebotomine sandfly. Of the five human volunteers, all five contracted leishmaniasis when bitten by a sandfly that had previously fed upon an infected individual (25, 26).

Life Cycle

Leishmania are digenetic protozoa, meaning they live in distinct stages, one within the insect vector and the other in the mammalian host (Figs 1.2 and 1.5). Within the female sandfly gut, *Leishmania* are flagellated extracellular promastigotes, where they mature into an infective promastigote form, called a "metacyclic promastigote". When an infected sandfly tries to feed on a mammalian host, the parasites are transmitted into the dermis and phagocytosed first by neutrophils, and subsequently by the macrophage where they exist as

non-motile intracellular amastigotes (27). These two environments differ dramatically—in the sandfly midgut, the temperature is about 26°C, the pH slightly alkaline, with high levels of sugar, this is in stark contrast to the mammalian phagolysosome where the temperature is around 37°C, the pH acidic, and lacking sugar, but full of amino acids and fatty acids. (28-30). Successful parasitism requires the quick and robust adaptation not only as it transitions between these distinct environments but also subsequent fluctuations in nutrient availability within each environment. The work presented in this thesis focuses on the promastigote form of the parasite, tractable for laboratory culture in defined medium as well specific stress induction.

Leishmaniasis

Leishmaniasis is a "neglected vector-borne tropical infection considered to be a disease of the poor" and the most deadly parasitic disease after malaria (31). The disease manifests in three major forms: visceral, cutaneous, and mucocutaneous leishmaniasis (**VL**, **CL**, and **MCL**, respectively). VL, also known as kala-azar or black fever, is caused by *L. donovani*, *L. infantum,* or *L. chagasi* colonizing the bone marrow, liver, and spleen, resulting in host immunosuppression, and is fatal if left untreated (32). In the latter forms, CL and MCL, parasite invasion is restricted to the epithelial tissues and often results in disfiguring lesions; *L. infantum*, *L. tropica*, and *L. major* are the common etiological agents.

With over 98 countries and territories endemic for leishmaniasis (Figs 1.3 and 1.4) (33), approximately 350 million people live in areas with active *Leishmania* transmission—which occurs through the bite of a sandfly (34). It is estimated that 14 million people are affected by the disease, with 0.2-0.4 million reported cases of VL (35) and up to 40,000 of those cases leading to death per year (31).

Treatment

Discovered by Gaspar Vianna, tartar emetic (antimony potassium tartrate, a trivalent antimony, Sb^{III}) was one of the first treatments for leishmaniasis, starting around 1913 (36). In 1922, pentavalent antimonials (Sb^{V}), such as sodium stibgluconate (Pentostam), were introduced and have remained a major component of treatment, as they are much safer than the trivalent antimonial (24). Unfortunately, in the 1970s an increasing number of patients with visceral leishmaniasis were unresponsive to treatment and it was found that isolates of *Leishmania* were resistant to these antimonial compounds (37). The antimonial compounds fell out of favor and the treatment of leishmaniasis saw the introduction of pentamidine in 1973 (38) liposomal amphotericin B (AmBisome) in 1996 (39), miltefosine in 2004 (40), and paromomycin in 2006 (41, 42). While these more recent treatments are safer and more efficacious than previous options, they require multi-week and supervised administration (all but miltefosine cannot be administered orally) and resistance to miltefosine is a

significant concern (43-46), thus, there exists an urgent need for new and more effective antileishmanial drugs.

1.4 ENVIRONMENTAL SENSING AND ADAPTATION IN *LEISHMANIA*

Overview

The sensing of extracellular and intracellular nutrient availability and adaptation to nutrient scarcity is essential for all forms of life, especially unicellular organisms that often inhabit disparate environments. Unlike a multicellular organism in which multiple types of cells contribute to maintaining systemic homeostasis, failure of a unicellular organism to adapt to an environmental changes results in the death of that cell (i.e. the *entire* organism).

Canonical sensing and signaling mechanisms

G-protein coupled receptors (**GPCRs**) are the largest and most diverse family of membrane receptors in eukaryotes, responsible for relaying the status of environmental information including availability of sugars, lipids, proteins, and the presence of hormones, or mating factors, for example (47). A beautifully simple system for direct sensing of the environment, GPCRs are absent from kinetoplastids (48), as are receptor protein kinases and phosphatases and heterotrimeric G proteins; while adenylyl and guanylyl cyclases have been described (49), their ligands remain elusive. It is likely that the canonical sensing and signaling pathways are absent or considerably different in these parasites. Adding another layer of complexity, many signaling pathways in other eukaryotes

result in the downstream activation of transcription factors altering the transcriptome. In contrast, transcription factors have not been identified in *Leishmania* (48). It should be noted that within the kinetoplastids, proteins have been identified that have characteristics of trimeric G proteins, though the functional consequence of these proteins in the parasite remains unknown (50).

Figure 1.6 by Parsons and Ruben (48) summarizes the absence in knowledge regard sensing and signaling in trypansomatids as compared to mammalian cells; little progress has been made since this figure was first published in 2000. A major goal of my thesis research is to delineate sensing and signaling mechanisms in trypanosomatids using purine starvation in *Leishmania* as a model system, as described below.

Review of purine starvation in *Leishmania*

Leishmania are unable to synthesis the purine ring *de novo* and must rely on a complement of nucleobase and nucleoside transporters at the cell surface to salvage extracellular purines, as well as enzymes for interconversion to meet purine requirements for growth. Previously, our laboratory established a robust system for starving *Leishmania* in culture by using defined medium (**DME**, Dulbecco's modified Eagle), modified for supporting *Leishmania* growth (51), supplemented with a serum lacking purines—for specific control of the parasite's purine environment by selective addition of purines; this medium allows for direct comparison between purine-replete and purine-starved cultured conditions as the only variable between the two is addition or absence of purines (52).

Studies using this model determined that purine starvation enhanced nucleobase and nucleoside transport in *Leishmania*, caused an elongation of the cell body (Fig. 1.7), and lead to growth arrest with cells accumulating in the G_1/G_0 stage of the cell cycle (52). Additionally, a number of proteins involved in purine salvage and interconversion are increased in abundance upon removal of purines, including adenine phosphoribosyltransferase, hypoxanthine-guanine phosphoribosyltransferase, and xanthine phosphoribosyltransferase (**APRT, HGPRT, XPRT**, respectively), as well as the nucleoside transporter LdNT2. The activities of LdNT1 and LdNT3 (nucleoside and nucleobase transporters, respectively) were also shown to increase due to purine starvation. Furthermore, total RNA for purine starved cells was decreased by about 3-fold after 48 h purine starvation, indicating a global decrease in transcription. However, some purine salvage gene mRNAs were upregulated, likely via post-transcriptional regulatory mechanisms as these parasites lack gene-specific transcriptional control (52). This model of purine starvation in *Leishmania* is the foundation for my dissertation and is essential to each of the studies described here.
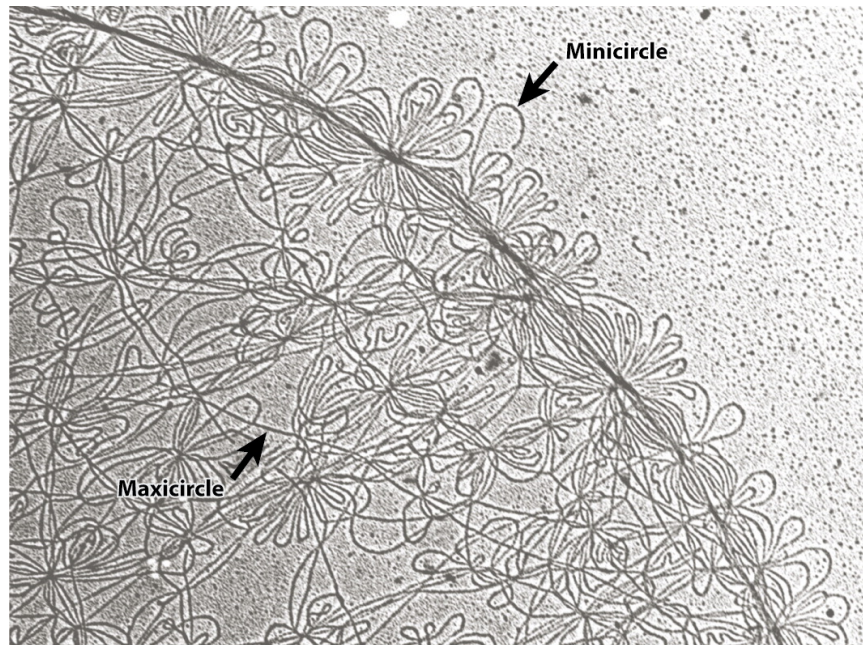
Figure 1.1 Electron micrograph of kDNA isolated from *Crithidia fasciculata.*
Minicircles are the small DNA loops and encode guide RNAs for editing
maxicircle transcripts, whereas the long strands of DNA are parts of maxicircles
that encode rRNAs and mitrochondrial proteins. Adapted from (53).
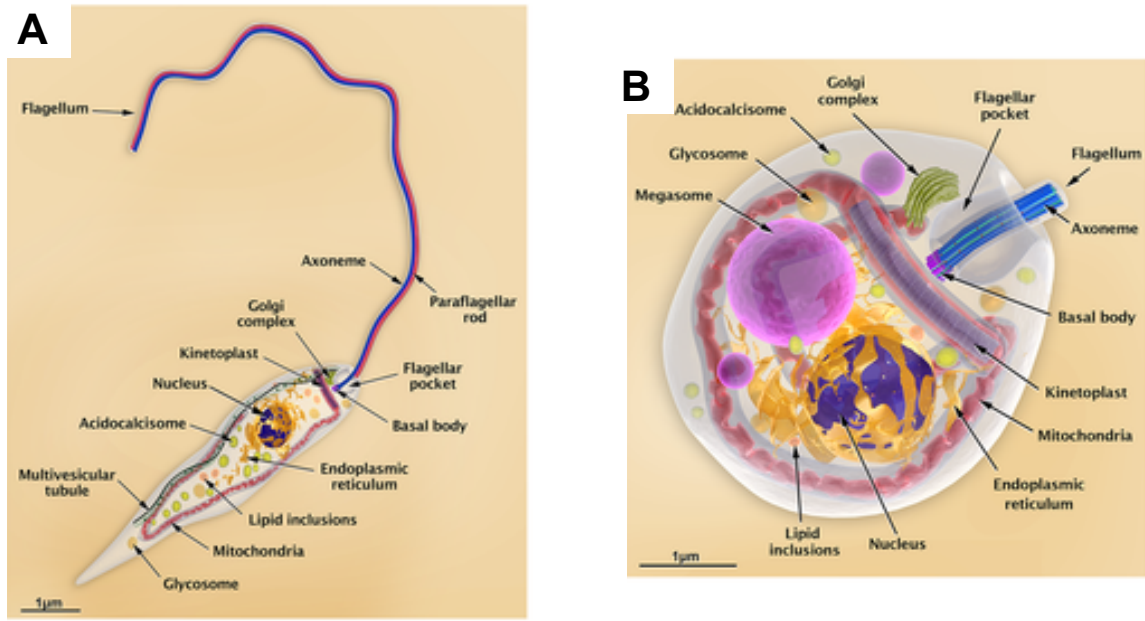
Figure 1.2 Structural organization of *Leishmania*

A) *Leishmania* promastigote B) *Leishmania* amastigote, source Teixeira et al (54).
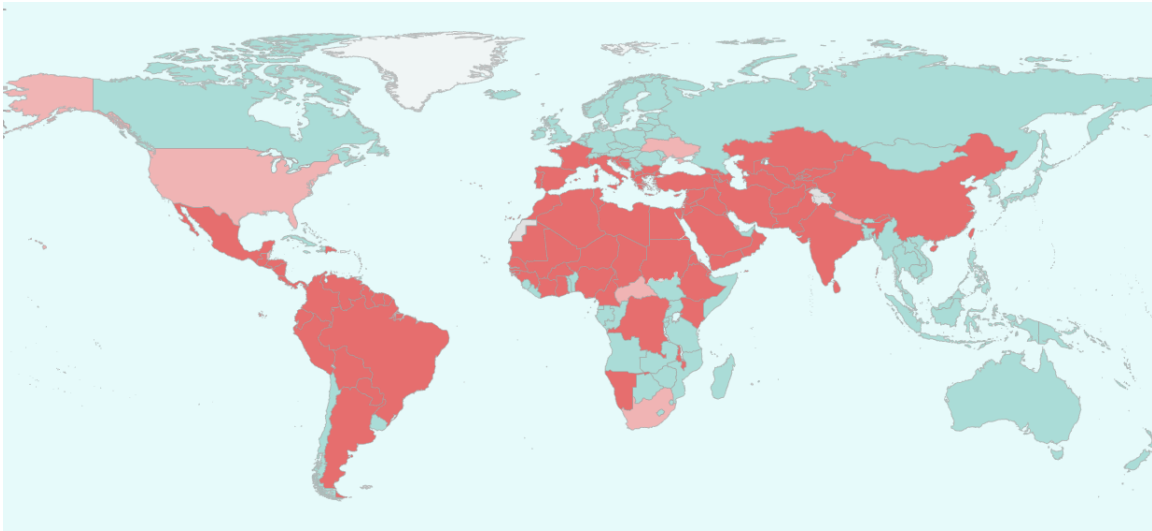
Figure 1.3 Status of endemicity of cutaneous leishmaniasis 2013

Dark red – countries with endemic leishmaniasis, light red – countries with previously reported cases, blue – no autochthonous cases reported, and grey – not applicable (33).
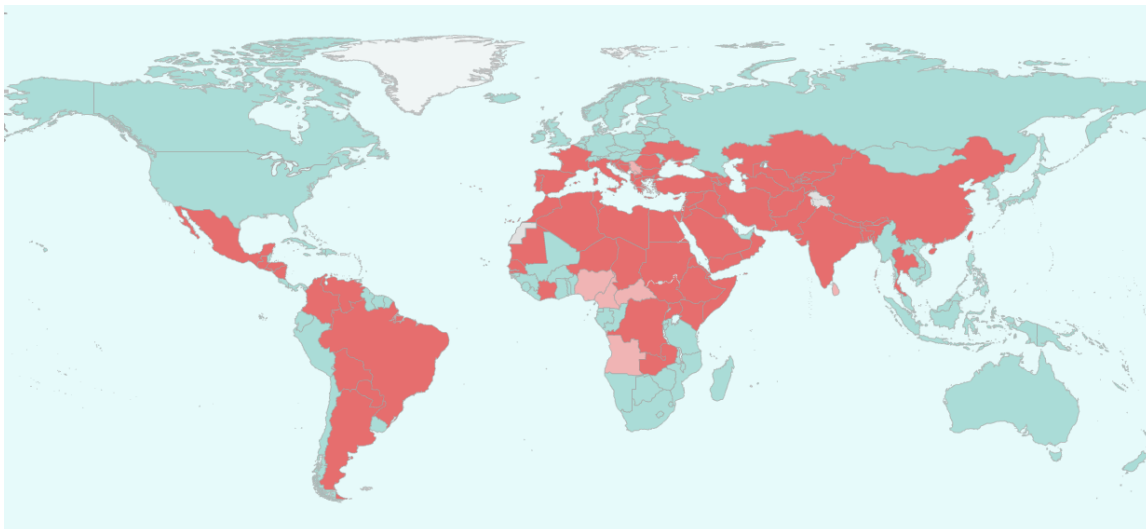
Figure 1.4 Status of endemicity of visceral leishmaniasis 2013

Dark red – countries with endemic leishmaniasis, light red – countries with previously reported cases, blue – no autochthonous cases reported, and grey – not applicable (33).
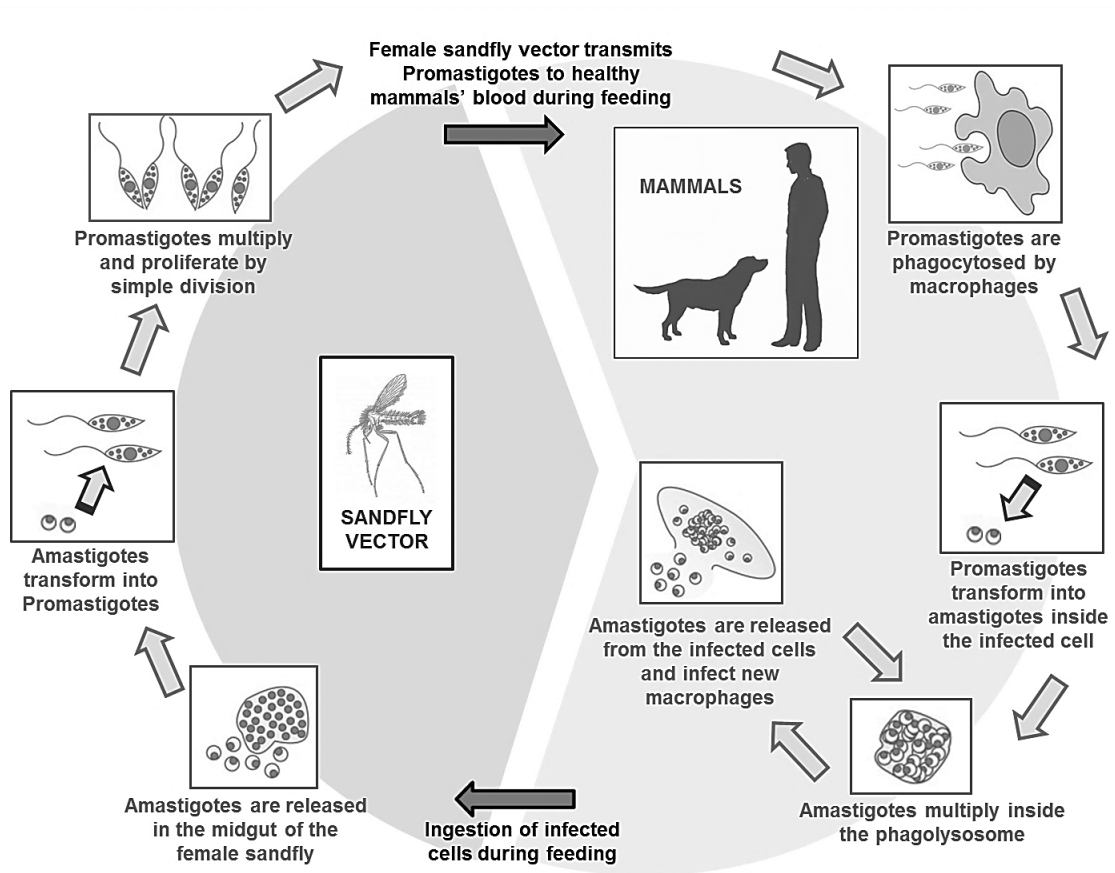
Figure 1.5 Life cycle of *Leishmania*

As published in (55).

Fig. 1. A simplified diagram of cell signaling. Many of the components and connections present in mammalian cells have not yet been found in trypanosomatids. PDE, cAMP phosphodiesterase; PIK, phosphatidylinositol kinases; PIPLC, phosphoinositide phospholipase C; PKA, cAMP-dependent protein kinase; PtdIns, phophatidylinositol; SH2, SRC homology region 2. Dashed arrows and dark grey shading indicate missing components and connections; solid arrows and pale grey shading indicate known components and connections.

Figure 1.6 An overview of known and unknowns in cell signaling as presented by Parsons et al in 2000 (50).
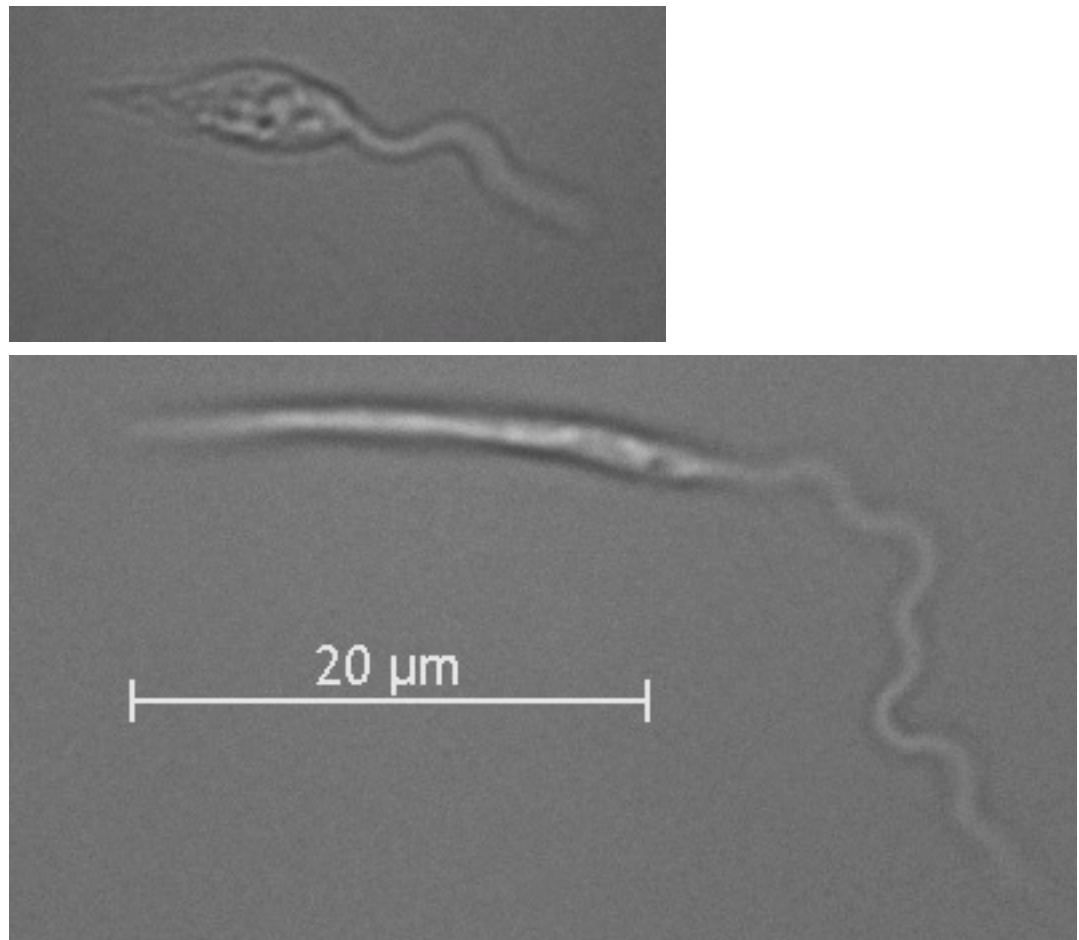
Fig 1.7 Morphological change after 24 h purine starvation
A) *Leishmania donovani* promastigotes cultured in DME-L medium with 100 μM
purine (standard culture conditions for work presented in this thesis) B) *L.
donovani* promastigote after 24 h purine starvation (DME-L medium with no
purine supplementation). Note the elongation of the cell body and increased
flagellum length.

Chapter 2

METABOLIC REPROGRAMMING DURING PURINE STRESS IN THE PROTOZOAN PATHOGEN LEISHMANIA DONOVANI

Jessica L. Martin[1][⊕], Phillip A. Yates[1][⊕], Radika Soysa[1], Joshua F. Alfaro[3], Feng Yang[3], Kristin E. Burnum-Johnson[3], Vladislav A. Petyuk[3], Karl. K. Weitz[3], David G. Camp II[3], Richard D. Smith[3], Phillip A. Wilmarth[1,2], Larry L. David[1,2], Gowthaman Ramasamy[4], Peter J. Myler[4,5], & Nicola S. Carter[1]*

Department of [1]Biochemistry & Molecular Biology and [2]Proteomics Shared Resource Core, Oregon Health & Science University, Portland, Oregon, United States of America; [3]Division of Biological Sciences, Pacific Northwest National Laboratory, Richland, Washington, United States of America; [4]Seattle Biomedical Research Institute, Seattle, Washington, United States of America; [5]Department of Global Health and Department of Biomedical Informatics & Medical Education, University of Washington, Seattle, Washington, United States of America.

[⊕]Both of these authors contributed equally to the work.

ABSTRACT

The ability of *Leishmania* to survive in their insect or mammalian host is dependent upon an ability to sense and adapt to changes in the microenvironment. However, little is known about the molecular mechanisms underlying the parasite response to environmental changes, such as nutrient availability. To elucidate nutrient stress response pathways in *Leishmania donovani*, we have used purine starvation as the paradigm. The salvage of purines from the host milieu is obligatory for parasite replication; nevertheless, purine-starved parasites can persist in culture without supplementary purine for over 3 months, indicating that the response to purine starvation is robust and engenders parasite survival under conditions of extreme scarcity. To understand metabolic reprogramming during purine starvation we have employed global approaches. Whole proteome comparisons between purine-starved and purine-replete parasites over a 6-48 h span have revealed a temporal and coordinated response to purine starvation. Purine transporters and enzymes involved in acquisition at the cell surface are upregulated within a few hours of purine removal from the media, while other key purine salvage components are upregulated later in the time-course and more modestly. After 48 h, the proteome of purine-starved parasites is extensively remodeled and adaptations to purine stress appear tailored to deal with both purine deprivation and general stress. To probe the molecular mechanisms affecting proteome remodeling in response to purine starvation, comparative RNA-seq analyses, qRT-PCR, and luciferase reporter assays were performed on purine-starved *versus* purine-replete

parasites. While the regulation of a minority of proteins tracked with changes at the mRNA level, for many regulated proteins it appears that proteome remodeling during purine stress occurs primarily *via* translational and/or post-translational mechanisms.

AUTHOR SUMMARY

Leishmania, the cause of a deadly spectrum of diseases in humans, surmounts a number of environmental challenges, including changes in the availability of salvageable nutrients, to successfully colonize its host. Adaptation to environmental stress is clearly of significance in parasite biology, but the underlying mechanisms are not well understood. To simulate the response to periodic nutrient scarcity *in vivo*, we have induced purine starvation *in vitro*. Purines are essential for growth and viability, and serve as the major energy currency of cells. *Leishmania* cannot synthesize purines and must salvage them from the surroundings. Extracellular purine depletion in culture induces a robust survival response in *Leishmania*, whereby growth arrests, but parasites persist for months. To profile the events that enable endurance of purine starvation, we used shotgun proteomics. Our data suggest that purine starvation induces extensive proteome remodeling, tailored to enhance purine capture and recycling, reduce energy expenditures, and maintain viability of the metabolically active, non-dividing population. Through global and targeted approaches, we reveal that proteome remodeling is multifaceted, and occurs through an array of responses at the mRNA, translational, and post-translational level. Our data provide one of the most inclusive views of adaptation to microenvironmental stress in *Leishmania*.

INTRODUCTION

Leishmania are protozoan parasites that are a significant human health burden, afflicting approximately 12 million people in 88 countries worldwide (24). These parasites cause a spectrum of diseases in humans ranging from cutaneous ulcerative lesions that can be localized or diffuse; disfiguring mucocutaneous lesions that manifest in the nose, mouth, and throat cavities; to fatal hepato- or splenomegaly arising from a visceralizing form of the disease (24). Due to the lack of an effective vaccine, management of leishmaniasis is predicated on just a few drugs, most of which exhibit toxic side effects and are costly and burdensome to administer, putting them beyond the reach of many of the affected countries. Of particular concern is the high level of resistance currently observed to the drug Pentostam, a mainstay of leishmaniasis treatment, especially in regions endemic for *Leishmania donovani*, the causative agent of deadly visceral leishmaniasis (37, 56). Thus, there is a compelling need for better therapeutic approaches for combating leishmaniasis in humans.

One long-standing approach to defining new pathways and targets for drug design has been to identify parasite pathways that are both different from their host and vital for parasite viability (57-59). An ability to adapt to host nutritional and physiological changes is a key feature of parasitism and ensures parasite survival, even under less than optimal conditions. *Leishmania*, in particular, overcome dramatic physiological alterations in their host milieu as they transition between extracellular promastigotes in the ambient, neutral

environment inside of the sandfly to intracellular amastigotes that reside in the acidic phagolysosome of mammalian macrophages at 37 ^{o}C (60). It is likely that salvageable nutrients that are essential for parasite viability also fluctuate throughout the *Leishmania* lifecycle, since these parasites have evolved robust mechanisms to deal with periods of nutrient paucity (52, 60-65). Indeed, nutrient depletion, at least *in vitro*, can be used as a trigger for metacyclogenesis in *Leishmania* (66-68), as well as in the closely related *Trypanosoma cruzi* (69, 70), implying that nutrient stress provokes substantial changes to the parasite proteome. Therefore, these parasites must sense and adapt to changing extracellular and intracellular conditions as they colonize the different microenvironments of each host.

Despite their significance for parasite survival, little is known about the molecular mechanisms used by these parasites to respond to environmental changes, such as nutrient availability (50, 71). Thus, to elucidate nutrient stress response pathways in *L. donovani*, we have used purine starvation as the paradigm. The salvage of purines from the host milieu is an obligatory process that impacts both cell viability and growth (72). *Leishmania*, like all parasitic protozoa characterized to date, are auxotrophic for purines and have evolved a unique set of purine transporters and salvage enzymes to scavenge these essential nutrients from their host (72-74). Because purine acquisition in *Leishmania* is an indispensable nutritional process, and the pathway is considered an attractive target for therapeutic exploration, the components of purine salvage have been extensively characterized at the molecular,

biochemical, and, in some cases, at the structural level (72, 74-78). However, the regulation of this pathway in response to changes in the extracellular purine milieu is poorly understood. Earlier studies in *Leishmania* and related parasites have revealed a marked augmentation in cell surface activities corresponding to 3'-nucleotidase/nuclease (**3'NT/NU**) and membrane-bound acid phosphatase in response to purine starvation (65, 79-83), and studies from our own laboratory (52, 84), as well as others (64, 85, 86), have shown augmentation of nucleoside and nucleobase transport activities and proteins. Purine starvation is easily induced *in vitro* by the withdrawal of purines from the growth medium, and we have previously developed conditions where the response to purine stress is both robust and readily tractable (52). Our preliminary studies have shown that removal of purines from the extracellular milieu provokes striking morphological and metabolic changes (52). Purine-starved parasites arrest growth after one division in G_1/G_0 phase of the cell cycle (52), and we have shown that they can persist in culture without the provision of purine for more than 3 months. Altogether, these observations suggest that the response to purine starvation is tailored for parasite survival even under extreme scarcity and that purine starvation in *Leishmania* is an ideal model for dissecting the response to nutrient stress.

The molecular mechanisms that lead to the upregulation of cell surface purine enzymes and transporters during purine stress are likely complex. Thus, as a first step towards uncovering the multi-faceted changes involved in adaptation to purine starvation, we have used global approaches. Here we

describe an extensive comparison of the proteomes of purine-starved and purine-replete *L. donovani* over a 6-48 h window. These analyses have revealed that there is a temporal component to purine starvation, with earlier proteome changes tailored to counteract the scarcity of purine in the extracellular milieu and later proteome changes reflective of general responses to cellular stress that might accompany the entrance of the cells into quiescence. These later changes involve an extensive remodeling of the cellular proteome and likely contribute to the prolonged viability of these cells while under purine stress. Since *Leishmania* exhibit an unusual mechanism of gene regulation, whereby the majority of the leishmanial genome is constitutively transcribed and changes in protein abundance are directed by post-transcriptional mechanisms (19, 87), we have profiled post-transcriptional changes in mRNA stability by Whole Transcriptome Shotgun Sequencing or RNA-seq (88-95) to dissect the molecular mechanisms underlying proteome remodeling during purine stress. These analyses suggest that the post-transcriptional mechanisms that lead to proteome remodeling are complex and likely involve a diverse array of responses including changes in mRNA abundance, translational efficiency, as well as changes in the post-translational stability of proteins.

RESULTS

Temporal Changes in the Leishmanial Proteome During Purine Restriction

We have previously shown that the removal of extracellular purines leads to morphological changes in *L. donovani* promastigotes that manifest by 24 h post-purine removal from the growth medium (52). Parasites starved for purines also cease growth and accumulate in G_1/G_0 phase of the cell cycle, indicating that the removal of purines from the extracellular milieu promotes entrance of these parasites into a quiescent-like state (52). Accompanying these morphological and growth changes, *L. donovani* promastigotes also upregulate certain purine transport and salvage enzyme activities, as well as their corresponding proteins (52, 64). To assess the additional effects of extracellular purine depletion upon the leishmanial proteome, we starved *L. donovani* promastigotes of purines over a 48 h time period and compared the proteome of these parasites with cells grown with an extracellular purine source at 6, 12, 24, and 48 h. Note that *Leishmania* are capable of growth in any of the naturally occurring purine nucleobases or nucleosides (72), but for these experiments 100 μM hypoxanthine was included as the sole purine supplement in the growth medium. Comparison of the proteomes of purine-starved and purine-replete parasites at each of these time points was performed by the label-free and ultra-sensitive proteomic accurate mass and time (**AMT**) tag method (96-98). By AMT tag analysis, a total of 24,283 distinct peptides were identified corresponding to ~4109 proteins, of which 2661 proteins were identified with ≥ 2 peptides (Table

A.1). (Note that the entire liquid chromatography-tandem mass spectrometry (**LC-MS/MS**) dataset for these analyses can be accessed at http://omics.pnl.gov/view/publication_1086.html). Given that the reference *Leishmania infantum* genome (14, 99), used in the generation of the theoretical peptide fragmentation library for these studies, comprises 8381 annotated protein coding sequences, this equated to a coverage of ~49 %. Of the ~2500 proteins identified at each time point, ~2.6, 12.2, 12.5, and 35.1 % were observed to be significantly different in abundance (p-value ≤ 0.05) at the 6, 12, 24, and 48 h time points, respectively (Fig. 2.1 and Table A.1). The median abundance change at 6, 12, 24 and 48 h for upregulated proteins was 1.49-, 1.36-, 1.58-, and 1.64-fold, respectively, and 0.69-, 0.70-, 0.51-, and 0.49-fold for downregulated proteins. For those proteins that were significantly regulated at 6 h, only 7 showed a difference of 2-fold or greater and these were all upregulated under purine-deplete conditions (Fig. 2.1). With prolonged purine restriction, progressively more proteins demonstrated altered abundance, and by 48 h, the profiled proteome for purine-starved cells harbored some 841 proteins significantly changed in abundance, of which 151 were upregulated and 105 downregulated by 2-fold or greater (Table A.1 and Fig. 2.1).

The accuracy of the AMT tag analyses for estimating modest, but significant, differences in the proteomes of purine-starved and purine-replete cells was exemplified by its comparison to an independent shotgun proteomic dataset collected after 24 h of purine starvation and evaluated by LC-MS/MS and spectral counting (see Supplementary Materials and Methods and Table A.2).

Comparison of the 24 h AMT tag and spectral counting datasets revealed 1877 common proteins (see Table A.2), and of the 301 proteins significantly upregulated or downregulated (p-value ≤ 0.05) at 24 h by the AMT tag method (Table A.1 and Fig. 2.1), 202 followed a similar trend in the spectral counting dataset, where 110 proteins were downregulated and 92 were upregulated (Table A.2).

Temporal Responses within the Purine Pathway Proteome of Purine-Starved Leishmania: Some of the earliest and most striking changes in the proteome following purine removal involved the upregulation of purine salvage components located at the cell surface. These included the purine nucleoside transport proteins, **LdNT1** (LinJ.15.1230-50) and **LdNT2** (LinJ.36.2040), which participate in adenosine and 6-oxopurine nucleoside acquisition, respectively (100, 101), the purine nucleobase transporter **LdNT3** (LinJ.13.1110) (102), and the membrane bound 3'NT/NUs (LinJ.12.0350 and LinJ.31.2380) and acid phosphatases (**MAP2**) (LinJ.36.2720) that digest nucleic acids and mononucleotides down to their respective nucleosides (65, 103-107) (Figs. 2.2A and 2.3). Thus, some of the earliest changes appear tailored to enhance purine acquisition at the cell surface. By 12-24 h, the levels of two of the major intracellular purine salvage enzymes, xanthine phosphoribosyltransferase (**XPRT**) (LinJ.21.0990) and hypoxanthine-guanine phosphoribosyltransferase (**HGPRT**) (LinJ.21.0980) (76), were also significantly (but modestly) increased. These enzymes catalyze the conversion of xanthine and hypoxanthine to XMP

and IMP, respectively, and provide a major route of conversion for all purine

nucleobases to the nucleotide level in these parasites (Figs. 2.2B and 2.3 and

refs. (72, 76, 108, 109)). By 48 h, more changes were evident in the pathway,

with increases observed for the purine nucleobase transporter **LdNT4**

(LinJ.11.0520) (110), and the purine salvage and interconversion enzymes,

adenine phosphoribosyltransferase (**APRT**) (LinJ.26.0120), guanosine

monophosphate reductase (**GMPR**) (LinJ.17.0870), adenylosuccinate synthetase

(**ADSS**) (LinJ.13.1090), one of the two profiled adenosine monophosphate

deaminases (**AMPDA-32**) (LinJ.32.2690), adenosine kinase (**AK**) (LinJ.30.0940),

purine-specific nucleoside hydrolase (**IAGNH**) (LinJ.29.2910), and the 6-

hydroxypurine nucleoside hydrolase (**IGNH**) (LinJ.14.0130) (Figs. 2.2B and 2.3).

By contrast, no significant change, and in one case even decreased abundance,

was observed for guanine deaminase (**GDA**) (LinJ.29.0920), the nonspecific

nucleoside hydrolase (**NH**) (LinJ.18.1570), adenylosuccinate lyase (**ASL**)

(LinJ.04.0440), GMP synthase (**GMPS**) (LinJ.22.0013), adenine aminohydrolase

(**AAH**) (LinJ.35.2200), the alternative AMPDA (**AMPDA-04**) (LinJ.04.0270), and

IMP dehydrogenase (**IMPDH**) (LinJ.19.1590). Although these later abundance

changes within the pathway at 48 h were modest (the majority being ~2-fold or

less) the cumulative effect of these changes would seem to suggest that flux

through the pathway is retooled to favor adenylate nucleotide production (Fig.

2.3). This supposition is supported by the following: that two putative adenylate

kinase orthologs (**ADKB** and **ADKC**) (LinJ.21.1490 and LinJ.36.1410), one of

which (ADKB) has a flagellar location in *Trypanosoma brucei* (111), were

28

significantly upregulated in purine-starved cells, whereas the reciprocal activity within the guanylate branch of the pathway, guanylate kinase (**GK**) (LinJ.33.1150), was decreased at the protein level (Figs. 2.2B and 2.3); that a putative methylthioadenosine phosphorylase (**MTAP**) (LinJ.05.0830) that catalyzes the conversion of methylthioadenosine (**MTA**) to adenine and 5-deoxy-5-(methylthio)ribose-1-phosphate (112) was upregulated, whereas the production of S-adenosylmethionine (**SAM**) from ATP and methionine by SAM synthetase (**SAMSYN**) (LinJ.30.3560) (113, 114) was disfavored (Fig. 2.2C); and that a spectrum of phosphodiesterases (**PDE**) (LinJ.15.1540-50, LinJ.18.1100, and LinJ.04.0030) that liberate AMP, and possibly GMP, from their respective cyclic nucleotides (115-117) were also upregulated at the protein level (Figs. 2.2C and 2.3). Finally, in addition to the other changes in the purine pathway, the formation of deoxyribonucleotides for DNA synthesis, unsurprisingly, also appeared suppressed in growth-arrested, purine-restricted cells, since the amounts of both the large and small subunits of ribonucleotide reductase (LinJ.22.1110, LinJ.27.1970, LinJ.28.0980) (118, 119) were decreased (Figs. 2.2C and 2.3).

Global Proteome Remodeling in Purine-Starved Cells:

We next asked whether other global changes in the proteome could be linked to the observed morphological and metabolic changes observed upon purine withdrawal from the media (52). Proteins that were significantly altered (p-value of ≤ 0.05) by a $\log_2$ abundance ratio of either ≥ 0.5 or ≤ -0.5 (which corresponds to either a 1.4-fold upregulation or more, and a 0.7-fold downregulation or less) in

purine-starved parasites were classified in terms of their biological and metabolic functions (see Fig. 2.4 and Table A.3). A total of 777 proteins were analyzed and 561 were categorized according to their GO category and molecular function, but the remaining 216 were of unknown function and therefore, could not be classified. The large number of unclassified proteins (~28 %) is reflective of the prevalence of hypothetical proteins within the annotated *L. infantum* genome (99).

The earliest changes (6 h) in the proteome predominantly involved the upregulation of transporter proteins, as well as catabolic activities involved in protein and nucleic acid digestion, with the latter category largely populated with digestive activities involved in purine acquisition at the cell surface (Figs. 2.2A and 2.4B and Table A.3). By 12-24 h, however, a diverse array of proteins was significantly upregulated, including proteins involved in intracellular purine interconversion (namely HGPRT and XPRT), carbohydrate metabolism (specifically involved in gluconeogenesis and NADPH production in the oxidative branch of the pentose phosphate pathway), signal transduction, flagella motility and structure, protein folding, and cellular redox response and homeostasis (Fig. 2.4B and Table A.3). Proteome restructuring was also facilitated at 12-24 h by the downregulation of certain cellular constituents (Fig. 2.4C and Table A.3). Predominant amongst the downregulated proteins were ribosome components, as well as other factors involved in protein synthesis, signifying that translation is reduced in purine-starved cells as early as 12 h post purine removal from the medium. Analysis of [^{3}H]-leucine incorporation into the trichloroacetic acid-

precipitable pool of cells starved for purine for 24 h indicated that the rate of incorporation was reduced by ~ 25 % in comparison to cells grown continuously in hypoxanthine (Fig. 2.5), signifying that protein synthesis is downregulated during purine starvation. In contrast, the rate of incorporation of [2-^{14}C]-uracil into the same trichloroacetic acid-precipitable pool was effectively equivalent between purine-starved and purine-replete cells over the same time course (Fig. 2.5). Proteins involved in nucleic acid metabolism were also significantly reduced in purine-starved cells. Specifically those involved in nucleic acid replication, processing, and repair, including ribonucleotide reductase, RNA helicases, and DNA topoisomerases, as well as various DNA and RNA binding proteins, including two universal minicircle sequence binding protein (**UMSBP**) orthologs (LinJ.36.1680 and LinJ.36.1720), which have been implicated in kinetoplast DNA (**kDNA**) replication and mitochondrial and nuclear segregation in trypanosomes (120). Remarkably, very few other metabolic activities were downregulated in purine-starved cells at 12-24 h, but amongst the downregulated activities were proline dehydrogenase (alternatively named proline oxidase) (LinJ.26.1590) and UDP-sugar pyrophosporylase (LinJ.17.1260), which participate in proline catabolism (121) and glycan precursor biosynthesis (122), respectively.

By 48 h the proteome of purine-starved cells was extensively changed. Although many of the changes that were detected were subtle, involving changes of two-fold or less (Fig. 2.1), many of the altered proteins could be grouped to either the same metabolic pathway or were similar in their molecular function (Fig. 2.4 and Table A.3), denoting, perhaps, a significant role for these biological

processes in the adaptive response to purine stress. Proteins involved in degradative or catabolic processes were generally upregulated within the proteome of growth-arrested, purine-starved cells, including those proteins involved in fatty acid ß-oxidation, the catabolism and interconversion of amino acids, and protein and nucleic acid degradation (Fig. 2.4B and Table A.3). In contrast, factors involved in protein and DNA synthesis, both of which are ATP-consuming reactions, remained substantially downregulated (Fig. 2.4C and Table A.3).

Amongst the other proteome constituents upregulated, proteins involved in cell redox homeostasis and oxidant defense, intracellular trafficking, and amino acid interconversion and degradation were prevalent. However, by far the predominant functional category of upregulated proteins at 48 h was that of carbohydrate metabolism, with 42 candidates out of 360 upregulated proteins with an assigned function allocated to this category (Fig. 2.4 and Table A.3). Specifically, those proteins associated with glycolysis and gluconeogenesis, the pentose phosphate pathway (Fig. A.1), and the tricarboxylic acid (**TCA**) cycle, were all augmented. Given that many of the components of these pathways are sequestered in glycosomes in *Leishmania*, peroxisome-like organelles (6-8), we compared the protein abundance data at 6-48 h for all known and *in silico* predicted glycosomal proteins (123) to determine whether a reduced turnover of this organelle could account for the observed protein upregulation (Table A.4). However, the data revealed little consensus at each time point, suggesting that

changes in glycosome turnover likely do not contribute towards proteome remodeling during purine starvation.

Since proteome profiling of purine-starved *versus* purine-replete cells revealed that multiple factors involved in oxidant defense were upregulated at the 24 and 48 h time points (Table A.3), we also investigated whether purine-starved cells were under increased duress from reactive oxygen species (**ROS**) by employing the cell-permeant ROS indicator 2',7'-dichlorodihydrofluorescein diacetate (**H$_2$DCFDA**). While cells starved for purine for 24, 48, and 72 h did not appear to harbor increased ROS (Fig. 2.6), incubation of these starved cells in the presence of increasing concentrations of menadione (2.5-10 µM) revealed an enhanced capacity to deal with increased levels of ROS, and consequently, oxidative stress, which was considerably greater than that observed in cells continuously grown in hypoxanthine (Fig. 2.6). Moreover, the antioxidant capacity of cells purine-starved for 24, 48, and 72 h was progressively amplified. A similar phenomenon was also observed with cells starved for purine for 24 and 48 h and incubated in the presence of either 2 or 4 mM H$_2$O$_2$ (Fig. A.2).

Within those proteins classified as participating in the catabolism and interconversion of amino acids (Table A.3), one pathway appeared particularly represented, namely that of proline biosynthesis and interconversion (Fig. A.3). Proteins encoding for a putative glutamate 5-kinase (LinJ.26.2740), pyrroline-5-carboxylate synthetase-like protein (LinJ.32.3340), and pyrroline-5-carboxylate reductase (LinJ.13.1420), that all participate in proline biosynthesis were modestly upregulated at 48 h, whilst proline dehydrogenase (LinJ.26.1590),

33

which is involved in proline catabolism, was significantly reduced at 12, 24 and 48 h post purine removal (Table A.3, and Fig. A.3). Proline is a key stress response metabolite in a number of organisms and, although its precise role remains rather enigmatic, it has been shown to enhance cell survival during environmental stress (124-128). Significantly, in *T. cruzi*, a parasite highly related to *Leishmania*, proline has emerged as an important nutrient in combating environmental stress (125) and is vital during metacyclogenesis, a process that has also been linked with nutrient stress (70, 129). Thus, we investigated whether proline levels were also augmented in *L. donovani* during purine starvation. A marked increase in intracellular proline was observed in purine-starved cells at 24 h and 48 h (9.7- and 5.7-fold, respectively) in comparison to those cells grown in hypoxanthine (Fig. 2.7). These data confirm the veracity of the proteomics results, and significantly, suggest that small, but cumulative changes at the protein level for multiple enzymes within the same pathway can lead to a significant modulation at the metabolite level.

Proteome remodeling, particularly during differentiation of the procyclic or insect stage of *Leishmania* to the mammalian infectious amastigote form, has also been described through autophagy (30, 68, 130, 131). Whether autophagy is also involved in proteome remodeling during purine deprivation is unclear. While purine-starved cells by 48 h had substantially boosted protein digestive activities, including cysteine peptidase A (LinJ.19.1460), which has also been implicated in autophagosome degradation (68), most of the described canonical autophagic machinery (68, 132, 133) was either not upregulated or could not be

profiled within the proteomics dataset (Table A.1). However, vacuolar protein

sorting-associated protein 4 (**VPS4**, LinJ.29.2610) (131) was upregulated 2-fold

by 48 h post purine removal from the medium, an activity previously shown to be

important for cytosolic autophagosome processing in *Leishmania* (131). Perhaps

more significantly, VPS4 in *Leishmania* has also been shown to be important for

survival during nutrient depletion, as well as for the differentiation of

promastigotes during metacyclogenesis (131). *De novo* phospholipid

biosynthesis has also been critically implicated in autophagosome formation

during autophagy (134), since phospholipids are core components of the

autophagosome membrane bilayer, and phosphatidylethanolamine (**PE**), in

particular, also functions to tether Autophagy-related protein (**Atg8**) to the

autophagosome membrane, a crucial step in autophagosome formation and

expansion (133-135). At 48 h in purine-starved cells the proteomics data

suggested that PE formation is favored, since both ethanolamine-phosphate

cytidylyltransferase (LinJ.32.0940) and sphingosine 1-phosphate lyase

(LinJ.30.2360) are augmented (Fig. A.4 and Table A.3). Note that the

degradation of sphingolipids by sphingosine 1-phosphate lyase provides the

major route for phosphoethanolamine synthesis in *Leishmania* (136). In addition,

the synthesis of the core phospholipid phosphatidylcholine from PE also

appeared enhanced, since phosphatidylethanolamine-methyltransferase-like

protein levels (LinJ.31.3250 and LinJ.31.2360) were also elevated (Fig. A.4 and

Table A.3).

Reconfiguration of the proteome during purine stress requires the removal of existing molecules from various cellular compartments, as well as the redistribution of new molecules. From the proteomics data, it appeared that the capacity for intracellular transport was greatly enhanced by 48 h post purine removal from the medium (Fig. 2.4 and Table A.3). Amongst the upregulated proteins at 48 h were a number of factors involved in intracellular vesicle formation, fusion, and exocytosis, as well as an array of kinesins and dyneins that likely facilitate the movement of these vesicles along the microtubular network. Notably, two polypeptides encoding kinesin K39 (LinJ.14.1600 and LinJ.14.1190) and a putative kinesin (LinJ.16.1550) were not amongst these upregulated molecular motors at 48 h, although LinJ.14.1190 and LinJ.16.1550 were initially upregulated at 6 h. By contrast, these kinesins were significantly downregulated at 24-48 h and, given that kinesin K39 (LinJ.14.1190), at least, is apparently enriched at the posterior poles of the cortical cytoskeleton in a cell cycle-dependent manner during cytokinesis (137), their downregulation would seem to correlate with the arrest in growth of the purine-starved cells.

Analysis of the Molecular Mechanisms Underlying Proteome Restructuring
Whole Transcriptome Analysis of Purine-Starved and Purine-Replete Cells:
Leishmania exhibit unusual mechanisms of gene regulation. The majority of the genome is constitutively transcribed by RNA polymerase II as long polycistrons (pre-mRNAs that contain multiple coding sequences) that are *trans*-spliced into mature mRNAs by the coordinated addition of a 5' capped 39 ribonucleotide

splice leader (**SL**) to the 5' untranslated region (**UTR**) and a polyadenylate tail to the 3' UTR of each mRNA (19, 87). Thus, in these parasites, classical transcriptional regulation is absent; instead, changes in protein abundance can arise from changes at the mRNA level, involving alterations in mRNA abundance, *trans*-splicing, and polyadenylation, or from changes at the translational or post-translational level. As a first step towards understanding the molecular mechanisms underlying proteome modification upon purine restriction, Whole Transcriptome Shotgun Sequencing (**RNA-seq**) was undertaken to quantitate mRNA abundance differences between purine-starved and purine-replete cells. Since the RNA-seq libraries were constructed using an SL-specific primer for 2nd strand cDNA synthesis (see *Materials and Methods*), this also enabled us to determine whether alternative *trans*-splice sites were used under conditions of purine restriction (89, 90, 92-95, 138). A total of 53,249,393 and 27,430,972 reads were gathered from the purine-replete and purine-starved samples, respectively. (The SL RNA-Seq data from this study have been submitted to the NCBI Gene Expression Omnibus (**GEO**) database at http://www.ncbi.nlm.nih.gov/geo/ under the accession no. GSE48394). These reads were mapped to 8185 genes of which 8075 had at least 100 reads across both conditions and accounted for ~96 % coverage within the reference *L. infantum* genome (99) (Table A.5 and Fig. 2.8). The median number of reads from purine-replete cells was 2,522 and from purine-starved cells was 1,132. After normalization of the data (see *Materials and Methods*), the number of mRNAs that were changed in abundance in purine-starved cells by two-fold or

more (log$_2$ expression ratio ≥1 or ≤ -1) at 24 h was 523 (Table S5 and Fig. 8). Of

these regulated mRNAs, 324 were upregulated and 199 were downregulated.

However, in general no substantial changes in the primary *trans*-splice sites used

for each mRNA were observed between purine-replete and purine-starved cells

(splice site data available at http://www.ncbi.nlm.nih.gov/geo/ under the

accession no. GSE48394), indicating that where differences in mRNA

abundance were observed they were unlikely due to differential mRNA

processing in these organisms. Of the regulated mRNAs, 13 were upregulated by

4-fold or more, and significantly amongst these were the mRNAs for two cell

surface purine activities *LdNT3* and *MAP2-36*, which were upregulated by 6.5

and 4.5-fold, respectively. A comparison of the mRNA levels for the key purine

pathway components that were regulated at the protein level at 24 and 48 h post

purine restriction (Fig. A.5 and Table 2.1) indicated that the fold-changes at the

mRNA and protein level for the most part tracked together, although there were

two notable exceptions (LdNT1 and LdNT2) where changes at the mRNA level

correlated poorly with the fold changes at the protein level. These nucleoside

transporters were highly (6- to 16-fold) upregulated at the protein level at 24 and

48 h, but showed only a modest change at the mRNA level (*LdNT1*) or an

apparent decrease (*LdNT2*) at 24 h. Comparison of the SL RNA-seq data to the

entire proteome datasets at 24 and 48 h showed considerable discordance

between the changes manifested at the protein and mRNA level in purine-

starved cells (Fig. 2.9 and Table A.6). Specifically, there were a number of

downregulated proteins where the corresponding mRNA was elevated in

abundance (Fig. 2.9 A and B, upper left quadrant and Table A.6) and

upregulated proteins where the corresponding mRNA was downregulated (Fig.

2.9 A and B, lower right quadrant). These correlations were consistent between

the 229 mRNA and protein pairs present in the 24 and 48 h proteome data,

where only one protein and mRNA pair (a putative ethanolamine-phosphate

cytidylyltransferase, LinJ.32.0940) showed a decreased mRNA and protein

abundance at 24 h but increased protein abundance at 48 h (see Table A.6 for

the matched protein and mRNA data). These data suggest that, in addition to

changes in mRNA abundance, proteome remodeling in response to purine stress

is likely orchestrated by translational and post-translational mechanisms.

Establishing Whether Translational Mechanisms Lead to the Augmentation

of Select Candidates within the Purine-Starved Proteome:

RNA-seq is particularly suited for the quantitative analysis of transcript

expression levels due to the massive amounts of sequence data and the number

of reads that can be generated for each mRNA (88, 89, 91-95), especially in a

genome as small as that of *L. donovani* (15, 99). Nevertheless, it was still

important to confirm the fold-changes observed at the mRNA level in purine-

starved cells for some of the most regulated mRNAs and proteins identified in

these analyses. Thus, the levels for those mRNAs described in Table 2.1 were

quantified from purine-replete and purine-starved cells at 24 h by quantitative

reverse transcriptase PCR (**qRT-PCR**). In general, the mRNA abundance

changes measured by SL RNA-seq or qRT-PCR at 24 h (Table 2.1) were in good

agreement, confirming the utility of RNA-seq for profiling mRNA abundance changes during purine starvation. The results were also comparable with our previous qRT-PCR analyses that established mRNA levels at 48 h for the purine permeases and key purine pathway components between purine-starved and purine-replete cells (52). There were, however, a few notable discrepancies between the qRT-PCR and SL RNA-seq data. In particular, the mRNA level for the La RNA binding protein (LinJ.21.0600) was significantly increased in purine-starved cells when measured by SL RNA-seq, but was not appreciably elevated when measured by qRT-PCR. While the cause of this discrepancy likely reflects the inherent differences between the two methodologies, it is noteworthy that the abundance of the La RNA binding protein was not augmented, but rather was decreased in purine-starved cells at the proteome level.

In most cases, the abundance changes for those subset of proteins listed in Table 2.1, as determined by proteomic analysis, corresponded closely to the changes in mRNA abundance determined by the SL RNA-seq and qRT-PCR analyses, implying that the regulation of these proteins during purine stress was predominantly mediated at the level of mRNA abundance. In contrast, the abundance of LdNT1.1 and LdNT2 proteins was significantly more augmented than the changes wrought at the mRNA level, where the increase was modest for *LdNT1.1* mRNA and non-existent for *LdNT2* mRNA, intimating that regulation occurs via translational and/or post-translational mechanisms during purine stress. Similarly, the incremental increase observed for LdNT3 protein in our proteomics analysis between 24-48 h time points was not reflected by our

combined qRT-PCR analysis of *LdNT3* mRNA abundance at these same time points (Table 2.1; ref. (52)), suggestive of an additional level of regulation at either the translational or post-translational level.

To investigate the contribution of translational mechanisms to proteome remodeling during purine stress, we used a novel Dual-Luciferase reporter system in which the firefly luciferase gene (**Fluc**) (KF035118) was integrated in place of the coding sequence of one allelic copy of the gene of interest in a manner such that the native 5' and 3' UTRs remained intact. This approach conserves the sites of *trans*-splicing and polyadenylation, as well as any potential *cis*-acting elements in the UTRs of each mRNA, which is of particular importance in *Leishmania* and other kinetoplastid parasites where it has been demonstrated that regulation of mRNA abundance and translation is often mediated by *cis*-acting elements encoded in the 5' and/or 3' UTRs (139-144). A *Renilla* luciferase gene (**Rluc**) (KF035116) integrated in place of one copy of *L. donovani* UMP synthase (**UMPS**) (LinJ.16.0560) (145), also referred to as orotidine-5-phosphate decarboxylase/orotate phosphoribosyltransferase, was used as a control to normalize the luciferase activity between experiments. Note that from our current and previous qRT-PCR analyses, western analyses, as well as from the SL RNA-seq and proteomics data described here, *UMPS* mRNA and protein levels do not appear to change significantly in response to purine stress (Tables 2.1, A.1, and A.5, and ref. (52)).

For each cell line with an integrated *Fluc* construct, both Fluc activity and *Fluc* mRNA levels were assessed to distinguish the contributions of mRNA

abundance and translational mechanisms to reporter regulation in response to purine stress. The mRNA and protein abundance of the purine nucleobase transporter LdNT4 was not substantially changed following 24 h purine starvation (Table 2.1), and this was directly mirrored by the activity and mRNA abundance of the *Fluc* reporter integrated at the *LdNT4* locus (Table 2.2), indicating that *Fluc* by itself does not affect mRNA abundance or confer a response to purine stress. In contrast to LdNT4, the change in mRNA abundance for the *Fluc* reporter arising from its integration into the locus of corresponding purine-responsive genes listed in Table 2.2 was two- to four-fold lower than the changes observed for the native mRNA, suggesting that the coding sequence (**CDS**) of these purine-responsive genes contributes to the regulation of mRNA abundance. The change in Fluc activity for those reporters integrated in place of one gene copy of *3' NT/NU-12*, *3' NT/NU-31*, and *MAP2-36*, which encode some of the most upregulated proteins detected within the proteome of purine-starved cells (Fig 2.2A), was commensurate with the change (~1.5 to 2-fold) at the corresponding *Fluc* mRNA level (Table 2). This concordance was also observed for the native locus, where the magnitude of change for the corresponding mRNA and protein was essentially equivalent. These data support a model whereby the regulation of these genes is primarily manifested at the mRNA level, and is bestowed, at least in part, through sequences in the 5' or 3' UTR. For the purine permeases (LdNT1.1, LdNT2, and LdNT3) and oxidoreductase (LinJ.29.0260), despite only modest changes, and in the case of LdNT2 even decreased abundance for the *Fluc* reporter mRNA, the increase in Fluc activity was significantly higher (~2.5 to

12-fold), indicating that native 5' and 3' UTRs are involved in the augmentation of their translation in response to purine stress. While translational and/or post-translational regulation was predicted for the purine permeases based on the discordance between mRNA and protein abundance data (see Table 2.1), the absence of protein abundance data for the oxidoreductase made such a prediction impossible. This highlights the utility of the Dual-Luciferase system for distinguishing regulatory mechanisms for candidates in which protein abundance data is either lacking or scant. Overall, the combination of proteomics, SL RNA-seq, and Dual-Luciferase reporter data revealed that regulation of gene expression in response to purine stress for several of the most upregulated proteins occurs at the level of mRNA abundance (3'NT/NU-12, 3'NT/NU-31, and MAP2-36), translation (LdNT2), or both (LdNT1.1, LdNT3, and oxidoreductase). It is also likely that post-translational mechanisms are also involved in purine stress-induced proteome remodeling, but this prospect has yet to be directly investigated.

Since the purine permeases LdNT1-3, the cell surface 3'NT/NUs, and MAP2-36 are some of the earliest regulated proteins detected within the global proteome (Fig. 2.2A), the activity arising from the *Fluc* reporter integrated at each of these loci was compared between purine-starved versus purine-replete cells at 6 h post purine removal from the medium (Table 2.3). For each of these candidates, the mechanisms of regulation at 6 h and 24 h were identical (Tables 2.2 and 2.3), demonstrating that regulatory mechanisms affecting mRNA abundance and translation are invoked early in the response to purine stress.

Interestingly, the mRNA level of the *Fluc* reporter integrated at the *LdNT3* locus was reduced over 2-fold at 6 h but increases 2.5-fold by 24 h of purine stress, implying the early destabilization of the *Fluc* mRNA is later reversed by a mechanism that stabilizes the mRNA. This biphasic temporal response was not observed for the wild type *LdNT3* allele, suggesting a role for the *LdNT3* CDS in protecting *LdNT3* mRNA from the general decrease in total RNA abundance that accompanies purine starvation (8). In contrast, the expression of the oxidoreductase, which was increased at both the mRNA and translational levels after 24 h purine stress, was essentially unchanged after 6 h.

DISCUSSION

Proteome Analyses Offer Insight into Metabolome Reconfiguration During Purine Stress

We undertook a large-scale global proteome profiling experiment to identify how *L. donovani* promastigotes reorganize their proteome to deal with purine stress, a type of nutrient stress. The label-free approach of AMT tag is highly suited to the analysis of multiple biological replicates (97), which enabled even subtle abundance changes between purine-starved and purine-replete cells to be detected reproducibly and with a high degree of confidence. It is noteworthy that for those proteins where fold changes had previously been measured by western analyses (52) (i.e., for the purine permeases and various phosphoribosyltransferases), or by spectral counting in a separate comparative shotgun proteomics experiment (see Table A.2), the comparative AMT tag data was in good agreement, emphasizing the accuracy of this approach in predicting even small protein abundance changes. Changes within the parasite proteome followed a chronological order with the first response primarily focused on enhancing purine acquisition at the cell surface, but this was succeeded by a broader transformation of the parasite proteome upon prolonged purine deprivation. With chronic purine stress, progressively more alterations within the parasite proteome were apparent. Indeed, by 48 h, approximately one-third of the proteins that could be detected by the AMT tag method within the parasite proteome were significantly changed in abundance. The challenge of future

explorations will be to identify changes induced upon purine stress for those lower abundance proteins not easily detected by current methods used to profile the whole cellular proteome. Nevertheless, the current results have provided significant insight into proteome changes, and in some cases metabolic alterations, within purine-starved cells, and by extrapolating these findings to the entire annotated parasite proteome it is clear that the adaptive response to purine stress is both extensive and multifaceted in nature.

Remarkably, despite being in quiescence, the metabolism of purine-starved cells appears to remain robust. Measurement of the reduction of resazurin to resorufin, a reaction which occurs primarily in the mitochondria of most cells and is essentially a measure of aerobic respiration and mitochondrial metabolism (146-148), indicated that even cells purine-starved for two weeks were essentially as metabolically active as those continuously grown in purine (Fig. A.6). Within the 48 h proteome, more than 78% of the proteins that were significantly changed in abundance were upregulated. In these chronically purine-deprived, quiescent cells, the proteomics data, supported by the leucine incorporation data (Fig. 2.5) and our previous cell cycle data, which showed an arrest in growth in G_1 phase (52), indicated that there was a decrease in energy-intensive biosynthetic pathways, such as DNA and protein synthesis, and the catabolism of proteins and nucleic acids into their precursor molecules appeared favored. This is likely a reflection of the differing metabolic needs of these non-dividing cells, which are unencumbered of the requirement to replicate nuclear and cellular material for proliferation. Instead, within these cells proteins involved

46

in digestive processes were generally upregulated, and in addition to promoting proteome remodeling, these factors would likely serve to facilitate the disposal of spent and potentially damaged macromolecules that would normally be dispersed during cell segregation.

The response to prolonged purine stress is complex and the proteomics data revealed upregulation of numerous proteins involved in cellular activities spanning amino acid and lipid metabolism, cell redox response, intracellular trafficking, and protein interaction. One pathway that was abundantly represented in the altered proteome of purine-starved cells was that of central carbon metabolism. By both AMT tag analysis and spectral counting, participants in glycolysis, gluconeogenesis, the pentose phosphate pathway, and TCA cycle were all observed to be upregulated (Tables A.1-3). Most of the changes were subtle (two-fold or less) and what (if any) impact these changes exert on flux through these pathways cannot, *a priori*, be predicted from the steady state levels revealed by the proteome data. However, it is conceivable that the increase observed in glycolytic and TCA cycle components in purine-starved cells serves to compensate for dwindling ATP levels, the reduction of which we have recently confirmed (Martin *et al.*, unpublished). On the other hand, the observed increase in the levels of the gluconeogenic enzymes, phosphoenolpyruvate carboxykinase (LinJ.27.1710), pyruvate diphosphate kinase (LinJ.11.1000), and fructose-1,6-bisphosphatase (LinJ.04.1170), could also signify a boost in the synthesis of glucose-6-phosphate from oxaloacetate or pyruvate, which, although resulting in a net loss of ATP currency in the cell, could

also favor flux through the pentose phosphate pathway. The pentose phosphate pathway has been critically implicated in the response to oxidative stress in *Leishmania* and other organisms (149, 150). Significantly, enzymes within the oxidative branch of the pathway that irreversibly catalyze the conversion of glucose-6-phosphate to ribulose-5-phosphate, providing a crucial mechanism for NADPH regeneration, were upregulated at the protein level, as were those enzymes responsible for the recycling of ribulose-5-phosphate back to glucose-6-phosphate (Fig. A.1). The importance of cellular reductive energy in the form of NADPH in purine-starved cells may also be underscored by the fact that two other lesser-known mechanisms for generating NADPH, NADP-linked malic enzyme (LinJ.24.0780) and isocitrate dehydrogenase (LinJ.10.0310), were also upregulated at the protein level in these parasites. It is notable that the changes recorded for central carbon metabolism in *Leishmania* during purine stress have also been described in response to assorted stresses in a variety of other organisms including bacteria, protozoa, yeast, nematodes, and mammalian cells (150-154), underscoring the importance of these pathways in the adaptive mechanism to microenvironmental stress.

Much of the evidence points to purine-starved cells being under greater oxidative stress during purine starvation. Proteins associated with protein folding and quality control, such as heat shock proteins, peptidyl-prolyl cis-trans isomerases, and calreticulin (LinJ.31.2670) were all upregulated during purine stress, as were those proteins involved in cell redox homeostasis. Moreover, the antioxidant capacity of purine-starved cells was significantly and progressively

improved in comparison to that of purine-replete cells (Figs. 2.6 and A.2). In particular, enzymes involved in first-line oxidant defense such as the superoxide dismutases (LinJ.32.1910 and LinJ.08.0300) and ascorbate-dependent peroxidase (LinJ.34.0070) were all augmented at the protein level, as were those enzymes γ-glutamylcysteine synthetase (LinJ.18.1660), ornithine decarboxylase (LinJ.12.0100), and spermidine synthase (LinJ.04.0570) that participate in the biosynthesis of trypanothione, a low molecular weight dithiol that acts as a glutathione surrogate in these parasites (155, 156). Most significantly, trypanothione reductase (LinJ.05.0350), an NADPH-linked activity solely responsible for trypanothione reduction, was upregulated, along with tryparedoxin (LinJ.29.1250), a glutaredoxin-like protein, and peroxiredoxin (LinJ.29.1250), which are all key constituents of trypanothione redox metabolism (157). Recently, the upregulation of these proteins, along with components of the pentose phosphate pathway and gluconeogenesis, was also implicated in the response to oxidative and nitrosative stress in *L. donovani* (158), suggesting that common stress response pathways are likely enacted regardless of the nature of the particular environmental stress.

Even though the majority of the proteome changes detected were modest, involving changes of two-fold or less (Fig. 2.1), many could be grouped to either the same metabolic pathway or were similar in their molecular function (Figs. 2.4, A.1, A.3-A.4 and Table A.3), denoting, perhaps, a significant role for these biological processes in acclimatization to purine stress. One pathway that exhibited multiple, but small changes at the protein level was that of proline

biosynthesis and interconversion, where the components of the pathway were increased or decreased by three-fold or less in a manner predicted to favor proline accumulation in purine-starved parasites (Fig. A.3 and Tables A.1 and A.3). Upon examination of intracellular free proline levels in purine-starved *versus* purine-replete cells, a significant increase at both 24 and 48 h was observed (Fig. 2.7). While these data support our proteomics findings, they also provide compelling evidence that small changes in the levels of multiple proteins within the same pathway can lead to significant metabolic alterations. Thus, we conjecture that the effect of these cumulative, subtle changes in multiple pathways might confer a metabolic flexibility on purine-starved parasites, enabling their rapid adaptation and response to fluctuations within the host nutritional and physiological environment.

Proteome Restructuring is Achieved by a Complex Assortment of Mechanisms

In addition to identifying the adaptive changes in the purine-starved cell proteome, it was also important to investigate the molecular mechanisms underlying proteome restructuring. Canonical regulation of the transcriptome through promoters and transcriptional enhancers is absent in these parasites, and instead, kinetoplastids rely on post-transcriptional regulatory mechanisms, many of which are still being defined within these parasites (19, 21, 87). To survey the changes in the parasite global transcriptome upon the induction of purine stress, we used the powerful method of RNA-seq to measure the fold

changes at the mRNA level and compared them with those quantified at the protein level. Significantly, there was a high degree of discordance between the mRNA and protein abundance data, and the results signified the complexity of proteome remodeling that is realized by a diverse assortment of mechanisms at the mRNA, translational, and post-translational level. For a select group of candidates, the role of 5' and 3' UTRs in directing changes produced at the translational level were distinguished from those at the mRNA level using a Dual-Luciferase reporter strategy, where one copy of the candidate gene was replaced with a *Fluc* reporter. While regulatory mechanisms could be ascribed for many of the candidates, it was also apparent that their regulation is complex and is achieved at multiple post-transcriptional levels. For example, the purine permeases LdNT1 and LdNT3 showed regulation at both the mRNA and translational level, while LdNT2, another purine transporter, was only regulated translationally. In the case of LdNT2, our previous work demonstrated that expression of GFP-tagged LdNT2 from an episome lacking the cognate *LdNT2* UTRs was upregulated 10-fold in response to purine starvation for 72 h, suggesting additional mechanisms involving post-translational stabilization of LdNT2 protein or perhaps a regulatory role for the *LdNT2* CDS (52). The complexity of post-transcriptional regulation invoked during purine starvation is also illustrated by the differing responses for those mRNAs arising from various *Fluc* integrations (Table 2.2), where the fold changes in mRNA abundance were consistently lower than those for the corresponding wild type allele, with the exception of LdNT4, which is not upregulated after 24 h of purine starvation.

Thus, it is likely that both the UTRs and the CDS of those purine responsive candidates described in Table 2.2 contribute to regulation. Indeed, modulation of mRNA levels by *cis*-acting regulatory elements encoded within various CDSs has been demonstrated in the related kinetoplastids *T. brucei* (159) and *T. cruzi* (160), and for numerous mammalian mRNAs (161). The discrepancy in mRNA abundance changes between *Fluc* and the corresponding allele may also be a reflection of the differences in the intracellular location of mRNA translation. Endoplasmic reticulum association has been shown to increase mRNA stability (162) and, under conditions of cellular stress, protect mRNAs from incorporation into stress granules, thus preserving their translational capacity (163), and potentially protecting the mRNA from degradation through association with processing bodies or P-bodies. All but one of the genes, that for oxidoreductase, examined *via* the Dual-Luciferase System (Table 2.2) encode membrane proteins whose obligatory translation at the ER could facilitate mRNA stabilization. In contrast, mRNAs from alleles in which a membrane protein CDS was replaced by *Fluc* (which encodes for a soluble protein lacking transmembrane domains) are likely translated in the cytosol and may not have access to ER-associated factors that protect specific mRNAs from the general decrease in cellular RNA content observed in response to purine stress (52).

In summary, it is highly probable that more complex regulatory mechanisms than could be uncovered here contribute to the dynamic changes in the proteome, including changes in mRNA subcellular location (*e.g.* stress granules, P-bodies, or ER association) that alter interactions with the translation

machinery and other *trans*-acting factors, and post-translation modifications that enhance or reduce protein stability. A broader survey of the post-transcriptional regulatory mechanisms for the other candidates identified in our proteomic screen will likely illuminate some of these mechanisms by identifying common regulatory *cis*-acting sequences and *trans*-acting factors involved in the coordinated and temporal response to purine stress.

Purine Stress and Parasite Differentiation

Previously, both nutrient depletion and environmental stressors such as decreased pH, increased temperature, and exposure to antimonial drugs have been observed to trigger parasite differentiation (70, 164-166), and recently an intriguing link between adenosine depletion and the induction of metacyclogenesis has also been proposed (67). Although we cannot rule out the possibility that some of the temporal proteome changes that we detected upon purine stress are due to the induction of parasite differentiation, it seems highly unlikely that the remodeling of those pathways involved in purine capture, salvage, and interconversion, is due to parasite differentiation. Evaluation of those mRNAs known to be increased in metacyclic and differentiating parasites by SL RNA-seq (Table A.5) or by qRT-PCR (Table 2.1), such as *SHERP* (LinJ.23.1210, LinJ.23.1230 and refs. (166, 167)), *A2* (LinJ.22.0670 and refs. (164, 168)), and *META1* (LinJ.17.0990 and ref. (169)), exhibited only a minor increase for *SHERP* (Table 2.1 and Table A.5) and even a decrease for *A2* (Table A.5), although the *META1* mRNA by SL RNA-seq showed an increase of

~2-fold (Table A.5). Purine stress appears to induce a pronounced elongation of the *L. donovani* cell body (52) that is distinctly different than the morphological changes ascribed to metacyclic parasites (170), although the morphology is similar to that described for the nectomonad stage, one of the earliest differentiating stages within the anterior abdominal mid-gut of the sand fly (171). Thus, it is not inconceivable that some of the stress response pathways triggered during purine starvation are also induced during the early stages of parasite differentiation. Indeed, some of the changes chronicled in this manuscript have also been described during the early stages of differentiation in culture when late log phase *L. donovani* promastigotes were induced to convert to amastigotes, the mammalian infectious life cycle form, by temperature and pH shift of the culture conditions (30, 164).

In summary, this manuscript provides a detailed examination of *L. donovani* proteome dynamics upon the induction of purine starvation, a type of nutrient stress. Moreover, the data revealed that a complex assortment of molecular mechanisms conspire to induce an extensive reprogramming of the parasite proteome, which in some cases could be extrapolated to the parasite metabolome, and enable parasite survival even under conditions of extreme purine scarcity. In large part, this is achieved by the rebalancing of intracellular ATP expenditure, signified by the apparent decrease in energy intensive processes such as protein and DNA synthesis, and consistent with the observed quiescence phenotype. Remarkably, despite being in quiescence, purine-starved

cells remained metabolically active, augmenting several pathways, many of which likely are part of a common stress response mechanism in these parasites (30, 158).

MATERIALS AND METHODS

Cell Lines and Cultivation

The visceralizing *L. donovani* strain 1S2D (172) clonal derivative LdBob (173) was employed in these studies. Wild type LdBob promastigotes were routinely cultured at 26 °C in 5% CO_2 in modified Dulbecco's Modified Eagle-Leishmania (**DME-L**) medium (51) that lacked bovine serum albumin and was supplemented with 5% serum plus (Sigma-Aldrich), 1 mM glutamine, 1X RPMI 1640 vitamin mix, 10 µM folate, hemin (2 ml from a 500X stock containing 2.5 g l^{-1}), and 100 µM hypoxanthine as a purine source. To elicit purine starvation conditions, cells were grown in DME-L lacking hypoxanthine but with all other media components present.

Treatment of Cells for Downstream Proteomic Analyses

Logarithmically growing cells were seeded at 2 x 10^6 cells ml^{-1} in 5 roller bottles corresponding to 5 individual biological replicates and grown for 24 h prior to the start of purine starvation in complete DME-L supplemented with 100 µM hypoxanthine. At t=0 h, 2 x 10^8 cells from each replicate were processed for downstream proteomic analyses as detailed below. The remaining cells in each replicate were prepared in parallel as described. Briefly, cells were washed twice in DME-L medium lacking purines and resuspended at 2 x 10^6 cells ml^{-1} in either purine-replete media (DME-L supplemented with 100 µM hypoxanthine) or in purine-deplete media (DME-L lacking hypoxanthine). At time points

corresponding to 6, 12, 24, and 48 h after the initiation of purine starvation, 2 x 10^8 cells were removed from both the purine-replete and purine-starved cultures and processed for downstream proteomic analyses as described below. Note that the densities for the cells growing in purine-replete media were adjusted every 24 h to ensure that they remained in the log phase of growth and thus, any differences identified between the proteomes of purine-starved and purine-replete cells were due solely to the effects of purine depletion.

Sample Preparation for Proteomic Analyses

The reserved cells for proteomic analyses, 45 samples in total, consisting of 5 biological replicates per condition (purine-starved or purine-replete) and at time points of 0 h (purine-replete only) and 6, 12, 24, and 48 h (purine-starved and purine-replete), were washed twice in 50 ml of Dulbecco's Phosphate Buffered Saline (D-PBS) to remove media contaminants, resuspended in 500 µl of D-PBS, and transferred to a microcentrifuge tube. Cells were pelleted at 1500 x *g*, the supernatant removed and the cell pellets put on ice. Each cell pellet was resuspended in 500 µl of complete lysis buffer (100 mM ammonium carbonate pH 7.8 containing 8 M urea) and incubated on ice for 10 min. After 10 min of incubation, a small aliquot of the cell lysate was reserved for analysis with the Micro BCA Protein Assay kit (Thermo Scientific) to determine protein concentration, and the rest of the lysate flash-frozen in liquid N_2 and stored at -80 $^{\circ}$C until ready for downstream proteomic analysis.

Protein Extraction and Digestion

For each of the 45 samples, 300 μg of protein extract was reduced with 5 mM

dithiothreitol for 1 h at 37 °C, and subsequently, alkylated with 15 mM

iodoacetamide (**IAA**) for 2 h at 25 °C in the dark. Each sample was then diluted

10-fold with 50 mM NH_4HCO_3 (pH 8) containing 1 mM $CaCl_2$ and digested for 3 h

at 37 °C with trypsin, added at a 1:50 trypsin to protein ratio. Samples were

acidified with trifluoroacetic acid prior to desalting with a Discovery-C18 SPE

cartridge (SUPELCO). Aliquots of peptides (20 μg) from each of the purine-

replete or the purine-starved digests were pooled into two samples (purine-

replete versus purine-starved). Peptides from each pooled sample at a

concentration of 350 μg were fractionated using a high pH (pH 10) reversed-

phase liquid chromatography strategy, which have been previously described

(174), and collected across 96 fractions, which were then concatenated into

groups of 4 to yield 24 fractions. The fractions were dried in a Speed-Vac to

remove the solvent and resuspended in 170 μl of Nanopure water.

Reversed-phase Capillary LC-MS/MS and LC-MS Analyses

LC-MS/MS analysis of the pooled fractions described above was used to

generate a reference database of peptide markers defined by accurate masses

and elution times, i.e., AMT tag (described in the paragraph below and refs. (96-

98)). The AMT tag database then served as a comprehensive "look up" table for

the subsequent higher throughput LC-MS analyses described below. For the

AMT tag database generation, each of the 24 fractions corresponding to the

purine-replete and purine-starved cells were analyzed using a 4-column, custom-built, capillary LC system coupled online via an in-house manufactured electrospray ionization (**ESI**) interface to an LTQ-Orbitrap mass spectrometer (Thermo Scientific, San Jose, CA) (175). To identify the eluting peptides, the LTQ-Orbitrap instrument was operated in a data-dependent MS/MS mode for the top six abundant precursor ions in each full MS scan. Following the AMT tag database generation, LC-MS analyses with full MS scan (400-2,000 *m/z* range) were performed on the 45 unfractionated purine-replete and purine-starved peptide samples described above to generate quantitative data. For this, samples were analyzed in random order using the same chromatographic and electrospray conditions as described for the LC-MS/MS analyses except that the LC system was interfaced to an Exactive Mass Spectrometer (Thermo Scientific).

Development of an AMT Tag Database for *L. donovani*

MS/MS data were searched against a decoy protein database consisting of forward and reversed sequences entries extracted from a May 18, 2010 download from the Wellcome Trust Sanger Institute (http://www.sanger.ac.uk/) of a *Leishmania infantum* FASTA protein database (LinJwholegenome_20080508.v3.0a.fasta) using SEQUEST analysis software (176). When searching, SEQUEST used a dynamic mass modification for methionine oxidation (15.9949 Da) and a static mass modification for IAA induced cysteine alkylation (57.0215 Da). Peptides with an estimated false discovery rate <0.1% based on a target-decoy database search (177) were

stored as AMT tags in a Microsoft SQL Server database. The elution times for these peptides were normalized to a range of 0 to 1 using a predictive peptide LC normalized elution time (**NET**) model and linear regression, as previously reported (177).

AMT Tag Identification of Tryptic Peptides from Purine-Replete and Purine-Starved Cells.

Identification and quantification of the detected peptide peaks were performed utilizing the AMT tag approach (96-98). Briefly, multiple in-house developed, but publicly available, informatics tools were used to process LC-MS data and correlate the resulting LC-MS features to build an AMT tag database containing accurate mass and LC separation elution time information for peptide tags generated from *Leishmania donovani* proteins. Among the tools used were algorithms for peak-picking and for determining isotopic distributions and charge states (178). Further downstream data analysis incorporated all of the possible detected peptides into a visualization program VIPER (179) to correlate LC-MS features to the peptide identifications in the AMT tag database. The VIPER results were matched with a refined mass tolerance of ± 2 ppm and a refined NET tolerance of ± 2%. VIPER provided an intensity report for all detected features, normalized LC elution times via alignment to the database, and feature identification. In DAnTE software (180), peptide peak intensity values were converted to a log_2 scale and proteins with ≥2 peptides (Rrollup parameters) were statistically compared between the two conditions (plus or minus purine) at

each time point utilizing ANOVA performed as a t-test (with a minimum of 3 data points per condition).

Gene Ontology Classifications

UniProt identifiers for all of those proteins with significantly altered abundance (p-value of ≤ 0.05 and $\log_2$ value of ≥ 0.5 or ≤ -0.5) were submitted to the AgBase server to assign a Gene Ontology (**GO**) classification (http://www.agbase.msstate.edu/cgi-bin/tools/goretriever_select.pl and ref. (181)). All proteins were then grouped according to their GO category, or, alternatively, based upon predicted or known molecular function based upon searches of the UniProt database (http://www.uniprot.org/) and ref. (182)), PubMed (http://www.ncbi.nlm.nih.gov/pubmed/), or by using the BLAST algorithm (http://blast.ncbi.nlm.nih.gov/Blast.cgi and ref. (183)). In those cases where neither a GO category nor molecular function could be ascribed, proteins were classified as of "unknown function".

Radiolabeled Leucine and Uracil Incorporation Assays

Logarithmic cells, either continuously grown in 100 µM hypoxanthine or starved for purine for 24 h, were washed twice in growth media (**DMEL-Bob-Leu⁻**) that lacked both leucine and uracil and supplemented with (purine-replete cells) or without (purine-starved cells) 100 µM hypoxanthine. Cells were resuspended in DMEL-Bob-Leu⁻ plus or minus 100 µM hypoxanthine at a density of 5×10^7 cells/ml to which 1 µCi ml^{-1} of [4,5-^{3}H]-leucine (Sp. Act. 144 Ci mmol^{-1}) and 0.1

μCi ml^{-1} of [2-^{14}C]-uracil (Sp. Act. 57mCi mmol^{-1}) was added. At t = 20, 40, 60, and 80 min, 5 x 10^7 cells from the purine-replete and purine-starved cultures were washed twice in ice-cold PBS, resuspended in 0.5 ml of ice-cold PBS to which an equal volume of a 20 % trichloroacetic acid/water mix was added, and precipitated on ice for 60 min. The acid-precipitated material was collected onto glass fiber filters *via* vacuum manifold, washed twice with 1 ml of a 10 % trichloroacetic acid/water mix, followed by two washes with 1 ml of ice-cold ethanol. The filters were dried and radioactivity incorporated into the trichloroacetic acid-precipitated pool quantitated by liquid scintillation counting on a Beckman LS6500 liquid scintillation counter.

Quantitation of ROS in Leishmania

ROS measurements were performed based upon the published method of ref. (184). Log phase promastigotes, either continuously grown in 100 µM hypoxanthine or starved for purine for 24 - 72 h, were washed twice in Hank's Balanced Salt Solution supplemented with 25 mM glucose (**HBSS-G**) and either plus (purine-replete cells) or minus (purine-starved cells) 100 µM hypoxanthine. Cells were seeded at a density of either 0.1, 0.5, or 1 X 10^8 cells per well in HBSS-G plus or minus 100 µM hypoxanthine and containing 25 µg ml^{-1} of the cell-permeant fluorescein derivative 2',7'-dichlorodihydrofluorescein diacetate (H$_2$DCFDA) (Sigma-Aldrich) and incubated at 25 °C for 30 min. Fluorescence was measured with a SpectraMax M2 Microplate Reader (MolecularDevices GmbH, Ismaning/München, Germany) at wavelengths of 485 nm for excitation

and 535 nm for emission. Relative fluorescence units (**RFU**) measured were normalized to 10^6 cells.

Determination of Free Intracellular Proline in Leishmania

The free intracellular L-proline concentration was determined for purine-replete and purine-starved cells by the method of (185). 10^8 promastigotes were harvested at 24 and 48 h post induction of purine starvation. Cells were washed in PBS and proteins precipitated using 20 % trichloroacetic acid in PBS for 30 min on ice. Lysates were centrifuged at 10,000 x *g* for 30 min at 4 °C. A 200 µl aliquot of the resultant supernatant was mixed *via* inversion with 200 µl of an acid ninhydrin solution (0.25 g ninhydrin, 6 ml of glacial acetic acid, and 4 ml of 6 M phosphoric acid) and 200 µl of glacial acetic acid, and incubated at 100 °C for 1 h. A standard curve for L-proline (0 - 500 µM) was prepared in parallel. All reactions were stopped by chilling of the samples on ice and the chromagen extracted into 400 µl of toluene. For enumeration, a 100 µl aliquot of the toluene solution was measured in a quartz microcuvette at 520 nm using a Beckman DU-600 spectrophotometer.

Whole Transcriptome Shotgun Sequencing (RNA-Seq)

Early log phase *L. donovani* promastigotes were cultivated in purine-replete and purine-deplete media for 24 h as described above for the AMT tag analyses, after which time 1 X 10^8 cells were removed from each condition, harvested by centrifugation and washed twice in D-PBS to remove all media components.

Total RNA from the purine-replete and purine-deplete cells was isolated using an RNeasy kit (Qiagen Inc., Valencia, CA) according to the manufacturer's protocol. Next Generation Sequencing (**NGS**) libraries were constructed by priming ~1 µg of total RNA from either the purine-starved or purine-replete sample with a random hexamer primer (TCCGATCTCTNNNNNNNN) for first strand cDNA synthesis and an oligonucleotide primer (TCAGTTTCTGTA) derived from the *Leishmania* splice leader (**SL**) sequence for second-strand cDNA synthesis. This strategy is effective in identifying the 5' end of individual mRNAs, as well as differences in splice site usage (138). The resultant cDNA was amplified by PCR for 12-15 cycles using the oligonucleotides (CAAGCAGAAGACGGCATACGAGCTCTTCCGATCTCT and AATGATACGGCGACCACCGACACTCTTTCCCTACATCAGTTTCTGTACTTTA) that overlapped with the initial primers and containing adapters for subsequent cluster generation and sequencing using Solexa sequencing by synthesis (**SBS**) technology. Short-read (36-nt) sequences were obtained using a SL-specific sequencing primer (CACTCTTTCCCTACATCAGTTTCTGTACTTTA) on the Genome Analyzer IIx platform at the University of Washington High Throughput Genomics Unit. The FASTQ sequence data files were analyzed at Seattle BioMed using a customized NGS analysis pipeline. After quality checking, the reads were aligned with the *L. donovani* genome using Bowtie (186), and the results uploaded into a relational database. These analyses identified both the major and alternative splice sites for each gene, as well as the number of reads at each site. The latter was used to determine the expression level of each

mRNA. To normalize the purine-starved and purine-replete samples for reads/mRNA comparison, read numbers were divided by the median number of reads per mRNA in each sample (187).

qRT-PCR Analyses

Total cellular RNA was isolated from 2 X 10^8 *L. donovani* promastigotes using an RNeasy Mini Kit (Qiagen Inc., Valencia, CA) following the manufacturer's protocol. All additional qRT-PCR reagents were from Life Technologies (Grand Island, NY). To minimize potential contamination by genomic DNA, the purified RNA was subjected to DNaseI digestion using the Turbo DNA-*free* kit. First-strand cDNA was synthesized with a High Capacity cDNA Reverse Transcription kit using 2 µg of total RNA as per the manufacturer's instructions. For qRT-PCR, 5 µl of diluted first-strand cDNA reaction corresponding to 20 ng of input RNA was included in a 20 µl reaction with 5 pmol primers (see Table S6) and 10 µl 2X SYBR Select Master Mix. The reactions were run on an Applied Biosystems 7500 Real-Time PCR System under the following conditions: 50°C for 2 min and 95°C for 10 min, followed by 40 cycles of 95°C for 15 s and 60°C for 1 min. A final thermal dissociation analysis was performed for each reaction to confirm that the PCR generated a single amplification product. The relative abundance of target amplicons between purine replete and starved samples was determined via the $2^{-\Delta\Delta C_T}$ method (188).

Dual-Luciferase Assay

Constructs containing the *Photinus pyralis* (firefly) luciferase gene fused at the 3'
end to the blasticidin-S deaminase gene (GenBank accession number
KF035118; designated as **Fluc** in the text and Tables 2 and 3) and flanked by ~ 1
kb of 5' and 3' sequence adjacent to the coding sequence of the corresponding
genes of interest were assembled by the method of multifragment ligation (189).
(See Table S7 for details about the primer sequences used for the amplification
of the 5' and 3' fragments). These constructs were linearized with *PacI* and
transfected using standard transfection techniques (173) into a recipient cell line
in which one copy of *UMPS* (145) had previously been replaced by the *Renilla
reniformis* luciferase gene fused at the 3' end to the puromycin acetyltransferase
gene (GenBank accession number KF035116; designated as **Rluc** in the text
and legend of Tables 2 and 3). *Rluc* integrated at the *UMPS* locus served as a
control for the Fluc reporter assays in both purine-replete and purine-starved
cells, since we have previously established by western analyses and qRT-PCR
(52), as well as by the proteomic and SL RNA-seq analyses described in this
manuscript, that the abundance of *UMPS* mRNA and its corresponding protein
does not alter during 48 h of purine starvation. Changes in *Fluc* activity arising
from integration at various loci was measured at 6 and 24 h post induction of
purine starvation and compared to the internal normalizer of *Rluc* using the Dual-
Luciferase® Reporter Assay System (Promega, Madison, WI). Briefly, 1 ml of
purine-replete or purine-starved cells (~2 x 10^6 cells) was harvested by
centrifugation at 16,000 x *g* for 1 min at ambient temperature and washed in 1 ml

66

of PBS. Cells were resuspended in 1 ml of 1X Passive Lysis Buffer provided with the Dual-Luciferase® Reporter Assay System kit, vortexed briefly, and then subjected to end-over-end rotation at ambient temperature for 20 min to achieve complete lysis. Twenty µl of the cell lysate was transferred to a well in a black flat-bottom 96-well assay plate (Corning, Amsterdam) and assayed according to the Dual-Luciferase® Reporter Assay System protocol using a Veritas™ Microplate Luminometer (Turner BioSystems, Sunnyvale, CA). For each cell lysate, the relative light units (**RLUs**) arising from Fluc was divided by the RLUs arising from Rluc to obtain a normalized value, and the fold change in purine-starved cells calculated by dividing the normalized value with that from the corresponding purine-replete sample. Note that details of the construction of *Fluc* and *Rluc* were unavailable at time of publication and can now be found in the publication by Soysa et al. (190).

ACKNOWLEDGEMENTS

6 h Proteome

2334 (61) 52 2 7

12 h Proteome

2132 (295) 135 142 7 11

24 h Proteome

2110 (301) 96 76 109 20

48 h Proteome

1555 (841) 508 77 105 151
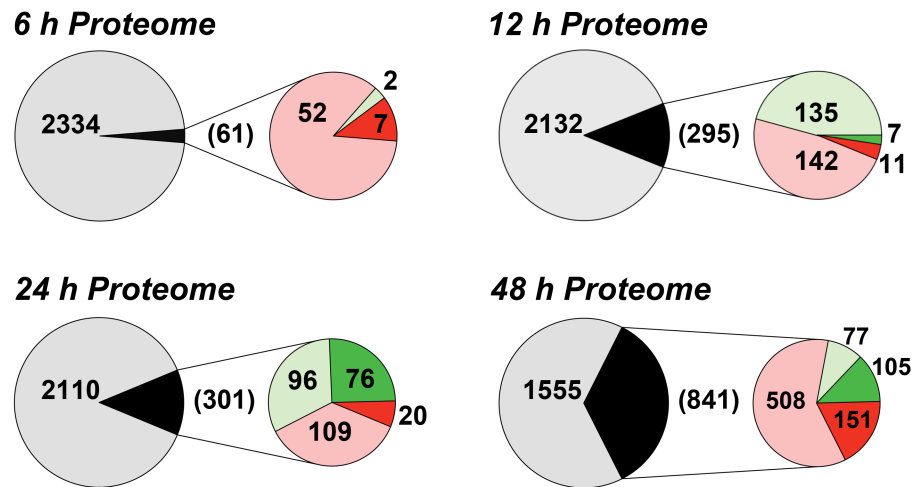
Figure 2.1 Summary of the Proteome Changes Accompanying Purine Starvation.

The proteomes of cells incubated in either purine-replete or in purine-deplete media were compared at 6, 12, 24, and 48 h post purine supplement removal. Large circles and the numbers within represent the total number of proteins that could be assigned between purine-replete and purine-deplete cells at each time point. Small circles and numbers in parentheses refer to the number of proteins significantly changed (p-value < 0.05) at each time point between purine-replete and purine-deplete cells. Light red and light green fractions and corresponding numbers indicate proteins upregulated or downregulated, respectively, by less than 2-fold, dark red and dark green portions and corresponding numbers indicate proteins upregulated or downregulated, respectively, by 2-fold or more.

A

	6	12	24	48	
					LdNT1 (LinJ.15.1240)
					LdNT2 (LinJ.36.2040)
					LdNT3 (LinJ.13.1110)
					LdNT4 (LinJ.11.0520)
					3'NT/NU-31 (LinJ.31.2380)
					3'NT/NU-12 (LinJ.12.0350)
					MAP2-23 (LinJ.23.1430)
					MAP2-36 (LinJ.36.2720)

B

	6	12	24	48	
					HGPRT (LinJ.21.0980)
					XPRT (LinJ.21.0990)
					APRT (LinJ.26.0120)
					AK (LinJ.30.0940)
					IGNH (LinJ.14.0130)
					NH (LinJ.18.1570)
					IAGNH (LinJ.29.2910)
					AAH (LinJ.35.2200)
					GDA (LinJ.29.0920)
					ADSS (LinJ.13.1090)
					ASL (LinJ.04.0440)
					AMPDA-32 (LinJ.32.2690)
					AMPDA-04 (LinJ.04.0270)
					IMPDH (LinJ.19.1590)
					GMPR (LinJ.17.0870)
					GMPS (LinJ.22.0013)
					ADKG (LinJ.04.0960)
					ADKB (LinJ.21.1490)
					ADKD (LinJ.36.1410)
					ADKF (LinJ.34.0120)
					ADKC (LinJ.34.0130)
					GK (LinJ.33.1150)

C

	6	12	24	48	
					NDKb (LinJ.32.3110)
					NDK (LinJ.35.3910)
					PDE-1 (LinJ.15.1540)
					PDE-2 (LinJ.18.1100)
					PDE-3 (LinJ.15.1550)
					PDE-4 (LinJ.04.0030)
					RR-S1 (LinJ.22.1110)
					RR-S2 (LinJ.27.1970)
					RR-L (LinJ.28.0980)
					MTAP (LinJ.05.0830)
					SAMSYN (LinJ.30.3560)

69

Figure 2.2 Heat Maps Depicting Temporal Changes in Purine Metabolism During Purine Starvation.

Heat maps were generated using the open-source analysis software Multi Experiment Viewer MeV v4.6 (http://www.tm4.org/mev/MeV_4_6) (191) to show the comparative log2 abundance ratios between purine-replete and purine-starved samples at 6, 12, 24, and 48 h. The log2 scale for each heat map is shown on the bar above. TriTrypDB accession numbers (http://tritrypdb.org/tritrypdb/) are included on the right of each panel. Upregulated proteins are depicted by red bars, downregulated proteins by green bars, and missing data points by grey bars. (A) Log2 abundance ratios for cell surface purine salvage components. (B) Log2 abundance ratios for various intracellular purine salvage pathway components. (C) Log2 abundance ratios for other intracellular purine metabolizing enzymes. Abbreviations: LdNT1-4, L. donovani nucleobase/nucleoside transporters 1-4; 3'NT/NU-31 and 3'NT/NU-12, 3'-nucleotidase/nucleases corresponding to sequences on chromosomes 31 and 12, respectively; MAP2-23 and MAP2-36, membrane acid phosphatases corresponding to sequences on chromosomes 23 and 36, respectively; HGPRT, hypoxanthine phosphoribosyltransferase; XPRT, xanthine phosphoribosyltransferase; APRT, adenine phosphoribosyltransferase; AK, adenosine kinase; IGNH, inosine-guanosine nucleoside hydrolase; NH, nonspecific nucleoside hydrolase; IAGNH, purine-specific nucleoside hydrolase; AAH, adenine aminohydrolase; GDA, guanine deaminase; ADSS, adenylosuccinate synthetase; ASL, adenylosuccinate lyase; AMPDA-32 and AMPDA-04, putative adenosine monophosphate (AMP) deaminases corresponding to sequences on chromosomes 32 and 4, respectively; IMPDH, inosine monophosphate dehydrogenase; GMPR, guanosine monophosphate (GMP) reductase; GMPS, GMP synthase; ADKG, ADKB, ADKD, ADKF, ADKC, multiple adenylate kinase activities; GK, putative guanylate kinase; NDKb and NDK, nucleoside diphosphate kinases; PDE-2, cAMP specific phosphodiesterase A; PDE-1, -3, -4, putative cAMP phosphodiesterases; RR-S1 and RR-S2, putative ribonucleoside diphosphate reductase small chains; RR-L, putative ribonucleoside diphosphate reductase large chain; MTAP, putative methylthioadenosine phosphorylase; and SAMSYN, S-adenosylmethionine synthetase.
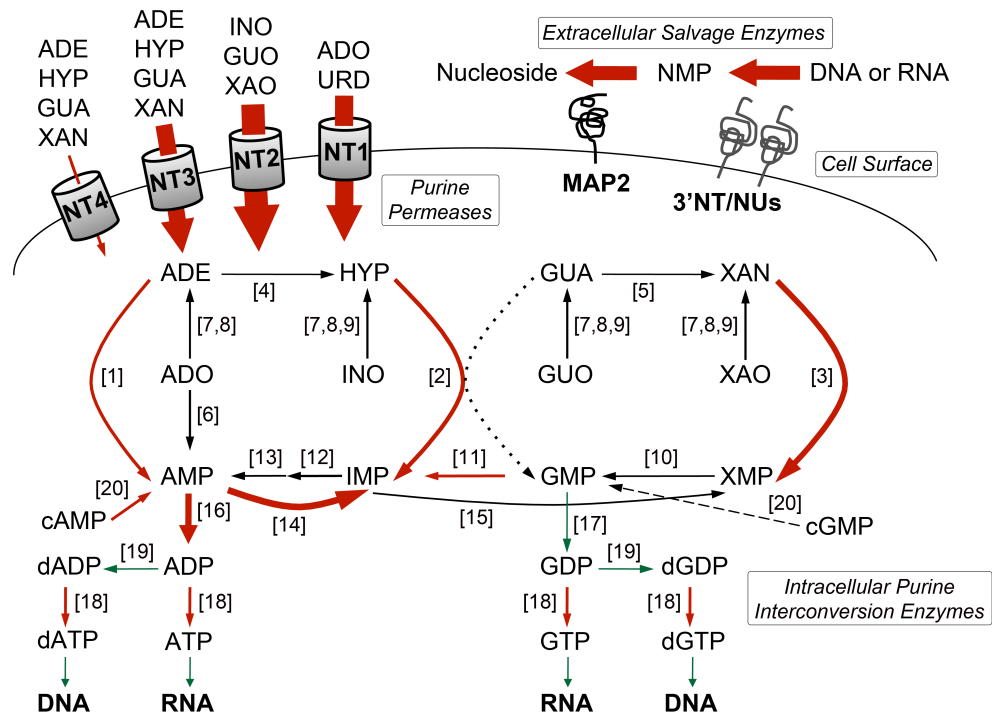
Figure 2.3 Purine Acquisition and Interconversion in Leishmania 48 h Post Induction of Purine Starvation.

The thickness of the arrows represents the magnitude of upregulation in the 48 h proteome and is used as a prediction of flux through the pathway. Activities upregulated by 2-fold or more are shown in red and those that are downregulated are shown in green. Dashed arrow indicates that the conversion of cGMP to GMP is predicted but has yet to be demonstrated in *Leishmania*. Dotted arrow indicates that the conversion of GUA to GMP by HGPRT is insubstantial in *L. donovani* (76). *Abbreviations*: NT1, LdNT1; NT2, LdNT2; NT3, LdNT3; NT4, LdNT4; ADE, adenine; HYP, hypoxanthine; GUA, guanine; XAN, xanthine; ADO, adenosine; INO, inosine; GUO, guanosine; XAO, xanthosine; URD, uridine; XMP, xanthosine monophosphate; NMP, nucleoside monophosphate; ADP, adenosine diphosphate; GDP, guanosine diphosphate; dADP, deoxyadenosine diphosphate; dGDP, deoxyguanosine diphosphate; ATP, adenosine triphosphate; GTP, guanosine triphosphate; dATP, deoxyadenosine triphosphate; dGTP, deoxyguanosine triphosphate; for all other abbreviations see the legend of Fig. 2. *Activities* (*see the legend of Fig. 2 for abbreviations*): [1] APRT; [2] HGPRT; [3] XPRT; [4] AAH; [5] GDA; [6] AK; [7] NH; [8] IAGNH; [9] IGNH; [10] GMPS; [11] GMPR; [12] ADSS; [13] ASL; [14] AMPDA; [15] IMPDH; [16] various ADK; [17] GK; [18] NDKb and NDK; [19] ribonucleoside diphosphate reductase; [20] various cyclic nucleotide phosphodiesterases.
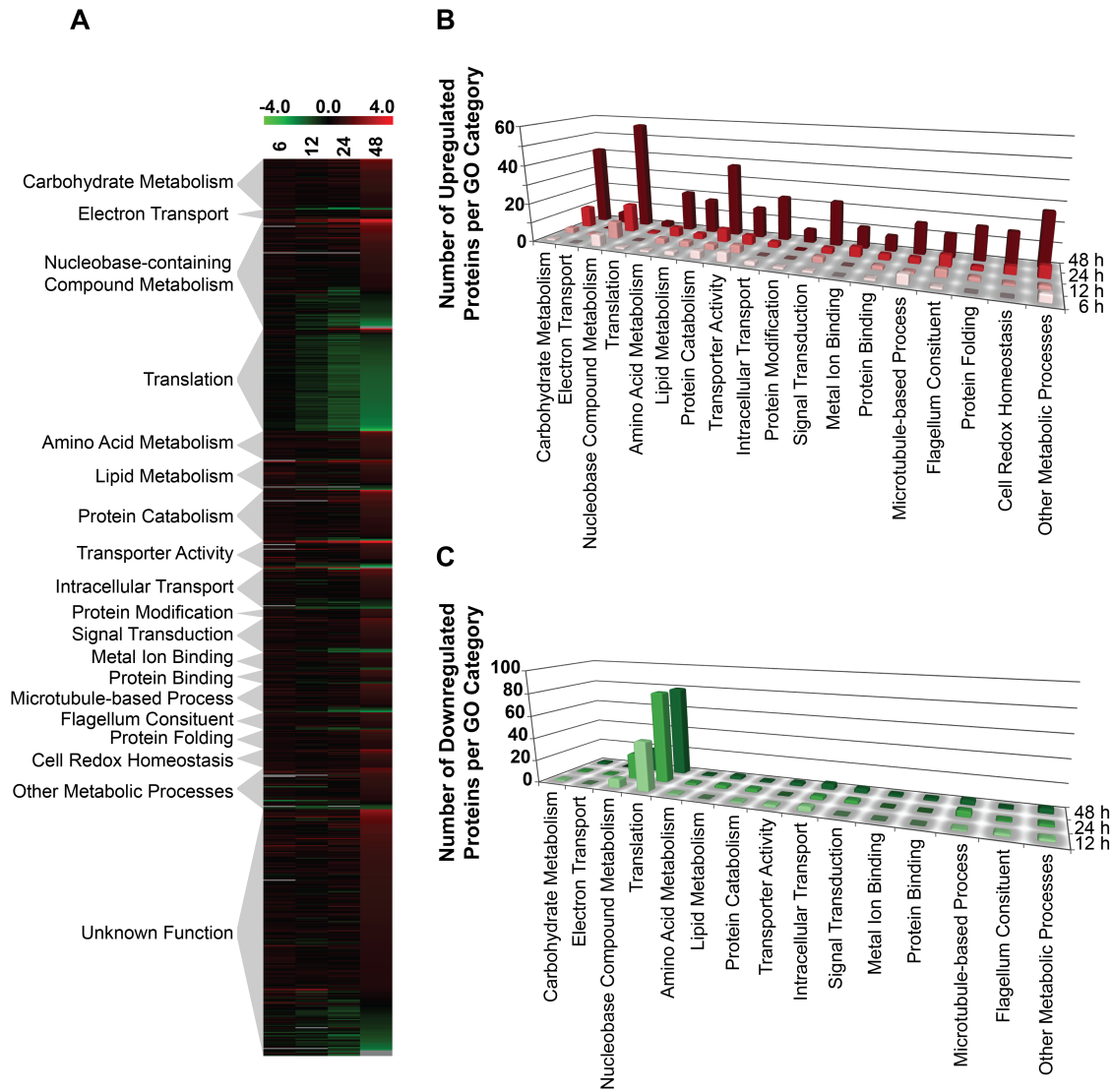
Figure 2.4 Global Proteome Remodeling in Purine-Starved Cells.

777 proteins that were significantly changed (p-value ≤ 0.05) and either up- or downregulated by a $\log_2$ value of 0.5 or more at 6, 12, 24, and 48 h were grouped according to their molecular function. (A) Heat map illustrating the temporal changes between purine-replete and purine-starved samples at 6, 12, 24, and 48 h. The $\log_2$ scale is shown on the bar above. Missing data points for particular proteins within the time-course are depicted by the grey bars. Proteins were sorted according to molecular function and the heat map generated using the open-source analysis software Multi Experiment Viewer MeV v4.6 (http://www.tm4.org/mev/MeV_4_6) (191). (B) and (C) 3-dimensional bar graphs showing the number of either upregulated (B) or downregulated (C) proteins in each functional category. Both the heat map and bar graphs were generated using the data in Table S3.
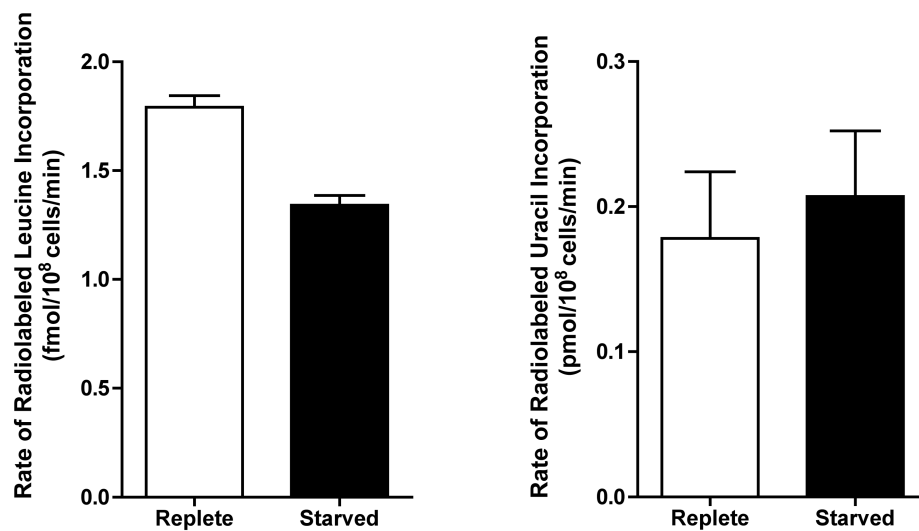
Figure 2.5 Rate of Incorporation of Radiolabeled Leucine and Uracil into Purine-Starved and Purine-Replete Cells.

The rate of incorporation of [4,5-^{3}H]-leucine and [2-^{14}C]-uracil was compared between purine-replete (open bars) and cells starved for purine for 24 h (closed bars). Rates were calculated based upon 3 biological replicates per time-point for each condition (purine-replete *versus* purine-starved) and the data represent the mean rate of incorporation from two independent assays.
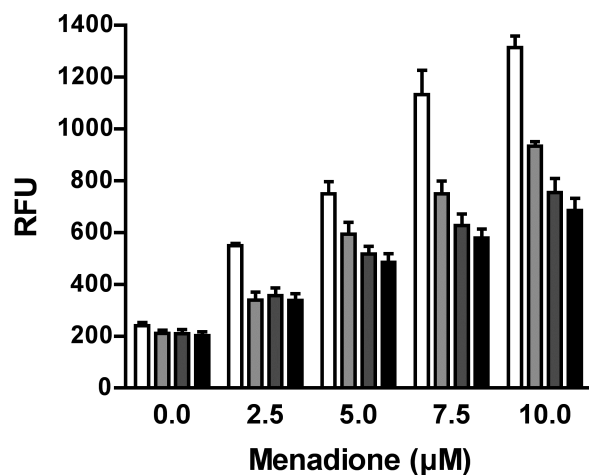
Figure 2.6 Response of Purine-Starved and Purine-Replete Parasites to ROS Induction.

Purine-replete and purine starved promastigotes were exposed to increasing concentrations (2.5-10 µM) of the ROS-generating compound menadione. Generation of ROS was measured by incubating parasites with the cell-permeant fluorescein derivative H_2DCFDA. The RFU attributable to ROS in 10^6 cells are depicted for parasites grown continuously in 100 µM hypoxanthine (open bars) or starved for purine for 24 h (light grey bars), 48 h (dark grey bars), or 72 h (black bars). The data represent three independent biological replicates. (Error bars indicate standard deviation).
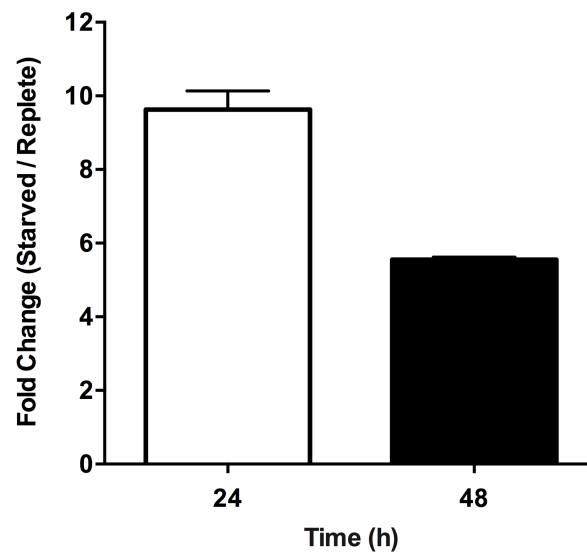
Figure 2.7 Effect of Purine Starvation on Intracellular Proline Levels.
The free intracellular L-proline concentration was determined for purine-replete
and purine-starved cells. Bars indicate the fold change between purine-starved
versus purine-replete parasites at 24 h (open bar) and 48 h (black bar) post
purine removal. Error bars indicate standard deviation; data represent two
independent biological replicates.
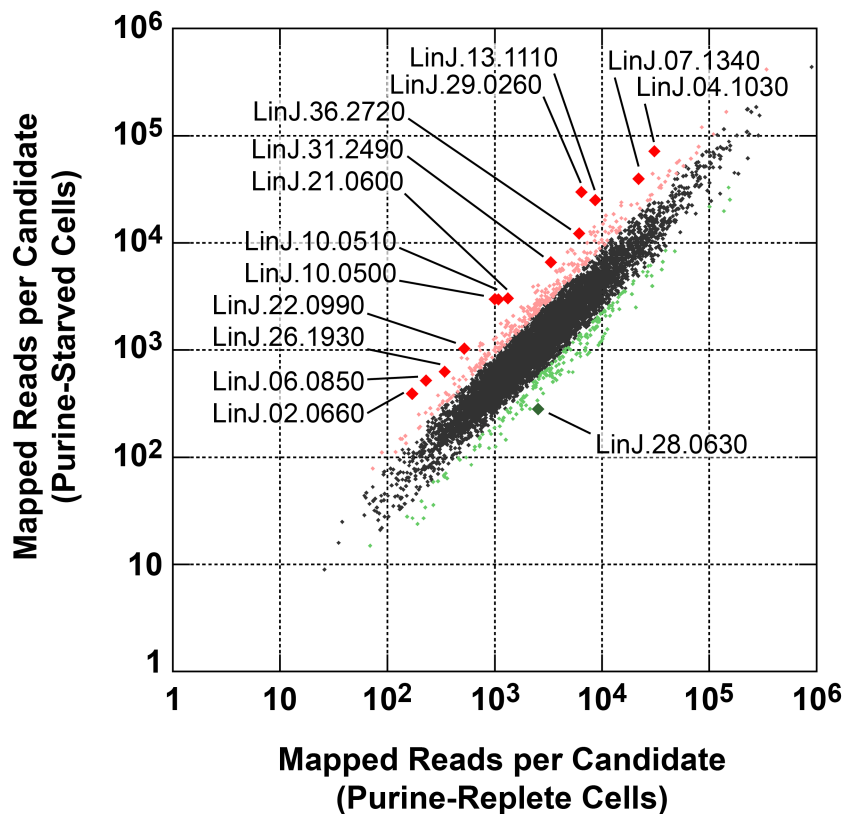
Figure 2.8 Scatter Plot of SL RNA-Seq Data Comparing mRNA Abundance Between Purine-Replete and Purine-Starved Cells.

The number of reads mapped to individual mRNA sequences (see Table S4) were compared between cells grown in medium supplemented with 100 µM hypoxanthine to those cultivated in medium without purine supplementation for 24 h. Those mRNAs changed by less than 2-fold are denoted by small black diamonds; mRNAs upregulated 2- to 4-fold are denoted by small pink diamonds; mRNAs downregulated 2- to 4-fold are denoted by small green diamonds; mRNAs upregulated by 4-fold or more are denoted by large red diamonds; mRNAs downregulated by 4-fold or more are denoted by large green diamonds. The TriTrypDB (14) accession numbers for those mRNAs most significantly changed are shown.
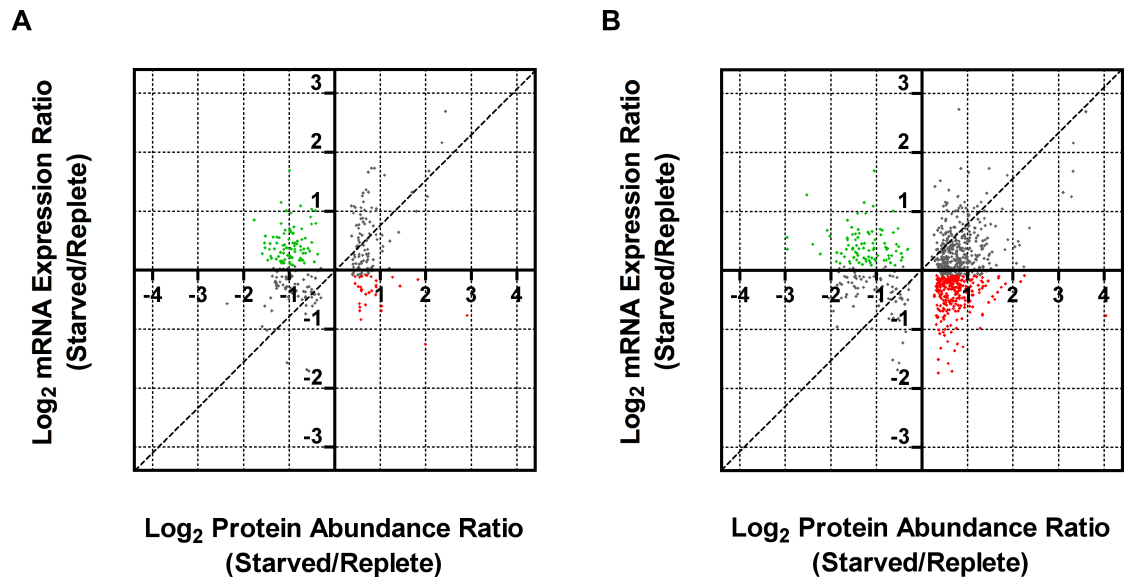
Figure 2.9 Comparison of Fold Changes at the Protein and mRNA Level in Purine-Starved Cells.

Proteins were sorted by $\log_2$ abundance ratio at both 24 h (A) and 48 h (B) and plotted against the $\log_2$ expression ratio at 24 h for the corresponding mRNA as measured by SL RNA-seq. Dashed lines indicate an exact correlation between the changes at the protein and mRNA level. Grey dots indicate those proteins that exhibit a similar trend at the mRNA level (upregulated, upper right quadrant, and downregulated, lower left quadrant), green dots correspond to those proteins that were downregulated but where the corresponding mRNA was upregulated (upper left quadrant), and red dots correspond to those proteins that were upregulated but where the corresponding mRNA was downregulated (lower right quadrant).

Descriptor, Accession Number	mRNA Fold	Change (24 h)	Protein	Fold Change
	SL RNA-seq	qRT-PCR	24 h	48 h
LdNT1.1, LinJ.15.1230-50	1.79	2.27±0.40	6.48	7.66[b]
LdNT2, LinJ.36.2040	0.59	1.07±0.41	7.46	16.45
LdNT3, LinJ.13.1110	6.45	5.75±0.23	5.39	12.13
LdNT4, LinJ.11.0520	0.97	1.70±0.44	1.34	2.03
3'NT/NU-12, LinJ.12.0350	3.20	5.07±0.61	4.19	9.97
3'NT/NU-31, LinJ.31.2380	1.48	5.06±0.05	4.11	9.71
MAP2-36, LinJ.36.2720	4.47	4.81±0.45	5.12	10
XPRT, LinJ.21.0990	3.05	1.97±0.19	2.13	3.68
AAT19, LinJ.07.1340	3.71	3.52±0.47	1.04	1.15
La RNA binding protein, LinJ.21.0600	5.10	1.13±0.05	0.75	0.85
Oxidoreductase, LinJ.29.0260	10.34	4.29±0.78	ND*	ND*
Hypothetical, LinJ.31.2490	4.41	3.67±0.31	ND*	1.27
Hypothetical, LinJ.04.1030	5.21	2.15±0.69	ND	ND
Hypothetical, LinJ.28.0630	0.25	1.04±0.06	ND	ND
SHERP, LinJ.23.1210, LinJ.23.1230	1.08±0.02	1.62±0.11	ND	ND
UMPS[a], LinJ.16.0560	0.91	1.00[a]	1.05	1.12

qRT-PCR data represents the mean fold change ± standard deviation from two independent biological replicates. ND, not detected in replete or starved sample set; ND* not detected in replete samples only;
[a]serves as an internal control normalized to 1.00 for each qRT-PCR assay;
[b]since LdNT1.1 peptides were not detected in the 48 h replete sample, the fold change was calculated by comparing the combined average AMT tag intensity recorded at 6, 12, and 24 h (replete samples, n = 11) with the average AMT tag intensity at 48 h (starved samples, n = 5).
doi:10.1371/journal.ppat.1003938.t001

Table 2.1 Comparison of relative mRNA abundance change during purine starvation by SL RNA-seq and qRT-PCR.

Descriptor, Accession Number	Fold Change (24 h)		
	Fluc Activity	**qRT-PCR** *Fluc*	**qRT-PCR Gene**
LdNT1.1, LinJ.15.1230-50	4.04±0.26	0.97±0.20	3.05±0.11
LdNT2, LinJ.36.2040	3.01±0.04	0.25±0.02	1.16±0.20
LdNT3, LinJ.13.1110	10.54±1.13	2.52±0.98	7.40±1.48
LdNT4, LinJ.11.0520	1.25±0.19	1.01±0.04	1.11±0.13
3'NT/NU-12, LinJ.12.0350	2.50±0.06	1.97±0.03	5.98±0.37
3'NT/NU-31, LinJ.31.2380	1.93±0.04	1.47±0.29	3.16±0.52
MAP2-36, LinJ.36.2720	2.21±0.04	1.85±0.15	3.73±0.46
Oxidoreductase, LinJ.29.0260	5.78±0.46	2.07±0.38	4.60±0.65

L donovani cell lines were generated in which a *Fluc* reporter was integrated in place of one allele of the indicated locus; each *Fluc* reporter line also contained an *Rluc* reporter integrated at the *UMPS* locus as an internal normalization control. Changes in Fluc activity and mRNA abundance (qRT-PCR *Fluc*), and mRNA abundance of the corresponding endogenous allele (qRT-PCR Gene) following 24 h purine starvation were determined in parallel from aliquots of the same culture. All qRT-PCR data were normalized to *UMPS*. The mean and standard deviation determined from two independent biological replicates is shown for each analysis.
doi:10.1371/journal.ppat.1003938.t002

Table 2.2 An assessment of the role of 5' and 3' UTRs from select purine-responsive candidates on mRNA abundance and translational regulation.

Descriptor, Accession Number	Fold Change (6 h)		
	Fluc Activity	qRT-PCR *Fluc*	qRT-PCR Gene
LdNT1.1, LinJ.15.1230-50	1.94±0.08	1.06±0.001	1.52±0.17
LdNT2, LinJ.36.2040	1.69±0.06	0.40±0.06	0.93±0.01
LdNT3, LinJ.13.1110	2.63±0.28	0.43±0.001	2.90±0.18
3'NT/NU-12, LinJ.12.0350	1.25±0.28	1.53±0.11	3.06±0.22
3'NT/NU-31, LinJ.31.2380	1.36±0.03	1.54±0.14	3.22±0.61
MAP2-36, LinJ.36.2720	1.33±0.30	0.97±0.13	1.63±0.02
Oxidoreductase, LinJ.29.0260	1.36±0.23	1.02±0.03	1.24±0.02

Table 2.3 Elucidation of the molecular mechanisms in the early response to purine starvation.

Descriptor	TriTrypDB Accession number (*L. infantum*)	GenBank Accession number	Primer Sequence - Forward Reverse
LdNT1.1	LinJ.15.1230-50	AF065311	5'-GTGATGGAGGTCATCTTCGGCTTCTC-3'
			5'-GCTTGCCGTCGTTGTCGATGC-3'
LdNT2	LinJ.36.2040	AF245276	5'-CGCACTCTTCATGTCGATCATCCAG-3'
			5'-CCGATTCCAATGCCGAAGTAGATGC-3'
LdNT3	LinJ.13.1110	HM147245	5'-GGTGAGTTCCGTGCCATCAAGC-3'
			5'-GCTGGTTGCTGCTGCTGAG-3'
LdNT4	LinJ.11.0520	HM147244	5'-CCATGCTTGTCACCAGCCTTGTG-3'
			5'-CCTTGTTGCCAGCGAGGTACTTGTAG-3'
3'NT/NU (Chr12)	LinJ.12.0350	XM_003859104	5'-GACACCATCTACAACCCACAG-3'
			5'-ATGAGGTTTGCGACAGAGG-3'
3'NT/NU (Chr31)	LinJ.31.2380	L35078	5'-GTTATCGACTCCAAGGGAACC-3'
			5'-GTACGTTGCTTCCAGATAGTCG-3'
MAP2	LinJ.36.2720	XM_003865339	5'-AGCAGATGGTGAAGAACATGGA-3'
			5'-GCGCTGTAGTGCATCAACTTG-3'
XPRT	LinJ.21.0990	XM_003860567	5'-GCTCGTCTGTCACCCAGCAC-3'
			5'-GGATGAAGTCGGATGTGAAGATGTAGCTG-3'
AAT19	LinJ.07.1340	XM_003858517	5'-TTCATCGGCTTCATCTTCCC-3'
			5'-ACTCTAGCAACCCCACATTC-3'
Oxidoreductase	LinJ.29.0260	XM_003862395	5'-CGTGGAGCGCATCTCGAT-3'
			5'-TTCGGCAGGCAGGAAATC-3'
La RNA binding protein	LinJ.21.0600	XM_003860529	5'-CATCTTTCAGGACGCCGAG-3'
			5'-CTCCTTCTCTACGTTCGCTATG-3'
Hypothetical	LinJ.31.2490	XM_003863288	5'-GCGTCTTTTCACTCTCTGGTGGACAC
			5'-GCTTTGCCACATCGCTGAAGCTC-3'
Hypothetical	LinJ.04.1030	XM_003858117	5'-TCGTTTGCGTCATCCTGG-3'
			5'-CGTTGAGCGATGAAAACTGC-3'
Hypothetical	LinJ.28.0630	XM_003862114	5'-GTGGAGCAAGCACCAGAGAAACG-3'
			5'-GACGTGTTGGAGTCGAACCACAG-3'
UMPS	LinJ.16.0560	JN882599	5'-GATTGAGCAGACGCACGAGTACG-3'
			5'-CGGCACGAATCACTTCCGACAG-3'
Firefly luciferase 2	Not applicable	AAV52869.1	5'-GGTCGTGCTCATGTACCGCTTC-3'
			5'-GCTTAGGTCGTACTTGTCGATGAGAGTG-3'

Table 2.4 Primers used for the qRT-PCR analyses.

81

Descriptor	TriTrypDB Accession number (*L. infantum*)	5'TS Primer Sequence - Forward *Reverse*	3'TS Primer Sequence - Forward *Reverse*
LdNT1.1	LinJ.15.1230-50	5'_**GAGGCCACCTAGGCC**GTAC GGCACCTGCTGGACCTAC_3' *5'_**GAGGCCACGCAGGCC**TGTC TATCTGGGCGGAATGGTG_3'*	5'_**GAGGCCTCTGTGGCC**CGCAG ACTATTCGCGCGACTTAC_3' *5'_**GAGGCCTGACTGGCC**TACGA GAAGGGTGGGTTCATCGAG_3'*
LdNT2	LinJ.36.2040	5'_**GAGGCCACCTAGGCC**TAAG CTGCTAGCAGTGGCACAGTC_3' *5'_**GAGGCCACGCAGGCC**TTCTT CCAACTTCAGCTTCGTCCAG_3'*	5'_**GAGGCCTCTGTGGCC**TTCCC GCAGTGGAGCTTCTG_3' *5'_**GAGGCCTGACTGGCC**GAGGT TGTGGAGAGATGCTTGCAG_3'*
LdNT3	LinJ.13.1110	5'_**GAGGCCACCTAGGCC**GCAT CCCTGAACGCATGTG_3' *5'_**GAGGCCACGCAGGCC**TTGC TGTACTAGGGCGAGGAG_3'*	5'_**GAGGCCTCTGTGGCC**TTCCT GCCCTAAGCACAATGC_3' *5'_**GAGGCCTGACTGGCC**GTGCA TGATCAAACACGACGAAG_3'*
LdNT4	LinJ.11.0520	5'_**GAGGCCACCTAGGCC**GAGG GATGCACGACGTGGCGATC_3' *5'_**GAGGCCACGCAGGCC**GCTC GCACTGCGCCGTG_3'*	5'_**GAGGCCTCTGTGGCC**ACTTA AGCGAAATGGCGATACG_3' *5'_**GAGGCCTGACTGGCC**TCGCT TAAAGTGACAGTATCTCC_3'*
3'NT/NU (Chr12)	LinJ.12.0350	5'_**GAGGCCACCTAGGCC**GTGC TCTGTTTACGAGTTGACCTG_3' *5'_**GAGGCCACGCAGGCC**ATGT CTGGTCCCGTTGAGG_3'*	5'_**GAGGCCTCTGTGGCC**GCGAG CCACGGAATCTGAG_3' *5'_**GAGGCCTGACTGGCC**TGCGC ACACACTGACGTACTC_3'*
3'NT/NU (Chr31)	LinJ.31.2380	5'_**GAGGCCACCTAGGCC**AGAC CTCTCCCTGACCTCAACTG_3' *5'_**GAGGCCACGCAGGCC**ATGT CTGCCGTAGCGTGCAC_3'*	5'_**GAGGCCTCTGTGGCC**CGCTT TGGTTCCTATGAGCACGTC_3' *5'_**GAGGCCTGACTGGCC**GACTC ACAGCCGAAACGAATCGAG_3'*
MAP2	LinJ.36.2720	5'_**GAGGCCACCTAGGCC**GGTT TCTTGCAGCTGAGCTTGGAGG_ 3' *5'_**GAGGCCACGCAGGCC**GCGG ACAGCAGCGGCCTCAAG_3'*	5'_**GAGGCCTCTGTGGCC**GCGCG AGAAGCAAGCAACAGG_3' *5'_**GAGGCCTGACTGGCC**ATTGC CACCGTCCGCATTCC_3'*
Oxido-reductase	LinJ.29.0260	5'_**GAGGCCACCTAGGCC**AGCG GTACGAGGCCTGCATGCAAG_3' *5'_**GAGGCCACGCAGGCC**TGGT GGGGGCGAGCGAGAGAGT_3'*	5'_**GAGGCCTCTGTGGCC**GGTGG GCTGTGGAGCAACTGAC_3' *5'_**GAGGCCTGACTGGCC**GATGC ACGCATGACACGCACAG_3'*
UMPS	LinJ.16.0560	5'_**GAGGCCACCTAGGCC**TGAT GCACCATGCGCTGTACC_3' *5'_**GAGGCCACGCAGGCC**ACGA TAAGACGAAGATGTGTTGGTGT CC_3'*	5'_**GAGGCCTCTGTGGCC**TACAC ACGCACACGCGAGGAG_3' *5'_**GAGGCCTGACTGGCC**TCTCT TTCACAGCCAGTGTTGC_3'*

Table 2.5 Primers used for the construction of fLuc or rLuc reporter constructs for integration at the indicated loci via homologous recombination.

Primer sequences corresponding to 5' or 3' targeting sequences (TS) flanking the indicated gene are in plain text, while the SfiI restriction sites that facilitate the single-step assembly of the targeting construct are highlighted in boldface type.

Chapter 3

A ROLE FOR ADENINE NUCLEOTIDES IN THE SENSING MECHANISM TO PURINE STARVATION IN *LEISHMANIA DONOVANI*

Jessica L. Martin[1], Phillip A. Yates[1], Jan M. Boitz[1], Dennis R. Koop[2], Audrey L. Fulwiler[1], Maria Belen Cassera[3], Buddy Ullman[1], Nicola S. Carter[1]*

[1]Department of Biochemistry and Molecular Biology, Oregon Health & Science University, 3181 SW Sam Jackson Park Road, Portland, OR 97239-3098, USA.
[2]Department of Physiology and Pharmacology, Oregon Health & Science University, 3181 SW Sam Jackson Park Road, Portland, OR 97239-3098, USA.
[3]Department of Biochemistry and Virginia Tech Center for Drug Discovery, M/C 0308, Virginia Tech, Blacksburg, Virginia 24061, USA.

ABSTRACT

Purine salvage by *Leishmania* is an obligatory nutritional process that impacts both cell viability and growth. Previously, we have demonstrated that the removal of purines in culture provokes significant metabolic changes that enable *Leishmania* to survive prolonged periods of purine starvation. In order to understand how *Leishmania* sense and respond to changes in their purine environment, we have exploited several purine pathway mutants, some in which adenine and guanine nucleotide metabolism is uncoupled. While wild type parasites grow in any one of a variety of naturally occurring purines, the proliferation of these purine pathway mutants requires specific types or combinations of exogenous purines. By culturing purine pathway mutants in high levels of extracellular purines that are either permissive or non-permissive for growth and monitoring for previously defined markers of the adaptive response to purine starvation, we determined that adaptation arises from a surveillance of intracellular purine nucleotide pools rather than from a direct sensing of the extracellular purine content of the environment. Specifically, our data suggest that perturbation of intracellular adenine-containing nucleotide pools provides a crucial signal for inducing the metabolic changes necessary for the long-term survival of *Leishmania* in a purine-scarce environment.

AUTHOR SUMMARY

Successful parasitism by *Leishmania* is based upon an ability to sense and respond to changes in the extracellular environment including fluctuations in nutrient availability. *Leishmania* that are starved for purines (essential nutrients that, therefore, must be scavenged) cease to grow and undergo a metabolic restructuring that allows them to persist for over three months in the absence of purines. Here, we describe a plausible purine sensing mechanism that prompts the adaptation of *Leishmania* to purine restriction. Using purine pathway mutants, we have established that this response to starvation can be elicited in the presence of an extracellular purine supplement that does not support growth. These studies also revealed that purine sensing and the ensuing metabolic adaptations that ensure long-term survival within a purine-deficient environment are contingent upon disruption of intracellular adenylate nucleotide metabolism. The experiments described here also emphasize the utility of purine pathway mutants as valuable tools for delineating the signaling networks involved in adaptation to purine starvation.

INTRODUCTION

Leishmania are protozoan parasites that are a significant human health and socioeconomic burden and the etiological agent of leishmaniasis, a disease afflicting approximately 12 million people in 98 countries (33). Due to the lack of an effective vaccine, management of leishmaniasis is based on a handful of drugs, most of which are cumbersome to administer, costly, and exhibit toxic side effects. Of growing concern is the high level of resistance to first-line drug treatments, particularly in regions endemic for *L. donovani* (56), the causative agent of deadly visceral leishmaniasis. Thus, there is an exigent need for improved therapeutic approaches.

An ideal strategy for the discovery of new and better therapeutic targets is to identify metabolic pathways in the parasite that are both different from the host and essential for parasite survival (57-59). *Leishmania*, like other related parasitic protozoa, have a complex digenetic life cycle during which they encounter dramatic physiological alterations in their host milieu as they transition from extracellular promastigotes in the insect vector to intracellular amastigotes that reside in the phagolysosome of mammalian macrophages (60). Although the precise profile of nutrients available to the parasite in either the vector or the host has not be defined, it is likely that nutrient availability fluctuates substantially during the *Leishmania* lifecycle; perhaps—as a consequence—these parasites have evolved robust adaptive mechanisms for dealing with nutrient scarcity (52, 60-65). As the parasite transitions between lifecycle stages, its survival depends on both sensing and adapting its metabolic repertoire to respond to the changing

microenvironment (16). Even though the signaling responses that underlie the parasite's acclimatization to environmental changes are essential, they are poorly understood (50, 71). While a great deal is known about how model organisms such as bacteria, yeast, and mammalian cells sense the intra- and extracellular milieu (often through cell surface receptors engaged in various signal transduction pathways (192)), there is no defined pathway for how kinetoplastid protozoa respond to any environmental stimulus. The leishmanial genome, although rich in kinase-like sequences, lacks canonical orthologs for both G protein-coupled receptors and receptor tyrosine kinases, and the classical signaling pathways present in higher Eukarya are either absent or undefined in the parasite (48, 99). Hence, understanding environmental sensing is a major frontier in the biology of kinetoplastid protozoa.

To elucidate nutrient stress response pathways in *L. donovani*, we have used purine starvation as the paradigm. *Leishmania*, like other parasitic protozoa, cannot synthesize the purine ring *de novo* and must scavenge purine metabolites from the extracellular milieu supplied by the host. Distinct metabolic changes are observed in *L. donovani* promastigotes 24–48 h after purines are removed from the growth medium (16, 52). Parasites starved for purines growth arrest, accumulate in the G_1/G_0 phase of the cell cycle, and persist without the provision of extracellular purines for more than 3 months in culture, indicating that absence of an extracellular purine source promotes entrance of these parasites into a quiescent-like state (52). Within hours of purine removal from the culture medium, *L. donovani* promastigotes upregulate key components of the

purine salvage pathway that enhance purine acquisition, including the nucleoside transporters **LdNT1** and **LdNT2**, the nucleobase transporter **LdNT3**, cell surface 3'-nucleotidase/nucleases (**3'NT/NU**) and membrane-bound acid phosphatases (**MAP2**), as well as the primary purine salvage enzymes hypoxanthine-guanine phosphoribosyltransferase (**HGPRT**) and xanthine phosphoribosyltransferase (**XPRT**). While our previous studies profiling the proteome and transcriptome of purine-starved parasites have provided an in-depth view of adaptation to purine starvation in *L. donovani* (16), the underlying molecular mechanisms that orchestrate this response have yet to be defined.

Purine salvage and interconversion in *Leishmania* is both complex and redundant (193) and wild type parasites can utilize any one of a multitude of naturally occurring purines for their survival. To test the hypothesis that purine sensing occurs through perturbations in intracellular purine pools (since canonical cell-surface signaling relays appear absent), a series of purine pathway mutants with defined purine growth requirements were used to conditionally perturb adenosine monophosphate (**AMP**) or guanosine monophosphate (**GMP**) production (**Fig. 3.1**). These mutant cell lines were exposed to high levels of various extracellular purines that cannot assimilate into either AMP or GMP, or their respective downstream metabolites, and, as a consequence, these parasites growth arrested after 48 h. We found that culturing purine pathway mutants in an extracellular purine source that is non-permissive for growth resulted in the upregulation of proteins and genes consistent with the phenotype observed when wild type *Leishmania* are purine starved (16, 52); with

one caveat, the degree of upregulation and long-term survival was specific to the intracellular purine nucleotide pool perturbed. Further investigation revealed that perturbation of intracellular AMP and its downstream metabolites are necessary for robust adaptation to and long-term survival during purine scarcity. We conclude that sensing of the available purine environment arises from surveillance of intracellular purine pools, and in particular it is the perturbation of adenylate nucleotides that triggers the adaptive response needed to survive long-term purine deprivation.

MATERIALS AND METHODS

Chemicals and reagents

SERUM PLUS™ was purchased from SAFC BioSciences/Sigma Aldrich (St.
Louis, MO, USA). Mini-PROTEAN TGX Precast Gels and nitrocellulose
membrane were procured from Bio-Rad (Hercules, CA, USA). Mouse
monoclonal anti-α-tubulin DM1A was purchased from EMD Biosciences (La
Jolla, CA, USA). Rabbit antisera against the *L. donovani* HGPRT and XPRT full-
length proteins have been previously described elsewhere (109, 194).
Biotinylated polyclonal goat anti-GFP antibody was obtained from Thermo-
Pierce. Secondary goat anti-rabbit IgG IRDye 800CW, goat anti-mouse IgG
IRDye 680, donkey anti-goat IgG IRDye 800CW, and Odyssey Blocking Buffer
were bought from LI-COR Biosciences (Lincoln, NE, USA). Streptavidin,
DyLight™ 800 conjugate was acquired from Thermo Scientific (Rockford, IL,
USA). The RNeasy Mini Kit was received from Qiagen (Valencia, CA, USA).
Additional qRT-PCR reagents were obtained from Applied Biosystems, Life
Technologies (Grand Island, NY, USA). All other reagents purchased were of the
highest grade possible.

Cell culture

Wild type *L. donovani* strain 1S2D parasites (172), specifically the visceralizing
clonal derivative LdBob (173), were used for these studies as well as for the
generation of the knock-out cell lines Δ*impdh* (195)*,* Δ*gmpr*, Δ*gmps*, Δ*aah*Δ*adss*
(196, 197)*,* Δ*ldnt1–4*, and Δ*gmpr*Δ*impdh.* (Note that details about the

constructions of the $\Delta ldnt1$–4, $\Delta gmpr$ and $\Delta gmpr\Delta impdh$ cell lines will be

described elsewhere, Carter *et al.* and Boitz *et al.* unpublished). Wild type,

$\Delta impdh$, $\Delta gmpr$, $\Delta gmps$, $\Delta aah\Delta adss$, $\Delta ldnt1$–4, and $\Delta gmpr\Delta impdh$ promastigotes

were routinely cultured at 26°C with 5% CO_2 in purine-replete (containing 100 µM

of specified purine) DME-L-Bob medium, described previously (52),

supplemented with 5% SERUM PLUS™ (Sigma-Aldrich). To satisfy the purine

requirements of the individual cell line, this medium was further supplemented

with 100 µM hypoxanthine (wild type, $\Delta ldnt1$–4, $\Delta gmpr$), xanthine ($\Delta impdh$),

guanine ($\Delta gmps$), adenine ($\Delta aah\Delta adss$), and 100 µM each of xanthine and

hypoxanthine ($\Delta gmpr\Delta impdh$).

<u>Purine starvation</u>

To elicit purine starvation, as described in (16, 52), logarithmically growing cells

were pelleted via centrifugation at 1,100 x *g* for 10 min at ambient temperature,

washed twice in an excess of DME-L-Bob medium without purine

supplementation, and resuspended in either purine-replete or purine-deficient

medium at a final density of 2 x 10^6 cells ml^{-1}. For those cells cultured in a purine

that is non-permissive for growth, essentially the same procedure was followed

with the exception that the cells were washed and resuspended in DME-L-Bob

medium supplemented with 100 µM of the non-permissive purine.

Growth curves

To assess the ability of wild type, Δ*impdh,* Δ*gmpr*, Δ*gmps*, Δ*aah*Δ*adss,* Δ*ldnt1–4*, and Δ*gmpr*Δ*impdh L. donovani* promastigotes to grow in each purine source tested, cells were seeded at 2 x 10^6 cells ml^{-1} in DME-L-Bob medium with 5% SERUM PLUS™ and 100 µM purine or in the absence of purine supplementation. Cells were incubated at 26°C with 5% CO_2, and the number of cells ml^{-1} enumerated with a Neubauer haemocytometer at 24, 48, 72, and 96 h.

Western blotting

At specific time points, ~1.0 x 10^8 purine-replete and purine-starved cells were collected by centrifugation at 1,100 x *g* for 5 min at ambient temperature, the majority of the supernatant was decanted, and the cell pellet was suspended in the small volume of remaining supernatant for transfer to a microcentrifuge tube. Samples were then pelleted at 16,100 x *g* speed for 30 s in a microcentrifuge and the cell pellets resuspended at a density of 4 x 10^5 cells $µl^{-1}$ in Bio-Rad 2X Laemmli sample buffer with 100 mM ß-mercaptoethanol. Cells were lysed by heating to 95 °C for 3 min, and lysates from 2 x 10^6 cells (5 µl of the 4 x 10^5 cells $µl^{-1}$ sample preparation) were fractionated by SDS-polyacrylamide gel electrophoresis on either 7.5 or 10% Bio-Rad Mini-PROTEAN TGX Precast Gels and transferred to a 0.2 µm nitrocellulose membrane by semi-dry transfer (using a Bio-Rad Trans-Blot® SD Semi-Dry Transfer Cell) for 36 min at 20V. Rabbit antisera against HGPRT and XPRT were used at 1:2,500 dilution, biotinylated polyclonal goat antisera against GFP and mouse antisera against α-tubulin was

used at a dilution of 1:10,000. The secondary goat anti-rabbit IgG IRDye 800CW

and goat anti-mouse IgG IRDye 680 were used at 1:5,000 dilution. All antibodies

were diluted in a 1:1 mixture of LI-COR Odyssey Blocking Buffer with phosphate

buffered saline containing 0.2% Tween® 20. Western blots were scanned for

infrared signal using the Odyssey Infrared Imaging System (LI-COR

Biosciences), and protein abundance fold changes calculations were based on

signal as determined via integrated intensity values (Image Studio Lite, LI-COR

Biosciences).

Statistical analysis

All statistical analyses were calculated using GraphPad Prism software version

6.0f. Two-way ANOVA was run with the goal of comparing each mean with every

other mean (e.g. purine source, time, or gene). Tukey's multiple comparison

correction was employed. Graphed data are the mean of at least two biological

replicates, unless otherwise indicated, and error bars depict standard deviation.

For simplicity only the statistical summary is graphically represented on each

graph, for individual comparisons see statistical summaries (Table S2).

Total RNA isolation and cDNA synthesis

Total RNA was isolated from 2 x 10^8 $\Delta gmpr\Delta impdh$ promastigotes cultured for

24 h in DME-L-Bob medium supplemented with 5% SERUM PLUS™ and one of

the following purine sources: 100 µM hypoxanthine and xanthine, 100 µM

hypoxanthine, 100 µM xanthine, or no purine using a Qiagen RNeasy Mini Kit

following the manufacturer's protocol. RNA was obtained from 2 x 10^8 Δ*gmps*

cells cultured in medium containing 100 μM guanine, 100 μM adenine, 100 μM

xanthine, or no purine. To remove any potentially contaminating genomic DNA,

purified RNA samples were treated with DNaseI using the Turbo DNA-*free* kit

(Ambion). A High Capacity cDNA Reverse Transcription kit was used for

synthesis of first strand cDNA using 2 μg of total RNA as per the manufacturer's

instructions.

qRT-PCR

A 20 μl reaction was set up containing 5 μl of the diluted cDNA reaction

equivalent to 20 ng of input RNA, 5 pmol primers (see Table S2), and 10 μl 2X

SYBR Select Master Mix (Applied Biosystems®). Reactions were run on an

ABI/Lifetech StepOne-Plus realtime PCR system under the following conditions:

50°C for 2 min and 95°C for 10 min, followed by 40 cycles of 95°C for 15 s and

60°C for 1 min. A final thermal dissociation analysis was performed for each

reaction to confirm that the PCR generated a single amplification product. The

relative abundance for target amplicons between purine-replete and purine-

starved samples was determined via the 2$^{-\Delta\Delta CT}$ method (188).

Determination of free intracellular proline in *Leishmania*

10^8 promastigotes were harvested at the specified time points and proline levels

determined using the method of Bates et al. (185) and our previous study (16).

Briefly, cells were washed in phosphate-buffered saline (PBS) and suspended in

20% trichloroacetic acid in PBS for 30 min on ice to precipitate proteins.
Following centrifugation at 10,000 x g for 30 min at 4°C, a 200 µl aliquot was
removed and mixed with 200 µl acid ninhydrin solution (0.25 g ninhydrin, 6 ml
glacial acetic acid, and 4 ml of 6 M phosphoric acid) and 200 µL glacial acetic
acid, and incubated at 100°C for 1 h. In parallel, a standard curve for L-proline (0
– 500 µM) was prepared. Samples were then placed on ice to stop the reaction
and the chromagen extracted into 400 µL toluene. 100 µL of each toluene extract
was used for quantitation in a 96 well quartz cuvette at 520 nm, using a
SpectraMax M2 Microplate Reader (MolecularDevices GmbH, Ismaning/Müchen,
Germany).

Nucleotide extraction

At specific time points, 2.0 x 10^8 cells were transferred to conical tubes and
rapidly quenched in an ethanol/dry ice bath for <20 s and immediately
centrifuged for 5 min at 1100 x g at ~2°C. The supernatant was aspirated and the
pellet suspended in 1 ml ice-cold PBS, then transferred to a pre-chilled
microcentrifuge tube and pelleted for 30 s at 20,937 x g at ~2°C. The PBS
supernatant was discarded and 200 µL ice-cold 0.5 M perchlorate was added
with rapid pipetting to suspend the pellet, 80 µL of 2 M potassium carbonate was
mixed thoroughly to neutralize pH and the samples then centrifuged for 5 min at
20,937 x g at ~2°C. The resultant supernatant was removed to new
microcentrifuge tube, flash frozen in liquid nitrogen, and stored at -80°C until
analysis.

Determination of relative intracellular nucleotide pools

Nucleotides present in acid extracts were separated by HPLC using solvents described by Stocchi et al. (198). The HPLC system was an Agilent 1100 quaternary system with column oven and diode array detector at 254 nm. Separation was performed on a Thermo Scientific Aquasil™ C18 HPLC column (150 x 3 mm inner diameter (I.D.), 5 µm particle size) with a 10 mm guard column with the same packing material and maintained at 35°C. The injection volume was 25 µl, and the autosampler was maintained at room temperature. The mobile phases consisted of solvent A: 0.1 M potassium phosphate, pH 6.0, containing 8 mM tetrabutylammonium hydrogen sulfate and solvent B: 0.1 M potassium phosphate, pH 6.0, containing 8 mM tetrabutylammonium hydrogen sulfate and 30% (v/v) of methanol. The following chromatographic conditions were used: flow rate was 1.0 ml ml^{-1}, 0 to 2.5 min, 0% B; 5 min 20% B; 13 min 40% B; 16-18 min 100% B; then returned to start conditions of 0% B for 7 min prior to the next injection. Instrument control, data acquisition and analysis were performed using Agilent ChemStation software. Peak identities were established by co-elution of nucleotide standards of known concentration.

RESULTS

The response to purine starvation is triggered by disruption of intracellular purine pools:

Little is known about environmental sensing in *Leishmania* or the intracellular

signaling mechanisms that orchestrate adaptation of the parasite to physiological

and nutritional environment fluctuations. To illuminate these processes, we have

used the response to purine starvation as our model because it is well defined

and can readily be induced by the removal of extracellular purines from the

culture medium. Previous studies in our laboratory indicated that purine

starvation in wild type cells leads to parasite growth arrest that was reversed

upon the reintroduction of an exogenous purine supplement. Moreover,

comparison of the proteomes of purine-starved versus purine-replete *Leishmania*

revealed extensive global proteome changes, including the upregulation of key

purine salvage enzymes such as HGPRT and XPRT and the inosine-guanosine

nucleoside transporter LdNT2 (16, 52). While these changes were induced by the

removal of exogenous purines from the medium, we were curious whether a

similar purine starvation phenotype could be elicited in *Leishmania* when a non-

growth supporting purine was the sole purine in the culture medium. Due to a

robust purine salvage and interconversion pathway (**Fig. 3.1A**) wild type

Leishmania are able to utilize any naturally occurring purine source to fulfill their

purine nucleotide requirements for growth. Thus, we employed a battery of

mutant cell lines that harbor defined lesions within the purine pathway and, as a

consequence, require the addition of specific purines to enable their growth. The

response to purine restriction was investigated in these mutant cell lines in the presence of various growth-permissive and growth-restrictive purine supplements by using the metric of XPRT protein upregulation (**Table 3.1**). As observed previously, wild type cells in the absence of an exogenous purine supplement became growth arrested between 24 and 48 h, and XPRT protein levels were augmented at 24 and 48 h (**Table 3.1**). Similarly, all of the purine pathway mutants listed in Table 1 growth arrested by 24–48 h when cultured with either no extracellular purine source or a non-permissive purine source (**Figs. 3.2A** and **B.1**) and, in the majority of cases, exhibited upregulation of XPRT protein after 48 h (**Table 3.1** and **Figs. 3.2B** and **B.2**). These data confirm that a purine starvation response can also be elicited in the presence of an extracellular purine source that is non-permissive for growth and imply that disruption of intracellular purine homeostasis, rather than direct sensing of extracellular purine abundance, is a key trigger for adaptation to purine stress.

Differential response of intracellular purine salvage enzymes to purine pathway perturbations:

Significantly, incubation of Δ*impdh*, Δ*gmpr*Δ*impdh*, or Δ*gmps* cells in an exogenous purine supplement that is predicted to fulfill the cellular requirement for AMP, but not for GMP (see **Figs. 3.1B** and **3.1C** for the proposed purine salvage and nucleotide interconversion pathways for the Δ*gmpr*Δ*impdh* mutant), failed to provoke a discernible upregulation in XPRT protein levels even after 48 h (**Table 3.1** and **Figs. 3.2B** and **B.2**, teal bars), even though these cells were

98

growth arrested by ~24 h (**Figs. 3.2A** and **B.1**). XPRT protein was, however, upregulated in these cells when AMP (Δ*gmpr*Δ*impdh* cells in presence of xanthine alone), or both AMP and GMP (Δ*impdh*, Δ*gmpr*Δ*impdh*, or Δ*gmps* cells in absence of purine supplementation) production was predicted to be compromised (**Table 3.1** and **Figs. 3.2B** and **B.2, purple** and **gray bars**), indicating that the overall effect of these mutations was not to incapacitate the purine starvation response in these cells, and significantly, that the responses observed were not an artifact of introducing the GMPR and IMPDH lesions.

Because the Δ*gmpr*Δ*impdh* cell line afforded the opportunity to perturb AMP and GMP synthesis separately, but within the same genetic background (see **Fig. 3.1B** and **3.1C**), we focused on this cell line to further investigate whether a differential response to purine starvation could be elicited when GMP, but not AMP, synthesis was perturbed. Thus, to determine whether the differential response in XPRT protein upregulation could be extended to other previously identified benchmarks of purine starvation (16, 52) Δ*gmpr*Δ*impdh* cells were cultured in xanthine, hypoxanthine, or in the absence of an extracellular purine source (**Fig. 3.1B** and **3.1C**), and the protein abundance for HGPRT (**Fig. 3.2C**) and the inosine-guanosine transporter, LdNT2, tagged at the N-terminus with Green Fluorescent Protein (**GFP-LdNT2**) (**Fig. 3.2D**), were monitored by western blot analysis. As previously observed, HGPRT protein was modestly upregulated in wild type cells during purine starvation. For the Δ*gmpr*Δ*impdh* cell line, changes in HGPRT protein levels were minor after 24 h of purine starvation under all the conditions assayed. However, HGPRT abundance was increased

after 48 h in xanthine, as well as in the absence of purine supplementation (3.5 and 4-fold, **Fig. 3.2C** teal and gray bars, respectively), but no change in protein abundance was evident after incubation in hypoxanthine (**Fig. 3.2C,** purple bars). Interestingly, GFP-LdNT2 showed a 2-fold increase in abundance within the Δ*gmpr*Δ*impdh* cell line under all of the assayed conditions after 6 h, but further upregulation of this protein at 24 and 48 h only occurred in the xanthine and no purine condition (**Fig. 3.2D**). This emphasizes the complexity of the response, signified by an early phase that is independent of the extracellular purine restriction and a later phase specific to AMP branch perturbations.

Differential effect of purine pathway perturbations on intracellular proline levels:

From our previous analyses of wild type *L. donovani*, we noted that proline, a key stress response metabolite (70, 125, 129), was elevated in purine-starved cells (16). We were interested as to whether a similar response might also be induced within the Δ*gmpr*Δ*impdh* cell line and whether perturbation of AMP or GMP production might affect a differential response. Δ*gmpr*Δ*impdh* cells showed minimal change in proline abundance in any purine condition after 24 h; however, a 3.5-fold upregulation of intracellular proline was observed when Δ*gmpr*Δ*impdh* cells were incubated in the absence of purine for 48 h (**Fig. 3.3**). Likewise, Δ*gmpr*Δ*impdh* cells cultured in the presence of xanthine showed a similar response (2.7-fold increase) after 48 h. In contrast, proline levels in Δ*gmpr*Δ*impdh* cells incubated in the presence of hypoxanthine were not

demonstrably altered. Note that a similar differential response in intracellular

proline accumulation was also observed for the Δ*gmps* cell line (**Fig**. **B.3**).

Together these data indicate that proline only accumulates under conditions

where AMP production is compromised and provides further evidence for a

causal link between disruption of adenine nucleotide homeostasis and adaptation

to purine starvation.

Differential response to purine pathway perturbations of purine-regulated

mRNAs:

We have previously shown that adaptation to purine scarcity in *Leishmania* also

induces changes at the mRNA level, some of which likely facilitate proteome

remodeling and cell survival during prolonged purine starvation (16, 52). To

ascertain whether perturbations in AMP or GMP production in Δ*gmpr*Δ*impdh*

cells induce differential responses at the mRNA level, we quantified a subset of

purine-responsive candidates, for which a response at the mRNA level had

previously been established by both qRT-PCR and RNA-seq analyses (16).

Removal of purine supplements from the culture medium for 24 h (a condition in

which both AMP and GMP production is anticipated to be perturbed) resulted in

the upregulation of mRNAs corresponding to *LdNT1.1*, *LdNT3*, *XPRT*, *MAP2-*

Chr36, *3'NT/NU-Chr12*, *3'NT/NU-Chr31*, *AAT19*, and a putative oxidoreductase

(**Fig. 3.4**, gray bars), though the observed increase in *LdNT1.1* mRNA was quite

modest. Incubation of Δ*gmpr*Δ*impdh* cells in xanthine for 24 h, a condition in

which only AMP synthesis is expected to be perturbed, led to similar increases at

the mRNA level for *XPRT*, *3'NT/NU-Chr31*, and the putative oxidoreductase; even more pronounced increases were measured for *MAP2-Chr36*, *3'NT/NU-Chr12*, *AAT19* (**Fig. 3.4**, teal bars), with the level of *3'NT/NU-Chr12* mRNA upregulated ~2.5 fold more than in cells cultured in medium containing no purine supplement. In contrast, the cultivation of Δ*gmpr*Δ*impdh* parasites in hypoxanthine for 24 h, a condition in which disruption of only GMP is predicted, resulted in a much smaller increase at the mRNA level for *MAP2-Chr36*, *3'NT/NU-Chr31*, *AAT19*, and the putative oxidoreductase, and no significant increase for *XPRT* and *3'NT/NU-Chr12* (**Fig. 3.4**, purple bars). By comparison, the abundance for *LdNT1.1*, *LdNT2,* and *LdNT3* mRNA was almost equivalent for Δ*gmpr*Δ*impdh* cells cultured in hypoxanthine, xanthine, or without purine supplementation. Regardless of the extracellular purine restriction, the *LdNT1.1* transcript level was only modestly upregulated, whereas the level of *LdNT2* mRNA was unchanged. *LdNT3* mRNA was increased ~3-fold for Δ*gmpr*Δ*impdh* cells cultured in hypoxanthine or xanthine, and was slightly more augmented in the absence of purines (~5.4 fold). These data are in agreement with our previous data for purine-starved wild type cells (16) and intimate that disruption of intracellular adenine nucleotide pools is a key progenitor for effecting adaptive changes at the mRNA level.

Measurement of adenine and guanine nucleotide pools in differentially

starved parasites:

Previous studies in our laboratory delineated the purine requirements for the

growth of various purine pathway mutants (196, 197, 199, 200). Based on these

data, we were able to predict with relative confidence the effects of different

purine supplements on AMP and GMP production and thus, disruption of

intracellular purine nucleotide homeostasis (**Table 3.1** and **Fig. 3.1**). However, it

was still important to confirm these predictions within the Δ*gmpr*Δ*impdh* cell line

by direct means, as well as measure the precise effect of the conditional purine

starvation conditions upon the adenine- and guanine-containing nucleotide pools.

Thus, a high-performance liquid chromatography (**HPLC**) method was employed

to empirically determine relative intracellular purine nucleotide abundance

changes. To begin, we established that wild type and Δ*gmpr*Δ*impdh* purine

nucleotide pools were virtually identical under purine-replete conditions (100 μM

each hypoxanthine and xanthine). Removal of purines from wild type cells

caused a precipitous decrease in ATP and ADP levels by 24 h, which persisted

throughout the 120 h time-course (**Fig. 3.5A**). AMP and GDP levels were also

decreased at 24 h but recovered to near-replete levels by 120 h (**Fig. 3.5A**). In

contrast, GTP and GMP levels were not reduced in purine-starved wild type cells

and increased by >2-fold by 120 h (**Fig. 3.5A**). AMP, ADP and ATP levels in

Δ*gmpr*Δ*impdh* cells cultured in xanthine or no purine exhibited a trend similar to

purine-starved wild type parasites (**Fig. 3.5B, middle** and **right panels**). As

expected, GMP, GDP, and GTP levels were not decreased in those

ΔgmprΔimpdh cells cultured in xanthine, while *ΔgmprΔimpdh* cells incubated in the absence of purine showed a similar trend to that of purine-starved wild type cells, although GTP was initially reduced at 24 h (**Fig. 3.5C, middle** and **right panels**). In contrast, intracellular ATP, AMP, GTP, GDP, and GMP levels did not decrease in *ΔgmprΔimpdh* cells cultured in hypoxanthine, and only a slight decrease in ADP levels was observed after 120 h (**Fig. 3.5B** and **C, left panels**). These data confirm that adenine nucleotide homeostasis is perturbed in purine-starved wild type cells and *ΔgmprΔimpdh* cells cultured in xanthine or in the absence of purine. In contrast, no perturbation is apparent in *ΔgmprΔimpdh* cells cultured in hypoxanthine. Thus, these data corroborate a purine-sensing mechanism based upon surveillance of intracellular adenine nucleotide pools.

Purine pathway perturbations impact the long-term survival of Leishmania during purine starvation:

Collectively, our data suggest that perturbation of adenine nucleotide synthesis is required for a complete and robust response to purine restriction, at least at the protein and mRNA level. We were intrigued as to whether perturbation of adenine nucleotide synthesis might also impact long-term cell survival during purine restriction. Although wild type cells growth arrest after purine is removed from the culture medium, they are able to survive prolonged bouts of purine starvation with little loss in cell number. Note that the reintroduction of a purine supplement to a population of wild type purine-starved cells anytime during the 90 day time period reversed the growth arrest and induced parasite growth. A similar phenotype was also observed for *ΔgmprΔimpdh* cells cultured in the

absence of purines or in the presence of xanthine for 90 days (**Fig. 3.6A**)—

conditions in which the synthesis of adenine nucleotides is disrupted (see **Fig.**

3.5B). Strikingly, prolonged incubation of the Δ*gmpr*Δ*impdh* in hypoxanthine as

the sole purine source led to a gradual decrease in cell number, which became

apparent at 5 days and was accompanied by changes in cell morphology (**Fig**

3.6B). A precipitous drop in cell number was subsequently observed between

days 10–31 (**Fig. 3.6A**). Indeed, no cells could be detected or rescued from

these cultures after 31 days. A similar differential survival phenotype was also

observed for the Δ*impdh* and Δ*gmps* cell lines, where long-term survival was

observed only in conditions predicted to perturb adenine-containing nucleotides

(**Table 3.1**). These findings suggest that perturbation of adenine nucleotide

synthesis is a likely progenitor of the signaling and metabolic responses required

for the long-term survival of purine starvation in these parasites.

Effect of purine pathway perturbations on the cell cycle:

While all cells grown under purine-restricted conditions growth arrest between

24–48 h (**Figs. 3.2A** and **B.1**), only those in which adenine nucleotide production

is impinged are able to survive over prolonged periods (**Table 3.1** and **Fig. 3.6**).

Previously, we have demonstrated that purine-starved wild type *Leishmania*

accumulate in G_1/G_0 phase of the cell cycle (52), and we surmise that the long-

term survival of these cells during purine starvation is likely due to exit from the

cell cycle. Thus, cell cycle analysis was undertaken on Δ*gmpr*Δ*impdh* cells

cultured in hypoxanthine, xanthine, or without purine to determine if a similar

accumulation in G_1/G_0 phase was apparent (**Fig. 3.7**). For $\Delta gmpr\Delta impdh$ cells in

the presence of xanthine or with no purine, conditions under which they are able

to persist for > 90 days (**Fig. 3.6A**), the bulk of the population was detected in

G_1/G_0 phase over the 8-day time course, with fewer than 25% of the cells

detected in either S or G_2/M phase (**Fig. 3.7A**). $\Delta gmpr\Delta impdh$ cells cultured in

hypoxanthine over the first 24 h showed a similar distribution between G_1/G_0

phase and S or G_2/M phase, but with prolonged incubation in hypoxanthine,

more cells (>35%) were detected in S and G_2/M with a concomitant decrease of

cells detected in G_1/G_0 (**Fig. 3.7B**), implying that these cells are either in the

process of or have completed DNA replication. We hypothesize that cells that

have stopped dividing and persist in G_1/G_0 phase are in a quiescent-like state

that aids in the parasite's survival during purine starvation and other

environmental insults (16, 151, 201, 202). Therefore, the failure of $\Delta gmpr\Delta impdh$

cells cultured in hypoxanthine to persist in the G_1/G_0 phase of cell cycle may

underlie their inability to survive purine limitation long-term.

DISCUSSION

Leishmania, like other parasitic protozoa, are completely dependent on their host environment for the continuous supply of a variety of essential nutrients and precursor metabolites needed to sustain their growth and viability. Since these unicellular pathogens have a limited capacity to store nutrients, their survival during times of nutrient scarcity is dependent upon an innate ability to sense and adapt rapidly to changes in nutrient availability both in the extracellular and intracellular milieus. To decipher the molecular programs that underlie adaption to nutrient stress in *Leishmania*, we have used induction of purine starvation as a paradigm (16, 52). Previous work in our laboratory demonstrated a robust adaptive response to purine starvation *in vitro* that resulted in proteome remodeling (52) and encompassed changes in both parasite morphology and metabolism. Purine-starved parasites appear to minimize intracellular ATP consumption by halting DNA replication, as evidenced by arrest in G_1/G_0 phase of the cell cycle, and decreasing the overall rate of protein synthesis. Despite being growth arrested, purine-starved cells remained metabolically active, and even augmented several metabolic processes, including purine acquisition and oxidant defense strategies (16, 52).

In this manuscript, we have parlayed these previous observations on the biological response to purine starvation to investigate the mechanism by which *Leishmania* sense extracellular purine availability. An array of purine pathway mutants, each of which harbor specialized purine requirements for growth, was cultured in various purine sources that restrict their growth and monitored for a

biological response to purine starvation. Growth arrest was observed after ~24 h for all cell lines when they were cultured in the presence of a growth-restricting purine source, as well as in the absence of any purine supplementation (**Table 3.1** and **Figs. 3.2A** and **B.1**). However, the induction of a robust response to purine starvation, including the ability to persist past ~30 days in culture, was only observed when manipulation of the purine content of the culture medium was projected to perturb intracellular adenine nucleotide pools (see **Table 3.1** and **Figs. 3.1–4**, and **3.6–7**). This observation was subsequently confirmed by HPLC analysis of the intracellular purine nucleotide content of purine-starved wild type cells cultured in the absence of any extracellular purines, as well as in *ΔgmprΔimpdh* cells differentially purine starved in the presence of either hypoxanthine or xanthine, as well as in the absence of a purine source (**Fig. 3.5**). These data suggest that diminished intracellular adenine nucleotide pools are one of the prompts for the molecular program that results in adaptation to and survival of prolonged purine starvation, and that *Leishmania*, and likely other related parasites, have evolved a purine-sensing mechanism that is predicated on intracellular adenine nucleotide pool surveillance, rather than direct sampling of the extracellular purine milieu. Mechanistically, this may involve sensing of adenine nucleotide levels directly and/or monitoring of the relative ratios between adenine and guanine nucleotide pools, the later of which remained near or above normal in the *ΔgmprΔimpdh* cells regardless of the extracellular purine source (**Fig. 3.5**).

The reliance of these parasites on the host environment for the provision of a diverse array of essential nutrients, combined with the absence of much of the canonical cell surface sensing machinery described in yeast and higher eukaryotes, support the possibility that the surveillance of intracellular metabolite pools may be a key feature of their nutrient sensing. This supposition is bolstered by a previous study in *L. amazonensis* in which AAP3 arginine transporter mRNA levels were linked to changes in intracellular arginine (203).

Moreover, G protein-coupled receptors (and their heterotrimeric G proteins) and receptor tyrosine kinases that coordinate direct interactions with extracellular ligands, have not been identified in the available genome data for *Leishmania* and related parasites (14, 15, 48, 50, 99, 204). Likewise, although *Leishmania* possess a variety of plasma membrane nutrient permeases (74, 205), none of them have been shown to function as transmembrane receptors (transceptors) as described in yeast (206, 207). Considering wild type *Leishmania* can thrive on any naturally occurring purine nucleobase or nucleoside, the specific purine composition of the extracellular environment is irrelevant, eliminating the benefit of monitoring individual purines at the cell surface. Moreover, our studies employing purine pathway mutants in which a purine starvation response was elicited in each purine nucleobase or nucleoside exclude the possibility of sensing through a universal purine receptor (**Table 3.1**). It should be noted that *Leishmania*, as well as other trypanosomatids, harbor a large family of transmembrane receptor-like adenylate cyclases within the genome that are capable of transducing a response to an extracellular stimulus through the

intracellular conversion of ATP to cAMP (49, 208-210). However, the ligand repertoire for this family remains obscure and a role in nutrient sensing has yet to be revealed.

Even though the signaling pathways responsible for relaying the metabolic changes needed to combat perturbation of intracellular adenine nucleotide levels still need to be delineated, one obvious candidate that is known to be sensitive to adenine nucleotide levels that is worthy of future evaluation is AMP-activated protein kinase (**AMPK**). AMPK acts as a cellular energy sensor, directing widespread metabolic adaptation to ensure continued cell growth and/or survival during times of starvation (211, 212). AMPK is activated in response to rising cellular AMP and ADP levels that result from the increased consumption of cellular ATP and functions to restore energy homeostasis by promoting the activity or expression of proteins favoring ATP production and by switching off biosynthetic pathways that consume ATP. AMPK is a heterotrimeric complex that is composed of a single catalytic α subunit comprising Ser/Thr kinase activity, one scaffolding β subunit, and one regulatory γ subunit that contains four cystathionine-beta-synthase (**CBS**) domains — domains that have been implicated in the regulation of AMPK activity due to their conformational change upon the binding of either AMP and ADP (activating) or ATP (inactivating) (213). The existence of AMPK and conservation of its function is nearly universal in all eukaryotes (212), and it appears that *Leishmania* is no exception as the genome harbors two putative orthologs for the α catalytic subunit (LdBPK_292140.1;

110

LdBPK_360960.1), as well as single β (LdBPK_230530.1) and γ (LdBPK_350780.1) subunits.

Whether AMPK is involved in the response to purine stress remains to be established. However, in the case of both purine-starved wild type cells, as well as in the *ΔgmprΔimpdh* cells incubated in xanthine or no purine, the increased ratio between AMP and ATP after 120 h of purine starvation would be expected to activate AMPK, suggesting that AMPK may be important for adaptation to prolonged purine starvation (**Figs. 3.5A** and **B**). In contrast, while the overall levels of adenine nucleotides decrease over the first 72 h of purine starvation, the adenylate charge is essentially unchanged, which is inconsistent with AMPK signaling during the early response to purine scarcity. However, it is possible that the earliest changes in adenine nucleotide abundance and ratios are confined to specific cellular domains or compartments. These changes may have been too subtle to be detected via our measurement of global nucleotide pools but may be readily detectable by AMPK and/or other unknown, compartment-specific sensors in the cell. The concept of compartmentalized adenine nucleotide pools is supported by the fact that kinetoplastid parasites encode a number of adenylate kinase (**ADK**) isoforms that are targeted to various net energy-producing (mitochondrion, glycosome) or net energy-consuming (flagella, nucleus, cytosol) subcellular compartments (111). ADK catalyzes the interconversion of ATP and AMP with ADP and, in addition to AMPK, plays a key role in the maintenance of cellular energy homeostasis. The differential localization of ADK isoforms may provide a means of accommodating

compartment-specific energy demands. Our previous proteome analyses, which measured temporal changes in protein abundance, found that 3 out of 5 leishmanial ADK isoforms were altered in purine-starved cells, some as early as 6 h (16). The change in ADK expression depended on the predicted localization of the isoform – ADKB (LdBPK_211490.1), which has a flagellar location in *T. brucei* (111) and ADKC (LdBPK_340130.1) were significantly upregulated after 24 h in purine-starved cells, whereas ADKD (LdBPK_361410.1), which contains a glycosomal targeting sequence in *Leishmania* and has been localized to the glycosome in *T. brucei* (111, 214), was downregulated after 6 h of purine starvation (16). This compartment-specific regulation of ADK isoforms lends credence to the notion of localized changes to adenine nucleotide pools in purine-starved cells.

It is likely that other signaling responses, distinct from AMPK, are also involved in directing the metabolic reprogramming that accompanies adaptation to purine stress. This supposition is supported by our previous global analyses on purine stressed cells, which demonstrated that proteome remodeling occurs in distinct temporal phases (16). The results detailed in this manuscript also support a complex, hierarchical signaling response. While Δ*gmpr*Δ*impdh* cells cultured in hypoxanthine, xanthine, or in the absence of purine, augment GFP-LdNT2 protein to a similar degree after 6 h, by 24 h the level of augmented GFP-LdNT2 protein diverges depending on the purine restriction (**Fig. 3.2D**). Likewise, the response observed at the mRNA level suggests that regulation is complex and

likely governed by multiple signals since some mRNAs are augmented regardless of the purine constraint (**Fig. 3.5**).

The work described herein has also highlighted the utility of metabolic mutants, such as the $\Delta gmpr\Delta impdh$ cell line, for dissecting the molecular response to purine starvation in *Leishmania*. In particular, this mutant provides a remarkable opportunity to identify changes in mRNA and protein abundance that contribute to the prolonged survival of these cells under purine limitation. This can be further explored by dissecting the molecular mechanisms that regulate the changes in mRNA and protein abundances, including *cis* and *trans*-acting factors, as well as translational and post-translational mechanisms affecting protein synthesis or stability. That a differential survival phenotype can be elicited by altering the purine content of the extracellular medium obviates the need for comparison with additional cell lines and eliminates cell line to cell line variability. Moreover, the fact that $\Delta gmpr\Delta impdh$ cells starved in hypoxanthine initially appear to stall in G_1/G_0 phase of the cell cycle and subsequently progress into G_2/M phase, which closely parallels their demise in culture, may enable exploration of the metabolic changes and signaling responses associated with entrance into and exit from cell quiescence. This work has also highlighted the tractability of *Leishmania* to both culture medium and genetic manipulation, which will provide a facile model in the future for the testing of key candidates identified in the response to purine stress, as well as in the response to other nutrient restrictions and microenvironmental stress.

In summary, these studies build upon our previous global analyses describing the molecular response to purine stress (16), and led us to propose a plausible nutrient-sensing mechanism in which the response to extracellular purine scarcity is, at least in part, mediated through internal adenine nucleotide pool perturbations. This research also provides the basis for future examination of the signaling pathways triggered by both local and global purine perturbation, which ultimately should reveal key candidates and signaling pathways involved in cell survival during times of nutrient paucity.

Cell line	Extracellular purine	Intracellular perturbation	XPRT protein abundance (48 h)	Long-term survival
Δaah Δadss	hypoxanthine	AMP	increased	yes
	xanthine	AMP	increased	yes
	no purine	AMP + GMP	increased	yes
Δgmpr	xanthine	AMP	increased	yes
	no purine	AMP + GMP	increased	yes
Δimpdh	**hypoxanthine**	**GMP**	**not increased**	**no**
	no purine	AMP + GMP	increased	yes
Δgmpr Δimpdh	**hypoxanthine**	**GMP**	**not increased**	**no**
	xanthine	AMP	increased	yes
	no purine	AMP + GMP	increased	yes
Δgmps	**adenine**	**GMP**	**not increased**	**no**
	xanthine	AMP + GMP	increased	yes
	no purine	AMP + GMP	increased	yes
Δldnt1-4	adenosine	AMP + GMP	increased	yes
	adenosine + EHNA	AMP + GMP	increased	yes
	inosine	AMP + GMP	increased	yes
	guanosine	AMP + GMP	increased	yes
	no purine	AMP + GMP	increased	yes

Table 3.1. Summary of XPRT protein abundance changes and long-term survival of
Leishmania **purine pathway mutants as a function of predicted intracellular purine**
perturbation.

For each purine pathway mutant the extracellular purine source and predicted
intracellular purine perturbation are indicated. The experimental results for
changes in XPRT protein abundance after 48 h and long-term survival (see
Materials and Methods for method information) are shown in the two rightmost
columns. Bold text indicates conditions in which the cells do not survive long
term. Δ*ldnt1–4* is a purine nucleoside and nucleobase transport null mutant with
residual purine nucleobase uptake capacity allowing for growth.

.
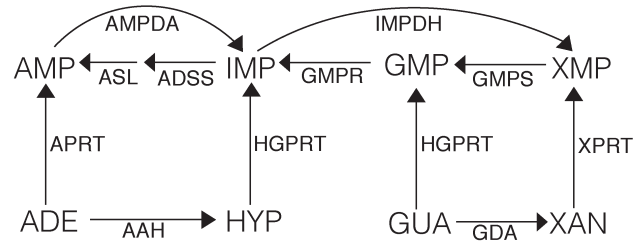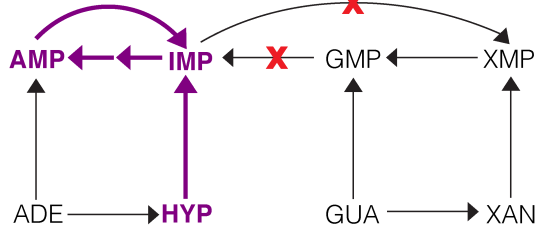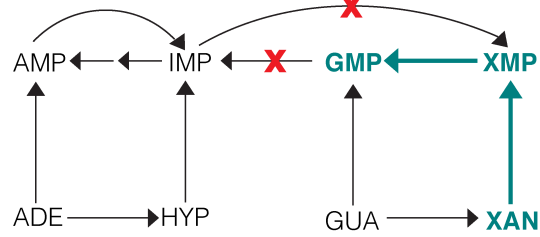
Figure 3.1 Predicted purine nucleotide synthesis pathways for wild type and ∆*gmpr*∆*impdh L. donovani*.

For simplicity, the salvage of purine nucleosides is not depicted. (A) Wild type *L. donovani* can convert any of the four naturally occurring nucleobases (adenine, xanthine, guanine, hypoxanthine) to GMP and AMP to fulfill their nucleotide requirements for growth. (B and C) Red Xs denote absence of GMPR and IMPDH enzyme activity due to gene knockout, (B) AMP production is denoted in purple; ∆*gmpr*∆*impdh* cultured in hypoxanthine (or adenine) can only produce AMP; GMP production is perturbed, (C) GMP production is denoted in teal; ∆*gmpr*∆*impdh* cultured in xanthine (or guanine) can only produce GMP; AMP production is perturbed. Abbreviations: AMP, adenosine 5'-monophosphate; GMP, guanosine 5'-monophosphate; IMP, inosine 5'-monophosphate; XMP, xanthosine 5'-monophosphate; ADE, adenine; GUA, guanine; HYP, hypoxanthine; XAN, xanthine; AAH, adenine aminohydrolase; ADSS, adenylosuccinate synthetase; AMPDA, AMP deaminase; APRT, adenine phosphoribosyltransferase; ASL, adenylosuccinate lyase; GDA, guanine deaminase; GMPR, GMP reductase; GMPS, GMP synthase; HGPRT, hypoxanthine-guanine phosphoribosyltransferase; IMPDH, IMP dehydrogenase; XPRT, xanthine phosphoribosyltransferase.
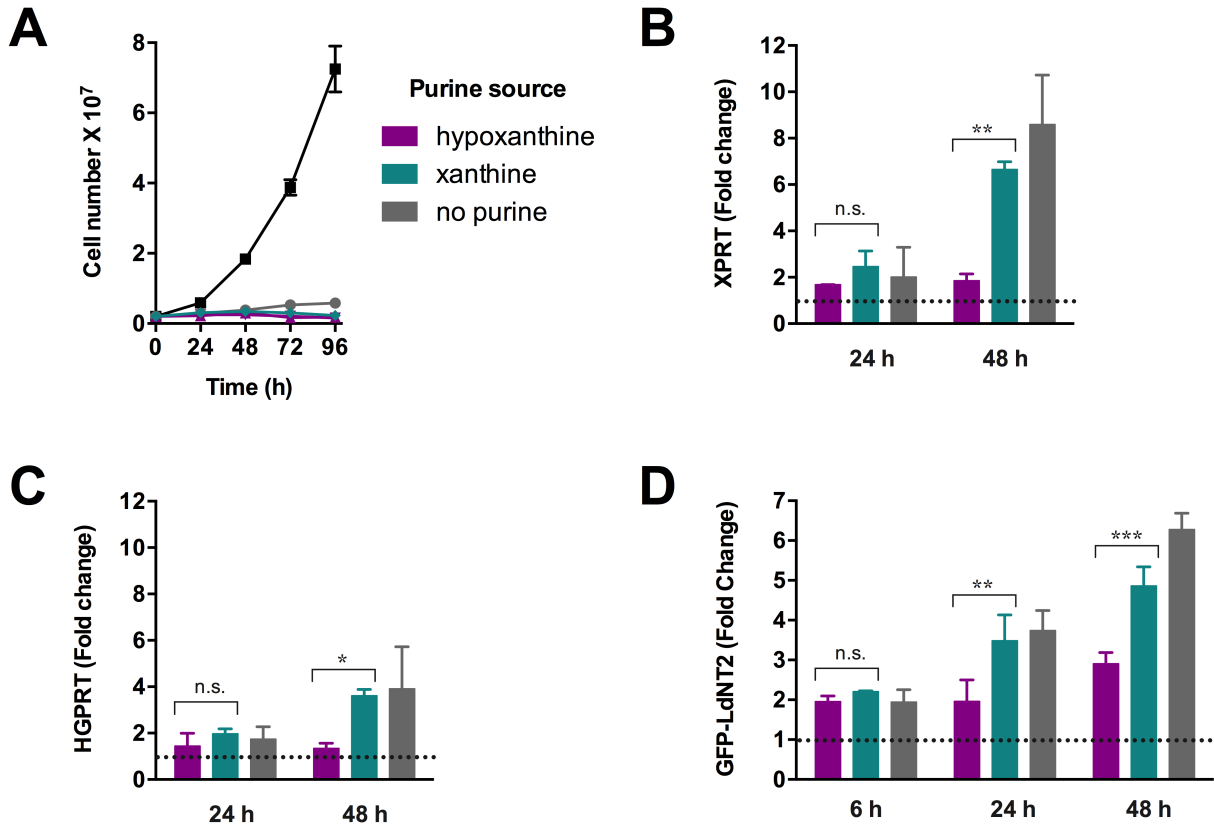
Figure 3.2 Effect of purine limitation on the growth phenotype and abundance of XPRT, HGPRT, and GFP-LdNT2 proteins.

Δ*gmpr*Δ*impdh* promastigotes were cultured in an extracellular purine source that can be assimilated into both AMP and GMP (black), into AMP but not GMP (purple), into GMP but not AMP (teal), or in the absence of purine (gray). (**A**) Growth was evaluated for each cell line as described in *Materials and Methods*. XPRT (**B**), HGPRT (**C**), protein abundance levels at 24 and 48 h were determined via anti-XPRT or anti-HGPRT western blotting as described in *Materials and Methods.* GFP-LdNT2 (**D**) protein abundance was determined at 6, 24, and 48 h using anti-GFP western blotting as an antibody against LdNT2 is unavailable. In all cases, tubulin was used as a loading control and fold changes are compared to the permissive condition for which the value was normalized to 1 (indicated by the dotted line). Ordinary two-way ANOVA calculated using GraphPad Prism; n.s. – non-significant, p-value (p) > 0.05; * p ≤ 0.05; ** p ≤ 0.01; *** p ≤ 0.001; **** p ≤ 0.0001; see *Materials and Methods* for more information.
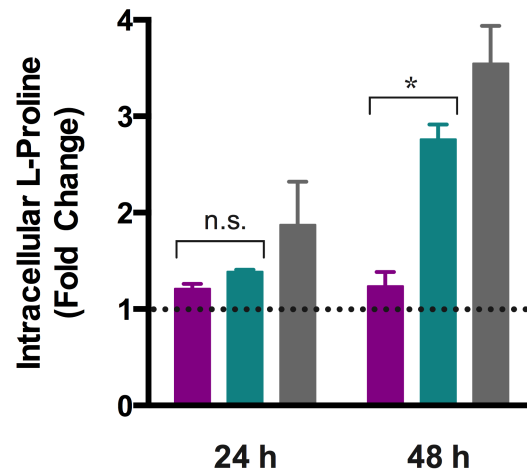
Figure 3.3 Changes in intracellular proline due to purine limitation.
Changes in free intracellular L-proline were determined for Δ*gmpr*Δ*impdh* promastigotes cultured in an extracellular purine source that is permissive for growth (set to 1, dashed line), predicted to perturb the guanylate branch (purple), adenylate branch (teal), or both (gray); fold changes were determined by comparing to the permissive condition. Ordinary two-way ANOVA calculated using GraphPad Prism; n.s. – non-significant, $p > 0.05$; * $p \leq 0.05$; ** $p \leq 0.01$; *** $p \leq 0.001$; **** $p \leq 0.0001$; see *Materials and Methods* for more information.
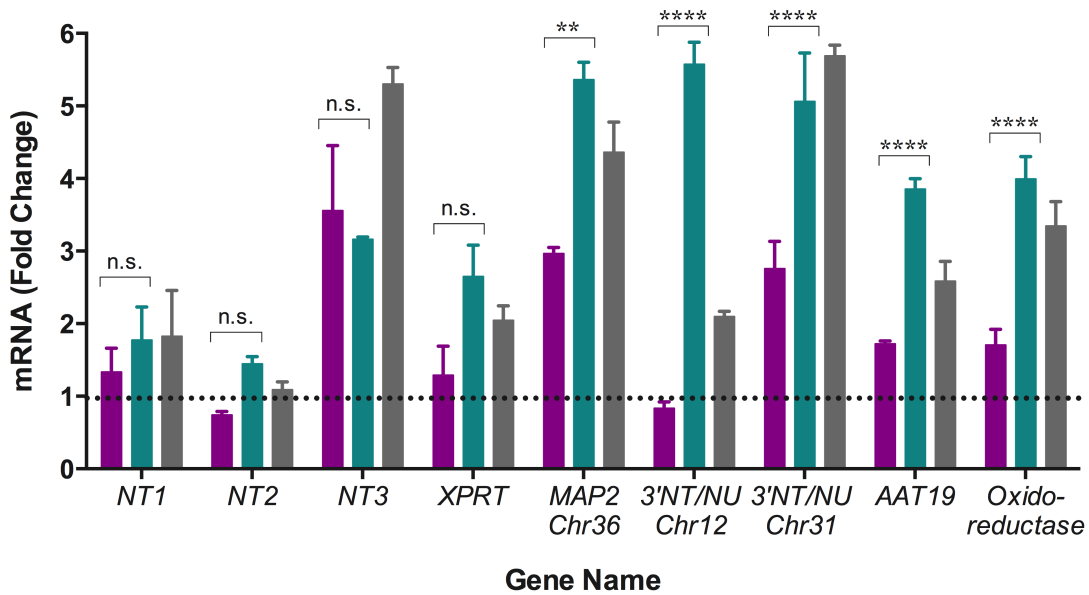
Figure 3.4 Changes in mRNA expression levels for a subset of genes as a result of purine pool perturbations.

ΔgmprΔimpdh promastigotes were cultured in an extracellular purine source that is permissive for growth (normalized to 1, dashed line), or in hypoxanthine (predicted to perturb GMP synthesis, purple bars), xanthine (predicted to perturb AMP synthesis teal bars), or the absence of purine (predicted to perturb both AMP and GMP synthesis, gray bars). mRNA abundance levels were determined by qRT-PCR at 24 h as described in *Materials and Methods.* Ordinary two-way ANOVA calculated using GraphPad Prism; n.s. – non-significant, $p > 0.05$; * $p \leq 0.05$; ** $p \leq 0.01$; *** $p \leq 0.001$; **** $p \leq 0.0001$; see *Materials and Methods* for more information.
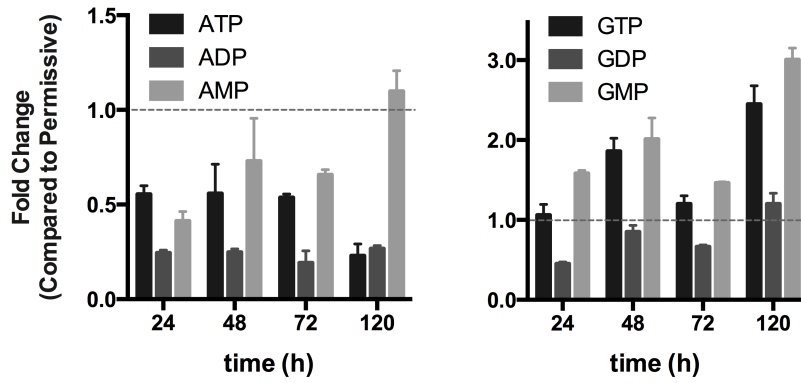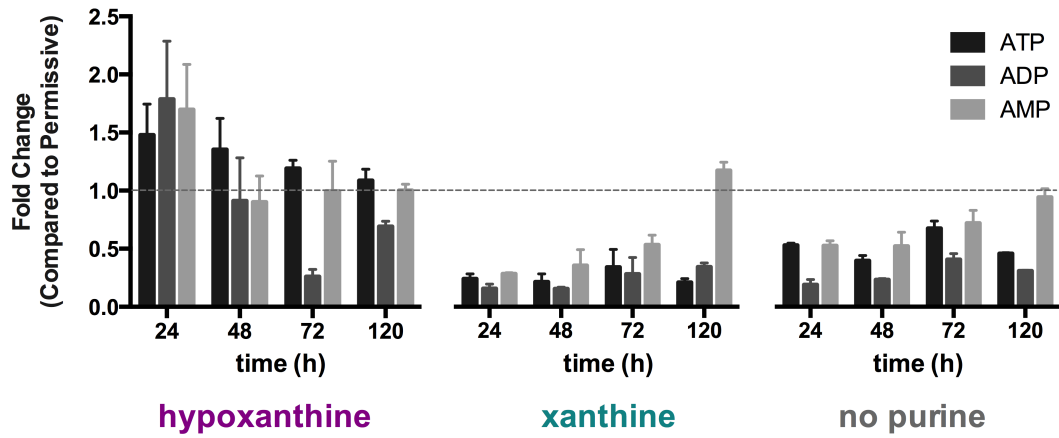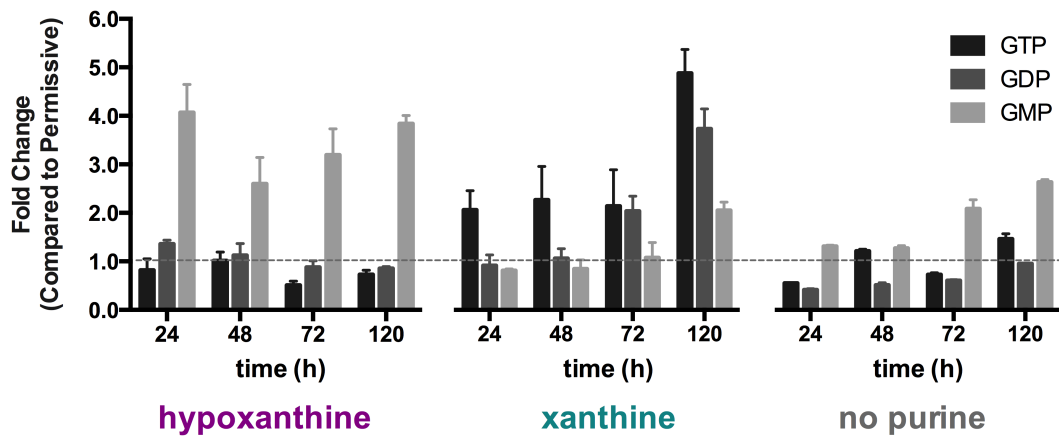
Figure 3.5 Determination of relative intracellular purine nucleotide pools.
(**A**) Wild type cells were cultured either in 100 µM hypoxanthine and 100 µM xanthine or in the absence of purine, and purine nucleotide levels assayed as described in *Materials and Methods*. The relative peak area for each adenine and guanine nucleotide under purine-replete conditions was set to 1 and used to calculate the fold change for wild type cells grown in the absence of purine supplement. (**B**) and (**C**) Δ*gmpr*Δ*impdh* cells were cultured in 100 µM hypoxanthine and 100 µM xanthine (conditions permissive for growth), or in 100 µM hypoxanthine (predicted to perturb GMP synthesis, AMP synthesis intact), or in 100 µM xanthine (predicted to perturb AMP synthesis, GMP synthesis intact), or in the absence of a purine supplement (predicted to perturb both AMP and GMP synthesis). Fold changes in ATP, ADP, and AMP levels (**B**) and GTP, GDP, and GMP levels (**C**) were calculated using the relative peak areas for Δ*gmpr*Δ*impdh* cells grown under the permissive condition as described above for wild type cells. Ordinary two-way ANOVA calculated using GraphPad Prism; n.s. – non-significant, $p > 0.05$; * $p \leq 0.05$; ** $p \leq 0.01$; *** $p \leq 0.001$; **** $p \leq 0.0001$; see *Materials and Methods* for more information.

A
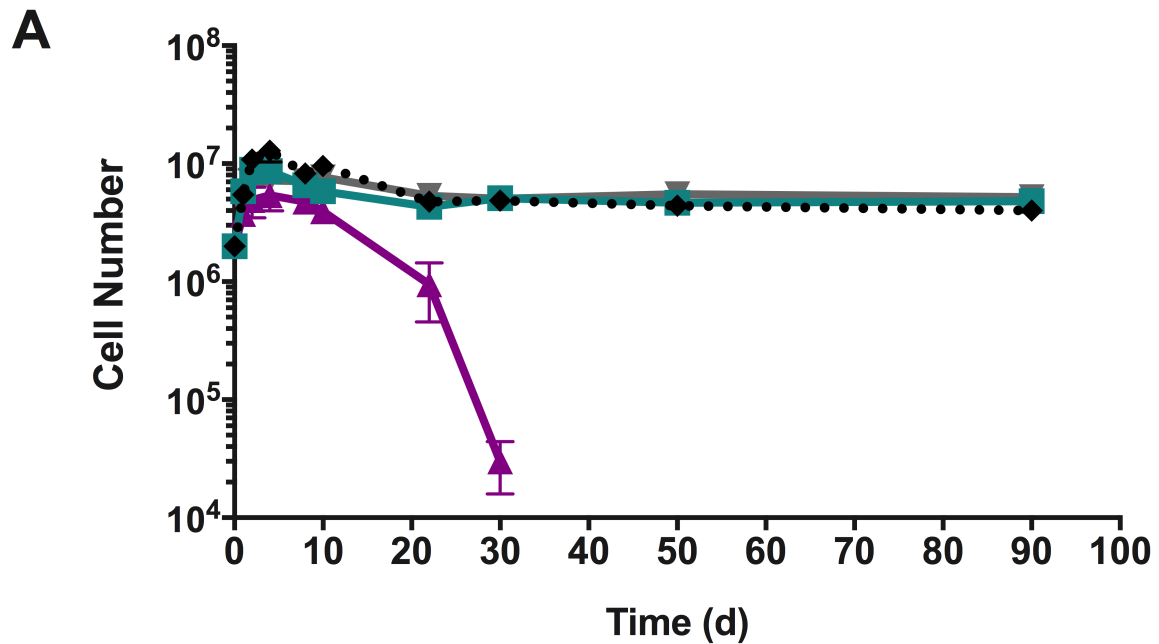
B
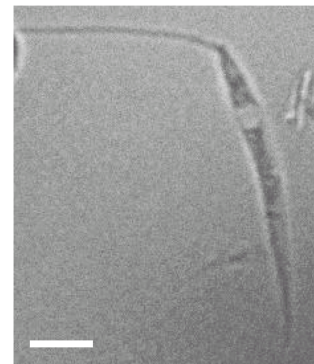
Hypoxanthine   **Xanthine**

Figure 3.6 Determination of long-term survival in Δ*gmpr*Δ*impdh* cells.
(**A**) Cells were cultured in hypoxanthine (purple), xanthine (teal), or without purine (gray), and cell numbers enumerated at various time points. Cell counts for purine-starved wild type *L. donovani* are shown by the black dotted line. Data plotted are the average of 2 biological replicates. The ability of each culture to recover from purine stress was evaluated by adding back purines permissive for growth and monitoring growth after 5 days. (**B**) DIC images of Δ*gmpr*Δ*impdh* cells cultured in hypoxanthine or xanthine after 5 days.
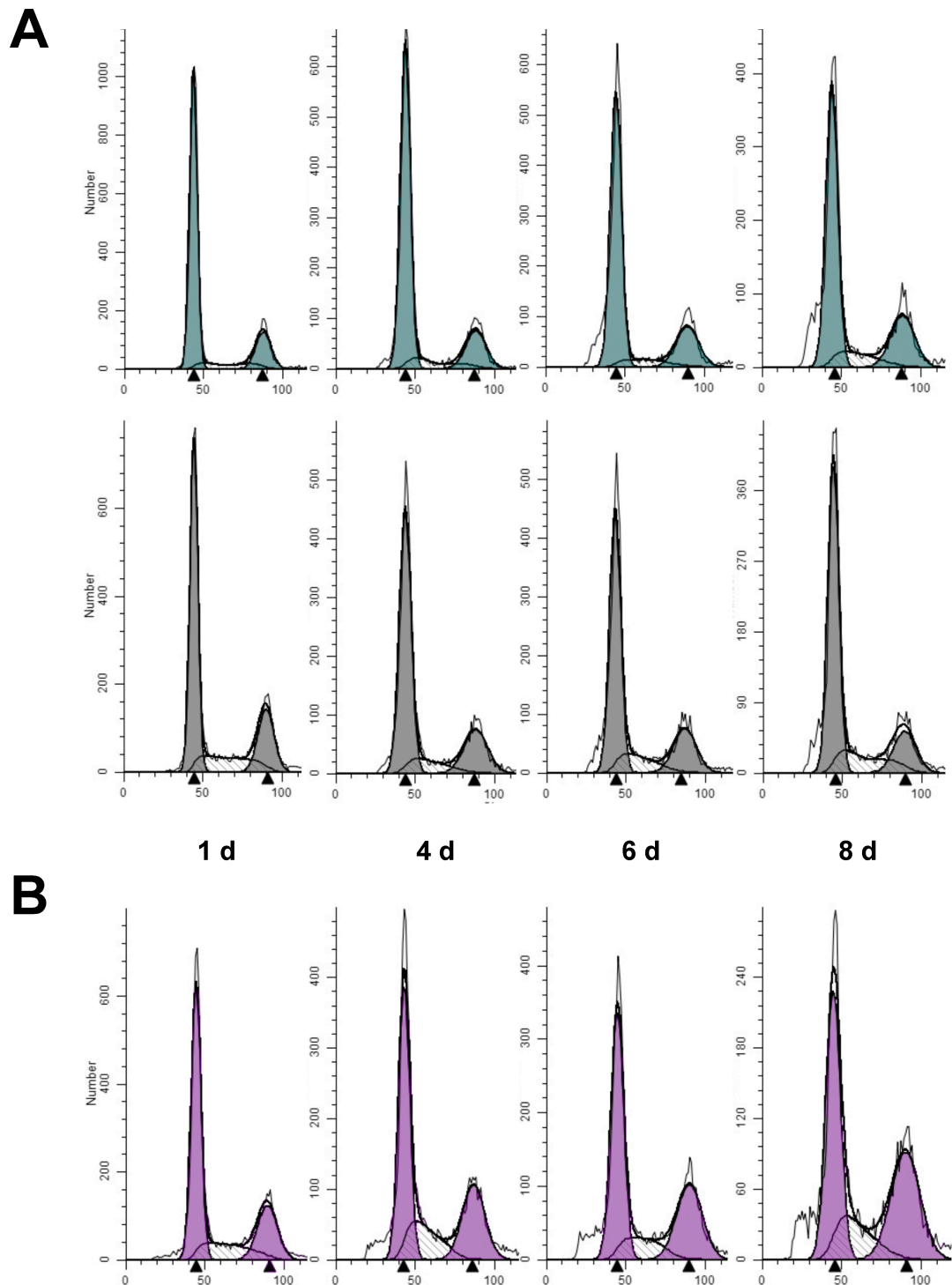
Figure 3.7 Analysis of cell cycle arrest in Δ*gmpr*Δ*impdh* cells.

Cells were cultured in: (**A**) xanthine, teal; no purine, gray; or (**B**) hypoxanthine, purple; harvested at 1, 4, 6, or 8 days then fixed and stained for cell cycle analysis as described in the *Materials and Methods*. Plotted are the representative counts of cells (y-axis) and fluorescent DNA signal (x-axis) corresponding to cells in the G_1/G_0 (triangle near 50) or G_2/M (triangle near 100) phase of the cell cycle.

Chapter 4

CONCLUSIONS AND A CASE FOR SYSTEMS BIOLOGY

In addition to my work (experimental design, sample preparation, data analysis and interpretation, and writing) the following people contributed the following to the data presented here:

Charles K. Ansong and Geremy C. Clair performed proteomics analysis.

Buddy Ullman, Phillip A. Yates, and Nicola S. Carter helped with experimental design and interpretation of the data.

OVERVIEW

Throughout the lifecycle of the digenetic parasites, an efficient sensing and response to disparate host environments is essential for successful parasitism. *Leishmania* navigates life through the sandfly gut as a motile promastigote, existing in an environment with neutral pH, ambient temperature, and substantial sucrose availability. Upon infection into the mammalian host, the parasite is engulfed by a macrophage, where it takes up residence as a non-motile amastigote living in the acidic phagolysosome, combating 37°C temperature, and persisting on amino acids and fatty acids (28-30).

Responses to environmental changes are realized at the metabolite, mRNA, and protein level, and despite their essential nature, very little is known about the signaling mechanisms underlying these changes. Considering that absent from the genome are G-protein coupled receptors and their heterotrimeric G-proteins, receptor protein kinases and phosphatases, many signaling mechanisms are likely non-canonical (48).

In the absence of traditional signaling mechanisms in this parasite, we considered the role of phosphorylation in survival of purine starvation. As described by Parsons *et. al* (48) the genomes of *Leishmania* and related organisms are rich with genes predicted to encode protein kinases, *Leishmania* are estimated to have about 200, making up approximately 2% of the genome. Furthermore, many studies on these parasites' development from the insect stage (promastigote) to the mammalian stage (amastigote) have demonstrated regulation of protein phosphorylation (28, 215-220) in response to the pH and

temperature stress these parasite encounter; it followed that a role for phosphorylation in the stress response to purine starvation likely exists.

The preliminary studies presented here, in Chapter 4, are my contributions to the establishment of an emerging research program that will work to further delineate regulatory mechanisms in *Leishmania*.

EXPERIMENTAL OVERVIEW

Wild type 90 minute global proteomics and phosphoproteomics

The goal of this study was to identify candidate proteins potentially involved in relaying the purine perturbation signal. Wild type cells were cultured in the presence or absence of purine supplementation for 90 min and then analyzed for both global protein abundance changes as well as phosphorylation changes.

Δ*gmpr*Δ*impdh* 24 h global proteomics and phosphoproteomics

Our previous proteome analysis (Chapter 2, (16)) identified a number of proteins significantly regulated in wild type cells after 24 h of purine starvation. It was the goal of this study to identify protein and phosphorylation differences in Δ*gmpr*Δ*impdh* cells cultured in xanthine or hypoxanthine to identify components required for long-term survival.

MATERIALS AND METHODS

Cell culture

Wild type *Leishmania donovani* strain 1S2D (172) parasites were used to generate a mutant cell line lacking the genes encoding GMP reductase and IMP dehydrogenase (Δ*gmpr*Δ*impdh*, details to be described elsewhere, Boitz, *et al*. unpublished) used for these studies. The Δ*gmpr*Δ*impdh* promastigotes were cultured at 26°C with 5% CO_2 in Dulbecco's Modified Eagle- Leishmania (**DME-L-Bob**) medium (as described by Carter *et al.* (52)) with 5% SERUM PLUS™

(Sigma-Aldrich), supplemented with purines (100 µM each hypoxanthine and xanthine) for robust growth.

Purine perturbation of Leishmania

As described in (16, 52) logarithmically growing promastigotes were pelleted via centrifugation at 1,1000 x g for 10 min, washed two times in DME-L-Bob supplemented with the specified purine source, and suspended in DME-L-Bob medium at a density of 2 x 10^6 cells ml^{-1}.

Growth and harvest of Leishmania samples

Logarithmically growing $\Delta gmpr\Delta impdh$ cells were cultured in either 100 µM hypoxanthine or 100 µM xanthine for 24 h and harvested at 1,100 x g for 5 minutes at room temperature. The cell pellet was washed twice with phosphate buffered saline. Finally, the cells were suspended in 1 mL of complete lysis buffer—100 mM ammonium carbonate pH 7.8 with 8 M urea; with 1x Phosphatase Inhibitor Cocktail 2 and 3 (Sigma-Aldrich) and incubated on ice for 10 min. Samples were flash frozen in liquid N_2 and stored at -80°C until analysis.

Tryptic digest and peptide cleanup

Dithiothreitol (**DTT**) was added to a final concentration of 5 mM and samples incubated with constant shaking at 37°C for 1 h. Iodoacetamide was added to 10 mM for alkylation and samples mixed again at 37°C for 1 h in the dark. Samples were diluted 2-fold with H_2O, $CaCl_2$ was added to a final concentration of 1 mM

and digested with trypsin at a 1:50 trypsin-to-protein ratio overnight at 37°C with constant shaking. Samples were acidified with trifluoroacetic acid (**TFA**) and then desalted using a Discovery-C18 SPE cartridge (SUPELCO) and 500 µg of eluted peptides were transferred to a new tube and vacuumed to dryness.

Peptide tandem mass tag labeling

Dried peptides were reconstituted in 500 mM triethylammonium bicarbonate (**TEAB**) and TMTsixplex™ Label Reagent (ThermoFisher, masses 126, 127, 128, 129, 130, 131) were prepared and labeling carried out as per the manufacturer's directions, and samples pooled. Following TFA acidification of the labeled sample, SPE cleanup was performed as above.

C18 reversed-phase fractionation

Peptides were fractionated using an XBridge C18 column, 250 x 4.6 mm, 5 µm, with a 4.6 x 20 mm guard column (Waters). Mobile phase A: 10 mM TEAB, pH 7.5 and mobile phase B: 10 mM TEAB, pH 7.5, 90% acetonitrile (**ACN**) at a flow rate of 0.5 mL/min using the following gradient: 100% A, 0% B 0-41 min; 10% B 41-127 min; 30% B 127-137 min; 43% B 137-142 min; 55% B 142-147 min; 100% B 147-148; 100% A 148-178 min. 96 fractions were collected from 48-164 min of the gradient at equal intervals of 1.2 min, collected fractions were dried down. Fractions were suspened in 100 uL of 50% methanol 0.05% TFA and pooled (fractions 1, 25, 49, and 73; fractions 2, 26, 50, 74; etc.) and the resulting 12 fractions were dried again and suspended in 0.05% TFA.

Global proteome analysis

5% of the total peptide pool from each of the final 12 fractions was submitted for LC-MS/MS global proteome analysis.

Phosphopeptide enrichment

The remaining 95% of the 12 peptide fractions were enriched using Fe-substituted Ni-NTA-agarose beads (Qiagen). Samples were incubated with activated beads for 30 min, then unbound peptides washed 4 times using 80% ACN, 0.1% TFA. Phosphopeptides were eluted and immediately acidified to pH 3.5-4.0 with TFA, concentrated via SpeedVac and stored at -80°C until analysis.

Mass spectrometry and data analysis

Samples were analyzed by reverse phase LC-MS/MS using a Waters nanoEquityTM UPLC system (Millford, MA) coupled with a Orbitrap-Velos MS (Thermo Scientific) as previously described (221). The LC was configured to load the sample first on a solid phase extraction (**SPE**) column followed by separation on an analytical column. Analytical columns were made in-house by slurry packing 3 µm Jupiter C18 stationary phase (Phenomenex, Torrence, CA) into a 70 cm long, 360 µm OD x 75 µm ID fused silica capillary tubing (Polymicro Technologies Inc., Phoenix, AZ). The SPE column (360 µm OD x 150 µm ID) of 5 cm length was similarly made with 3.6 µm Aeries C18 particles. Mobile phase A (**MP-A**) consisted of 0.1% formic acid in water mobile phase B (**MP-B**) was 0.1%

formic acid in acetonitrile. Samples were suspended to a final concentration of ~

0.1 µg/µL and 5 µL loaded on the SPE column via a 5 µL sample loop for 30 min

at a flow rate of 3 µL min^{-1} and then separated by the analytical column using a

215 min gradient from 99% MP-A to 25% MP-A at a flow rate of 0.3 µL min^{-1}.

Mass spectrometry analysis was started 30 min after the sample was moved to

the analytical column and mass spectra were recorded for 180 min. After the

gradient was completed, column was washed with 100% MP-B and then

reconditioned with 99% MP-A for 30 minutes.

Raw mass spectrometry data were converted to peak lists (DTA files) using the

DeconMSn (version 2.3.1.2, http://omics.pnl.gov/software/DeconMSn.php) and

searched with MS-GF+ (222) against the *Leishmania donovani* BPK282A1

(8,028 sequences), bovine trypsin, and human keratin sequences (all in correct

and reverse orientations, 16,088 total sequences). Search parameters included

tryptic digestion of at least one of the peptide ends (partially tryptic), 20 ppm

peptide mass tolerance, methionine oxidation as variable modification, and

carbamidomethylation and lysine labeling with TMT reagent as fixed

modifications. Identified MS/MS spectra were filtered with an MS-GF+ score of

3.99432E-09 resulting for the phospho-enriched samples in a false-discovery

rate (**FDR**) ≤ 0.5% at the spectral level and a Peptide FDR ≤ 0.86% and for the

global samples (not phospho-enriched) in a spectral FDR ≤ 0.5, a peptide FDR ≤

0.71% and a protein FDR ≤ 0.21% (only proteins identified with two

proteospecific peptides were retained). At the peptide level, the TMT reporter

intensities of the peptides fragmented various times were summed. For the

phospho-sites, aScore was used to filter only the peptide with a high probability

of correct phosphorylation site and localization (aScore ≥ 13.0) (223). For

quantitative analysis, the TMT reporter ion intensities were extracted with MASIC

(MS/MS Automated Selected Ion Chromatogram Generator, version v2.6.5421,

http://omics.pnl.gov/software/MASIC.php) (224). All data were normalized using

the median signal of the global proteins/peptides for the corresponding TMT

SixPlex isobaric label. Missing values were imputed with a value corresponding

to the minimal value of the table divided by two and the data log2 transformed.

Statistically significant changes in protein, peptide and phoshpo-peptide

abundances were determined using two-tailed, homoscedastic t-test in Microsoft

Excel 2010 (V14.0.7145.5000).

RESULTS

Wild type 90 minute global proteomics and phosphoproteomics

After 90 minutes of purine starvation, only 6 proteins were significantly up or

downregulated in abundance (Table 4.1). However, 2,779 phosphosites were

identified, corresponding to 2,468 phosphopeptides, resulting in a total of 1,286

phosphoproteins identified. Of these, 119 phosphopeptides (117

phosphoproteins) were significantly altered between the two conditions and could

be clustered in to 3 groups based on regulation (Fig 4.1). 84 (71%) of the data

set matched to proteins of unknown function. The remaining 33 were assigned to

a biological function using gene ontology annotations available in TriTrypDB (Fig.

4.2), with the greatest number of identifications in the signaling transduction

category. Further information and the complete list of significantly regulated

phosphopeptides can be found in Table 4.2 The phosphosite distribution

resembles that of higher eukaryotes and previous studies in *Leishmania*, with

serine residues making up 80%, threonine 19.6% and tyrosine 0.4% (28).

Δ*gmpr*Δ*impdh* 24 h global proteomics and phosphoproteomics

Preliminary analysis of the global proteome changes of Δ*gmpr*Δ*impdh* cells

cultured in hypoxanthine or xanthine extracellular purine source resulted in 336

proteins significantly (p-value < 0.05) regulated with a log2 fold change > 0.3 or

< -0.3. A more stringent evaluation of those with a log2 fold change <-0.5,

revealed 32 downregulated proteins, 19 had functional annotation (Fig. 4.4,

Table 4.3). However, 71 proteins were significantly upregulated with a log2 fold

change > 0.5, only 43 proteins could be assigned a function (Figs. 4.5-4.8).

However, reviewing the number of phoshopeptides changed showed 1,322

significantly changed between the two conditions (Fig. 4.6).

Upon review of the Δ*gmpr*Δ*impdh* global proteome remodeling, I noticed a

large number of proteins involved in calcium ion binding, or calcium-dependent

activity (Table 4.5). Our previous studies had not indicated, necessarily, a role for

calcium in the response to purine starvation. However calcium signaling in

Leishmania has been shown to affect the transition from promastigote to axenic

amastigote, it is thought, then, that calcium is a likely second messenger (225).

These data also revealed a change in phosohporylation status of AMPK, a

protein that we speculated in Chapter 3 is important in the sensing and response

to adenylate nucleotide perturbations. From the global dataset, I determined that

AMPK protein abundance does not change (p-value > 0.05, and log2 fold change < 0.3), however, as shown in Table 4.6, the pattern of phosphorylation varies dramatically between Δ*gmpr*Δ*impdh* cells cultured in xanthine versus in hypoxanthine. These data will be further validated by ongoing studies in our laboratory.

CONCLUSION

In Chapter 4, I've presented a bird's eye view of preliminary data for a number of systems biology-level investigations I've undertaken with collaborators into the global proteome and phosphoproteome of the wild type and $\Delta gmpr\Delta impdh$ mutant cell line of *Leishmania donovani*. It is the nature of such studies, as shown in Chapters 2 and 3, that global analysis leads to specific hypothesis-driven research, and this hypothesis-driven research leads right back to a need for global analysis. For example, the work in Chapter 3 suggested a role for AMPK in the sensing mechanism to purine limitation and in the absence of robust commercially available reagents to investigate changes in phosphorylation status of AMPK subunits we undertook a systems-level evaluation of the phosphoproteome. This identified a number of differential phosphorylation patterns (Table 4.5) and is justification for further investigation that is currently underway in our laboratory.

As highlighted in both this chapter and Chapter 2, as of this writing, over 63% (5,170 of 8,195) of the proteins predicted in the *L. donovani* BPK282A1 proteome are "hypothetical" or of "unknown function," making the interpretation of biological significance for these proteins difficult. However, it is through comparison of systems-level analyses of the parasite's response to various stress conditions (e.g. temperature, pH, osmolarity, nutrient starvation) that we can begin to find proteins of unknown function that are commonly regulated in abundance or phosphorylation status between these conditions—perhaps revealing new biological functions or pathway assignments for these proteins.

This type of analysis is not limited to within species, however, by utilizing resources such as OrthoMCL (226-228) and TriTrypDB (14) the regulation of orthologs within a genus (e.g. *Leishmania and Trypanosoma*) can be compared, thereby greatly increasing the utility of systems-level datasets.

One particularly attractive feature of these proteins of unknown function is that in the absence of conserved domains and other characteristics typically used to infer function, it is likely that they are substantially different from host proteins. The ideal therapeutic target is dissimilar from the host to minimize the risk of the drug binding host proteins and creating potential toxic side effects. By determining if a hypothetical protein of unknown function is involved in a number of stress responses, a case can be made for further investigation of the protein and perhaps even rational drug design.

It is from this dissertation work that the hallmarks of the adaptive response to purine starvation in *Leishmania* were identified on a proteome-wide scale. Further demonstrated by the data were the modest changes in multiple proteins in a single pathway leading to substantial changes in related intracellular metabolite levels. A case for protein abundance changes conferred by alterations of the mRNA abundance level, translation, and post-translational level were established. Finally, this is amongst the most inclusive studies yet in response to nutrient stress in *Leishmania*.

Following the analysis of molecular mechanisms underlying proteome remodeling in purine-starved parasites, I was fascinated with the idea of how *Leishmania* sense their purine environment. A battery of purine salvage and

interconversion pathway mutants previously characterized in our laboratory was repurposed for the investigation of intracellular versus extracellular purine sensing. Not only was this study the first to identify intracellular nutrient sensing as a proxy for monitoring the extracellular environment, it resulted in the discovery of the adenine-nucleotide pool perturbation being the essential component for inducing the adaptive response to purine starvation phenotype and thereby allowing long-term survival of *Leishmania* in the absence of nucleotide requirements for growth.

The long-term impact of a model system like the $\Delta gmpr\Delta impdh$ cell line cannot be understated. This system allows for the parallel comparison of the *Leishmania* $\Delta gmpr\Delta impdh$ mutant's survival or death during purine limitation. The only experimental variable is the purine source, otherwise, the conditions are identical. Thus far, mRNA, protein, and metabolite abundance changes have been observed utilizing this system, however, as described in Chapter 3, the questions that can be asked of this system are endless.

As stated before, it is my hope that the data generated by my thesis work not only continues to contribute to the fundamental understanding of molecular mechanisms of these unique parasites, but also leads to identification of essential processes such that therapeutic intervention and treatment of leishmaniasis can be realized.

			log2 (starved/replete)			
TriTrypID	Description	p-value	Rep 1	Rep 2	Rep 3	Average
LdBPK_220380.1	hypothetical protein, conserved	0.00	-0.35	-0.24	-0.38	-0.32
LdBPK_211690.1	methyltransferase-like protein	0.01	0.41	0.20	0.38	0.33
LdBPK_051030.1	hypothetical protein, conserved	0.02	-0.49	-0.28	-0.37	-0.38
LdBPK_340030.1	protein kinase, putative	0.03	0.78	0.27	0.30	0.45
LdBPK_321870.1	hypothetical protein, conserved	0.03	-0.31	-0.37	-0.24	-0.31
LdBPK_353000.1	hypothetical protein, conserved	0.05	0.51	0.33	0.14	0.33

Table 4.1 Proteins significantly regulated in response to 90 min purine starvation in wild type *L. donovani*
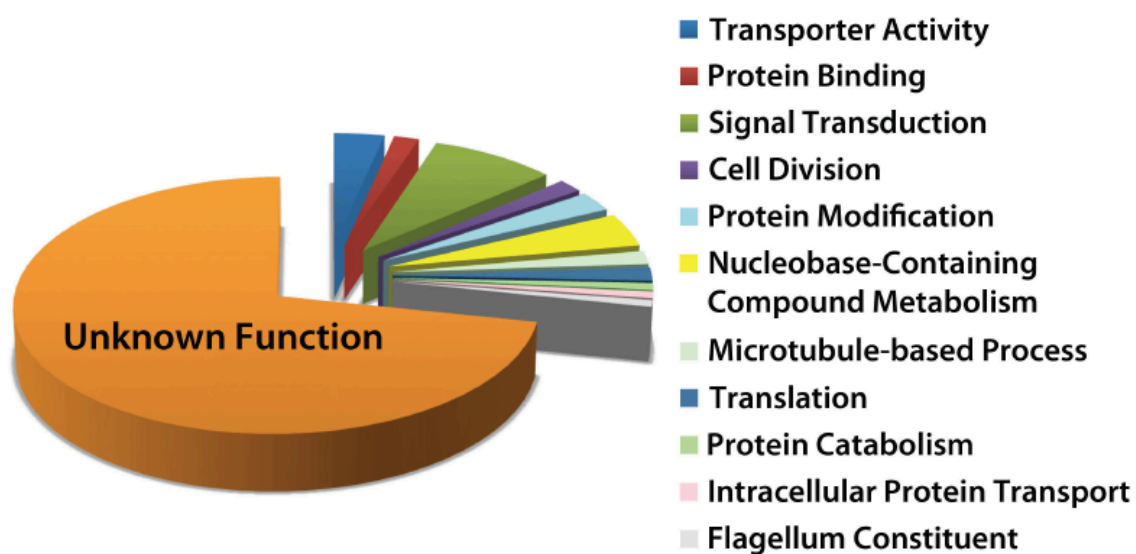
Figure 4.1 Biological function assignment of 117 differentially regulated phosphoproteins after 90 minutes of purine starvation
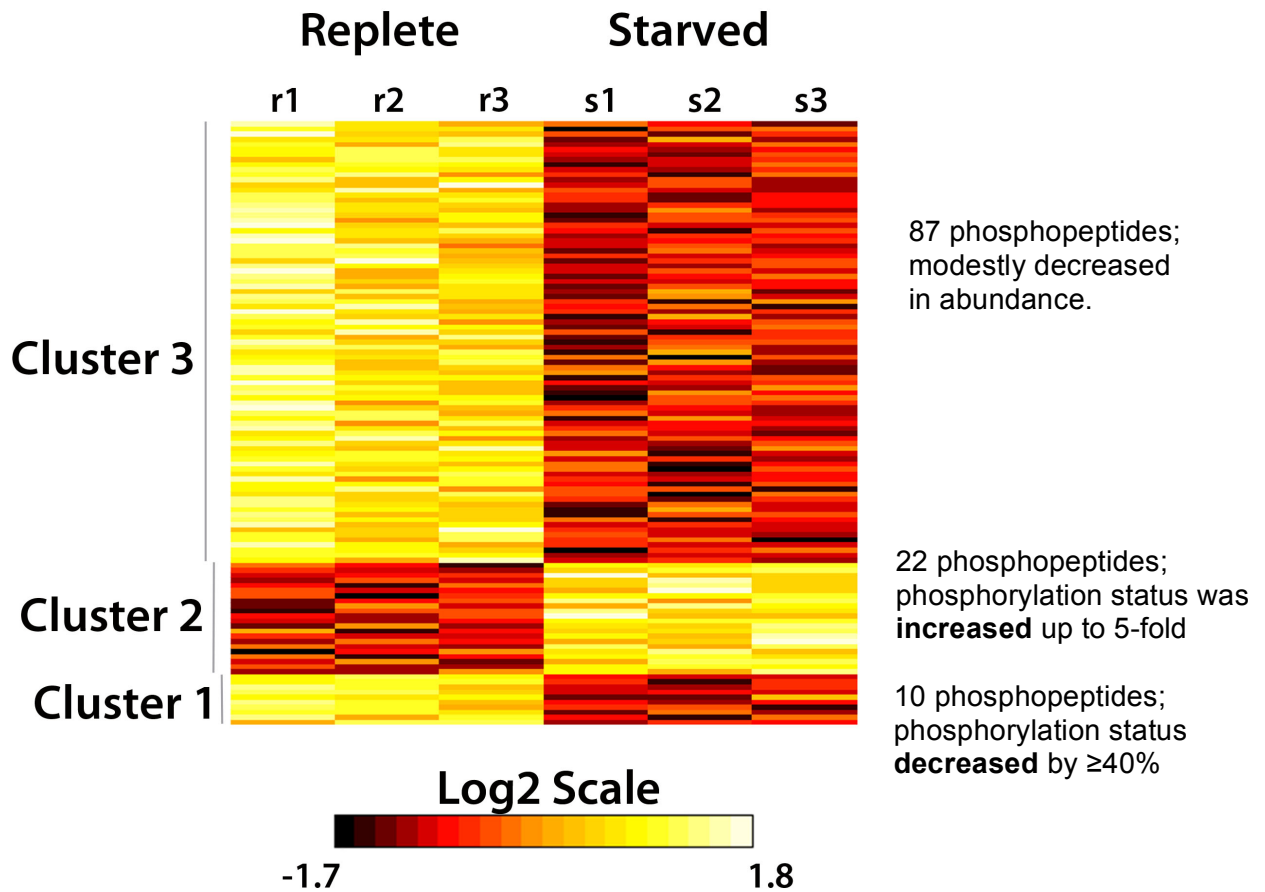
Figure 4.2 Similarly regulated phosphopeptides after 90 minutes of purine starvation in wild type cells.
Phosphopeptides were clustered into 3 groups based on the fold change in response to purine starvation.

Peptide	TriTrypID	Description	S-mods	T-Mods	Y-Mods	Total Sites	pvalue	log2 (starved/replete)			
								Rep 1	Rep 2	Rep 3	Average
K.S*AS*GPQLDHYTR.S	LdBPK_271290.1	protein kinase, putative	2	0	0	2	0.05	-0.22	-0.33	-0.27	-0.28
R.GGAS*T*PDAVAEAALPTR.D	LdBPK_050940.1	hypothetical protein, conserved	1	1	0	2	0.05	0.56	0.29	0.15	0.33
R.AQAS*S*GEYDHNEYSLR.E	LdBPK_342850.1	protein kinase, putative	2	0	0	2	0.05	0.65	0.39	1.24	0.76
R.RPS*S*PNTTSVSPLAR.G	LdBPK_221140.1	hypothetical protein, conserved	2	0	0	2	0.04	0.47	0.45	0.59	0.50
R.MPTLS*PAAS*PLTVQGR.S	LdBPK_211400.1	hypothetical protein, conserved	2	0	0	2	0.03	1.14	0.33	0.35	0.61
K.AS*RTPLS*ASVATITPASEQR.D	LdBPK_050640.1	hypothetical protein, conserved	2	0	0	2	0.03	-0.55	-0.31	-0.12	-0.33
G.S*APVS*PVTAHMMR.M	LdBPK_280320.1	hypothetical protein, conserved	2	0	0	2	0.03	0.28	0.19	0.20	0.22
R.QKS*AS*PDRVPVTLPPSSR.T	LdBPK_331460.1	hypothetical protein, conserved	2	0	0	2	0.03	-0.19	-0.15	-0.07	-0.13
R.GAGADNSDS*PDHS*PAATGR.A	LdBPK_110400.1	tubulin-tyrosine ligase-like protein	2	0	0	2	0.02	-0.91	-0.14	-0.86	-0.64
K.DAES*RGS*DADAEAAR.A	LdBPK_230290.1	ABC-thiol transporter	2	0	0	2	0.02	-0.70	-0.64	-0.37	-0.57
R.RS*VS*PVLSR.Q	LdBPK_221160.1	hypothetical protein, unknown function	2	0	0	2	0.01	0.23	0.46	0.28	0.32
R.SVS*GVGS*PTSDATAATWGR.S	LdBPK_341230.1	hypothetical protein, conserved	2	0	0	2	0.01	0.26	0.36	0.64	0.42
R.S*LQNS*PIIQPSR.L	LdBPK_300460.1	eukaryotic translation initiation factor 4e, putative	2	0	0	2	0.00	-1.07	-0.97	-0.69	-0.91
K.NDVTDVEHS*IAGHTDGR.D	LdBPK_361890.1	hypothetical protein, conserved	1	0	0	1	0.05	1.12	0.99	0.15	0.75
R.QMS*GFSTR.R	LdBPK_040060.1	hypothetical protein, conserved	1	0	0	1	0.05	-0.22	-0.28	-0.02	-0.18
R.SLS*EEGGDAGK.G	LdBPK_040920.1	hypothetical protein	1	0	0	1	0.05	-0.27	-0.48	-0.03	-0.26
R.AT*PAVMNGSADSRPVFLEAPLGYK.E	LdBPK_221450.1	ser/thr protein phosphatase, putative	0	1	0	1	0.05	0.05	0.40	0.37	0.27
T.LGDS*PVVAMQR.A	LdBPK_210250.1	hypothetical protein, conserved	1	0	0	1	0.05	-0.67	-0.54	-0.54	-0.58
R.FAVSTS*PVGSAEGLDTATAR.A	LdBPK_110460.1	hypothetical protein, unknown function	1	0	0	1	0.05	-0.40	-0.24	-0.41	-0.35
R.S*GSPPAVTGANATVSNNTVDHNR.F	LdBPK_350970.1	hypothetical protein, conserved	1	0	0	1	0.05	-1.36	-1.25	-0.28	-0.96
R.QAAVLT*PEEEESEELR.S	LdBPK_364160.1	hypothetical protein, conserved	0	1	0	1	0.04	-0.70	-0.08	-0.47	-0.42
K.RLS*TASAVSPSTSASR.A	LdBPK_211850.1	hypothetical protein, conserved	1	0	0	1	0.04	-0.35	-0.68	-0.45	-0.50
R.S*LPSTAPAAATVVR.N	LdBPK_080540.1	protein kinase , putative	1	0	0	1	0.04	-0.37	-0.16	-0.11	-0.21
R.S*GAGLWNR.L	LdBPK_010690.1	hypothetical protein, conserved	1	0	0	1	0.04	-0.47	-0.40	-0.20	-0.36
R.EAGS*GDDNEEGLEETELGR.G	LdBPK_343060.1	hypothetical protein, conserved	1	0	0	1	0.04	-0.36	-0.05	-0.21	-0.20
R.S*SREDFAQMLR.R	LdBPK_332570.1	hypothetical protein, conserved	1	0	0	1	0.04	-1.00	-0.18	-0.44	-0.54
R.LAS*AQDFSR.R	LdBPK_333170.1	hypothetical protein, conserved	1	0	0	1	0.04	-0.34	-0.09	-0.09	-0.17
R.EGS*LTTEHR.L	LdBPK_280630.1	hypothetical protein, unknown function	1	0	0	1	0.04	-0.76	-0.21	-0.24	-0.40
R.EVS*PSYTTR.S	LdBPK_170810.1	protein kinase, putative	1	0	0	1	0.04	-0.17	-0.19	-0.17	-0.17
R.AEDPGCADS*PDPR.G	LdBPK_311160.1	hypothetical protein, conserved	1	0	0	1	0.04	-0.19	-0.22	-0.10	-0.17
R.GGQS*PQQAGAPPTVLDILR.L	LdBPK_231780.1	hypothetical protein, conserved	1	0	0	1	0.04	-0.21	-0.03	-0.22	-0.15
R.VGDSVAS*PTAPSSMR.L	LdBPK_366600.1	ubiquitin-protein ligase, putative	1	0	0	1	0.04	-0.37	-0.29	-0.14	-0.26
R.NPES*PVTKPLPPPPVTK.T	LdBPK_363670.1	hypothetical protein, conserved	1	0	0	1	0.04	-0.27	-0.35	-0.06	-0.23
K.GTDAET*DGGEENQTVR.V	LdBPK_190230.1	hypothetical protein, conserved	0	1	0	1	0.04	-0.64	-0.15	-0.21	-0.33
R.ASSAT*PGGPAYQER.F	LdBPK_050560.1	hypothetical protein, conserved	0	1	0	1	0.04	-0.49	-0.54	-0.23	-0.42
K.EAVEDEEEQS*AKEEK.K	LdBPK_091020.1	elongation factor-1 gamma	1	0	0	1	0.04	-0.30	-0.08	-0.56	-0.31
K.S*VDGANVAGNASHR.R	LdBPK_322110.1	hypothetical protein, conserved	1	0	0	1	0.04	-0.53	-0.22	-0.39	-0.38
R.RTDSAQVDDTTAVPS*ENNFAASSAK.E	LdBPK_040830.1	hypothetical protein, conserved	1	0	0	1	0.04	0.52	2.26	1.06	1.28
R.QNS*TTLHPLCR.H	LdBPK_342320.1	protein phosphatase 2C-like protein	1	0	0	1	0.04	-0.91	-0.12	-0.51	-0.51
K.VHLLPSSETGEETLGSVAT*PTAHAVQR.T	LdBPK_050920.1	paraflagellar rod protein, putative	0	1	0	1	0.04	-1.55	-1.15	-0.95	-1.22
K.AVENDET*EDADEQGTGVSR.A	LdBPK_302840.1	hypothetical protein, conserved	0	1	0	1	0.04	0.12	0.15	0.30	0.19
R.WAS*DGNSYASGAEDGMVR.V	LdBPK_271140.1	hypothetical protein, conserved	1	0	0	1	0.04	-0.87	-0.36	-0.25	-0.49
K.LPAT*PSMGTQDGASAPDAAR.A	LdBPK_367080.1	beta-adaptin, putative	0	1	0	1	0.03	-1.12	-0.36	-0.59	-0.69
R.RIS*LDEQK.G	LdBPK_231890.1	hypothetical protein, unknown function	1	0	0	1	0.03	-0.62	-0.17	-0.27	-0.35
R.S*AGLGVDCAALVANGR.G	LdBPK_211400.1	hypothetical protein, conserved	1	0	0	1	0.03	-0.28	-0.38	-0.12	-0.26
R.TMS*PAEAPPDTAK.A	LdBPK_220020.1	hypothetical protein, conserved	1	0	0	1	0.03	-0.10	-0.02	-0.11	-0.08

Table 4.2 Summary of significantly regulated phosphopeptides in wild type _L. donovani_ after 90 min purine starvation

143

Peptide	TriTrypID	Description	S-mods	T-Mods	Y-Mods	Total Sites	pvalue	Rep 1	Rep 2	Rep 3	Average
								log2 (starved/replete)			
R.QLS*EGVASGVK.I	LdBPK_230090.1	hypothetical protein, conserved	1	0	0	1	0.03	-0.16	-0.20	-0.20	-0.19
R.RGS*DGAGSGESVNELR.S	LdBPK_220430.1	kinesin, putative	1	0	0	1	0.03	-0.27	-0.21	-0.38	-0.29
R.RNS*AATTTAGVSPR.T	LdBPK_241470.1	kinesin, putative	1	0	0	1	0.03	-0.49	-0.11	-0.26	-0.29
R.AMS*DHSISGNR.R	LdBPK_270550.1	hypothetical protein, conserved	1	0	0	1	0.03	-0.40	-0.36	-0.39	-0.38
R.RGS*LAQTLK.C	LdBPK_242040.1	hypothetical protein, conserved	1	0	0	1	0.03	-0.33	-0.07	-0.15	-0.18
R.TLS*DDGQPQNARPR.S	LdBPK_030330.1	protein kinase, putative	1	0	0	1	0.03	-0.36	-0.18	-0.25	-0.26
R.S*STAATLSSR.S	LdBPK_130570.1	hypothetical protein, conserved	1	0	0	1	0.03	-0.94	-0.25	-0.52	-0.57
R.AVPS*DAFVAK.S	LdBPK_362040.1	nucleoside transporter 1, putative	1	0	0	1	0.03	0.49	0.10	0.62	0.40
R.S*ASATAVAPDADAAPAR.T	LdBPK_230800.1	hypothetical protein, conserved	1	0	0	1	0.03	0.43	1.07	0.27	0.59
R.AAS*VPAVLSSR.L	LdBPK_013360.1	unspecified product	1	0	0	1	0.03	-0.23	-0.38	-0.21	-0.27
R.DPGARS*PISMR.N	LdBPK_320270.1	protein kinase, putative	1	0	0	1	0.03	-0.20	-0.06	-0.18	-0.15
R.DSS*TGSVAAAPLLR.G	LdBPK_340640.1	hypothetical protein, conserved	1	0	0	1	0.03	-0.12	-0.18	-0.11	-0.14
R.SESTAADSVAAS*PPPR.V	LdBPK_300740.1	CDC16, putative	1	0	0	1	0.03	-0.56	-0.37	-1.22	-0.72
R.ENDDMAS*LSTPSQSIR.S	LdBPK_120720.1	hypothetical protein, conserved	1	0	0	1	0.03	-0.27	-0.24	-0.04	-0.18
R.RPS*SPNTTSVSPLAR.G	LdBPK_221140.1	hypothetical protein, conserved	1	0	0	1	0.03	0.49	0.15	0.31	0.32
R.GAS*AQGSGVDDMSQTASGDAR.Q	LdBPK_270550.1	hypothetical protein, conserved	1	0	0	1	0.03	-0.32	-0.63	-0.39	-0.45
R.SPATAAASS*PVCVTK.D	LdBPK_211200.1	hypothetical protein, conserved	1	0	0	1	0.03	0.51	0.21	0.22	0.31
R.LSVS*PVAGVPSPPSR.F	LdBPK_070770.1	protein kinase, putative	1	0	0	1	0.02	-0.11	-0.41	-0.17	-0.23
R.ECPEAGGS*YGGSR.G	LdBPK_361720.1	universal minicircle sequence binding protein (UMSBP),	1	0	0	1	0.02	-0.38	-0.18	-0.18	-0.25
R.S*QEMAIAEEQELR.D	LdBPK_231720.1	hypothetical protein, conserved	1	0	0	1	0.02	-0.19	-0.14	-0.10	-0.14
K.EGEEAAAAT*PTATHR.A	LdBPK_201470.1	hypothetical protein, conserved	0	1	0	1	0.02	-0.18	-0.29	-0.57	-0.35
R.HWLPS*PQYR.G	LdBPK_344190.1	RNA-binding protein-like protein	1	0	0	1	0.02	-0.81	-0.50	-0.39	-0.57
R.DVFQNQS*PLQHQLAH.A	LdBPK_291440.1	RNA-binding protein, putative	1	0	0	1	0.02	-0.35	-0.22	-0.23	-0.27
R.SAT*PTLPPMSVSAAPR.A	LdBPK_130600.1	hypothetical protein, conserved	0	1	0	1	0.02	-0.16	-0.33	-0.17	-0.22
R.LS*PPPVHQVESK.D	LdBPK_351790.1	hypothetical protein, conserved	1	0	0	1	0.02	-0.93	-0.82	-0.83	-0.86
K.LRPNS*GSIVNAR.Q	LdBPK_282790.1	leucine rich repeat protein, putative	1	0	0	1	0.02	-0.66	-0.23	-0.31	-0.40
K.AHESYATVAAAS*DSGAGAVK.T	LdBPK_311050.1	hypothetical protein, unknown function	1	0	0	1	0.02	-0.33	-0.11	-0.47	-0.30
R.ENS*QQTMSSHR.A	LdBPK_280980.1	ribonucleoside-diphosphate reductase large chain, puta	1	0	0	1	0.02	-0.55	-0.33	-0.22	-0.37
R.DRDDDS*AEEPPLPADR.H	LdBPK_250320.1	hypothetical protein, conserved	1	0	0	1	0.02	-0.55	-0.30	-0.39	-0.41
K.DGFPEPERVPQPCDS*NADDADEPR.L	LdBPK_060690.1	hypothetical protein, conserved	1	0	0	1	0.02	-1.43	-1.98	-2.42	-1.95
L.AILQPECAADS*PTVVR.A	LdBPK_170460.1	hypothetical protein, conserved	1	0	0	1	0.02	0.41	0.33	0.63	0.46
R.S*SSTLGIEK.A	LdBPK_080520.1	ribose-phosphate pyrophosphokinase, putative	1	0	0	1	0.02	-0.74	-0.23	-0.36	-0.44
R.LPAS*HSMR.K	LdBPK_242010.1	hypothetical protein, conserved	1	0	0	1	0.02	-0.78	-0.24	-0.66	-0.56
R.S*FAVVTADEAEK.D	LdBPK_151340.1	hypothetical protein, conserved	1	0	0	1	0.01	-0.57	-0.31	-0.29	-0.39
R.S*APSSPSNVPGR.K	LdBPK_271720.1	hypothetical protein, unknown function	1	0	0	1	0.01	-0.34	-0.41	-0.16	-0.30
R.DAGS*DAGDAADEEDR.E	LdBPK_251270.1	hypothetical protein, conserved	1	0	0	1	0.01	-0.29	-0.20	-0.20	-0.23
K.GS*PAFGMPDSAIQNK.K	LdBPK_362260.1	DEAD box RNA helicase, putative	1	0	0	1	0.01	-0.36	-0.59	-0.29	-0.41
R.ATSVVPECVS*DADAAPAR.R	LdBPK_060620.1	hypothetical protein, conserved	1	0	0	1	0.01	-0.25	-0.76	-0.78	-0.60
R.SHS*DEGVEGAVR.D	LdBPK_100400.1	folate/biopterin transporter, putative	1	0	0	1	0.01	-0.84	-0.24	-0.66	-0.58
R.S*PANAGAPGAAGGGGVHR.T	LdBPK_060750.1	hypothetical protein, conserved	1	0	0	1	0.01	-0.64	-0.29	-0.27	-0.40
R.AGS*CGATGGHVGVYH.R	LdBPK_262390.1	hypothetical protein, conserved	1	0	0	1	0.01	-0.32	-0.74	-0.50	-0.52
K.GAVSDTLRHS*QJADGILAAQDQGAR.Q	LdBPK_323050.1	hypothetical protein, conserved	1	0	0	1	0.01	0.40	0.89	0.53	0.61
R.AS*PATVVAPEDK.K	LdBPK_201670.1	hypothetical protein, conserved	1	0	0	1	0.01	0.26	0.23	0.47	0.32
R.S*GGGGGQAPVAGVTASSLR.S	LdBPK_141300.1	hypothetical protein, conserved	1	0	0	1	0.01	0.24	0.28	0.22	0.24
R.ERS*PTSLSIK.L	LdBPK_250290.1	hypothetical protein, conserved	1	0	0	1	0.01	-0.43	-0.24	-0.18	-0.29
K.RGS*DSTAEEVEAR.A	LdBPK_201300.1	hypothetical protein, unknown function	1	0	0	1	0.01	-0.29	-0.27	-0.18	-0.25

Table 4.2 continued

Peptide	TriTrypID	Description	S-mods	T-Mods	Y-Mods	Total Sites	pvalue	log2 (starved/replete)			
								Rep 1	Rep 2	Rep 3	Average
R.RNS*VTAVCSK.D	LdBPK_301810.1	hypothetical protein, conserved	1	0	0	1	0.01	-0.76	-0.63	-0.28	-0.56
R.ANS*LEDVKR.A	LdBPK_262070.1	SUMO1/Ulp2, putative	1	0	0	1	0.01	-0.58	-0.38	-0.27	-0.41
R.S*PYMTPMPSDMAPDADR.S	LdBPK_270550.1	hypothetical protein, conserved	1	0	0	1	0.01	-1.06	-1.06	-0.40	-0.84
K.ES*GPSNAAICDAYATR.L	LdBPK_333000.1	D-alanyl-glycyl endopeptidase-like protein	1	0	0	1	0.01	-0.65	-0.26	-0.51	-0.47
R.S*PSEEHWQQR.G	LdBPK_110940.1	hypothetical protein, unknown function	1	0	0	1	0.01	-0.15	-0.21	-0.17	-0.18
R.S*STAGPSLTAGASR.M	LdBPK_321280.1	hypothetical protein, conserved	1	0	0	1	0.01	-0.51	-0.23	-0.27	-0.33
R.SAS*PCTEEVR.R	LdBPK_333240.1	hypothetical protein, unknown function	1	0	0	1	0.01	-0.23	-0.20	-0.23	-0.22
R.SQS*PLPQQK.Q	LdBPK_333170.1	hypothetical protein, conserved	1	0	0	1	0.01	-0.37	-0.31	-0.19	-0.29
R.LREDEAS*VADDDDDGGSFQLNK.F	LdBPK_151090.1	hypothetical protein, conserved	1	0	0	1	0.01	-2.92	-1.59	-2.26	-2.26
R.SS*VADAGATDTMGSAVTDAVGR.S	LdBPK_272090.1	hypothetical protein, conserved	1	0	0	1	0.01	-0.26	-0.34	-0.32	-0.31
R.QVDEQGNEIAVMT*PRPR.G	LdBPK_220320.1	hypothetical protein, conserved	0	1	0	1	0.00	-1.38	-1.43	-0.78	-1.20
R.NLSDHFPVEDS*PMNAR.P	LdBPK_332570.1	hypothetical protein, conserved	1	0	0	1	0.00	-0.29	-0.23	-0.14	-0.22
R.SYAAGAS*STALVPR.S	LdBPK_090120.1	hypothetical protein, conserved	1	0	0	1	0.00	-0.29	-0.37	-0.17	-0.28
R.SQTNSPSS*PAAESLQPSNK.A	LdBPK_366430.1	hypothetical protein, conserved	1	0	0	1	0.00	0.38	0.83	0.89	0.70
K.S*ASTAVEPAMTEGR.S	LdBPK_341610.1	hypothetical protein, conserved	1	0	0	1	0.00	-0.31	-0.41	-0.28	-0.33
R.SAT*PLNNSDAYAPPR.R	LdBPK_120070r.1	unspecified product	0	1	0	1	0.00	-0.40	-0.43	-0.32	-0.38
K.EEVPTTTVGT*DPTESR.N	LdBPK_366880.1	hypothetical protein, conserved	0	1	0	1	0.00	-0.37	-0.39	-0.56	-0.44
R.S*VEGAPHEEVNLDEEYR.W	LdBPK_363340.1	hypothetical protein, conserved	1	0	0	1	0.00	-0.64	-1.11	-0.72	-0.82
R.SPT*PEPQPVESAINR.D	LdBPK_170310.1	hypothetical protein, conserved	0	1	0	1	0.00	-0.48	-0.44	-0.26	-0.39
K.AEGAGGSDELS*ECDEVR.V	LdBPK_131110.1	nucleobase transporter	1	0	0	1	0.00	1.72	2.73	2.54	2.33
R.RGS*LGGANAQQR.Y	LdBPK_241000.1	hypothetical protein, conserved	1	0	0	1	0.00	-0.48	-0.31	-0.37	-0.39
R.T*PTPLGESGGSTGAK.N	LdBPK_160180.1	hypothetical protein, conserved	0	1	0	1	0.00	-0.32	-0.51	-0.29	-0.37
R.AAGAPS*PAPHQYR.T	LdBPK_080630.1	hypothetical protein, conserved	1	0	0	1	0.00	-0.41	-0.49	-0.44	-0.45
R.AGS*AGGAAAASSLAQR.A	LdBPK_090520.1	serine/threonine protein phosphatase, putative	1	0	0	1	0.00	-0.39	-0.35	-0.40	-0.38
R.SLQNS*PIIQPSR.L	LdBPK_300460.1	eukaryotic translation initiation factor 4e, putative	1	0	0	1	0.00	-0.75	-0.91	-0.81	-0.83
K.ALSTQAVS*PALEAR.T	LdBPK_261910.1	hypothetical protein, conserved	1	0	0	1	0.00	-0.78	-0.72	-0.61	-0.71
R.EGAVS*EDEFAGDSSDTSR.T	LdBPK_311980.1	transcription like protein nupm1, putative	1	0	0	1	0.00	1.66	1.92	1.71	1.77

Table 4.2 continued

Figure 4.4 Distribution of GO annotations for significantly downregulated proteins in the Δ*gmpr*Δ*impdh* cell line between xanthine and hypoxanthine culture supplementation

32 proteins were significantly (p-value <0.05) downregulated with a log2 fold change less than -0.5. The figure shows the GO annotations that could be assigned to 19 of these proteins, some proteins had multiple annotations assigned; see Table 4.3 for further information.

TriTrypID	Product	pvalue	log2(X1/H1)	log2(X2/H2)	log2(X3/H3)	Average log2(X/H)	Predicted GO Function Term and ID	Predicted GO Process Term and ID	Predicted GO Component Term and ID
LdBPK_190630.1	histone H3 variant, putative	0.012	-0.36	-0.75	-0.40	-0.50	DNA binding, protein heterodimerization activity, GO:0003677, GO:0046982	nucleosome assembly, GO:0006334	nucleosome, GO:0000786
LdBPK_323820.1	3-hydroxyisobutyryl-coenzyme a hydrolase-like protein	0.006	-0.50	-0.48	-0.60	-0.53	catalytic activity, GO:0003824	metabolic process, GO:0008152	
LdBPK_323980.1	hypothetical protein, conserved	0.004	-0.42	-0.61	-0.56	-0.53			
LdBPK_030350.1	hypothetical protein, conserved	0.046	-0.57	-0.33	-0.71	-0.54			membrane, GO:0016020
LdBPK_330290.1	hypothetical protein, conserved	0.018	-0.58	-0.54	-0.50	-0.54			integral to membrane, GO:0016021
LdBPK_342240.1	ribosomal protein 135a, putative	0.003	-0.45	-0.68	-0.49	-0.54	structural constituent of ribosome, GO:0003735	translation, GO:0006412	intracellular, ribosome, GO:0005622, GO:0005840
LdBPK_363020.1	40S ribosomal protein S24e	0.009	-0.38	-0.56	-0.72	-0.56	structural constituent of ribosome, GO:0003735	translation, GO:0006412	intracellular, ribosome, GO:0005622, GO:0005840
LdBPK_131410.1	60S ribosomal protein L44, putative	0.015	-0.48	-0.82	-0.42	-0.57	structural constituent of ribosome, GO:0003735	translation, GO:0006412	intracellular, ribosome, GO:0005622, GO:0005840
LdBPK_323810.1	3-hydroxyisobutyryl-coenzyme a hydrolase-like protein	0.011	-0.57	-0.52	-0.64	-0.57			
LdBPK_333100.1	hypothetical protein, conserved	0.003	-0.57	-0.57	-0.68	-0.61			
LdBPK_281030.1	oxidoreductase-like protein	0.031	-0.70	-0.15	-0.97	-0.61			
LdBPK_261290.1	hypothetical protein, conserved	0.022	-0.68	-0.74	-0.44	-0.62			
LdBPK_050490.1	hypothetical protein, conserved	0.000	-0.78	-0.57	-0.58	-0.64			
LdBPK_060410.1	60S ribosomal protein L19, putative	0.010	-0.50	-1.00	-0.44	-0.64	structural constituent of ribosome, GO:0003735	translation, GO:0006412	intracellular, ribosome, GO:0005622, GO:0005840
LdBPK_330750.1	hypothetical protein, conserved	0.001	-0.64	-0.57	-0.73	-0.65	protein binding, GO:0005515		
LdBPK_140760.1	fatty acid elongase, putative	0.016	-0.44	-0.80	-0.74	-0.66			integral to membrane, GO:0016021
LdBPK_100080.1	hypothetical protein, conserved	0.001	-0.78	-0.55	-0.70	-0.68			
LdBPK_080960.1	cathepsin L-like protease	0.002	-0.62	-0.67	-0.77	-0.69	cysteine-type peptidase activity, GO:0008234	proteolysis, GO:0006508	
LdBPK_180300.1	hypothetical protein, conserved	0.003	-0.80	-0.53	-0.73	-0.69		transport, GO:0006810	intracellular, GO:0005622
LdBPK_100070.1	dehydrogenase-like protein	0.005	-0.48	-0.89	-0.70	-0.69	oxidoreductase activity, GO:0016491	metabolic process, GO:0008152	
LdBPK_333140.1	hypothetical protein, conserved	0.005	-0.69	-0.60	-0.80	-0.70			
LdBPK_313180.1	iron/zinc transporter protein-like protein	0.008	-0.86	-0.39	-0.86	-0.70	metal ion transmembrane transporter activity, GO:0046873	metal ion transport, transmembrane transport, GO:0030001, GO:0055085	membrane, GO:0016020
LdBPK_211180.1	hypothetical protein, conserved	0.009	-0.78	-0.78	-0.60	-0.72			
LdBPK_361720.1*	universal minicircle sequence binding protein (UMSBP), putative	0.012	-1.01	-0.33	-0.85	-0.73	nucleic acid binding, zinc ion binding, GO:0003676, GO:0008270		
LdBPK_050900.1	surface antigen-like protein	0.005	-0.75	-0.83	-0.78	-0.78			
LdBPK_290640.1	ATP-binding cassette protein subfamily A, member 10, putative	0.001	-0.86	-0.68	-0.93	-0.82	ATP binding, ATPase activity, nucleoside-triphosphatase activity, nucleotide binding, GO:0005524, GO:0016887, GO:0017111, GO:0000166		
LdBPK_242320.1	hypothetical predicted multi-pass transmembrane protein	0.006	-0.89	-0.79	-0.90	-0.86			
LdBPK_332070.1	60S ribosomal protein L37	0.000	-1.08	-0.78	-0.95	-0.94	structural constituent of ribosome, GO:0003735	translation, GO:0006412	intracellular, ribosome, GO:0005622, GO:0005840
LdBPK_363930.1	60S ribosomal protein L34, putative	0.004	-0.76	-1.33	-0.87	-0.99	structural constituent of ribosome, GO:0003735	translation, GO:0006412	intracellular, ribosome, GO:0005622, GO:0005840
LdBPK_181380.1	60S ribosomal protein L34, putative	0.002	-1.43	-0.94	-0.78	-1.05	structural constituent of ribosome, GO:0003735	translation, GO:0006412	intracellular, ribosome, GO:0005622, GO:0005840
LdBPK_070970.1	hypothetical protein, conserved	0.001	-1.14	-0.99	-1.19	-1.11			
LdBPK_362710.1	related to multifunctional cyclin-dependent kinase pho85-like protein	0.001	-1.46	-0.95	-1.73	-1.38	glycerophosphodiester phosphodiesterase activity, phosphoric diester hydrolase activity, GO:0008889, GO:0008081	glycerol metabolic process, lipid metabolic process, GO:0006071, GO:0006629	

* manually annotated as mitochondrial DNA inheritance, mitosis (GO process IDs GO:0033955, GO:0007067)

Table 4.3 Summary of significantly downregulated proteins in Δ*gmpr*Δ*impdh* *L. donovani* after 24 hour purine limitation

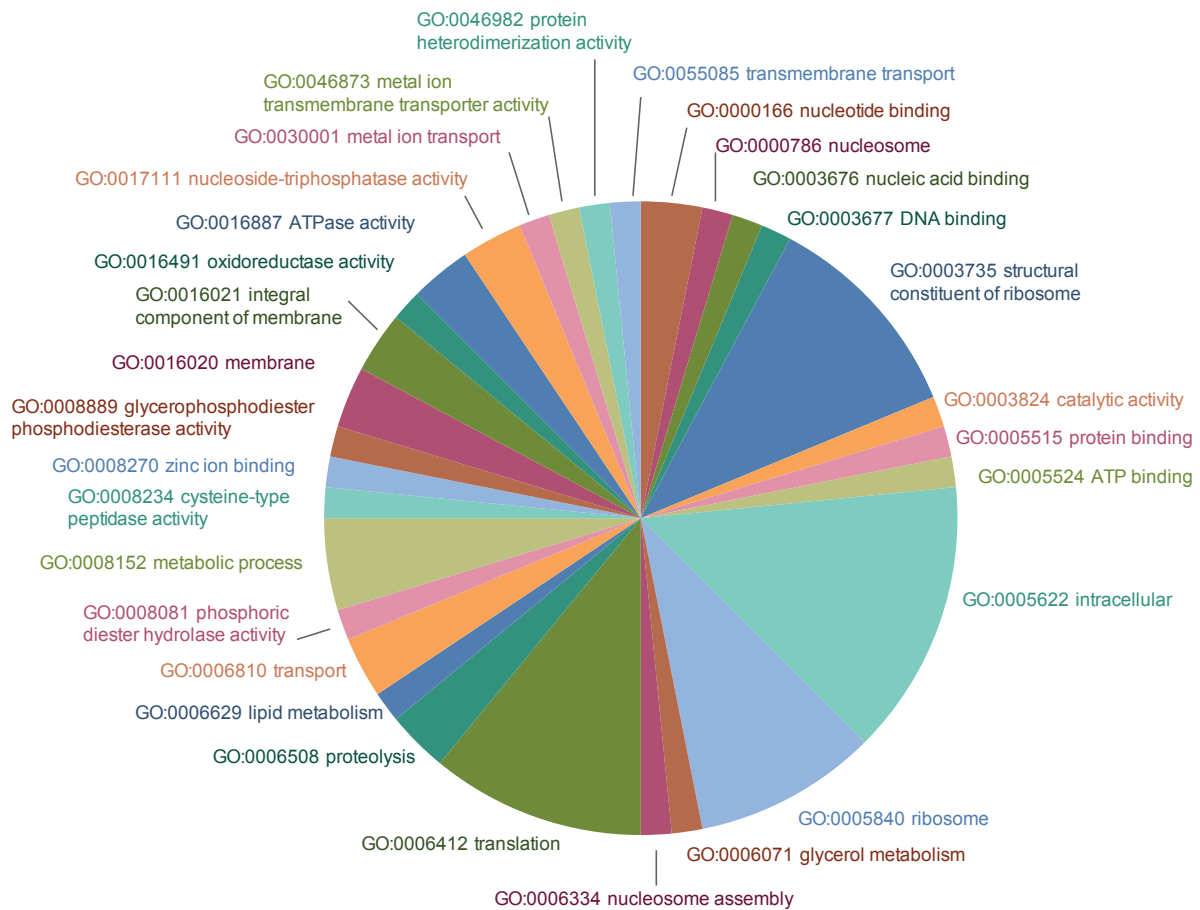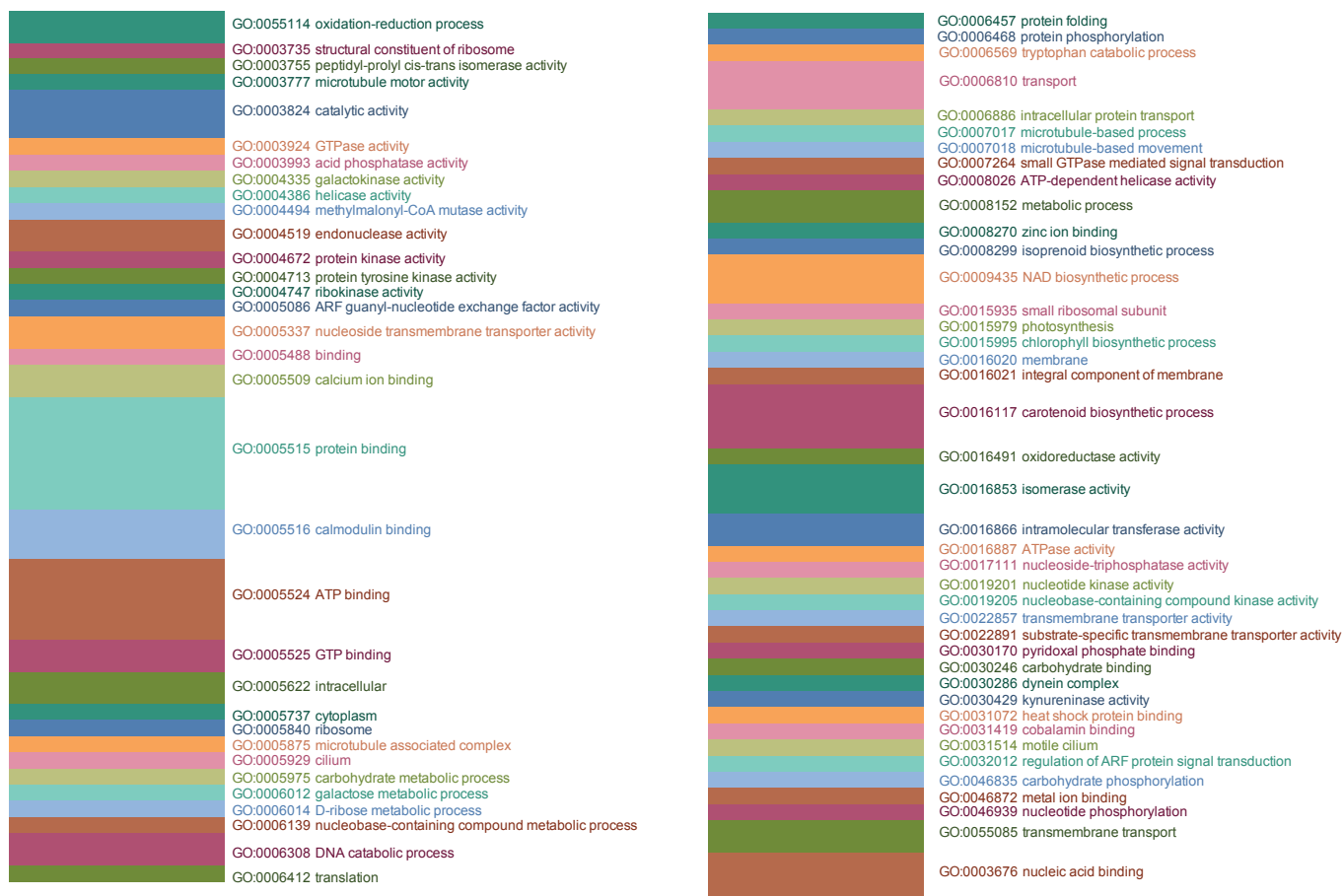**Figure 4.5 Distribution of GO annotations for significantly upregulated proteins in the Δ*gmpr*Δ*impdh* cell line between xanthine and hypoxanthine culture supplementation**

71 proteins were significantly (p-value <0.05) upregulated with a log2 fold change greater than 0.5. The figure shows the GO annotations that could be assigned to 43 of these proteins, some proteins had multiple annotations assigned, the size of each box indicates the relative proportion of each GO category. see Table 4.?? for further information.

Figure 4.6 Number of significantly changed phosphopeptides between
Δ*gmpr*Δ*impdh* **cells cultured in xanthine or hypoxanthine**
Comparing the phosphopeptide abundance of Δ*gmpr*Δ*impdh* cells cultured in
hypoxanthine versus xanthine resulted in 1322 significantly regulated
phosphopeptides, 418 of those were upregulated (red) and 904 were
downregulated (green).

TriTrypID	Product	pvalue	log2(X1/H1)	log2(X2/H2)	log2(X3/H3)	Average log2(X/H)	Predicted GO Function Term and ID	Predicted GO Process Term and ID	Predicted GO Component Term and ID
LdBPK_262250.1	kynureninase, putative	0.016	1.92	0.72	1.55	1.40	kynureninase activity, pyridoxal phosphate binding, GO:0030429, GO:0030170	NAD biosynthetic process, metabolic process, tryptophan catabolic process, GO:0009435, GO:0008152, GO:0006569	cytoplasm, GO:0005737
LdBPK_020500.1	hypothetical protein, conserved	0.035	0.37	1.37	1.58	1.11			
LdBPK_050060.1	major vault protein, putative	0.007	0.57	1.15	1.28	1.00			
LdBPK_321760.1 (a)	hypothetical protein, conserved	0.024	1.42	1.08	0.46	0.99			
LdBPK_262340.1	hypothetical protein, conserved	0.044	0.73	0.47	1.57	0.93	protein binding, GO:0005515		
LdBPK_241630.1	hypothetical protein, conserved	0.004	0.98	0.84	0.80	0.87			
LdBPK_362010.1	hypothetical protein, conserved	0.023	0.94	0.95	0.68	0.86			
LdBPK_290260.1	thymine-7-hydroxylase, putative	0.003	1.02	0.80	0.62	0.81	oxidoreductase activity, GO:0016491	oxidation-reduction process, GO:0055114	
LdBPK_281360.1	hypothetical protein, conserved	0.035	0.95	0.69	0.77	0.80			
LdBPK_363780.1	hypothetical protein, conserved	0.022	1.22	0.46	0.70	0.79			
LdBPK_362040.1	nucleoside transporter 1, putative	0.007	0.86	0.74	0.73	0.78	nucleoside transmembrane transporter activity, GO:0005337	transport, GO:0006810	integral to membrane, GO:0016021
LdBPK_291890.1	paraflagellar rod protein 1D, putative	0.005	0.84	0.82	0.66	0.77	calmodulin binding, GO:0005516		microtubule-based flagellum, GO:0009434
LdBPK_181640.1	hypothetical protein, conserved	0.018	0.90	0.90	0.51	0.77			
LdBPK_342700.1	selenocysteine-specific elongation factor, putative	0.026	0.40	0.74	1.10	0.75	GTP binding, GTPase activity, GO:0005525, GO:0003924		
LdBPK_351000.1	aldose 1-epimerase-like protein	0.003	0.83	0.68	0.67	0.73	carbohydrate binding, catalytic activity, isomerase activity, GO:0030246, GO:0003824, GO:0016853	carbohydrate metabolic process, GO:0005975	
LdBPK_361430.1	hypothetical protein, conserved	0.003	0.76	0.77	0.64	0.73	binding, catalytic activity, GO:0005488, GO:0003824		
LdBPK_161500.1	hypothetical protein, conserved	0.002	0.79	0.62	0.76	0.72			
LdBPK_151230.1	nucleoside transporter 1, putative	0.006	0.78	0.76	0.60	0.71	nucleoside transmembrane transporter activity, GO:0005337	transport, GO:0006810	integral to membrane, GO:0016021
LdBPK_100640.1	hypothetical protein, conserved	0.005	0.79	0.85	0.50	0.71			
LdBPK_312380.1	3'-nucleotidase/nuclease precursor, putative	0.004	0.71	0.79	0.60	0.70	endonuclease activity, nucleic acid binding, GO:0004519, GO:0003676	DNA catabolic process, GO:0006308	
LdBPK_170310.1	hypothetical protein, conserved	0.004	0.85	0.70	0.52	0.69			
LdBPK_291260.1	hypothetical protein, conserved	0.003	0.77	0.58	0.70	0.69			
LdBPK_300020.1	cyclophilin, putative	0.033	0.46	0.57	0.99	0.67	peptidyl-prolyl cis-trans isomerase activity, GO:0003755	protein folding, GO:0006457	
LdBPK_361220.1	hypothetical protein, conserved	0.012	0.65	0.67	0.65	0.66	calmodulin binding, GO:0005516		
LdBPK_161510.1	paraflagellar rod protein 2C	0.012	0.75	0.63	0.57	0.65			microtubule-based flagellum, GO:0009434
LdBPK_352790.1	galactokinase-like protein	0.002	0.73	0.66	0.56	0.65	ATP binding, galactokinase activity, GO:0005524, GO:0004335	carbohydrate phosphorylation, galactose metabolic process, GO:0046835, GO:0006012	
LdBPK_332270.1	hypothetical protein, conserved	0.016	0.90	0.71	0.30	0.64			
LdBPK_365010.1	hypothetical protein, conserved	0.003	0.60	0.66	0.64	0.63	protein binding, GO:0005515		
LdBPK_302380.1	ADP-ribosylation factor-like protein	0.021	0.57	0.84	0.49	0.63	GTP binding, GO:0005525	intracellular protein transport, small GTPase mediated signal transduction, GO:0006886, GO:0007264	intracellular, GO:0005622
LdBPK_283120.1	hypothetical protein, conserved	0.018	0.84	0.55	0.50	0.63			
LdBPK_320240.1	dynein light chain, flagellar outer arm, putative	0.007	0.62	0.69	0.55	0.62		microtubule-based process, GO:0007017	microtubule associated complex, GO:0005875
LdBPK_020280.1	hypothetical protein, conserved	0.011	0.67	0.54	0.62	0.61			
LdBPK_341620.1	hypothetical protein, conserved	0.013	0.65	0.71	0.48	0.61			
LdBPK_071080.1	hypothetical protein, conserved	0.005	0.74	0.72	0.36	0.61			
LdBPK_290280.1	hypothetical protein, conserved	0.009	0.55	0.73	0.53	0.61			
LdBPK_190070.1	hypothetical protein, conserved	0.036	0.74	0.46	0.61	0.61	heat shock protein binding, GO:0031072		
LdBPK_090580.1	leucine-rich repeat protein, putative	0.006	0.69	0.54	0.57	0.60	protein binding, GO:0005515		
LdBPK_251750.1	hypothetical protein, unknown function	0.008	0.70	0.48	0.62	0.60			
LdBPK_120350.1	3'-nucleotidase/nuclease, putative	0.013	0.74	0.52	0.54	0.60	endonuclease activity, nucleic acid binding, GO:0004519, GO:0003676	DNA catabolic process, GO:0006308	
LdBPK_361410.1	adenylate kinase, putative	0.002	0.58	0.76	0.44	0.59	ATP binding, nucleobase-containing compound kinase activity, nucleotide kinase activity, GO:0005524, GO:0019205,	nucleobase-containing compound metabolic process, nucleotide phosphorylation, GO:0006139, GO:0046939	
LdBPK_340430.1	hypothetical protein, conserved	0.023	0.68	0.46	0.63	0.59	oxidoreductase activity, GO:0016491		
LdBPK_366080.1	hypothetical protein, conserved	0.019	0.59	0.54	0.64	0.59			
LdBPK_342340.1	hypothetical protein, conserved	0.018	0.74	0.69	0.32	0.59	ARF guanyl-nucleotide exchange factor activity, GO:0005086	regulation of ARF protein signal transduction, GO:0003012	intracellular, GO:0005622
LdBPK_260490.1	hypothetical protein, conserved	0.013	0.66	0.56	0.52	0.58	protein binding, GO:0005515		

150

Table 4.4 Summary of significantly downregulated proteins in Δ*gmpr*Δ*impdh L. donovani* after 24 hour purine limitation
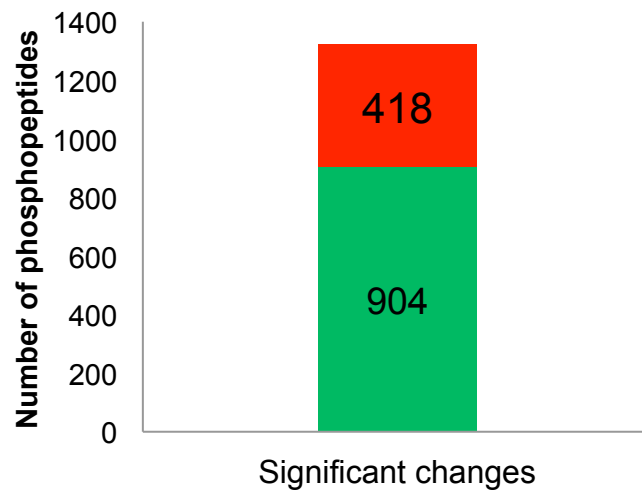
TriTrypID	Product	pvalue	log2(X1/H1)	log2(X2/H2)	log2(X3/H3)	Average log2(X/H)	Predicted GO Function Term and ID	Predicted GO Process Term and ID	Predicted GO Component Term and ID
LdBPK_330660.1 (b)	hypothetical protein, conserved	0.032	0.76	0.38	0.59	0.58			
LdBPK_141130.1	dynein heavy chain, putative	0.005	0.48	0.40	0.83	0.57	microtubule motor activity, GO:0003777	microtubule-based movement, GO:0007018	dynein complex, GO:0030286
LdBPK_091390.1	paraflagellar rod component, putative	0.012	0.59	0.57	0.55	0.57	calmodulin binding, GO:0005516		microtubule-based flagellum, GO:0009434
LdBPK_130950.1	hypothetical protein, conserved	0.006	0.60	0.57	0.51	0.56			
LdBPK_362720.1	membrane-bound acid phosphatase 2, putative	0.020	0.68	0.52	0.48	0.56	acid phosphatase activity, GO:0003993		
LdBPK_361680.1	universal minicircle sequence binding protein, putative	0.004	0.63	0.43	0.61	0.56	nucleic acid binding, zinc ion binding, GO:0003676, GO:0008270		
LdBPK_351720.1	casein kinase II, putative	0.027	0.76	0.78	0.12	0.56	ATP binding, protein kinase activity, protein tyrosine kinase activity, GO:0005524, GO:0004672, GO:0004713	protein phosphorylation, GO:0006468	
LdBPK_060460.1	hypothetical protein, conserved	0.014	0.54	0.58	0.52	0.55	protein binding, GO:0005515		
LdBPK_090970.1	calmodulin, putative	0.033	0.64	0.52	0.48	0.55	calcium ion binding, GO:0005509		
LdBPK_130160.1 (c)	protein kinase A regulatory subunit, putative	0.009	0.46	0.63	0.54	0.55			
LdBPK_366560.1 (d)	glucose transporter, lmgt1	0.021	0.56	0.57	0.47	0.53	substrate-specific transmembrane transporter activity, transmembrane transporter activity, GO:0022891,	transmembrane transport, GO:0055085	integral to membrane, membrane, GO:0016021, GO:0016020
LdBPK_190340.1	hypothetical protein, conserved	0.023	0.79	0.21	0.59	0.53			
LdBPK_321840.1	hypothetical protein, conserved	0.010	0.64	0.60	0.36	0.53			
LdBPK_320410.1	ATP-dependent RNA helicase, putative	0.019	0.59	0.51	0.48	0.53	ATP binding, ATP-dependent helicase activity, helicase activity, nucleic acid binding, GO:0005524, GO:0008026, GO:0004386, GO:0003676		
LdBPK_090230.1	hypothetical protein, conserved	0.030	0.69	0.46	0.43	0.53			
LdBPK_050380.1	microtubule-associated protein, putative	0.034	0.53	0.27	0.76	0.52			
LdBPK_240860.1	dynein arm light chain, putative	0.032	0.79	0.28	0.50	0.52			
LdBPK_311460.1	pentamidine resistance protein 1	0.029	0.73	0.54	0.29	0.52	ATP binding, ATPase activity, nucleoside-triphosphatase activity, nucleotide binding, GO:0005524, GO:0016887, GO:0017111, GO:0000166	transmembrane transport, transport, GO:0055085, GO:0006810	integral to membrane, GO:0016021
LdBPK_366370.1	centrin, putative	0.025	0.65	0.53	0.38	0.52	calcium ion binding, GO:0005509		
LdBPK_161490.1	hypothetical protein, conserved	0.032	0.34	0.65	0.56	0.52	protein binding, GO:0005515		
LdBPK_220310.1	40S ribosomal protein S15, putative	0.049	0.56	0.71	0.29	0.52	structural constituent of ribosome, GO:0003735	translation, GO:0006412	ribosome, small ribosomal subunit, GO:0005840, GO:0015935
LdBPK_270310.1	methylmalonyl-coenzyme a mutase, putative	0.018	0.68	0.47	0.39	0.52	catalytic activity, cobalamin binding, intramolecular transferase activity, isomerase activity, metal ion binding, methylmalonyl-CoA mutase activity, GO:0003824, GO:0031419, GO:0016866, GO:0016853, GO:0046872, GO:0004494	metabolic process, GO:0008152	
LdBPK_363490.1	hypothetical protein, conserved	0.017	0.60	0.50	0.44	0.52			
LdBPK_190210.1	polyprenyl synthase, putative	0.013	0.38	0.66	0.49	0.51	oxidoreductase activity, GO:0016491	carotenoid biosynthetic process, chlorophyll biosynthetic process, isoprenoid biosynthetic process, oxidation-reduction process, photosynthesis, GO:0016117, GO:0015995, GO:0008299, GO:0055114, GO:0015979	
LdBPK_366100.1	kinetoplast-associated protein, putative	0.046	0.68	0.44	0.39	0.51	protein binding, GO:0005515		
LdBPK_270430.1	ribokinase, putative	0.008	0.59	0.47	0.46	0.51	ribokinase activity, GO:0004747	D-ribose metabolic process, GO:0006014	
LdBPK_141300.1	hypothetical protein, conserved	0.016	0.54	0.60	0.37	0.50			

a manually annotated as cilium, GO:0005929

b manually annotated as eukaryotic translation initiation factor 4F complex, GO:0016281

c manually annotated as cilium movement involved in cell motility, modulation of development of symbiont involved in interaction with host, quorum sensing involved in interaction with host, GO:0060294, GO:0044145, GO:0052106, cilium, GO:0005929

d manually annotated as fructose transmembrane transporter activity, galactose transmembrane transporter activity, glucose transmembrane transporter activity, mannose transmembrane transporter activity, GO:0005353, GO:0005354, GO:0005355, GO:0015578, glucose transport, GO:0015758, motile cilium, GO:0031514, glucose transport, GO:0031514, glucose transport, GO:0015758, motile cilium, GO:0031514
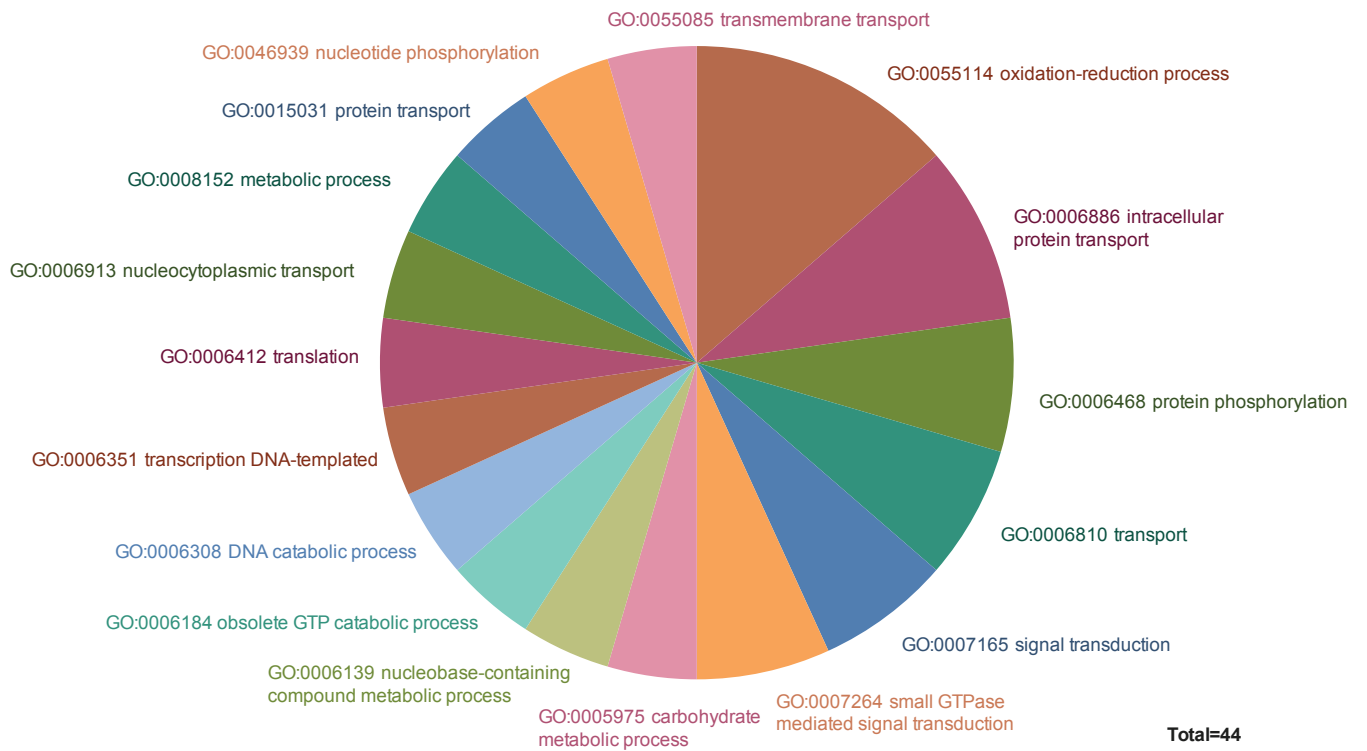
Table 4.4 continued

Figure 4.7 GO function process with more than 1 protein significantly upregulated in Δ*gmpr*Δ*impdh* cultured in xanthine versus hypoxanthine.
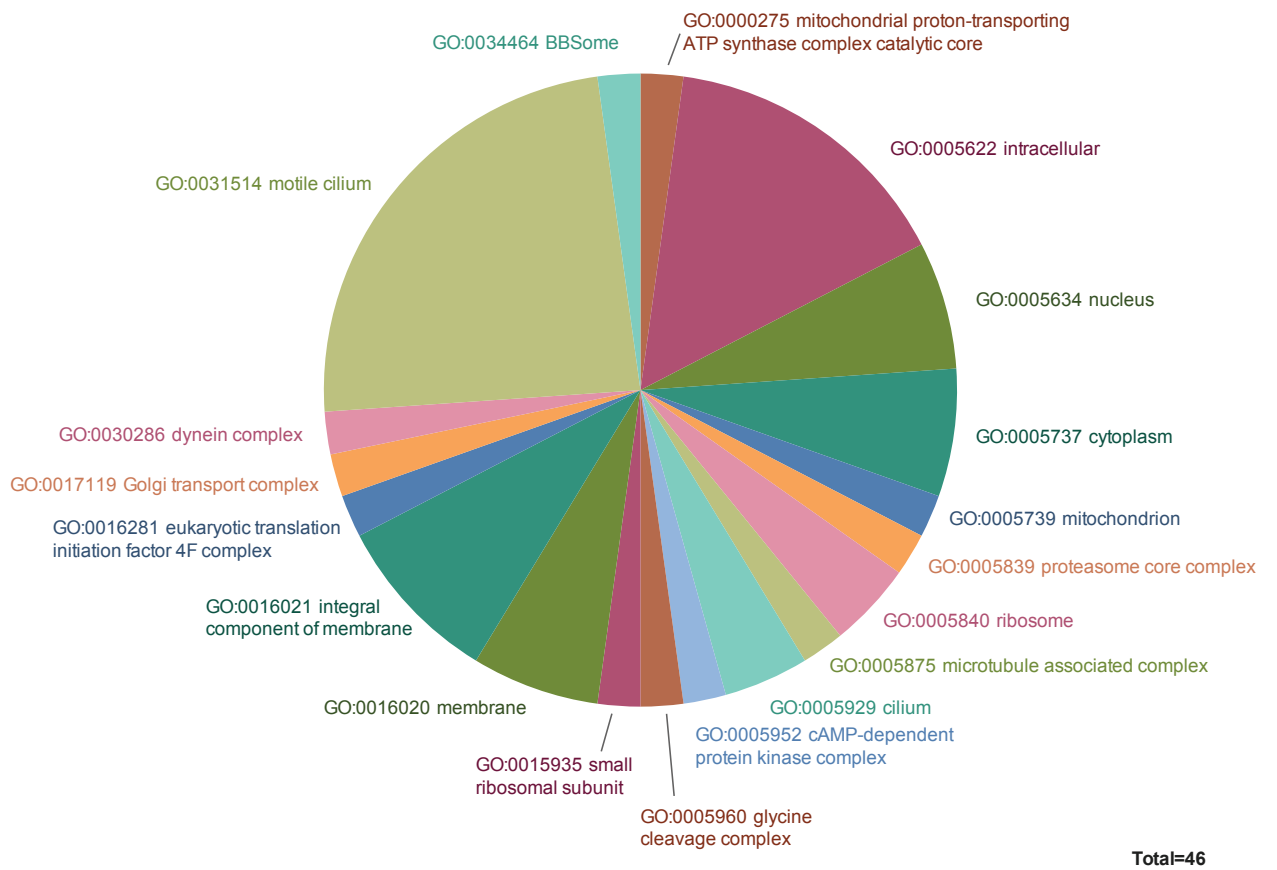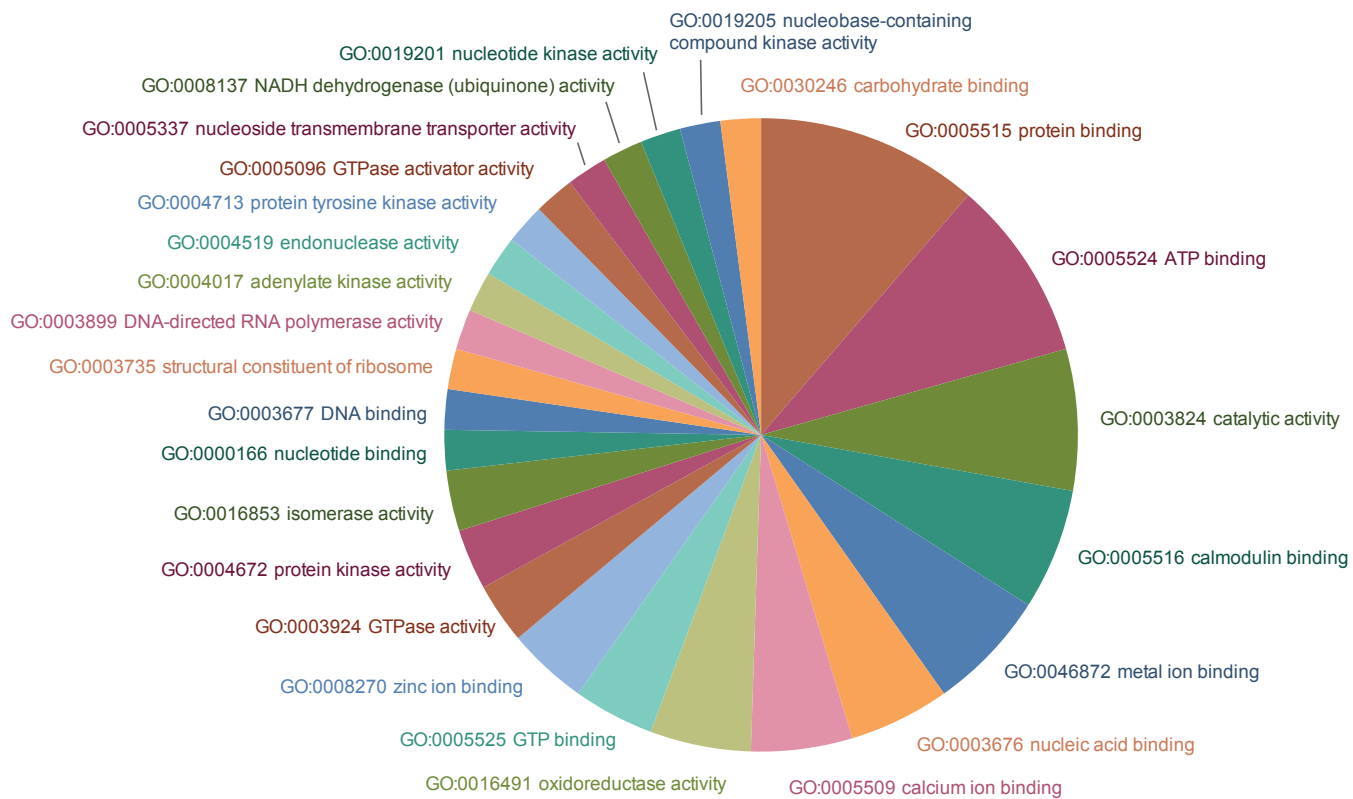
Figure 4.8 GO component categories with more than 1 protein significantly upregulated in Δ*gmpr*Δ*impdh* cultured in xanthine versus hypoxanthine.

Figure 4.9 GO function categories with more than 1 protein significantly upregulated in Δ*gmpr*Δ*impdh* cultured in xanthine versus hypoxanthine.

Protein	Product	pvalue	log2(X1/H1)	log2(X2/H2)	log2(X3/H3)	Average log2(X/H)	Gene ontology (GO)	Gene ontology (molecular function)	Gene ontology (cellular component)	Gene ontology IDs
LdBPK_363780.1	hypothetical protein, conserved	0.022	1.22	0.46	0.70	0.79	calcium ion binding [GO:0005509]	calcium ion binding [GO:0005509]		GO:0005509
LdBPK_291260.1	hypothetical protein, conserved	0.003	0.77	0.58	0.70	0.69	calcium ion binding [GO:0005509]	calcium ion binding [GO:0005509]		GO:0005509
LdBPK_090970.1	calmodulin, putative	0.033	0.64	0.52	0.48	0.55	calcium ion binding [GO:0005509]	calcium ion binding [GO:0005509]		GO:0005509
LdBPK_366370.1	centrin, putative	0.025	0.65	0.53	0.38	0.52	calcium ion binding [GO:0005509]	calcium ion binding [GO:0005509]		GO:0005509
LdBPK_272520.1	cysteine peptidase, Clan CA, family C2, putative	0.012	0.47	0.42	0.38	0.42	intracellular [GO:0005622]; calcium-dependent cysteine-type endopeptidase activity [GO:0004198]	calcium-dependent cysteine-type endopeptidase activity [GO:0004198]	intracellular [GO:0005622]	GO:0004198; GO:0005622
LdBPK_303410.1	calmodulin-related protein, putative	0.025	0.39	0.42	0.40	0.40	calcium ion binding [GO:0005509]	calcium ion binding [GO:0005509]		GO:0005509
LdBPK_070790.1	centrin, putative	0.078	0.40	0.55	0.18	0.38	calcium ion binding [GO:0005509]	calcium ion binding [GO:0005509]		GO:0005509
LdBPK_110810.1	hypothetical protein, conserved	0.053	0.32	0.46	0.25	0.34	calcium ion binding [GO:0005509]	calcium ion binding [GO:0005509]		GO:0005509
LdBPK_210280.1	calmodulin-like protein	0.089	0.54	0.40	0.05	0.33	calcium ion binding [GO:0005509]	calcium ion binding [GO:0005509]		GO:0005509
LdBPK_321020.1	calpain-like cysteine peptidase, putative	0.027	0.33	0.33	0.33	0.33	intracellular [GO:0005622]; calcium-dependent cysteine-type endopeptidase activity [GO:0004198]	calcium-dependent cysteine-type endopeptidase activity [GO:0004198]	intracellular [GO:0005622]	GO:0004198; GO:0005622
LdBPK_366660.1	hypothetical protein, conserved	0.100	0.41	0.27	0.29	0.32	calcium ion binding [GO:0005509]	calcium ion binding [GO:0005509]		GO:0005509
LdBPK_341100.1	hypothetical protein, conserved	0.062	0.32	0.18	0.45	0.32	calcium ion binding [GO:0005509]	calcium ion binding [GO:0005509]		GO:0005509
LdBPK_342780.1	hypothetical protein, conserved	0.015	0.51	0.31	0.13	0.32	calcium ion binding [GO:0005509]	calcium ion binding [GO:0005509]		GO:0005509
LdBPK_354120.1	hypothetical protein, conserved	0.015	0.26	0.35	0.30	0.30	calcium ion binding [GO:0005509]	calcium ion binding [GO:0005509]		GO:0005509
LdBPK_270720.1	hypothetical protein, conserved	0.081	0.33	0.28	0.27	0.29	calcium ion binding [GO:0005509]	calcium ion binding [GO:0005509]		GO:0005509
LdBPK_081030.1	hypothetical protein, conserved	0.002	0.30	0.29	0.27	0.29	calcium ion binding [GO:0005509]	calcium ion binding [GO:0005509]		GO:0005509
LdBPK_070700.1	vacuolar-type Ca2-ATPase, putative	0.076	-0.15	-0.23	-0.28	-0.22	integral component of membrane [GO:0016021]; ATP binding [GO:0005524]; calcium-transporting ATPase activity [GO:0005388]; metal ion binding [GO:0046872]	ATP binding [GO:0005524]; calcium-transporting ATPase activity [GO:0005388]; metal ion binding [GO:0046872]	integral component of membrane [GO:0016021]	GO:0005524; GO:0005388; GO:0016021; GO:0046872
LdBPK_280760.1	hypothetical protein, conserved	0.099	-0.14	-0.37	-0.32	-0.28	calcium ion binding [GO:0005509]	calcium ion binding [GO:0005509]		GO:0005509
LdBPK_201230.1	calpain-like cysteine peptidase, putative	0.004	-0.44	-0.39	-0.64	-0.49	intracellular [GO:0005622]; calcium-dependent cysteine-type endopeptidase activity [GO:0004198]	calcium-dependent cysteine-type endopeptidase activity [GO:0004198]	intracellular [GO:0005622]	GO:0004198; GO:0005622

Table 4.5 Summary of calcium metabolism proteins regulated in Δ*gmpr*Δ*impdh* L. *donovani* after 24 hour purine limitation

155

AMPK component	TriTrypID	Peptide	MSGF_SpecProb	AScore	pvalue	log2 (xan/hyp)			
						replicate 1	replicate 2	replicate 3	average
gamma, regulatory	LdBPK_350780.1	K.NTTSVAGDSDLSS*PQHNNSHQLR.S	3.8E-21	19	0.00	1.59	1.58	1.34	1.50
beta, scaffolding	LdBPK_230530.1	Y.SHLPANPVDPLES*LQA.-	1.4E-11	181	0.71	0.27	-0.38	-0.15	-0.09
		S.HLPANPVDPLES*LQA.-	6.8E-13	1000	0.08	0.21	0.06	0.34	0.20
		Y.YSHLPANPVDPLES*LQA.-	7.2E-15	78	0.09	0.11	0.06	0.34	0.17
		H.LRYT*PLNT*PPTLVR.C	2.7E-09	15	0.12	-0.07	-0.26	-0.44	-0.25
		R.YTPLNT*PPTLVR.C	4.7E-14	43	0.03	-0.28	-0.52	-0.12	-0.30
alpha catalytic	LdBPK_292140.1	R.GAS*PPASAAASTSAIAEPASSPANPVVISLY.F	2.0E-10	44	0.12	8.83	0.00	8.49	5.77
		R.S*FGSAPGGGFNT*SSSQVAR.G	5.8E-13	28	0.02	0.79	0.20	0.57	0.52
		G.S*APGGGFNTSSSQVAR.G	7.3E-12	224	0.13	0.65	-0.16	0.73	0.41
		R.S*FGSAPGGGFNTSSSQVAR.G	6.6E-13	77	0.00	0.51	0.30	0.30	0.37
		R.RNT*LS*TYSVESSAPIR.I	1.2E-09	32	0.04	0.50	0.17	0.47	0.38
		R.RNT*LSTYSVESSAPIR.I	1.7E-10	46	0.19	0.35	0.37	-0.03	0.23
		R.NTLSTYS*VESSAPIR.I	2.2E-13	17	0.29	0.35	-0.02	0.30	0.21
		G.SAPGGGFNTS*SSQVAR.G	1.2E-10	21	0.30	0.34	-0.13	0.25	0.15
		G.SAPGGGFNTSSS*QVAR.G	1.6E-13	24	0.12	0.21	0.00	0.31	0.18
		R.GAAGLTGGSSS*YRR.A	2.2E-09	21	0.14	0.16	0.38	0.00	0.18
		R.S*FGS*APGGGFNTSSSQVAR.G	6.2E-13	158	0.03	0.13	0.33	0.12	0.19
		R.GAAGLTGGSSSY*RR.A	3.8E-14	22	0.42	0.12	0.02	0.06	0.07
		R.S*FGSAPGGGFNTSSS*QVAR.G	3.4E-13	24	0.16	0.07	0.07	0.38	0.18
		R.AGMQSS*TGGTAASQLGANLSDQPR.V	6.0E-13	14	0.31	0.05	0.08	1.11	0.41
		G.SSSYAPGS*LR.G	1.6E-09	58	0.45	0.05	-0.13	0.43	0.11
		G.SGSVGSSSYAPGS*LR.G	1.6E-13	56	0.65	0.03	-0.16	0.26	0.04
		R.GAAGLTGGS*SSYR.R	1.5E-09	20	0.14	0.00	-0.21	-0.10	-0.10
		K.VSDTSLSDGSGNGGPGGSIAVGS*FR.I	3.1E-17	61	0.36	-0.03	-0.03	-0.34	-0.14
		R.GAAGLTGGSS*S*YRR.A	1.9E-10	22	0.40	-0.32	0.12	-0.09	-0.09
alpha catalytic	LdBPK_360960.1	L.QPQRS*PTTR.T	1.6E-09	15	0.05	0.71	0.18	0.22	0.37
		Q.QLTGNSS*FTGLSFK.E	3.3E-12	22	0.45	0.35	-0.33	0.46	0.16
		K.VEVGLS*DPHSPIPTGR.P	1.4E-10	60	0.40	0.13	0.46	-0.09	0.17
		K.VEVGLSDPHS*PIPTGR.P	1.3E-18	33	0.05	0.06	0.74	0.71	0.50
		R.FFET*SCGTPNYASPEVVSGR.L	3.6E-16	27	0.55	0.06	-0.16	0.01	-0.03
		N.SLQQLTGNSS*FTGLSFK.E	1.8E-16	32	0.98	-0.08	-0.12	0.19	0.00

Table 4.6 Differential phosphorylation of AMPK subunit peptides

The four predicted subunits of AMPK are listed with their identified phosphorylated peptides. As determined by the global proteome analysis of ΔgmprΔimpdh cells cultured in xanthine versus hypoxanthine, none of these four proteins was significantly changed; the log2 transform of each protein fold change was < 0.3 and each had a p-value > 0.05.

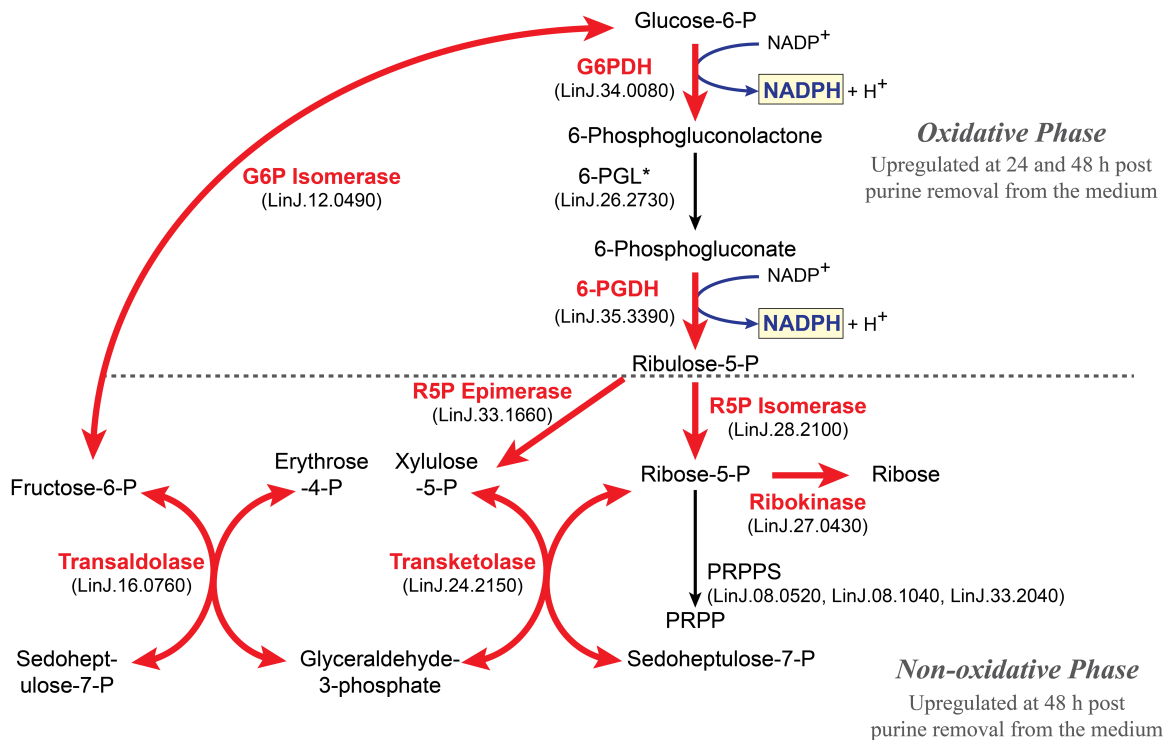# Appendix A: Chapter 2 Supporting information

Figure A.1 A Schematic of the Changes in the Pentose Phosphate Pathway Upon Purine Starvation.

Thick red arrows indicate those steps catalyzed by proteins (in red) that are upregulated and black arrows indicate those steps catalyzed by activities that are unchanged during purine starvation. The conversion of NADP$^+$ to NADPH is represented by the blue arrows. Proteins marked by an * were absent from the 6 - 48 h proteome datasets. TriTrypDB accession numbers are given for each protein. *Abbreviations:* G6PDH, glucose-6-phosphate dehydrogenase; 6-PGL, 6-phosphogluconolactonase; 6-PGDH, 6-phosphogluconate dehydrogenase; R5P Isomerase, putative ribose-5-phosphate isomerase; R5P Epimerase, putative ribulose-5-phosphate-4-epimerase; PRPPS, phosphoribosyl pyrophosphate synthetase; G6P Isomerase, glucose-6-phosphate isomerase.
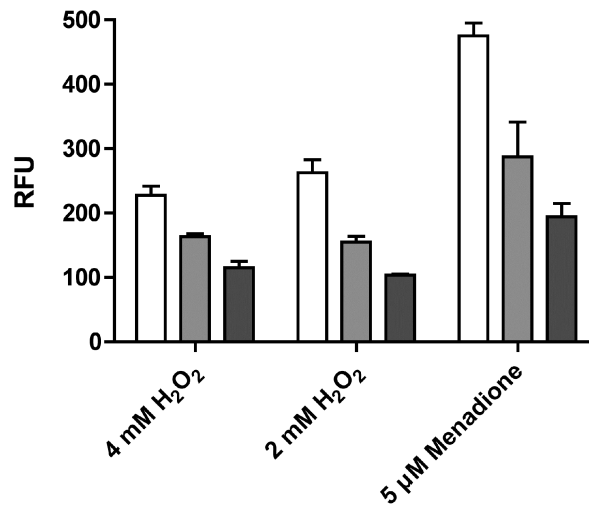
Figure A.2 Response of Purine-Starved and Purine-Replete Parasites to H₂O₂.

Purine-replete (open bars) and purine starved (24, 48 h, light and dark grey bars, respectively) promastigotes were exposed to 4 and 2 mM H_2O_2 as well as 5 µM of the ROS-generating compound menadione. Generation of ROS was measured by incubating parasites with the cell-permeant fluorescein derivative H_2DCFDA. Error bars indicate standard deviation; data represent three independent biological replicates.

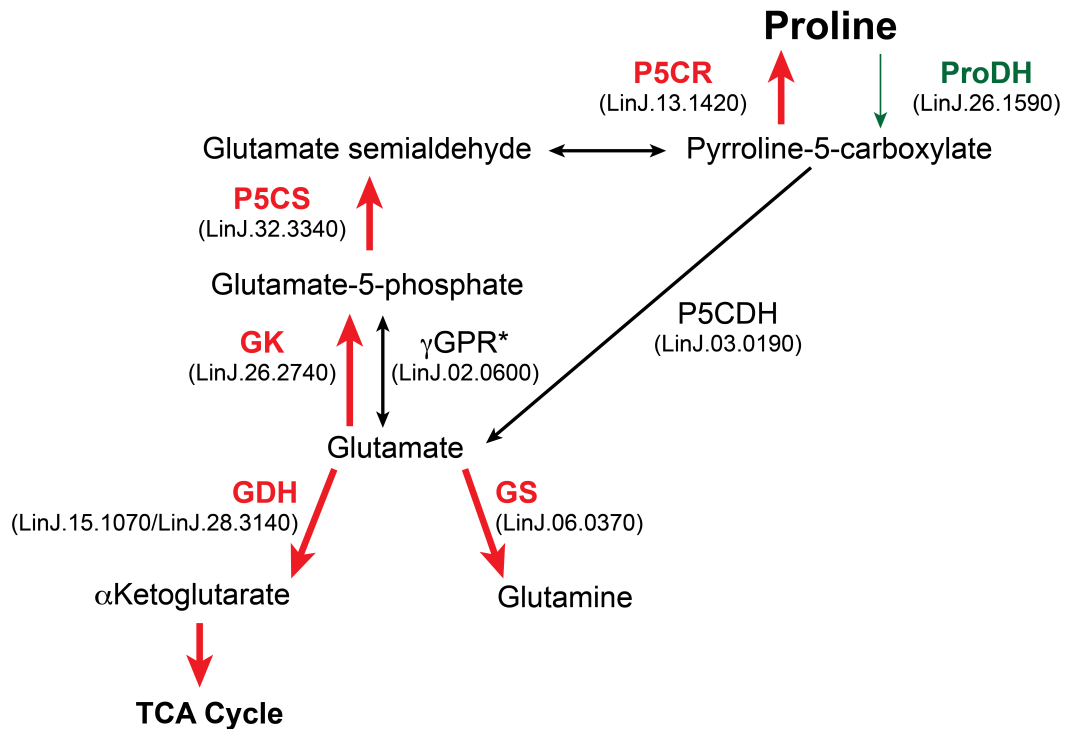**Figure A.3 A Schematic of the Changes in Proline and Glutamate Metabolism Upon Purine Starvation.**

Thick red arrows indicate those steps catalyzed by proteins (in red) that are upregulated, the thin green arrow represents the step catalyzed by ProDH (in green) that is downregulated, and the black arrows indicate those steps that are unchanged during purine starvation. γGPR* could not be detected in the 6 - 48 h proteome datasets. TriTrypDB accession numbers are given for each protein. *Abbreviations:* P5CR, pyrroline-5-carboxylate reductase, putative; ProDH, proline dehydrogenase, putative; P5CDH, delta-1-pyrroline-5-carboxylate dehydrogenase, putative; P5CS, pyrroline-5-carboxylate synthetase-like protein; GK, putative glutamate 5-kinase; γGPR, putative γ-glutamyl phosphate reductase; GDH, glutamate dehydrogenase; GS, putative glutamine synthetase.
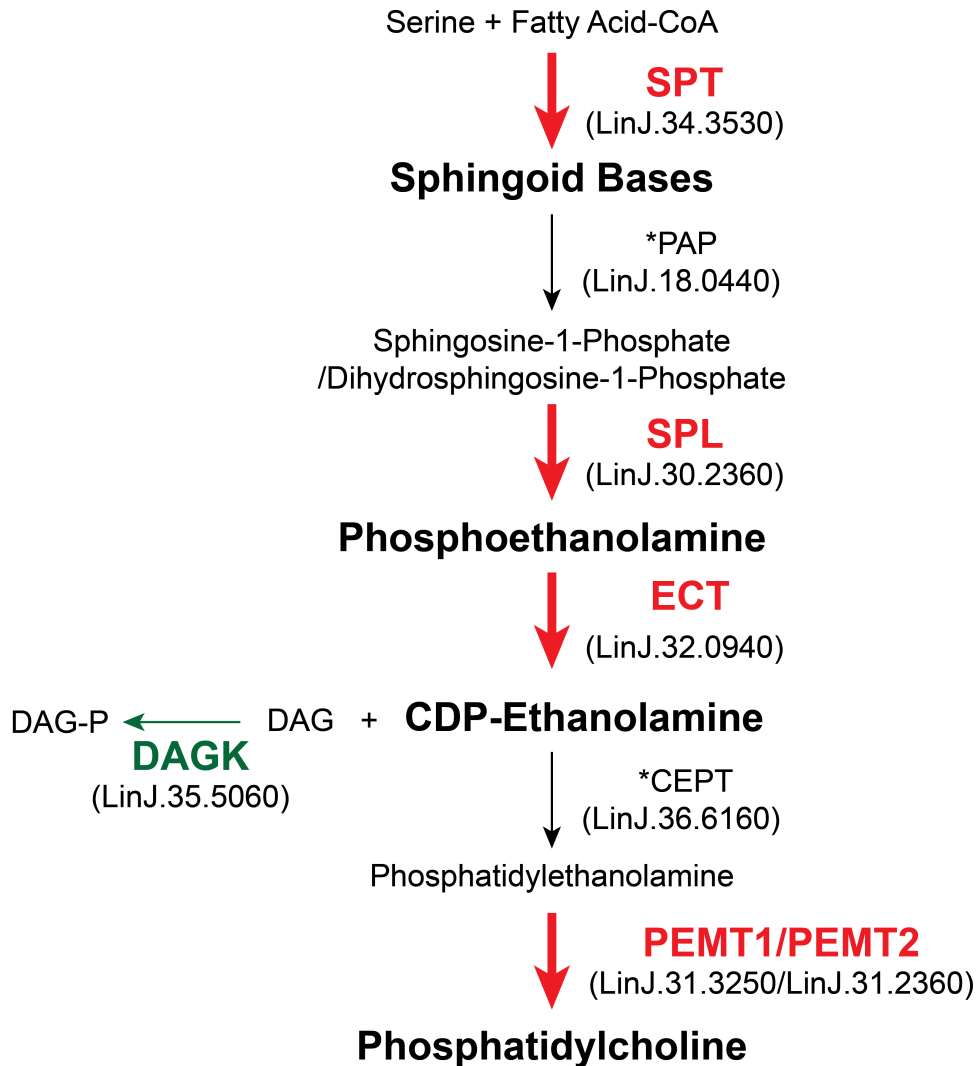
Serine + Fatty Acid-CoA

$\downarrow$ **SPT**
(LinJ.34.3530)

Sphingoid Bases

$\downarrow$ *PAP
(LinJ.18.0440)

Sphingosine-1-Phosphate
/Dihydrosphingosine-1-Phosphate

$\downarrow$ **SPL**
(LinJ.30.2360)

Phosphoethanolamine

$\downarrow$ **ECT**
(LinJ.32.0940)

DAG-P $\longleftarrow$ DAG + ## CDP-Ethanolamine
DAGK
(LinJ.35.5060)

$\downarrow$ *CEPT
(LinJ.36.6160)

Phosphatidylethanolamine

$\downarrow$ **PEMT1/PEMT2**
(LinJ.31.3250/LinJ.31.2360)

Phosphatidylcholine

Figure A.4 A Schematic of the Changes in Sphingoid Base and Phospholipid Metabolism Upon Purine Starvation.

Thick red arrows indicate those steps catalyzed by proteins (in red) that are upregulated, green arrows indicate those steps catalyzed by proteins (in green) that are downregulated, and black arrows indicate those steps catalyzed by activities that are unchanged during purine starvation. Proteins marked by an * were absent from the 6 - 48 h proteome datasets. TriTrypDB accession numbers are given for each protein. *Abbreviations:* SPT, serinepalmitoyltransferase-like protein; PAP, phosphatidic acid phosphatase; SPL, putative sphingosine 1-phosphate lyase; ECT, putative ethanolamine-phosphate cytidylyltransferase; CEPT, putative choline/ethanolamine phosphotransferase; PEMT1/2, phosphatidylethanolamine-methyltransferase-like proteins 1 and 2; DAGK, diacylglycerol kinase-like protein.
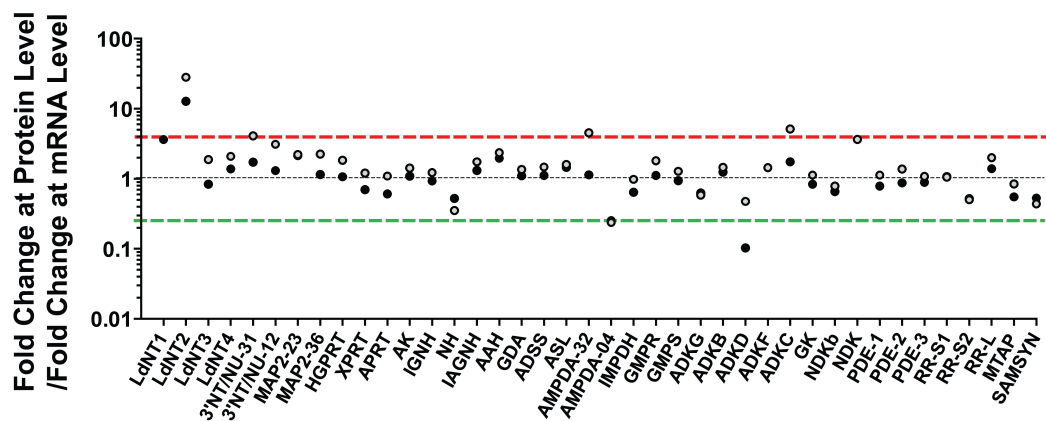
Figure A.5 A Comparison of the Fold Changes at the Protein Level with those at the mRNA Level for Various Purine Pathway Activities.

For purine-starved cells the fold changes at the protein level at 24 h (closed circles) and 48 h (grey circles) were divided by the fold change at the mRNA level as measured by RNA-seq. Black dotted line represents an exact correlation between the fold changes at the protein and mRNA level, and the dashed lines a 4-fold difference between the protein and mRNA levels either up (red) or down (green). See the legend of Fig. 2 for a list of the abbreviations.
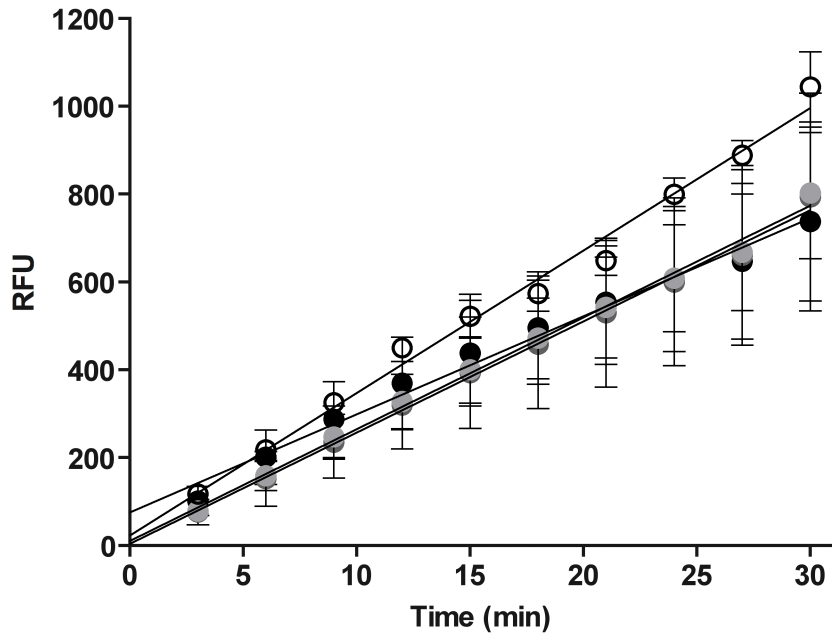
Figure A.6. Rates of Resazurin Reduction by Purine-Starved and Purine-Replete Parasites.

Generation of fluorescence arising from the irreversible reduction of resazurin to the fluorescent product resorufin was measured over time for purine-replete cells (open circles), 24 h purine-starved cells (light grey circles), 48 h purine-starved cells (dark grey circles), and cells starved for purine for two weeks (closed circles). Error bars indicate standard deviation, data represent two biological replicates for purine-replete cells and 3 biological replicates for all sets of purine-starved cells.

SUPPLEMENTARY MATERIALS AND METHODS

Comparative Shotgun Proteomics Using Spectral Count Data

Sample collection, digestion, chromatographic separations, and mass spectrometry. Promastigotes of the clonal derivative LdBob from *Leishmania donovani* strain 1S2D were cultured in DME-L with additional supplements, including 100 μM hypoxanthine, as described in the *Materials and Methods*. To induce purine starvation exponentially growing cells were washed twice in DME-L medium with (purine-replete sample) or without 100 μM hypoxanthine (purine-starved samples) and resuspended at 2 x 10^6 cells ml^{-1} in purine-replete or purine-deplete media, respectively. After 24 h, 2 x 10^8 cells were harvested from both the purine-replete and purine-starved cultures by centrifugation at 1,500 x *g*, washed once in D-PBS, and resuspended in 0.5 ml of 25 mM ammonium bicarbonate buffer. Cells were disrupted by sonication using a Sonic Dismembrator, model F60 (Fisher Scientific) at a setting of 2 and with 3 x 15 sec bursts with cooling in between. The protein content of each sample was determined by bicinchoninic acid assay using the BCA assay kit (Pierce, Rockville, IL) and 1 mg portions of protein dried by centrifugal evaporation. Samples were suspended in 8M urea buffer, reduced with dithioerythritol, alkylated with idoacetamide, and digested overnight with trypsin. Following addition of formic acid to a final 5% concentration, digests were solid phase extracted on Sep Pak Light Cartridges (Waters Corp., Milford, MA) and peptides separated by strong-cation exchange (**SCX**) chromatography into 32 fractions

using a polysulfoethyl A column (PolyLC Inc., Columbia MD). The digestion and SCX methods have been previously described (229). Forty percent of each cation exchange fraction was then separated by reverse phase chromatography and 100 minutes of tandem mass spectrometry data were collected for each of the 32 fractions using an LTQ linear ion trap (Thermo Scientific, San Jose, CA) operated as described in ref. (230).

Database searches

The closest species to *L. donovani* with a sequenced genome at the time of the study was *L. infantum* and RefSeq entries were extracted from a Dec. 28, 2009 download of the NCBI nr database using in-house tools (available at www.ProteomicAnalysisWorkbench.com). A target/decoy database was created by adding 179 contaminant entries to 7,872 *L. infantum* entries and then concatenating the 8,051 sequence-reversed entries. DTA files were created by BioWorks 3.3 (Thermo Scientific) with a molecular weight range of 550 to 4,000, an absolute threshold of 500, 1 group scan, more than 25 ions, and charge state analysis using ZSA. The numbers of DTA files ranged from 405,000 to 466,000 for the four samples. SEQUEST (version 27, rev. 12, Thermo Scientific) searches were configured with an average parent ion mass tolerance of 2.5 Da, a monoisotopic fragment ion tolerance of 1 Da, trypsin cleavage specificity, static +57 Da mass modification of cysteine residues, and variable modifications of +16 Da on methionine and +80 Da on serine, threonine, and tyrosine residues.

Peptide and protein identification

A flexible proteomic analysis pipeline developed in-house was used to accurately identify peptides and proteins (231). Briefly, SEQUEST scores were combined into discriminate function scores (176, 232) and histograms of scores for matches to the target and to the decoy database were tabulated for different peptide classes with a 7 amino acid minimum peptide length. The target and decoy score distributions were used to estimate peptide false discovery rates (**FDR**) for each peptide class and set thresholds to filter out incorrect matches. Correct peptide sequences were mapped to protein sequences using peptide-subset-removal parsimony filtering. Peptide sequences from all samples in the experiment were mapped in total followed by removal of any proteins lacking sufficient per sample evidence (two distinct peptides per protein). Peptide thresholds were iteratively determined based on overall protein FDR estimated from decoy protein matches and a peptide FDR of 0.7% was used. Previously, peptides were separated into different classes for FDR analysis based on charge state. In this work, additional classes were added for unmodified peptides, peptides containing M+16 modifications, and peptides containing STY+80 modifications.

Protein differential expression

Protein abundances were estimated using spectral counting (233). Total spectral counts were normalized across samples using quantile normalization, a method that works well in large-scale studies (234). The counts of peptides mapped to

multiple proteins were fractionally split based on the relative unique peptide counts of those proteins. Two methods for determining statistical significance of differential expression candidates were used. A basic Chi square test was computed using the average spectral counts from the purine-replete and purine-deplete samples where the null hypothesis was equal expression in both conditions. A second method ranked proteins from highest total spectral count to lowest, computed the $\log_2$ of the abundance ratio of the average counts in the two conditions for each protein, and renormalized the ratios (a Z-transfomation using trimmed ratios where the top 5 and bottom 5 ratios were excluded) in a 101-protein sliding window. This removes intensity-dependent dispersion in the expression ratios (235) and is, in essence, an adaptive fold-change test. Candidates from each test were determined by applying a Benjamini-Hochberg correction to p-values (236) and the union of the two sets of candidates was formed. We averaged spectral counts across the 4 samples and imposed a minimum count cutoff of 2.5 to reduce missing data points to negligible levels (less than 1%) and reduce the impact of small count fluctuations.

Measurement of Resazurin Reduction in Purine-Starved and Purine-Replete Parasites

Log-phase promastigotes cultured continuously in 100 μM hypoxanthine or without purine for 24 h, 48 h, or 2 weeks, were resuspended in growth media plus or minus purine at a density of 5 X 10^8 cells. A 100 μl of each cell suspension was transferred to a black, polystyrene 96-well plate along with a 10

µl of a 10x resazurin (alamarBlue®) solution (Life Technologies). Fluorescence attributable to the reduction of resazurin to resorufin was monitored at 560 nm_{ext} / 590 nm_{em} for 60 min using a SpectraMax M2 Microplate Reader (MolecularDevices GmbH, Ismaning/München, Germany). Heat-killed parasites (heated at 75 ºC for 10 min) and wells without the addition of cells served as controls.

Appendix B: Chapter 3 supporting information
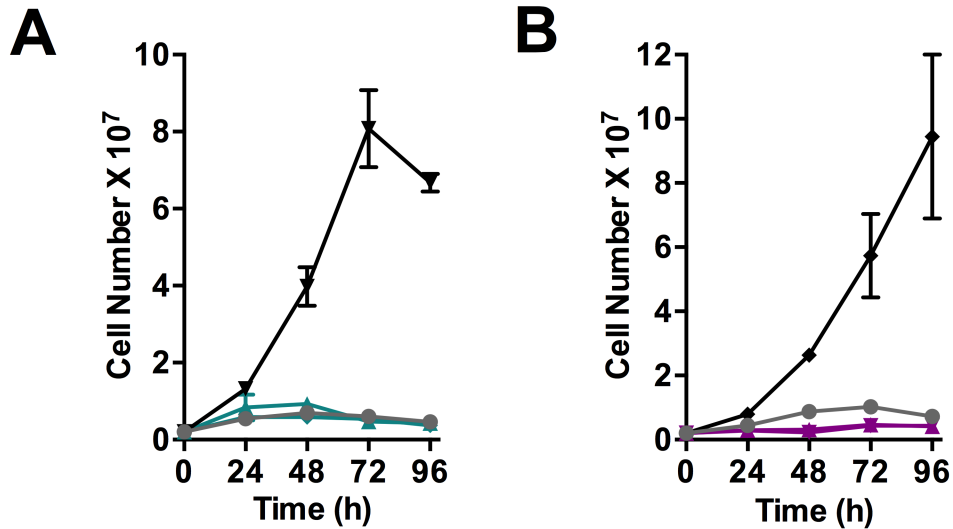
Figure B.1 Growth phenotypes for ∆*aah*∆*adss* and ∆*impdh* cell lines.
(**A**) ∆*aah*∆*adss* promastigotes were cultured in adenine (black triangle); hypoxanthine (teal triangle); xanthine (teal diamond) or no purine (gray); (**B**) ∆*impdh* promastigotes were cultured in xanthine (black); hypoxanthine (purple triangle up); adenine (purple triangle down); or no purine (gray) and growth was evaluated as described in *Materials and Methods*.
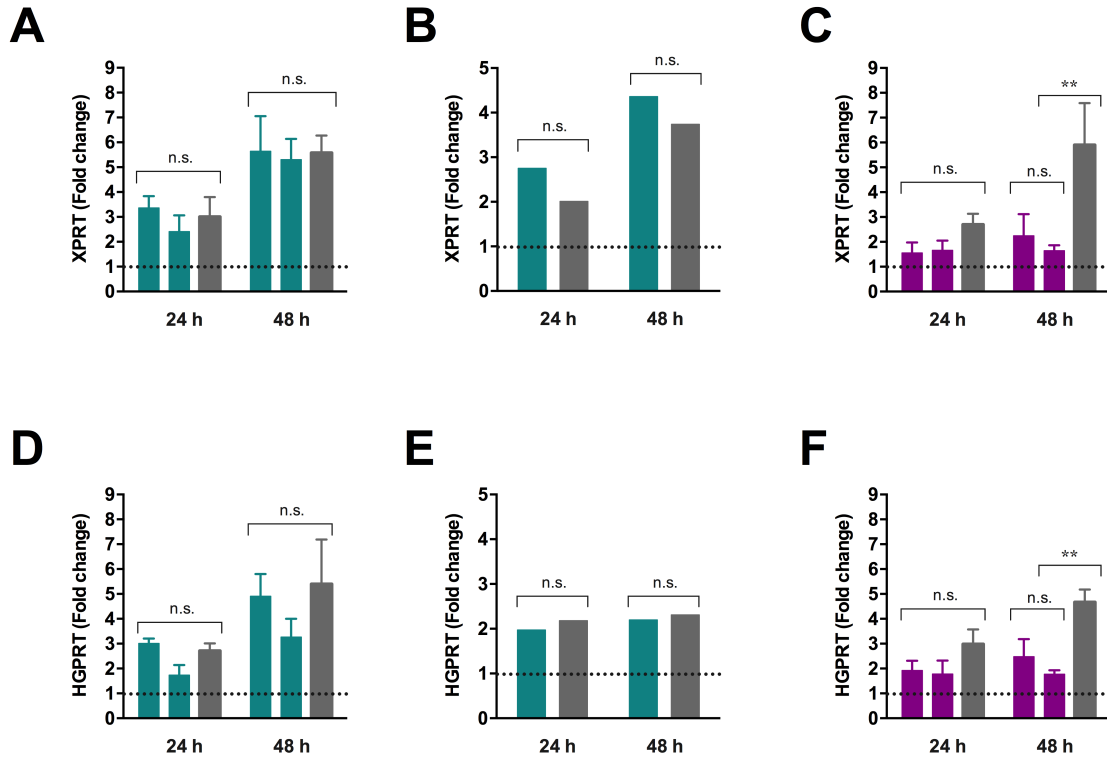
Figure B.2 Effect of intracellular purine pool perturbations on the abundance of XPRT and HGPRT proteins.

(**A, D**) Δ*aah*Δ*adss* promastigotes were cultured in hypoxanthine or xanthine (teal, predicted to perturb the adenylate pool) or no purine (gray); (**B, E**) Δ*gmpr* promastigotes were cultured in xanthine (teal, predicted to perturb the adenylate branch) or no purine (gray); (**C, F**) Δ*impdh* promastigotes were cultured in hypoxanthine or adenine (purple, predicted to perturb the guanylate branch) or no purine (gray). XPRT (**A, B, C**) and HGPRT (**D, E, F**) protein abundance levels at 24 and 48 h were determined via western blotting as described in *Materials and Methods.* Tubulin was used as a loading control and fold changes are compared to the permissive condition, normalized to 1. For panels A, C, D, F n = 3; B, E n = 1.
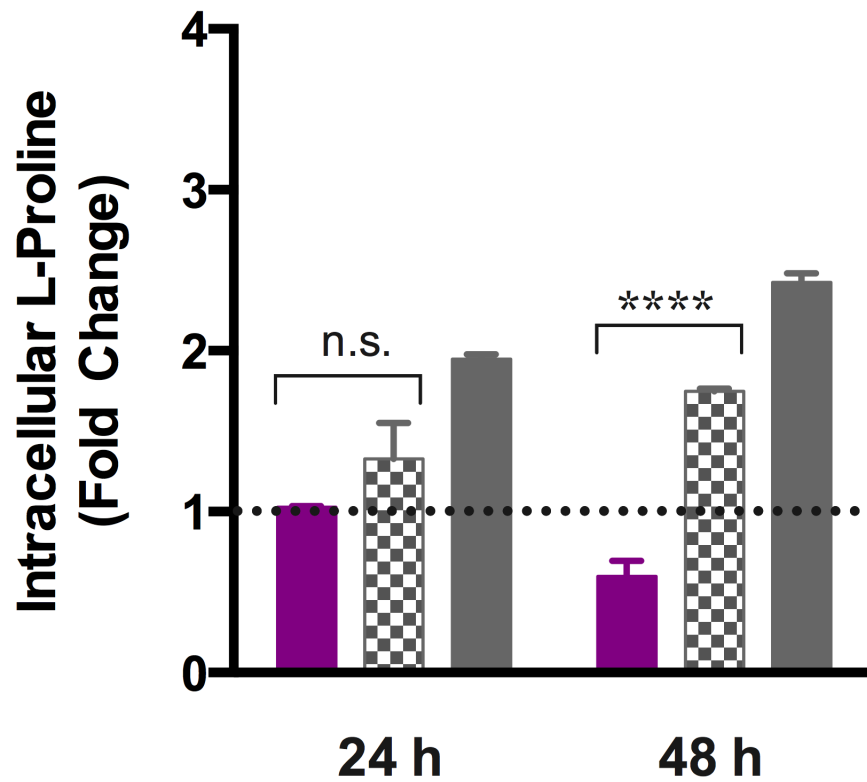
Figure B.3 Changes in free intracellular L-proline for Δ*gmps*.
Intracellular L-proline levels were determined for Δ*gmps* promastigotes cultured
in an extracellular purine source that is permissive for growth (guanine, set to 1,
dashed line), predicted to perturb GMP production (hypoxanthine, purple) or both
AMP and GMP synthesis (xanthine, gray and white checkered square, no purine,
gray solid); fold changes were determined by comparing to the permissive
condition, normalized to 1.

Description	TriTrypDB ID (*L. infantum*)	GenBank Accession Number	Primer Sequence - Forward / Primer Sequence - Reverse
LdNT1.1	LinJ.15.1230-50	AF065311	5'-GTGATGGAGGTCATCTTCGGCTTCTC-3' / 5'-GCTTGCCGTCGTTGTCGATGC-3'
LdNT2	LinJ.36.2040	AF245276	5'-CGCACTCTTCATGTCGATCATCCAG-3' / 5'-CCGATTCCAATGCCGAAGTAGATGC-3'
LdNT3	LinJ.13.1110	HM147245	5'-GGTGAGTTCCGTGCCATCAAGC-3' / 5'-GCTGGTTGCTGCTGCTGAG-3'
3'NT/NU (Chr12)	LinJ.12.0350	XM_003859104	5'-GACACCATCTACAACCCACAG-3' / 5'-ATGAGGTTTGCGACAGAGG-3'
3'NT/NU (Chr31)	LinJ.31.2380	L35078	5'-GTTATCGACTCCAAGGGAACC-3' / 5'-GTACGTTGCTTCCAGATAGTCG-3'
MAP2	LinJ.36.2720	XM_003865339	5'-AGCAGATGGTGAAGAACATGGA-3' / 5'-GCGCTGTAGTGCATCAACTTG-3'
XPRT	LinJ.21.0990	XM_003860567	5'-GCTCGTCTGTCACCCAGCAC-3' / 5'-GGATGAAGTCGGATGTGAAGATGTAGCTG-3'
AAT19	LinJ.07.1340	XM_003858517	5'-TTCATCGGCTTCATCTTCCC-3' / 5'-ACTCTAGCAACCCCACATTC-3'
Oxidoreductase	LinJ.29.0260	XM_003862395	5'-CGTGGAGCGCATCTCGAT-3' / 5'-TTCGGCAGGCAGGAAATC-3'
OMPDC/OPRT	LinJ.16.0560	JN882599	5'-GATTGAGCAGACGCACGAGTACG-3' / 5'-CGGCACGAATCACTTCCGACAG-3'

Table B.1 qRT-PCR primers

References

1.   Lopes AH, Souto-Padrón T, Dias FA, Gomes MT, Rodrigues GC, Zimmermann LT, Alves e Silva TL, Vermelho AB. Trypanosomatids: Odd Organisms, Devastating Diseases. The Open Parasitology Journal. 2010;4:30-59. doi: 10.2174/1874421401004010030.

2.   Dacks JB, Walker G, Field MC. Implications of the new eukaryotic systematics for parasitologists. Parasitol Int. 2008;57(2):97-104. Epub 2008/01/09. doi: 10.1016/j.parint.2007.11.004. PubMed PMID: 18180199.

3.   Lukes J, Guilbride DL, Votypka J, Zikova A, Benne R, Englund PT. Kinetoplast DNA network: evolution of an improbable structure. Eukaryot Cell. 2002;1(4):495-502. Epub 2002/11/29. PubMed PMID: 12455998; PMCID: 117999.

4.   Shapiro TA, Englund PT. The structure and replication of kinetoplast DNA. Annu Rev Microbiol. 1995;49:117-43. Epub 1995/01/01. doi: 10.1146/annurev.mi.49.100195.001001. PubMed PMID: 8561456.

5.   Shlomai J. The structure and replication of kinetoplast DNA. Curr Mol Med. 2004;4(6):623-47. Epub 2004/09/11. PubMed PMID: 15357213.

6.   Parsons M. Glycosomes: parasites and the divergence of peroxisomal purpose. Mol Microbiol. 2004;53(3):717-24. Epub 2004/07/17. doi: 10.1111/j.1365-2958.2004.04203.x

MMI4203 [pii]. PubMed PMID: 15255886.

7.   Michels PA, Bringaud F, Herman M, Hannaert V. Metabolic functions of glycosomes in trypanosomatids. Biochim Biophys Acta. 2006;1763(12):1463-77. Epub 2006/10/07. doi: S0167-4889(06)00231-X [pii]

10.1016/j.bbamcr.2006.08.019. PubMed PMID: 17023066.

8.   Opperdoes FR. Compartmentation of carbohydrate metabolism in trypanosomes. Annu Rev Microbiol. 1987;41:127-51. Epub 1987/01/01. doi: 10.1146/annurev.mi.41.100187.001015. PubMed PMID: 3120638.

9.   Hannaert V, Michels PA. Structure, function, and biogenesis of glycosomes in kinetoplastida. J Bioenerg Biomembr. 1994;26(2):205-12. Epub 1994/04/01. PubMed PMID: 8056787.

10.   Bakker BM, Michels PA, Opperdoes FR, Westerhoff HV. Glycolysis in bloodstream form Trypanosoma brucei can be understood in terms of the kinetics of the

glycolytic enzymes. J Biol Chem. 1997;272(6):3207-15. Epub 1997/02/07. PubMed PMID: 9013556.

11.   Bakker BM, Westerhoff HV, Opperdoes FR, Michels PA. Metabolic control analysis of glycolysis in trypanosomes as an approach to improve selectivity and effectiveness of drugs. Mol Biochem Parasitol. 2000;106(1):1-10. Epub 2000/04/01. PubMed PMID: 10743606.

12.   Bakker BM, Mensonides FI, Teusink B, van Hoek P, Michels PA, Westerhoff HV. Compartmentation protects trypanosomes from the dangerous design of glycolysis. Proc Natl Acad Sci U S A. 2000;97(5):2087-92. Epub 2000/02/19. doi: 10.1073/pnas.030539197. PubMed PMID: 10681445; PMCID: 15758.

13.   Gualdron-Lopez M, Brennand A, Hannaert V, Quinones W, Caceres AJ, Bringaud F, Concepcion JL, Michels PA. When, how and why glycolysis became compartmentalised in the Kinetoplastea. A new look at an ancient organelle. Int J Parasitol. 2012;42(1):1-20. Epub 2011/12/07. doi: 10.1016/j.ijpara.2011.10.007. PubMed PMID: 22142562.

14.   Aslett M, Aurrecoechea C, Berriman M, Brestelli J, Brunk BP, Carrington M, Depledge DP, Fischer S, Gajria B, Gao X, Gardner MJ, Gingle A, Grant G, Harb OS, Heiges M, Hertz-Fowler C, Houston R, Innamorato F, Iodice J, Kissinger JC, Kraemer E, Li W, Logan FJ, Miller JA, Mitra S, Myler PJ, Nayak V, Pennington C, Phan I, Pinney DF, Ramasamy G, Rogers MB, Roos DS, Ross C, Sivam D, Smith DF, Srinivasamoorthy G, Stoeckert CJ, Jr., Subramanian S, Thibodeau R, Tivey A, Treatman C, Velarde G, Wang H. TriTrypDB: a functional genomic resource for the Trypanosomatidae. Nucleic Acids Res. 2010;38(Database issue):D457-62. Epub 2009/10/22. doi: gkp851 [pii]

10.1093/nar/gkp851. PubMed PMID: 19843604; PMCID: 2808979.

15.   Downing T, Imamura H, Decuypere S, Clark TG, Coombs GH, Cotton JA, Hilley JD, de Doncker S, Maes I, Mottram JC, Quail MA, Rijal S, Sanders M, Schonian G, Stark O, Sundar S, Vanaerschot M, Hertz-Fowler C, Dujardin JC, Berriman M. Whole genome sequencing of multiple Leishmania donovani clinical isolates provides insights into population structure and mechanisms of drug resistance. Genome Res. 2011;21(12):2143-56. Epub 2011/11/01. doi: gr.123430.111 [pii]

10.1101/gr.123430.111. PubMed PMID: 22038251; PMCID: 3227103.

16.   Martin JL, Yates PA, Soysa R, Alfaro JF, Yang F, Burnum-Johnson KE, Petyuk VA, Weitz KK, Camp DG, 2nd, Smith RD, Wilmarth PA, David LL, Ramasamy G, Myler PJ, Carter NS. Metabolic reprogramming during purine stress in the protozoan pathogen Leishmania donovani. PLoS Pathog. 2014;10(2):e1003938. Epub 2014/03/04. doi: 10.1371/journal.ppat.1003938. PubMed PMID: 24586154; PMCID: 3937319.

17.   Nirujogi RS, Pawar H, Renuse S, Kumar P, Chavan S, Sathe G, Sharma J, Khobragade S, Pande J, Modak B, Prasad TS, Harsha HC, Patole MS, Pandey A. Moving from unsequenced to sequenced genome: reanalysis of the proteome of

Leishmania donovani. J Proteomics. 2014;97:48-61. doi: 10.1016/j.jprot.2013.04.021. PubMed PMID: 23665000.

18.   Palenchar JB, Bellofatto V. Gene transcription in trypanosomes. Mol Biochem Parasitol. 2006;146(2):135-41. Epub 2006/01/24. doi: 10.1016/j.molbiopara.2005.12.008. PubMed PMID: 16427709.

19.   Requena JM. Lights and shadows on gene organization and regulation of gene expression in Leishmania. Front Biosci. 2011;16:2069-85. Epub 2011/05/31. doi: 3840 [pii]. PubMed PMID: 21622163.

20.   Liang XH, Haritan A, Uliel S, Michaeli S. trans and cis splicing in trypanosomatids: mechanism, factors, and regulation. Eukaryot Cell. 2003;2(5):830-40. Epub 2003/10/14. PubMed PMID: 14555465; PMCID: 219355.

21.   Clayton C, Shapira M. Post-transcriptional regulation of gene expression in trypanosomes and leishmanias. Mol Biochem Parasitol. 2007;156(2):93-101. Epub 2007/09/04. doi: S0166-6851(07)00210-1 [pii]

10.1016/j.molbiopara.2007.07.007. PubMed PMID: 17765983.

22.   Tharakaram S. CHARLES Donovan, M.D. Br Med J. 1951;2(4740):1158. Epub 1951/11/10. PubMed PMID: 14869848.

23.   Gibson ME. The identification of kala-azar and the discovery of Leishmania donovani. Med Hist. 1983;27(2):203-13. Epub 1983/04/01. PubMed PMID: 6345968; PMCID: 1139308.

24.   W.H.O. Control of the leishmaniasis: report of a meeting of the WHO Expert Committee on the Control of Leishmaniases, Geneva, 22-26 March 2010. WHO technical report series: no 949 (http://whqlibdocwhoint/trs/WHO_TRS_949_engpdf) [Internet]. Available from: http://www.who.int/leishmaniasis/en/).

25.   Swaminath CS, Shortt HE, Anderson LA. Transmission of Indian kala-azar to man by the bites of Phlebotomus argentipes, ann and brun. 1942. Indian J Med Res. 2006;123(3):473-7. Epub 2006/06/23. PubMed PMID: 16789343.

26.   Adler S, Ber M. The transmission of *Leishmania tropica* by the bite of *Phlebotomus papatasi*. Indian Journal of Medical Research. 1942;29:803-9.

27.   Pulvertaft RJ, Hoyle GF. Stages in the life-cycle of Leishmania donovani. Trans R Soc Trop Med Hyg. 1960;54:191-6. Epub 1960/03/01. PubMed PMID: 14435316.

28.   Tsigankov P, Gherardini PF, Helmer-Citterich M, Spath GF, Zilberstein D. Phosphoproteomic analysis of differentiating Leishmania parasites reveals a unique

stage-specific phosphorylation motif. J Proteome Res. 2013;12(7):3405-12. Epub 2013/05/22. doi: 10.1021/pr4002492. PubMed PMID: 23688256.

29.   McConville MJ, Naderer T. Metabolic pathways required for the intracellular survival of Leishmania. Annu Rev Microbiol. 2011;65:543-61. Epub 2011/07/05. doi: 10.1146/annurev-micro-090110-102913. PubMed PMID: 21721937.

30.   Rosenzweig D, Smith D, Opperdoes F, Stern S, Olafson RW, Zilberstein D. Retooling Leishmania metabolism: from sand fly gut to human macrophage. FASEB J. 2008;22(2):590-602. Epub 2007/09/22. doi: fj.07-9254com [pii]

10.1096/fj.07-9254com. PubMed PMID: 17884972.

31.   Savoia D. Recent updates and perspectives on leishmaniasis. J Infect Dev Ctries. 2015;9(6):588-96. Epub 2015/07/06. doi: 10.3855/jidc.6833. PubMed PMID: 26142667.

32.   Zucca M, Scutera S, Savoia D. New chemotherapeutic strategies against malaria, leishmaniasis and trypanosomiases. Curr Med Chem. 2013;20(4):502-26. Epub 2012/12/06. PubMed PMID: 23210775.

33.   Organization WH. Global Health Observatory Data - Leishmaniasis 2014 [cited 2015 July 12]. Available from: http://www.who.int/gho/neglected_diseases/leishmaniasis/en/.

34.   Pace D. Leishmaniasis. J Infect. 2014;69 Suppl 1:S10-8. Epub 2014/09/23. doi: 10.1016/j.jinf.2014.07.016. PubMed PMID: 25238669.

35.   Alvar J, Velez ID, Bern C, Herrero M, Desjeux P, Cano J, Jannin J, den Boer M. Leishmaniasis worldwide and global estimates of its incidence. PLoS One. 2012;7(5):e35671. Epub 2012/06/14. doi: 10.1371/journal.pone.0035671. PubMed PMID: 22693548; PMCID: 3365071.

36.   Vianna G. Tratamento da leishmaniose tegumentar por injeções intravenosas

de tártaro emético. 7 Congresso Brasileiro de Medicina Tropical de São Paulo,

São Paulo, Brasil,. 1912:4.

37.   Lira R, Sundar S, Makharia A, Kenney R, Gam A, Saraiva E, Sacks D. Evidence that the high incidence of treatment failures in Indian kala-azar is due to the emergence of antimony-resistant strains of Leishmania donovani. J Infect Dis. 1999;180(2):564-7. Epub 1999/07/09. doi: JID981498 [pii]

10.1086/314896. PubMed PMID: 10395884.

38. Lai AFEJ, Vrede MA, Soetosenojo RM, Lai AFRF. Pentamidine, the drug of choice for the treatment of cutaneous leishmaniasis in Surinam. Int J Dermatol. 2002;41(11):796-800. Epub 2002/11/28. PubMed PMID: 12453009.

39. Davidson RN, di Martino L, Gradoni L, Giacchino R, Gaeta GB, Pempinello R, Scotti S, Cascio A, Castagnola E, Maisto A, Gramiccia M, di Caprio D, Wilkinson RJ, Bryceson AD. Short-course treatment of visceral leishmaniasis with liposomal amphotericin B (AmBisome). Clin Infect Dis. 1996;22(6):938-43. Epub 1996/06/01. PubMed PMID: 8783690.

40. Sundar S, Singh A, Rai M, Prajapati VK, Singh AK, Ostyn B, Boelaert M, Dujardin JC, Chakravarty J. Efficacy of miltefosine in the treatment of visceral leishmaniasis in India after a decade of use. Clin Infect Dis. 2012;55(4):543-50. Epub 2012/05/11. doi: 10.1093/cid/cis474. PubMed PMID: 22573856.

41. Sundar S, Rai M. Treatment of visceral leishmaniasis. Expert Opin Pharmacother. 2005;6(16):2821-9. Epub 2005/12/02. doi: 10.1517/14656566.6.16.2821. PubMed PMID: 16318433.

42. Sinha PK, Jha TK, Thakur CP, Nath D, Mukherjee S, Aditya AK, Sundar S. Phase 4 pharmacovigilance trial of paromomycin injection for the treatment of visceral leishmaniasis in India. J Trop Med. 2011;2011:645203. Epub 2011/12/17. doi: 10.1155/2011/645203. PubMed PMID: 22174722; PMCID: 3235903.

43. Cojean S, Houze S, Haouchine D, Huteau F, Lariven S, Hubert V, Michard F, Bories C, Pratlong F, Le Bras J, Loiseau PM, Matheron S. Leishmania resistance to miltefosine associated with genetic marker. Emerg Infect Dis. 2012;18(4):704-6. Epub 2012/04/04. doi: 10.3201/eid1804.110841. PubMed PMID: 22469394; PMCID: 3309694.

44. Rai K, Cuypers B, Bhattarai NR, Uranw S, Berg M, Ostyn B, Dujardin JC, Rijal S, Vanaerschot M. Relapse after treatment with miltefosine for visceral leishmaniasis is associated with increased infectivity of the infecting Leishmania donovani strain. MBio. 2013;4(5):e00611-13. Epub 2013/10/10. doi: 10.1128/mBio.00611-13. PubMed PMID: 24105765; PMCID: 3791894.

45. Rijal S, Ostyn B, Uranw S, Rai K, Bhattarai NR, Dorlo TP, Beijnen JH, Vanaerschot M, Decuypere S, Dhakal SS, Das ML, Karki P, Singh R, Boelaert M, Dujardin JC. Increasing failure of miltefosine in the treatment of Kala-azar in Nepal and the potential role of parasite drug resistance, reinfection, or noncompliance. Clin Infect Dis. 2013;56(11):1530-8. Epub 2013/02/22. doi: 10.1093/cid/cit102. PubMed PMID: 23425958.

46. Uranw S, Ostyn B, Dorlo TP, Hasker E, Dujardin B, Dujardin JC, Rijal S, Boelaert M. Adherence to miltefosine treatment for visceral leishmaniasis under routine conditions in Nepal. Trop Med Int Health. 2013;18(2):179-87. Epub 2012/12/04. doi: 10.1111/tmi.12025. PubMed PMID: 23199340.

47.   Kobilka BK. G protein coupled receptor structure and activation. Biochim Biophys Acta. 2007;1768(4):794-807. Epub 2006/12/26. doi: 10.1016/j.bbamem.2006.10.021. PubMed PMID: 17188232; PMCID: 1876727.

48.   Parsons M, Worthey EA, Ward PN, Mottram JC. Comparative analysis of the kinomes of three pathogenic trypanosomatids: Leishmania major, Trypanosoma brucei and Trypanosoma cruzi. BMC Genomics. 2005;6:127. Epub 2005/09/17. doi: 1471-2164-6-127 [pii]

10.1186/1471-2164-6-127. PubMed PMID: 16164760; PMCID: 1266030.

49.   Sanchez MA, Zeoli D, Klamo EM, Kavanaugh MP, Landfear SM. A family of putative receptor-adenylate cyclases from Leishmania donovani. J Biol Chem. 1995;270(29):17551-8. Epub 1995/07/21. PubMed PMID: 7615561.

50.   Parsons M, Ruben L. Pathways involved in environmental sensing in trypanosomatids. Parasitol Today. 2000;16(2):56-62. Epub 2000/02/01. doi: S0169-4758(99)01590-2 [pii]. PubMed PMID: 10652488.

51.   Iovannisci DM, Ullman B. High efficiency plating method for Leishmania promastigotes in semidefined or completely-defined medium. J Parasitol. 1983;69(4):633-6. Epub 1983/08/01. PubMed PMID: 6631633.

52.   Carter NS, Yates PA, Gessford SK, Galagan SR, Landfear SM, Ullman B. Adaptive responses to purine starvation in Leishmania donovani. Mol Microbiol. 2010;78(1):92-107. Epub 2010/10/07. doi: 10.1111/j.1365-2958.2010.07327.x. PubMed PMID: 20923417; PMCID: 2964060.

53.   Jensen RE, Englund PT. Network news: the replication of kinetoplast DNA. Annu Rev Microbiol. 2012;66:473-91. Epub 2012/09/22. doi: 10.1146/annurev-micro-092611-150057. PubMed PMID: 22994497.

54.   Teixeira DE, Benchimol M, Rodrigues JC, Crepaldi PH, Pimenta PF, de Souza W. The cell biology of Leishmania: how to teach using animations. PLoS Pathog. 2013;9(10):e1003594. Epub 2013/10/17. doi: 10.1371/journal.ppat.1003594. PubMed PMID: 24130476; PMCID: 3795027.

55.   Cardosa EA, da Silva AR, de Carvalho GC, Fraga AGM, Barbosa MLdC, dos Santos ALS, Castro HC, Lione V. Leishmaniasis: History, Evolution of Treatment and the Need for New

Drugs. Current Biotechnology. 2014;3(4):10. doi: 10.2174/2211550104666150303231736.

56.   Croft SL, Sundar S, Fairlamb AH. Drug resistance in leishmaniasis. Clin Microbiol Rev. 2006;19(1):111-26. Epub 2006/01/19. doi: 19/1/111 [pii]

10.1128/CMR.19.1.111-126.2006. PubMed PMID: 16418526; PMCID: 1360270.

57.   Fairlamb AH. Chemotherapy of human African trypanosomiasis: current and future prospects. Trends Parasitol. 2003;19(11):488-94. Epub 2003/10/29. doi: S1471492203002423 [pii]. PubMed PMID: 14580959.

58.   Frearson JA, Wyatt PG, Gilbert IH, Fairlamb AH. Target assessment for antiparasitic drug discovery. Trends Parasitol. 2007;23(12):589-95. Epub 2007/10/27. doi: S1471-4922(07)00253-X [pii]

10.1016/j.pt.2007.08.019. PubMed PMID: 17962072; PMCID: 2979298.

59.   Stuart K, Brun R, Croft S, Fairlamb A, Gurtler RE, McKerrow J, Reed S, Tarleton R. Kinetoplastids: related protozoan pathogens, different diseases. J Clin Invest. 2008;118(4):1301-10. Epub 2008/04/03. doi: 10.1172/JCI33945. PubMed PMID: 18382742; PMCID: 2276762.

60.   Burchmore RJ, Barrett MP. Life in vacuoles--nutrient acquisition by Leishmania amastigotes. Int J Parasitol. 2001;31(12):1311-20. Epub 2001/09/22. doi: S0020-7519(01)00259-4 [pii]. PubMed PMID: 11566299.

61.   Darlyuk I, Goldman A, Roberts SC, Ullman B, Rentsch D, Zilberstein D. Arginine homeostasis and transport in the human pathogen Leishmania donovani. J Biol Chem. 2009;284(30):19800-7. Epub 2009/05/15. doi: M901066200 [pii]

10.1074/jbc.M901066200. PubMed PMID: 19439418; PMCID: 2740405.

62.   Feng X, Feistel T, Buffalo C, McCormack A, Kruvand E, Rodriguez-Contreras D, Akopyants NS, Umasankar PK, David L, Jardim A, Beverley SM, Landfear SM. Remodeling of protein and mRNA expression in Leishmania mexicana induced by deletion of glucose transporter genes. Mol Biochem Parasitol. 2011;175(1):39-48. Epub 2010/09/28. doi: S0166-6851(10)00231-8 [pii]

10.1016/j.molbiopara.2010.08.008. PubMed PMID: 20869991; PMCID: 2974008.

63.   Feng X, Rodriguez-Contreras D, Buffalo C, Bouwer HG, Kruvand E, Beverley SM, Landfear SM. Amplification of an alternate transporter gene suppresses the avirulent phenotype of glucose transporter null mutants in Leishmania mexicana. Mol Microbiol. 2009;71(2):369-81. Epub 2008/11/20. doi: MMI6531 [pii]

10.1111/j.1365-2958.2008.06531.x. PubMed PMID: 19017272; PMCID: 2729070.

64.   Ortiz D, Valdes R, Sanchez MA, Hayenga J, Elya C, Detke S, Landfear SM. Purine restriction induces pronounced translational upregulation of the NT1 adenosine/pyrimidine nucleoside transporter in Leishmania major. Mol Microbiol. 2010;78(1):108-18. Epub 2010/08/26. doi: 10.1111/j.1365-2958.2010.07328.x. PubMed PMID: 20735779; PMCID: 2971681.

65.   Sacci JB, Jr., Campbell TA, Gottlieb M. Leishmania donovani: regulated changes in the level of expression of the surface 3'-nucleotidase/nuclease. Exp Parasitol. 1990;71(2):158-68. Epub 1990/08/01. doi: 0014-4894(90)90018-8 [pii]. PubMed PMID: 2164952.

66.   Bhattacharya A, Biswas A, Das PK. Identification of a protein kinase A regulatory subunit from Leishmania having importance in metacyclogenesis through induction of autophagy. Mol Microbiol. 2012;83(3):548-64. Epub 2011/12/16. doi: 10.1111/j.1365-2958.2011.07950.x. PubMed PMID: 22168343.

67.   Serafim TD, Figueiredo AB, Costa PA, Marques-da-Silva EA, Goncalves R, de Moura SA, Gontijo NF, da Silva SM, Michalick MS, Meyer-Fernandes JR, de Carvalho RP, Uliana SR, Fietto JL, Afonso LC. Leishmania metacyclogenesis is promoted in the absence of purines. PLoS Negl Trop Dis. 2012;6(9):e1833. Epub 2012/10/11. doi: 10.1371/journal.pntd.0001833

PNTD-D-12-00349 [pii]. PubMed PMID: 23050028; PMCID: 3458635.

68.   Williams RA, Tetley L, Mottram JC, Coombs GH. Cysteine peptidases CPA and CPB are vital for autophagy and differentiation in Leishmania mexicana. Mol Microbiol. 2006;61(3):655-74. Epub 2006/06/29. doi: MMI5274 [pii]

10.1111/j.1365-2958.2006.05274.x. PubMed PMID: 16803590.

69.   Tonelli RR, Augusto Lda S, Castilho BA, Schenkman S. Protein synthesis attenuation by phosphorylation of eIF2alpha is required for the differentiation of Trypanosoma cruzi into infective forms. PLoS One. 2011;6(11):e27904. Epub 2011/11/25. doi: 10.1371/journal.pone.0027904

PONE-D-11-15942 [pii]. PubMed PMID: 22114724; PMCID: 3218062.

70.   Figueiredo RC, Rosa DS, Soares MJ. Differentiation of Trypanosoma cruzi epimastigotes: metacyclogenesis and adhesion to substrate are triggered by nutritional stress. J Parasitol. 2000;86(6):1213-8. Epub 2001/02/24. doi: 10.1645/0022-3395(2000)086[1213:DOTCEM]2.0.CO;2. PubMed PMID: 11191893.

71.   Naula C, Seebeck T. Cyclic AMP signaling in trypanosomatids. Parasitol Today. 2000;16(1):35-8. Epub 2000/01/19. doi: S0169-4758(99)01582-3 [pii]. PubMed PMID: 10637587.

72.   Carter NS, Yates P, Arendt CS, Boitz JM, Ullman B. Purine and pyrimidine metabolism in Leishmania. Adv Exp Med Biol. 2008;625:141-54. Epub 2008/03/28. doi: 10.1007/978-0-387-77570-8_12. PubMed PMID: 18365665.

73.   Carter NS, Landfear SM, Ullman B. Nucleoside transporters of parasitic protozoa. Trends Parasitol. 2001;17(3):142-5. Epub 2001/04/05. doi: S1471-4922(00)01806-7 [pii]. PubMed PMID: 11286799.

74.   Landfear SM, Ullman B, Carter NS, Sanchez MA. Nucleoside and nucleobase transporters in parasitic protozoa. Eukaryot Cell. 2004;3(2):245-54. Epub 2004/04/13. PubMed PMID: 15075255; PMCID: 387651.

75.   Berg M, Van der Veken P, Goeminne A, Haemers A, Augustyns K. Inhibitors of the purine salvage pathway: a valuable approach for antiprotozoal chemotherapy? Curr

Med Chem. 2010;17(23):2456-81. Epub 2010/05/25. doi: BSP/CMC/E-Pub/ 144 [pii]. PubMed PMID: 20491648.

76.   Boitz JM, Ullman, B., Jardim, A., and Carter, N. S. Purine salvage in Leishmania: complex or simple by design? Trends Parasitol. 2012;28(8):345-52. Epub 2012 Jun 20.

77.   Carter NS, Rager N, Ullman B. Purine and Pyrimidine Transport and Metabolism. In: Marr JJ, Nilsen T, Komuniecki R, editors. Molecular and Medical Parasitology: Academic Press Limited, London; 2003. p. 197-223.

78.   Datta AK, Datta R, Sen B. Antiparasitic chemotherapy: tinkering with the purine salvage pathway. Adv Exp Med Biol. 2008;625:116-32. Epub 2008/03/28. doi: 10.1007/978-0-387-77570-8_10. PubMed PMID: 18365663.

79.   Alleman MM, Gottlieb M. Crithidia luciliae: starvation for purines and/or phosphate leads to the enhanced surface expression of a protein responsible for 3'-nucleotidase/nuclease activity. Exp Parasitol. 1990;71(2):146-57. Epub 1990/08/01. doi: 0014-4894(90)90017-7 [pii]. PubMed PMID: 2164951.

80.   Gottlieb M. Enzyme regulation in a trypanosomatid: effect of purine starvation on levels of 3'-nucleotidase activity. Science. 1985;227(4682):72-4. Epub 1985/01/04. PubMed PMID: 2981117.

81.   Sopwith WF, Debrabant A, Yamage M, Dwyer DM, Bates PA. Developmentally regulated expression of a cell surface class I nuclease in Leishmania mexicana. Int J Parasitol. 2002;32(4):449-59. Epub 2002/02/19. doi: S0020751901003721 [pii]. PubMed PMID: 11849641.

82.   Yamage M, Debrabant A, Dwyer DM. Molecular characterization of a hyperinducible, surface membrane-anchored, class I nuclease of a trypanosomatid parasite. J Biol Chem. 2000;275(46):36369-79. Epub 2000/08/18. doi: 10.1074/jbc.M004036200

M004036200 [pii]. PubMed PMID: 10945983.

83.   Yamage M, Joshi MB, Dwyer DM. Episomally driven antisense mRNA abrogates the hyperinducible expression and function of a unique cell surface class I nuclease in the primitive trypanosomatid parasite, Crithidia luciliae. J Mol Biol. 2007;373(2):296-307. Epub 2007/09/14. doi: S0022-2836(07)01084-4 [pii]

10.1016/j.jmb.2007.08.014. PubMed PMID: 17850817; PMCID: 2100425.

84.   Liu W, Arendt CS, Gessford SK, Ntaba D, Carter NS, Ullman B. Identification and characterization of purine nucleoside transporters from Crithidia fasciculata. Mol Biochem Parasitol. 2005;140(1):1-12. Epub 2005/02/08. doi: S0166-6851(04)00312-3 [pii]

10.1016/j.molbiopara.2004.11.018. PubMed PMID: 15694482.

85.	de Koning HP, Watson CJ, Sutcliffe L, Jarvis SM. Differential regulation of nucleoside and nucleobase transporters in Crithidia fasciculata and Trypanosoma brucei brucei. Mol Biochem Parasitol. 2000;106(1):93-107. Epub 2000/04/01. doi: S0166-6851(99)00203-0 [pii]. PubMed PMID: 10743614.

86.	Hall ST, Hillier CJ, Gero AM. Crithidia luciliae: regulation of purine nucleoside transport by extracellular purine concentrations. Exp Parasitol. 1996;83(3):314-21. Epub 1996/08/01. doi: S0014-4894(96)90079-X [pii]

10.1006/expr.1996.0079. PubMed PMID: 8823248.

87.	Ouellette M, Papadopoulou B. Coordinated gene expression by post-transcriptional regulons in African trypanosomes. J Biol. 2009;8(11):100. Epub 2009/12/19. doi: jbiol203 [pii]

10.1186/jbiol203. PubMed PMID: 20017896; PMCID: 2804284.

88.	Marguerat S, Bahler J. RNA-seq: from technology to biology. Cell Mol Life Sci. 2010;67(4):569-79. Epub 2009/10/28. doi: 10.1007/s00018-009-0180-6. PubMed PMID: 19859660; PMCID: 2809939.

89.	Mortazavi A, Williams BA, McCue K, Schaeffer L, Wold B. Mapping and quantifying mammalian transcriptomes by RNA-Seq. Nat Methods. 2008;5(7):621-8. Epub 2008/06/03. doi: nmeth.1226 [pii]

10.1038/nmeth.1226. PubMed PMID: 18516045.

90.	Nagalakshmi U, Wang Z, Waern K, Shou C, Raha D, Gerstein M, Snyder M. The transcriptional landscape of the yeast genome defined by RNA sequencing. Science. 2008;320(5881):1344-9. Epub 2008/05/03. doi: 1158441 [pii]

10.1126/science.1158441. PubMed PMID: 18451266; PMCID: 2951732.

91.	Ozsolak F, Milos PM. RNA sequencing: advances, challenges and opportunities. Nat Rev Genet. 2011;12(2):87-98. Epub 2010/12/31. doi: nrg2934 [pii]

10.1038/nrg2934. PubMed PMID: 21191423; PMCID: 3031867.

92.	Sultan M, Schulz MH, Richard H, Magen A, Klingenhoff A, Scherf M, Seifert M, Borodina T, Soldatov A, Parkhomchuk D, Schmidt D, O'Keeffe S, Haas S, Vingron M, Lehrach H, Yaspo ML. A global view of gene activity and alternative splicing by deep sequencing of the human transcriptome. Science. 2008;321(5891):956-60. Epub 2008/07/05. doi: 1160342 [pii]

10.1126/science.1160342. PubMed PMID: 18599741.

93.	Wang Z, Gerstein M, Snyder M. RNA-Seq: a revolutionary tool for transcriptomics. Nat Rev Genet. 2009;10(1):57-63. Epub 2008/11/19. doi: nrg2484 [pii]
10.1038/nrg2484. PubMed PMID: 19015660; PMCID: 2949280.

94.   Wilhelm BT, Marguerat S, Goodhead I, Bahler J. Defining transcribed regions using RNA-seq. Nat Protoc. 2010;5(2):255-66. Epub 2010/02/06. doi: nprot.2009.229 [pii]

10.1038/nprot.2009.229. PubMed PMID: 20134426.

95.   Wilhelm BT, Marguerat S, Watt S, Schubert F, Wood V, Goodhead I, Penkett CJ, Rogers J, Bahler J. Dynamic repertoire of a eukaryotic transcriptome surveyed at single-nucleotide resolution. Nature. 2008;453(7199):1239-43. Epub 2008/05/20. doi: nature07002 [pii]

10.1038/nature07002. PubMed PMID: 18488015.

96.   Burnum KE, Hirota Y, Baker ES, Yoshie M, Ibrahim YM, Monroe ME, Anderson GA, Smith RD, Daikoku T, Dey SK. Uterine deletion of Trp53 compromises antioxidant responses in the mouse decidua. Endocrinology. 2012;153(9):4568-79. Epub 2012/07/05. doi: en.2012-1335 [pii]

10.1210/en.2012-1335. PubMed PMID: 22759378; PMCID: 3423619.

97.   Pasa-Tolic L, Masselon C, Barry RC, Shen Y, Smith RD. Proteomic analyses using an accurate mass and time tag strategy. Biotechniques. 2004;37(4):621-4, 6-33, 36 passim. Epub 2004/11/03. PubMed PMID: 15517975.

98.   Qian WJ, Jacobs JM, Liu T, Camp DG, 2nd, Smith RD. Advances and challenges in liquid chromatography-mass spectrometry-based proteomics profiling for clinical applications. Mol Cell Proteomics. 2006;5(10):1727-44. Epub 2006/08/05. doi: M600162-MCP200 [pii]

10.1074/mcp.M600162-MCP200. PubMed PMID: 16887931; PMCID: 1781927.

99.   Peacock CS, Seeger K, Harris D, Murphy L, Ruiz JC, Quail MA, Peters N, Adlem E, Tivey A, Aslett M, Kerhornou A, Ivens A, Fraser A, Rajandream MA, Carver T, Norbertczak H, Chillingworth T, Hance Z, Jagels K, Moule S, Ormond D, Rutter S, Squares R, Whitehead S, Rabbinowitsch E, Arrowsmith C, White B, Thurston S, Bringaud F, Baldauf SL, Faulconbridge A, Jeffares D, Depledge DP, Oyola SO, Hilley JD, Brito LO, Tosi LR, Barrell B, Cruz AK, Mottram JC, Smith DF, Berriman M. Comparative genomic analysis of three Leishmania species that cause diverse human disease. Nat Genet. 2007;39(7):839-47. Epub 2007/06/19. doi: ng2053 [pii]

10.1038/ng2053. PubMed PMID: 17572675; PMCID: 2592530.

100.   Carter NS, Drew ME, Sanchez M, Vasudevan G, Landfear SM, Ullman B. Cloning of a novel inosine-guanosine transporter gene from Leishmania donovani by functional rescue of a transport-deficient mutant. J Biol Chem. 2000;275(27):20935-41. Epub 2000/04/28. doi: 10.1074/jbc.M002418200

M002418200 [pii]. PubMed PMID: 10783393.

101.   Vasudevan G, Carter NS, Drew ME, Beverley SM, Sanchez MA, Seyfang A, Ullman B, Landfear SM. Cloning of Leishmania nucleoside transporter genes by rescue

of a transport-deficient mutant. Proc Natl Acad Sci U S A. 1998;95(17):9873-8. Epub 1998/08/26. PubMed PMID: 9707568; PMCID: 21429.

102.   Ortiz D, Sanchez MA, Pierce S, Herrmann T, Kimblin N, Archie Bouwer HG, Landfear SM. Molecular genetic analysis of purine nucleobase transport in Leishmania major. Mol Microbiol. 2007;64(5):1228-43. Epub 2007/06/05. doi: MMI5730 [pii]

10.1111/j.1365-2958.2007.05730.x. PubMed PMID: 17542917.

103.   Debrabant A, Gottlieb M, Dwyer DM. Isolation and characterization of the gene encoding the surface membrane 3'-nucleotidase/nuclease of Leishmania donovani. Mol Biochem Parasitol. 1995;71(1):51-63. Epub 1995/04/01. doi: 016668519500035Y [pii]. PubMed PMID: 7630383.

104.   Dwyer DM, Gottlieb M. Surface membrane localization of 3'- and 5'-nucleotidase activities in Leishmania donovani promastigotes. Mol Biochem Parasitol. 1984;10(2):139-50. Epub 1984/02/01. PubMed PMID: 6321980.

105.   Gottlieb M, Dwyer DM. Leishmania donovani: surface membrane acid phosphatase activity of promastigotes. Exp Parasitol. 1981;52(1):117-28. Epub 1981/08/01. doi: 0014-4894(81)90067-9 [pii]. PubMed PMID: 7238722.

106.   Gottlieb M, Dwyer DM. Protozoan parasite of humans: surface membrane with externally disposed acid phosphatase. Science. 1981;212(4497):939-41. Epub 1981/05/22. PubMed PMID: 7233189.

107.   Gottlieb M, Dwyer DM. Evidence for distinct 5'- and 3'-nucleotidase activities in the surface membrane fraction of Leishmania donovani promastigotes. Mol Biochem Parasitol. 1983;7(4):303-17. Epub 1983/04/01. PubMed PMID: 6308442.

108.   Allen TE, Hwang HY, Jardim A, Olafson R, Ullman B. Cloning and expression of the hypoxanthine-guanine phosphoribosyltransferase from Leishmania donovani. Mol Biochem Parasitol. 1995;73(1-2):133-43. Epub 1995/07/01. PubMed PMID: 8577321.

109.   Jardim A, Bergeson SE, Shih S, Carter N, Lucas RW, Merlin G, Myler PJ, Stuart K, Ullman B. Xanthine phosphoribosyltransferase from Leishmania donovani. Molecular cloning, biochemical characterization, and genetic analysis. J Biol Chem. 1999;274(48):34403-10. Epub 1999/11/24. PubMed PMID: 10567419.

110.   Ortiz D, Sanchez MA, Koch HP, Larsson HP, Landfear SM. An acid-activated nucleobase transporter from Leishmania major. J Biol Chem. 2009;284(24):16164-9. Epub 2009/04/16. doi: M109.006718 [pii]

10.1074/jbc.M109.006718. PubMed PMID: 19366701; PMCID: 2713545.

111.   Ginger ML, Ngazoa ES, Pereira CA, Pullen TJ, Kabiri M, Becker K, Gull K, Steverding D. Intracellular positioning of isoforms explains an unusually large adenylate

kinase gene family in the parasite Trypanosoma brucei. J Biol Chem. 2005;280(12):11781-9. Epub 2005/01/20. doi: M413821200 [pii]

10.1074/jbc.M413821200. PubMed PMID: 15657034.

112.	Koszalka GW, Krenitsky TA. 5'-Methylthioadenosine (MTA) phosphorylase from promastigotes of Leishmania donovani. Adv Exp Med Biol. 1986;195 Pt B:559-63. Epub 1986/01/01. PubMed PMID: 3094329.

113.	Perez-Pertejo Y, Reguera RM, Ordonez D, Balana-Fouce R. Characterization of a methionine adenosyltransferase over-expressing strain in the trypanosomatid Leishmania donovani. Biochim Biophys Acta. 2006;1760(1):10-9. Epub 2005/11/11. doi: S0304-4165(05)00281-3 [pii]

10.1016/j.bbagen.2005.09.003. PubMed PMID: 16280200.

114.	Reguera RM, Balana-Fouce R, Perez-Pertejo Y, Fernandez FJ, Garcia-Estrada C, Cubria JC, Ordonez C, Ordonez D. Cloning expression and characterization of methionine adenosyltransferase in Leishmania infantum promastigotes. J Biol Chem. 2002;277(5):3158-67. Epub 2001/11/08. doi: 10.1074/jbc.M105512200

M105512200 [pii]. PubMed PMID: 11698393.

115.	Johner A, Kunz S, Linder M, Shakur Y, Seebeck T. Cyclic nucleotide specific phosphodiesterases of Leishmania major. BMC Microbiol. 2006;6:25. Epub 2006/03/09. doi: 1471-2180-6-25 [pii]

10.1186/1471-2180-6-25. PubMed PMID: 16522215; PMCID: 1431542.

116.	Seebeck T, Schaub R, Johner A. cAMP signalling in the kinetoplastid protozoa. Curr Mol Med. 2004;4(6):585-99. Epub 2004/09/11. PubMed PMID: 15357210.

117.	Shakur Y, de Koning HP, Ke H, Kambayashi J, Seebeck T. Therapeutic potential of phosphodiesterase inhibitors in parasitic diseases. Handb Exp Pharmacol. 2011(204):487-510. Epub 2011/06/23. doi: 10.1007/978-3-642-17969-3_20. PubMed PMID: 21695653.

118.	Ingram GM, Kinnaird JH. Ribonucleotide reductase: A new target for antiparasite therapies. Parasitol Today. 1999;15(8):338-42. Epub 1999/07/17. doi: S0169-4758(99)01478-7 [pii]. PubMed PMID: 10407382.

119.	Lye LF, Hsieh YH, Su KE, Lee ST. Cloning and functional analysis of the ribonucleotide reductase gene small subunit from hydroxyurea-resistant Leishmania mexicana amazonensis. Mol Biochem Parasitol. 1997;90(1):353-8. Epub 1998/03/13. doi: S0166-6851(97)00159-X [pii]. PubMed PMID: 9497060.

120.	Milman N, Motyka SA, Englund PT, Robinson D, Shlomai J. Mitochondrial origin-binding protein UMSBP mediates DNA replication and segregation in trypanosomes.

Proc Natl Acad Sci U S A. 2007;104(49):19250-5. Epub 2007/12/01. doi: 0706858104 [pii]

10.1073/pnas.0706858104. PubMed PMID: 18048338; PMCID: 2148276.

121.   Bringaud F, Barrett MP, Zilberstein D. Multiple roles of proline transport and metabolism in trypanosomatids. Front Biosci. 2012;17:349-74. Epub 2011/12/29. doi: 3931 [pii]. PubMed PMID: 22201748.

122.   Damerow S, Lamerz AC, Haselhorst T, Fuhring J, Zarnovican P, von Itzstein M, Routier FH. Leishmania UDP-sugar pyrophosphorylase: the missing link in galactose salvage? J Biol Chem. 2010;285(2):878-87. Epub 2009/11/13. doi: M109.067223 [pii]

10.1074/jbc.M109.067223. PubMed PMID: 19906649; PMCID: 2801289.

123.   Opperdoes FR, Szikora JP. In silico prediction of the glycosomal enzymes of Leishmania major and trypanosomes. Mol Biochem Parasitol. 2006;147(2):193-206. Epub 2006/03/21. doi: S0166-6851(06)00067-3 [pii]

10.1016/j.molbiopara.2006.02.010. PubMed PMID: 16546274.

124.   Berney M, Weimar MR, Heikal A, Cook GM. Regulation of proline metabolism in mycobacteria and its role in carbon metabolism under hypoxia. Mol Microbiol. 2012;84(4):664-81. Epub 2012/04/18. doi: 10.1111/j.1365-2958.2012.08053.x. PubMed PMID: 22507203.

125.   Magdaleno A, Ahn IY, Paes LS, Silber AM. Actions of a proline analogue, L-thiazolidine-4-carboxylic acid (T4C), on Trypanosoma cruzi. PLoS One. 2009;4(2):e4534. Epub 2009/02/21. doi: 10.1371/journal.pone.0004534. PubMed PMID: 19229347; PMCID: 2645137.

126.   Phang JM, Liu W, Zabirnyk O. Proline metabolism and microenvironmental stress. Annu Rev Nutr. 2010;30:441-63. Epub 2010/04/27. doi: 10.1146/annurev.nutr.012809.104638. PubMed PMID: 20415579.

127.   Verbruggen N, Hermans C. Proline accumulation in plants: a review. Amino Acids. 2008;35(4):753-9. Epub 2008/04/02. doi: 10.1007/s00726-008-0061-6. PubMed PMID: 18379856.

128.   Takagi H. Proline as a stress protectant in yeast: physiological functions, metabolic regulations, and biotechnological applications. Appl Microbiol Biotechnol. 2008;81(2):211-23. Epub 2008/09/20. doi: 10.1007/s00253-008-1698-5. PubMed PMID: 18802692.

129.   Tonelli RR, Silber AM, Almeida-de-Faria M, Hirata IY, Colli W, Alves MJ. L-proline is essential for the intracellular differentiation of Trypanosoma cruzi. Cell Microbiol. 2004;6(8):733-41. Epub 2004/07/09. doi: 10.1111/j.1462-5822.2004.00397.x

CMI397 [pii]. PubMed PMID: 15236640.

130.   Besteiro S, Williams RA, Coombs GH, Mottram JC. Protein turnover and differentiation in Leishmania. Int J Parasitol. 2007;37(10):1063-75. Epub 2007/05/12. doi: S0020-7519(07)00103-8 [pii]

10.1016/j.ijpara.2007.03.008. PubMed PMID: 17493624; PMCID: 2244715.

131.   Besteiro S, Williams RA, Morrison LS, Coombs GH, Mottram JC. Endosome sorting and autophagy are essential for differentiation and virulence of Leishmania major. J Biol Chem. 2006;281(16):11384-96. Epub 2006/02/25. doi: M512307200 [pii]

10.1074/jbc.M512307200. PubMed PMID: 16497676.

132.   Brennand A, Gualdron-Lopez M, Coppens I, Rigden DJ, Ginger ML, Michels PA. Autophagy in parasitic protists: unique features and drug targets. Mol Biochem Parasitol. 2011;177(2):83-99. Epub 2011/02/15. doi: S0166-6851(11)00068-5 [pii]

10.1016/j.molbiopara.2011.02.003. PubMed PMID: 21315770.

133.   Williams RA, Woods KL, Juliano L, Mottram JC, Coombs GH. Characterization of unusual families of ATG8-like proteins and ATG12 in the protozoan parasite Leishmania major. Autophagy. 2009;5(2):159-72. Epub 2008/12/11. doi: 7328 [pii]. PubMed PMID: 19066473; PMCID: 2642932.

134.   Girardi JP, Pereira L, Bakovic M. De novo synthesis of phospholipids is coupled with autophagosome formation. Med Hypotheses. 2011;77(6):1083-7. Epub 2011/10/04. doi: S0306-9877(11)00461-0 [pii]

10.1016/j.mehy.2011.09.008. PubMed PMID: 21963355.

135.   Nebauer R, Rosenberger S, Daum G. Phosphatidylethanolamine, a limiting factor of autophagy in yeast strains bearing a defect in the carboxypeptidase Y pathway of vacuolar targeting. J Biol Chem. 2007;282(23):16736-43. Epub 2007/04/13. doi: M611345200 [pii]

10.1074/jbc.M611345200. PubMed PMID: 17428789.

136.   Zhang K, Pompey JM, Hsu FF, Key P, Bandhuvula P, Saba JD, Turk J, Beverley SM. Redirection of sphingolipid metabolism toward de novo synthesis of ethanolamine in Leishmania. EMBO J. 2007;26(4):1094-104. Epub 2007/02/10. doi: 7601565 [pii]

10.1038/sj.emboj.7601565. PubMed PMID: 17290222; PMCID: 1852826.

137.   Gerald NJ, Coppens I, Dwyer DM. Molecular dissection and expression of the LdK39 kinesin in the human pathogen, Leishmania donovani. Mol Microbiol. 2007;63(4):962-79. Epub 2007/01/30. doi: MMI5487 [pii]

10.1111/j.1365-2958.2006.05487.x. PubMed PMID: 17257310.

138.   Mittra B, Cortez M, Haydock A, Ramasamy G, Myler PJ, Andrews NW. Iron uptake controls the generation of Leishmania infective forms through regulation of ROS levels. J Exp Med. 2013;210(2):401-16. Epub 2013/02/06. doi: jem.20121368 [pii]

10.1084/jem.20121368. PubMed PMID: 23382545; PMCID: 3570109.

139.   Abanades DR, Ramirez L, Iborra S, Soteriadou K, Gonzalez VM, Bonay P, Alonso C, Soto M. Key role of the 3' untranslated region in the cell cycle regulated expression of the Leishmania infantum histone H2A genes: minor synergistic effect of the 5' untranslated region. BMC Mol Biol. 2009;10:48. Epub 2009/05/23. doi: 1471-2199-10-48 [pii]

10.1186/1471-2199-10-48. PubMed PMID: 19460148; PMCID: 2691400.

140.   Bringaud F, Muller M, Cerqueira GC, Smith M, Rochette A, El-Sayed NM, Papadopoulou B, Ghedin E. Members of a large retroposon family are determinants of post-transcriptional gene expression in Leishmania. PLoS Pathog. 2007;3(9):1291-307. Epub 2007/10/03. doi: 07-PLPA-RA-0036 [pii]

10.1371/journal.ppat.0030136. PubMed PMID: 17907803; PMCID: 2323293.

141.   David M, Gabdank I, Ben-David M, Zilka A, Orr I, Barash D, Shapira M. Preferential translation of Hsp83 in Leishmania requires a thermosensitive polypyrimidine-rich element in the 3' UTR and involves scanning of the 5' UTR. RNA. 2010;16(2):364-74. Epub 2009/12/31. doi: rna.1874710 [pii]

10.1261/rna.1874710. PubMed PMID: 20040590; PMCID: 2811665.

142.   Garcia-Estrada C, Perez-Pertejo Y, Ordonez D, Balana-Fouce R, Reguera RM. Characterization of the 5' region of the Leishmania infantum LORIEN/MAT2 gene cluster and role of LORIEN flanking regions in post-transcriptional regulation. Biochimie. 2008;90(9):1325-36. Epub 2008/04/19. doi: S0300-9084(08)00078-3 [pii]

10.1016/j.biochi.2008.03.007. PubMed PMID: 18420039.

143.   Haile S, Dupe A, Papadopoulou B. Deadenylation-independent stage-specific mRNA degradation in Leishmania. Nucleic Acids Res. 2008;36(5):1634-44. Epub 2008/02/06. doi: gkn019 [pii]

10.1093/nar/gkn019. PubMed PMID: 18250085; PMCID: 2275140.

144.   Holzer TR, Mishra KK, LeBowitz JH, Forney JD. Coordinate regulation of a family of promastigote-enriched mRNAs by the 3'UTR PRE element in Leishmania mexicana. Mol Biochem Parasitol. 2008;157(1):54-64. Epub 2007/11/21. doi: S0166-6851(07)00273-3 [pii]

10.1016/j.molbiopara.2007.10.001. PubMed PMID: 18023890; PMCID: 2692640.

145.   French JB, Yates PA, Soysa DR, Boitz JM, Carter NS, Chang B, Ullman B, Ealick SE. The Leishmania donovani UMP synthase is essential for promastigote viability and has an unusual tetrameric structure that exhibits substrate-controlled oligomerization. J Biol Chem. 2011;286(23):20930-41. Epub 2011/04/22. doi: M111.228213 [pii]

10.1074/jbc.M111.228213. PubMed PMID: 21507942; PMCID: 3121495.

146.   Khera A, Vanderlelie JJ, Perkins AV. Selenium supplementation protects trophoblast cells from mitochondrial oxidative stress. Placenta. 2013;34(7):594-8. Epub 2013/05/11. doi: S0143-4004(13)00184-7 [pii]

10.1016/j.placenta.2013.04.010. PubMed PMID: 23660306.

147.   Morten KJ, Badder L, Knowles HJ. Differential regulation of HIF-mediated pathways increases mitochondrial metabolism and ATP production in hypoxic osteoclasts. J Pathol. 2013;229(5):755-64. Epub 2013/01/11. doi: 10.1002/path.4159. PubMed PMID: 23303559; PMCID: 3618370.

148.   Zhang HX, Du GH, Zhang JT. Assay of mitochondrial functions by resazurin in vitro. Acta Pharmacol Sin. 2004;25(3):385-9. Epub 2004/03/06. PubMed PMID: 15000895.

149.   Maugeri DA, Cazzulo JJ, Burchmore RJ, Barrett MP, Ogbunude PO. Pentose phosphate metabolism in Leishmania mexicana. Mol Biochem Parasitol. 2003;130(2):117-25. Epub 2003/08/30. doi: S0166685103001737 [pii]. PubMed PMID: 12946848.

150.   Ralser M, Wamelink MM, Kowald A, Gerisch B, Heeren G, Struys EA, Klipp E, Jakobs C, Breitenbach M, Lehrach H, Krobitsch S. Dynamic rerouting of the carbohydrate flux is key to counteracting oxidative stress. J Biol. 2007;6(4):10. Epub 2007/12/25. doi: jbiol61 [pii]

10.1186/jbiol61. PubMed PMID: 18154684; PMCID: 2373902.

151.   Lemons JM, Feng XJ, Bennett BD, Legesse-Miller A, Johnson EL, Raitman I, Pollina EA, Rabitz HA, Rabinowitz JD, Coller HA. Quiescent fibroblasts exhibit high metabolic activity. PLoS Biol. 2010;8(10):e1000514. Epub 2010/11/05. doi: 10.1371/journal.pbio.1000514. PubMed PMID: 21049082; PMCID: 2958657.

152.   Petti AA, Crutchfield CA, Rabinowitz JD, Botstein D. Survival of starving yeast is correlated with oxidative stress response and nonrespiratory mitochondrial function. Proc Natl Acad Sci U S A. 2011;108(45):E1089-98. Epub 2011/07/08. doi: 1101494108 [pii]

10.1073/pnas.1101494108. PubMed PMID: 21734149; PMCID: 3215077.

153.   Rui B, Shen T, Zhou H, Liu J, Chen J, Pan X, Liu H, Wu J, Zheng H, Shi Y. A systematic investigation of Escherichia coli central carbon metabolism in response to superoxide stress. BMC Syst Biol. 2010;4:122. Epub 2010/09/03. doi: 1752-0509-4-122 [pii]

10.1186/1752-0509-4-122. PubMed PMID: 20809933; PMCID: 2944137.

154.   Husain A, Sato D, Jeelani G, Soga T, Nozaki T. Dramatic Increase in Glycerol Biosynthesis upon Oxidative Stress in the Anaerobic Protozoan Parasite Entamoeba histolytica. PLoS Negl Trop Dis. 2012;6(9):e1831. Epub 2012/10/03. doi: 10.1371/journal.pntd.0001831

PNTD-D-12-00389 [pii]. PubMed PMID: 23029590; PMCID: 3459822.

155. Fairlamb AH, Cerami A. Metabolism and functions of trypanothione in the Kinetoplastida. Annu Rev Microbiol. 1992;46:695-729. Epub 1992/01/01. doi: 10.1146/annurev.mi.46.100192.003403. PubMed PMID: 1444271.

156. Krauth-Siegel LR, Comini MA, Schlecker T. The trypanothione system. Subcell Biochem. 2007;44:231-51. Epub 2007/12/19. PubMed PMID: 18084897.

157. Krauth-Siegel RL, Comini MA. Redox control in trypanosomatids, parasitic protozoa with trypanothione-based thiol metabolism. Biochim Biophys Acta. 2008;1780(11):1236-48. Epub 2008/04/09. doi: S0304-4165(08)00062-7 [pii]

10.1016/j.bbagen.2008.03.006. PubMed PMID: 18395526.

158. Sardar AH, Kumar S, Kumar A, Purkait B, Das S, Sen A, Kumar M, Sinha KK, Singh D, Equbal A, Ali V, Das P. Proteome changes associated with Leishmania donovani promastigote adaptation to oxidative and nitrosative stresses. J Proteomics. 2013. Epub 2013/02/05. doi: S1874-3919(13)00039-0 [pii]

10.1016/j.jprot.2013.01.011. PubMed PMID: 23376486.

159. Schurch N, Furger A, Kurath U, Roditi I. Contributions of the procyclin 3' untranslated region and coding region to the regulation of expression in bloodstream forms of Trypanosoma brucei. Mol Biochem Parasitol. 1997;89(1):109-21. Epub 1997/09/23. doi: S0166-6851(97)00107-2 [pii]. PubMed PMID: 9297705.

160. Weston D, La Flamme AC, Van Voorhis WC. Expression of Trypanosoma cruzi surface antigen FL-160 is controlled by elements in the 3' untranslated, the 3' intergenic, and the coding regions. Mol Biochem Parasitol. 1999;102(1):53-66. Epub 1999/09/07. doi: S0166-6851(99)00079-1 [pii]. PubMed PMID: 10477176.

161. Lee EK, Gorospe M. Coding region: the neglected post-transcriptional code. RNA Biol. 2011;8(1):44-8. Epub 2011/02/04. doi: 13863 [pii]. PubMed PMID: 21289484; PMCID: 3127077.

162. Hyde M, Block-Alper L, Felix J, Webster P, Meyer DI. Induction of secretory pathway components in yeast is associated with increased stability of their mRNA. J Cell Biol. 2002;156(6):993-1001. Epub 2002/03/20. doi: 10.1083/jcb.200112008

jcb.200112008 [pii]. PubMed PMID: 11901166; PMCID: 2173461.

163. Unsworth H, Raguz S, Edwards HJ, Higgins CF, Yague E. mRNA escape from stress granule sequestration is dictated by localization to the endoplasmic reticulum. FASEB J. 2010;24(9):3370-80. Epub 2010/05/11. doi: fj.09-151142 [pii]

10.1096/fj.09-151142. PubMed PMID: 20453113.

164.   Barak E, Amin-Spector S, Gerliak E, Goyard S, Holland N, Zilberstein D. Differentiation of Leishmania donovani in host-free system: analysis of signal perception and response. Mol Biochem Parasitol. 2005;141(1):99-108. Epub 2005/04/07. doi: S0166-6851(05)00063-0 [pii]

10.1016/j.molbiopara.2005.02.004. PubMed PMID: 15811531.

165.   Bates PA, Tetley L. Leishmania mexicana: induction of metacyclogenesis by cultivation of promastigotes at acidic pH. Exp Parasitol. 1993;76(4):412-23. Epub 1993/06/01. doi: S0014-4894(83)71050-7 [pii]

10.1006/expr.1993.1050. PubMed PMID: 8513879.

166.   Ouakad M, Vanaerschot M, Rijal S, Sundar S, Speybroeck N, Kestens L, Boel L, De Doncker S, Maes I, Decuypere S, Dujardin JC. Increased metacyclogenesis of antimony-resistant Leishmania donovani clinical lines. Parasitology. 2011;138(11):1392-9. Epub 2011/08/09. doi: S0031182011001120 [pii]

10.1017/S0031182011001120. PubMed PMID: 21819638.

167.   Sadlova J, Price HP, Smith BA, Votypka J, Volf P, Smith DF. The stage-regulated HASPB and SHERP proteins are essential for differentiation of the protozoan parasite Leishmania major in its sand fly vector, Phlebotomus papatasi. Cell Microbiol. 2010;12(12):1765-79. Epub 2010/07/20. doi: CMI1507 [pii]

10.1111/j.1462-5822.2010.01507.x. PubMed PMID: 20636473; PMCID: 3015063.

168.   Zhang WW, Charest H, Ghedin E, Matlashewski G. Identification and overexpression of the A2 amastigote-specific protein in Leishmania donovani. Mol Biochem Parasitol. 1996;78(1-2):79-90. Epub 1996/06/01. PubMed PMID: 8813679.

169.   Nourbakhsh F, Uliana SR, Smith DF. Characterisation and expression of a stage-regulated gene of Leishmania major. Mol Biochem Parasitol. 1996;76(1-2):201-13. Epub 1996/02/01. PubMed PMID: 8920007.

170.   Zakai HA, Chance ML, Bates PA. In vitro stimulation of metacyclogenesis in Leishmania braziliensis, L. donovani, L. major and L. mexicana. Parasitology. 1998;116 (Pt 4):305-9. Epub 1998/05/20. PubMed PMID: 9585932.

171.   Rogers ME, Chance ML, Bates PA. The role of promastigote secretory gel in the origin and transmission of the infective stage of Leishmania mexicana by the sandfly Lutzomyia longipalpis. Parasitology. 2002;124(Pt 5):495-507. Epub 2002/06/07. PubMed PMID: 12049412.

172.   Dwyer DM. Antibody-induced modulation of Leishmania donovani surface membrane antigens. J Immunol. 1976;117(6):2081-91. Epub 1976/12/01. PubMed PMID: 792338.

173.   Goyard S, Segawa H, Gordon J, Showalter M, Duncan R, Turco SJ, Beverley SM. An in vitro system for developmental and genetic studies of Leishmania donovani phosphoglycans. Mol Biochem Parasitol. 2003;130(1):31-42. Epub 2003/10/11. doi: S0166685103001427 [pii]. PubMed PMID: 14550894.

174.   Wang Y, Yang F, Gritsenko MA, Wang Y, Clauss T, Liu T, Shen Y, Monroe ME, Lopez-Ferrer D, Reno T, Moore RJ, Klemke RL, Camp DG, 2nd, Smith RD. Reversed-phase chromatography with multiple fraction concatenation strategy for proteome profiling of human MCF10A cells. Proteomics. 2011;11(10):2019-26. Epub 2011/04/19. doi: 10.1002/pmic.201000722. PubMed PMID: 21500348; PMCID: 3120047.

175.   Livesay EA, Tang K, Taylor BK, Buschbach MA, Hopkins DF, LaMarche BL, Zhao R, Shen Y, Orton DJ, Moore RJ, Kelly RT, Udseth HR, Smith RD. Fully automated four-column capillary LC-MS system for maximizing throughput in proteomic analyses. Anal Chem. 2008;80(1):294-302. Epub 2007/11/30. doi: 10.1021/ac701727r. PubMed PMID: 18044960; PMCID: 2516349.

176.   Eng JK, McCormack, A. L., Yates, J. R. An approach to correlate tandem mass spectral data of peptides with amino acid sequences in a protein database. Journal of the American Society for Mass Spectrometry. 1994;5(11):976-89. doi: doi:10.1016/1044-0305(94)80016-2

177.   Qian WJ, Liu T, Monroe ME, Strittmatter EF, Jacobs JM, Kangas LJ, Petritis K, Camp DG, 2nd, Smith RD. Probability-based evaluation of peptide and protein identifications from tandem mass spectrometry and SEQUEST analysis: the human proteome. J Proteome Res. 2005;4(1):53-62. Epub 2005/02/15. doi: 10.1021/pr0498638. PubMed PMID: 15707357.

178.   Jaitly N, Mayampurath A, Littlefield K, Adkins JN, Anderson GA, Smith RD. Decon2LS: An open-source software package for automated processing and visualization of high resolution mass spectrometry data. BMC Bioinformatics. 2009;10:87. Epub 2009/03/19. doi: 1471-2105-10-87 [pii]

10.1186/1471-2105-10-87. PubMed PMID: 19292916; PMCID: 2666663.

179.   Monroe ME, Tolic N, Jaitly N, Shaw JL, Adkins JN, Smith RD. VIPER: an advanced software package to support high-throughput LC-MS peptide identification. Bioinformatics. 2007;23(15):2021-3. Epub 2007/06/05. doi: btm281 [pii]

10.1093/bioinformatics/btm281. PubMed PMID: 17545182.

180.   Polpitiya AD, Qian WJ, Jaitly N, Petyuk VA, Adkins JN, Camp DG, 2nd, Anderson GA, Smith RD. DAnTE: a statistical tool for quantitative analysis of -omics data. Bioinformatics. 2008;24(13):1556-8. Epub 2008/05/06. doi: btn217 [pii]

10.1093/bioinformatics/btn217. PubMed PMID: 18453552; PMCID: 2692489.

181.   McCarthy FM, Wang N, Magee GB, Nanduri B, Lawrence ML, Camon EB, Barrell DG, Hill DP, Dolan ME, Williams WP, Luthe DS, Bridges SM, Burgess SC. AgBase: a

functional genomics resource for agriculture. BMC Genomics. 2006;7:229. Epub 2006/09/12. doi: 1471-2164-7-229 [pii]

10.1186/1471-2164-7-229. PubMed PMID: 16961921; PMCID: 1618847.

182.   Reorganizing the protein space at the Universal Protein Resource (UniProt). Nucleic Acids Res. 2012;40(Database issue):D71-5. Epub 2011/11/22. doi: gkr981 [pii]

10.1093/nar/gkr981. PubMed PMID: 22102590; PMCID: 3245120.

183.   Altschul SF, Gish W, Miller W, Myers EW, Lipman DJ. Basic local alignment search tool. J Mol Biol. 1990;215(3):403-10. Epub 1990/10/05. doi: 10.1016/S0022-2836(05)80360-2

S0022-2836(05)80360-2 [pii]. PubMed PMID: 2231712.

184.   Mukherjee A, Boisvert S, Monte-Neto RL, Coelho AC, Raymond F, Mukhopadhyay R, Corbeil J, Ouellette M. Telomeric gene deletion and intrachromosomal amplification in antimony-resistant Leishmania. Mol Microbiol. 2013;88(1):189-202. Epub 2013/02/21. doi: 10.1111/mmi.12178. PubMed PMID: 23421749.

185.   Bates LS. Rapid determination of free proline for water-stress studies. Plant Soil. 1973;39:205-7.

186.   Langmead B, Trapnell C, Pop M, Salzberg SL. Ultrafast and memory-efficient alignment of short DNA sequences to the human genome. Genome Biol. 2009;10(3):R25. Epub 2009/03/06. doi: gb-2009-10-3-r25 [pii]

10.1186/gb-2009-10-3-r25. PubMed PMID: 19261174; PMCID: 2690996.

187.   Dillies MA, Rau A, Aubert J, Hennequet-Antier C, Jeanmougin M, Servant N, Keime C, Marot G, Castel D, Estelle J, Guernec G, Jagla B, Jouneau L, Laloe D, Le Gall C, Schaeffer B, Le Crom S, Guedj M, Jaffrezic F. A comprehensive evaluation of normalization methods for Illumina high-throughput RNA sequencing data analysis. Brief Bioinform. 2012. Epub 2012/09/19. doi: bbs046 [pii]

10.1093/bib/bbs046. PubMed PMID: 22988256.

188.   Livak KJ, Schmittgen TD. Analysis of relative gene expression data using real-time quantitative PCR and the 2(-Delta Delta C(T)) Method. Methods. 2001;25(4):402-8. Epub 2002/02/16. doi: 10.1006/meth.2001.1262. PubMed PMID: 11846609.

189.   Fulwiler AL, Soysa DR, Ullman B, Yates PA. A rapid, efficient and economical method for generating leishmanial gene targeting constructs. Mol Biochem Parasitol. 2011;175(2):209-12. Epub 2010/11/09. doi: S0166-6851(10)00274-4 [pii]

10.1016/j.molbiopara.2010.10.008. PubMed PMID: 21055426; PMCID: 3018707.

190.   Soysa R, Carter NS, Yates PA. A dual luciferase system for analysis of post-transcriptional regulation of gene expression in Leishmania. Mol Biochem Parasitol.

2014;195(1):1-5. Epub 2014/06/01. doi: 10.1016/j.molbiopara.2014.05.002. PubMed PMID: 24878002; PMCID: 4142068.

191.   Saeed AI, Sharov V, White J, Li J, Liang W, Bhagabati N, Braisted J, Klapa M, Currier T, Thiagarajan M, Sturn A, Snuffin M, Rezantsev A, Popov D, Ryltsov A, Kostukovich E, Borisovsky I, Liu Z, Vinsavich A, Trush V, Quackenbush J. TM4: a free, open-source system for microarray data management and analysis. Biotechniques. 2003;34(2):374-8. Epub 2003/03/05. PubMed PMID: 12613259.

192.   Chantranupong L, Wolfson RL, Sabatini DM. Nutrient-sensing mechanisms across evolution. Cell. 2015;161(1):67-83. Epub 2015/03/31. doi: 10.1016/j.cell.2015.02.041. PubMed PMID: 25815986; PMCID: 4384161.

193.   Boitz JM, Ullman B, Jardim A, Carter NS. Purine salvage in Leishmania: complex or simple by design? Trends Parasitol. 2012;28(8):345-52. Epub 2012/06/26. doi: 10.1016/j.pt.2012.05.005. PubMed PMID: 22726696; PMCID: 3429121.

194.   Allen T, Henschel EV, Coons T, Cross L, Conley J, Ullman B. Purification and characterization of the adenine phosphoribosyltransferase and hypoxanthine-guanine phosphoribosyltransferase activities from Leishmania donovani. Mol Biochem Parasitol. 1989;33(3):273-81. Epub 1989/03/15. PubMed PMID: 2704389.

195.   Fulwiler AL, Boitz JM, Yates PA, Carter NS, Ullman B. Characterization of amplicons that suppress the conditional lethal growth phenotype of a Leishmania donovani mutant lacking normal purine salvage mechanisms. Mol Biochem Parasitol. 2011;175(1):76-82. Epub 2010/10/05. doi: S0166-6851(10)00250-1 [pii]

10.1016/j.molbiopara.2010.09.006. PubMed PMID: 20888372.

196.   Boitz JM, Strasser R, Hartman CU, Jardim A, Ullman B. Adenine aminohydrolase from Leishmania donovani: unique enzyme in parasite purine metabolism. J Biol Chem. 2012;287(10):7626-39. Epub 2012/01/13. doi: 10.1074/jbc.M111.307884. PubMed PMID: 22238346; PMCID: 3293595.

197.   Boitz JM, Strasser R, Yates PA, Jardim A, Ullman B. Adenylosuccinate synthetase and adenylosuccinate lyase deficiencies trigger growth and infectivity deficits in Leishmania donovani. J Biol Chem. 2013;288(13):8977-90. Epub 2013/02/14. doi: 10.1074/jbc.M112.431486. PubMed PMID: 23404497; PMCID: 3610970.

198.   Stocchi V, Cucchiarini L, Canestrari F, Piacentini MP, Fornaini G. A very fast ion-pair reversed-phase HPLC method for the separation of the most significant nucleotides and their degradation products in human red blood cells. Anal Biochem. 1987;167(1):181-90. Epub 1987/11/15. PubMed PMID: 2829656.

199.   Boitz JM, Ullman B. Adenine and adenosine salvage in Leishmania donovani. Mol Biochem Parasitol. 2013;190(2):51-5. Epub 2013/07/13. doi: 10.1016/j.molbiopara.2013.06.005. PubMed PMID: 23845934; PMCID: 3767402.

200.   Fulwiler AL, Boitz JM, Gilroy C, Yates PA, Jardim A, Ullman B. IMP dehydrogenase deficiency in Leishmania donovani causes a restrictive growth phenotype in promastigotes but is not essential for infection in mice. Mol Biochem Parasitol. 2011;180(2):123-6. Epub 2011/09/13. doi: 10.1016/j.molbiopara.2011.08.006. PubMed PMID: 21907738; PMCID: 3202435.

201.   Gray JV, Petsko GA, Johnston GC, Ringe D, Singer RA, Werner-Washburne M. "Sleeping beauty": quiescence in Saccharomyces cerevisiae. Microbiology and molecular biology reviews : MMBR. 2004;68(2):187-206. doi: 10.1128/MMBR.68.2.187-206.2004. PubMed PMID: 15187181; PMCID: 419917.

202.   Laporte D, Lebaudy A, Sahin A, Pinson B, Ceschin J, Daignan-Fornier B, Sagot I. Metabolic status rather than cell cycle signals control quiescence entry and exit. J Cell Biol. 2011;192(6):949-57. doi: 10.1083/jcb.201009028. PubMed PMID: 21402786; PMCID: 3063145.

203.   Castilho-Martins EA, Laranjeira da Silva MF, dos Santos MG, Muxel SM, Floeter-Winter LM. Axenic Leishmania amazonensis promastigotes sense both the external and internal arginine pool distinctly regulating the two transporter-coding genes. PLoS One. 2011;6(11):e27818. doi: 10.1371/journal.pone.0027818. PubMed PMID: 22114701; PMCID: PMC3218042.

204.   El-Sayed NM, Myler PJ, Blandin G, Berriman M, Crabtree J, Aggarwal G, Caler E, Renauld H, Worthey EA, Hertz-Fowler C, Ghedin E, Peacock C, Bartholomeu DC, Haas BJ, Tran AN, Wortman JR, Alsmark UC, Angiuoli S, Anupama A, Badger J, Bringaud F, Cadag E, Carlton JM, Cerqueira GC, Creasy T, Delcher AL, Djikeng A, Embley TM, Hauser C, Ivens AC, Kummerfeld SK, Pereira-Leal JB, Nilsson D, Peterson J, Salzberg SL, Shallom J, Silva JC, Sundaram J, Westenberger S, White O, Melville SE, Donelson JE, Andersson B, Stuart KD, Hall N. Comparative genomics of trypanosomatid parasitic protozoa. Science. 2005;309(5733):404-9. Epub 2005/07/16. doi: 10.1126/science.1112181. PubMed PMID: 16020724.

205.   Landfear SM. Nutrient transport and pathogenesis in selected parasitic protozoa. Eukaryot Cell. 2011;10(4):483-93. doi: 10.1128/EC.00287-10. PubMed PMID: 21216940; PMCID: 3127635.

206.   Conrad M, Schothorst J, Kankipati HN, Van Zeebroeck G, Rubio-Texeira M, Thevelein JM. Nutrient sensing and signaling in the yeast Saccharomyces cerevisiae. FEMS microbiology reviews. 2014;38(2):254-99. doi: 10.1111/1574-6976.12065. PubMed PMID: 24483210; PMCID: 4238866.

207.   Kriel J, Haesendonckx S, Rubio-Texeira M, Van Zeebroeck G, Thevelein JM. From transporter to transceptor: signaling from transporters provokes re-evaluation of complex trafficking and regulatory controls: endocytic internalization and intracellular trafficking of nutrient transceptors may, at least in part, be governed by their signaling function. BioEssays : news and reviews in molecular, cellular and developmental biology. 2011;33(11):870-9. doi: 10.1002/bies.201100100. PubMed PMID: 21913212; PMCID: 3258547.

208. Lopez MA, Saada EA, Hill KL. Insect stage-specific adenylate cyclases regulate social motility in African trypanosomes. Eukaryot Cell. 2015;14(1):104-12. doi: 10.1128/EC.00217-14. PubMed PMID: 25416239; PMCID: 4279026.

209. Saada EA, Kabututu ZP, Lopez M, Shimogawa MM, Langousis G, Oberholzer M, Riestra A, Jonsson ZO, Wohlschlegel JA, Hill KL. Insect stage-specific receptor adenylate cyclases are localized to distinct subdomains of the Trypanosoma brucei Flagellar membrane. Eukaryot Cell. 2014;13(8):1064-76. doi: 10.1128/EC.00019-14. PubMed PMID: 24879126; PMCID: 4135804.

210. Salmon D, Vanwalleghem G, Morias Y, Denoeud J, Krumbholz C, Lhomme F, Bachmaier S, Kador M, Gossmann J, Dias FB, De Muylder G, Uzureau P, Magez S, Moser M, De Baetselier P, Van Den Abbeele J, Beschin A, Boshart M, Pays E. Adenylate cyclases of Trypanosoma brucei inhibit the innate immune response of the host. Science. 2012;337(6093):463-6. doi: 10.1126/science.1222753. PubMed PMID: 22700656.

211. Carling D, Viollet B. Beyond energy homeostasis: the expanding role of AMP-activated protein kinase in regulating metabolism. Cell metabolism. 2015;21(6):799-804. doi: 10.1016/j.cmet.2015.05.005. PubMed PMID: 26039446.

212. Hardie DG. AMP-activated protein kinase: an energy sensor that regulates all aspects of cell function. Genes Dev. 2011;25(18):1895-908. doi: 10.1101/gad.17420111. PubMed PMID: 21937710; PMCID: 3185962.

213. Ereno-Orbea J, Oyenarte I, Martinez-Cruz LA. CBS domains: Ligand binding sites and conformational variability. Arch Biochem Biophys. 2013;540(1-2):70-81. doi: 10.1016/j.abb.2013.10.008. PubMed PMID: 24161944.

214. Guther ML, Urbaniak MD, Tavendale A, Prescott A, Ferguson MA. High-confidence glycosome proteome for procyclic form Trypanosoma brucei by epitope-tag organelle enrichment and SILAC proteomics. J Proteome Res. 2014;13(6):2796-806. doi: 10.1021/pr401209w. PubMed PMID: 24792668; PMCID: 4052807.

215. Aboagye-Kwarteng T, ole-MoiYoi OK, Lonsdale-Eccles JD. Phosphorylation differences among proteins of bloodstream developmental stages of Trypanosoma brucei brucei. Biochem J. 1991;275 (Pt 1):7-14. Epub 1991/04/01. PubMed PMID: 2018486; PMCID: 1150005.

216. Dell KR, Engel JN. Stage-specific regulation of protein phosphorylation in Leishmania major. Mol Biochem Parasitol. 1994;64(2):283-92. Epub 1994/04/01. PubMed PMID: 7935606.

217. Parsons M, Valentine M, Deans J, Schieven GL, Ledbetter JA. Distinct patterns of tyrosine phosphorylation during the life cycle of Trypanosoma brucei. Mol Biochem Parasitol. 1991;45(2):241-8. Epub 1991/04/01. PubMed PMID: 1710035.

218.   Morales MA, Watanabe R, Dacher M, Chafey P, Osorio y Fortea J, Scott DA, Beverley SM, Ommen G, Clos J, Hem S, Lenormand P, Rousselle JC, Namane A, Spath GF. Phosphoproteome dynamics reveal heat-shock protein complexes specific to the Leishmania donovani infectious stage. Proc Natl Acad Sci U S A. 2010;107(18):8381-6. Epub 2010/04/21. doi: 10.1073/pnas.0914768107. PubMed PMID: 20404152; PMCID: 2889574.

219.   Morales MA, Watanabe R, Laurent C, Lenormand P, Rousselle JC, Namane A, Spath GF. Phosphoproteomic analysis of Leishmania donovani pro- and amastigote stages. Proteomics. 2008;8(2):350-63. Epub 2008/01/19. doi: 10.1002/pmic.200700697. PubMed PMID: 18203260.

220.   Foucher AL, Spath GF, Pemberton IK. Probing the dynamic nature of signalling pathways by IMAC and SELDI-tof MS. Arch Physiol Biochem. 2010;116(4-5):163-73. Epub 2010/07/02. doi: 10.3109/13813455.2010.495129. PubMed PMID: 20590411.

221.   Mertins P, Yang F, Liu T, Mani DR, Petyuk VA, Gillette MA, Clauser KR, Qiao JW, Gritsenko MA, Moore RJ, Levine DA, Townsend R, Erdmann-Gilmore P, Snider JE, Davies SR, Ruggles KV, Fenyo D, Kitchens RT, Li S, Olvera N, Dao F, Rodriguez H, Chan DW, Liebler D, White F, Rodland KD, Mills GB, Smith RD, Paulovich AG, Ellis M, Carr SA. Ischemia in tumors induces early and sustained phosphorylation changes in stress kinase pathways but does not affect global protein levels. Mol Cell Proteomics. 2014;13(7):1690-704. doi: 10.1074/mcp.M113.036392. PubMed PMID: 24719451; PMCID: PMC4083109.

222.   Granholm V, Kim S, Navarro JC, Sjolund E, Smith RD, Kall L. Fast and accurate database searches with MS-GF+Percolator. J Proteome Res. 2014;13(2):890-7. doi: 10.1021/pr400937n. PubMed PMID: 24344789; PMCID: PMC3975676.

223.   Beausoleil SA, Villen J, Gerber SA, Rush J, Gygi SP. A probability-based approach for high-throughput protein phosphorylation analysis and site localization. Nat Biotechnol. 2006;24(10):1285-92. doi: 10.1038/nbt1240. PubMed PMID: 16964243.

224.   Monroe ME, Shaw JL, Daly DS, Adkins JN, Smith RD. MASIC: a software program for fast quantitation and flexible visualization of chromatographic profiles from detected LC-MS(/MS) features. Comput Biol Chem. 2008;32(3):215-7. doi: 10.1016/j.compbiolchem.2008.02.006. PubMed PMID: 18440872; PMCID: PMC2487672.

225.   Prasad A, Kaur S, Malla N, Ganguly NK, Mahajan RC. Ca2+ signaling in the transformation of promastigotes to axenic amastigotes of Leishmania donovani. Mol Cell Biochem. 2001;224(1-2):39-44. PubMed PMID: 11693198.

226.   Chen F, Mackey AJ, Stoeckert CJ, Jr., Roos DS. OrthoMCL-DB: querying a comprehensive multi-species collection of ortholog groups. Nucleic Acids Res. 2006;34(Database issue):D363-8. doi: 10.1093/nar/gkj123. PubMed PMID: 16381887; PMCID: PMC1347485.

227.	Fischer S, Brunk BP, Chen F, Gao X, Harb OS, Iodice JB, Shanmugam D, Roos DS, Stoeckert CJ, Jr. Using OrthoMCL to assign proteins to OrthoMCL-DB groups or to cluster proteomes into new ortholog groups. Curr Protoc Bioinformatics. 2011;Chapter 6:Unit 6 12 1-9. doi: 10.1002/0471250953.bi0612s35. PubMed PMID: 21901743; PMCID: PMC3196566.

228.	Li L, Stoeckert CJ, Jr., Roos DS. OrthoMCL: identification of ortholog groups for eukaryotic genomes. Genome Res. 2003;13(9):2178-89. doi: 10.1101/gr.1224503. PubMed PMID: 12952885; PMCID: PMC403725.

229.	Wilmarth PA, Tanner S, Dasari S, Nagalla SR, Riviere MA, Bafna V, Pevzner PA, David LL. Age-related changes in human crystallins determined from comparative analysis of post-translational modifications in young and aged lens: does deamidation contribute to crystallin insolubility? J Proteome Res. 2006;5(10):2554-66. Epub 2006/10/07. doi: 10.1021/pr050473a. PubMed PMID: 17022627; PMCID: 2536618.

230.	Bassnett S, Wilmarth PA, David LL. The membrane proteome of the mouse lens fiber cell. Mol Vis. 2009;15:2448-63. Epub 2009/12/04. doi: 261 [pii]. PubMed PMID: 19956408; PMCID: 2786885.

231.	Wilmarth PA, Riviere MA, David LL. Techniques for accurate protein identification in shotgun proteomic studies of human, mouse, bovine, and chicken lenses. J Ocul Biol Dis Infor. 2009;2(4):223-34. Epub 2010/02/17. doi: 10.1007/s12177-009-9042-6. PubMed PMID: 20157357; PMCID: 2816815.

232.	Keller A, Nesvizhskii AI, Kolker E, Aebersold R. Empirical statistical model to estimate the accuracy of peptide identifications made by MS/MS and database search. Anal Chem. 2002;74(20):5383-92. Epub 2002/10/31. PubMed PMID: 12403597.

233.	Liu H, Sadygov RG, Yates JR, 3rd. A model for random sampling and estimation of relative protein abundance in shotgun proteomics. Anal Chem. 2004;76(14):4193-201. Epub 2004/07/16. doi: 10.1021/ac0498563. PubMed PMID: 15253663.

234.	Fei SS, Wilmarth PA, Hitzemann RJ, McWeeney SK, Belknap JK, David LL. Protein database and quantitative analysis considerations when integrating genetics and proteomics to compare mouse strains. J Proteome Res. 2011;10(7):2905-12. Epub 2011/05/11. doi: 10.1021/pr200133p. PubMed PMID: 21553863; PMCID: 3128464.

235.	Yang IV, Chen E, Hasseman JP, Liang W, Frank BC, Wang S, Sharov V, Saeed AI, White J, Li J, Lee NH, Yeatman TJ, Quackenbush J. Within the fold: assessing differential expression measures and reproducibility in microarray assays. Genome Biol. 2002;3(11):research0062. Epub 2002/11/14. PubMed PMID: 12429061; PMCID: 133446.

236.	Thissen D, Steinberg L, Kuang D. Quick and Easy Implementation of the Benjamini-Hochberg Procedure for Controlling the False Positive Rate in Multiple

Comparisons. Journal of Educational and Behavioral Statistics. 2002;27(1):77-83. doi: 10.3102/10769986027001077.